

A quantitative evaluation of the impact of railway track characteristics on the magnitude of dynamic loads

by

Danial Behnia

A thesis submitted in partial fulfillment of the requirements for the degree of

Doctor of Philosophy

in

Geotechnical Engineering

Department of Civil and Environmental Engineering

University of Alberta

© Danial Behnia, 2024

Abstract

Canada has one of the largest railway networks globally, with more than 48,000 route kilometers of track. The Canadian railway network is primarily a heavy freight railway network that highlights the importance of the railway industry for the Canadian economy and the requirement for its fast and safe operation. The substantial intensity of dynamic loads can damage the railway track, such as rail breaks and failures in track components. In Canada, the leading causes of derailments are rail breaks and rail component failures. In light of continuing rail failures, it is worth revisiting the understanding of the magnitude of loads that the rail is subjected to.

The current literature needs to address the relationship between dynamic loads and railway track structures, particularly in understanding the magnitude of these loads. Track geometry and stiffness changes are two primary factors contributing to the variability and escalation of dynamic loads. A significant limitation of existing understanding stems from data predominantly gathered under constant track conditions at instrumented sections, focusing on numerous wheel loads without considering variable conditions. As dynamic load factor (ϕ) values find widespread application in the analysis and design of railway tracks, this research centers on evaluating this factor. The ϕ values play a significant role in track structure analysis, design, and selection of rail steel and cross-sectional characteristics (weight).

An extensive study was conducted on a track section of over 340 km in the Canadian Prairies, operated by a North American Class 1 freight railway. This study utilized a train-mounted system comprising the Instrumented Wheelset (IWS) and MRail measurement systems. In contrast to previous investigations that focused on specific track sections (i.e., instrumented section), the measurements used in this research primarily result from variations in track characteristics.

Evaluating the impact of observable track characteristics indicates a noteworthy influence, resulting in dynamic load ranges and ϕ values for the track that exceed those typically estimated through conventional means. This augmentation is particularly pronounced for non-tangent track segments, which include curves, switches, crossings, and bridges. The impact of track surface longitudinal level (in terms of rail profile) on ϕ values revealed a more pronounced effect of the longitudinal level of the rail vertical deviations, train speed, and track conditions on the magnitude of dynamic loads in non-tangent sections compared to tangent sections. Track surface vertical deviations can lead to a 15-36% increase in dynamic load magnitudes within the typical range of rail profile changes (0-20 mm), diverging from prevalent North American railway design practices.

The assessment of subgrade track stiffness (VTD_{sub}) conditions highlighted the significance of the average track conditions range (3.1-4.4 mm), demonstrating a critical association with observable increases in ϕ values. This association can increase dynamic load magnitudes by 20-30%. In curves, heightened subgrade vertical track deflection (VTD_{sub}) conditions, particularly in tracks of average to poor quality, may lead to increased dynamic loads on the lower rail compared to good tracks. The investigation into the effects of transition directions on dynamic load magnitudes indicated that transitions from soft-to-stiff conditions amplify dynamic loads, while transitions from stiff-to-soft conditions attenuate them. Notably, soft-to-stiff transitions exhibited ϕ values approximately 10% higher than those observed in stiff-to-soft transitions. This analysis also highlighted that subgrade track conditions contribute to the effectiveness of the influence of transition direction, potentially diminishing the discrepancy between the two transition scenarios. These quantitative insights pave the way for proactively optimizing maintenance schedules to prevent rail breaks and failures.

Preface

This is a “paper-format” style dissertation, with Chapters 3, 4, 5, and 6 either submitted for publication or published as detailed below. Versions of the individual manuscripts as presented in this thesis may differ slightly from the published versions.

Chapter 3 is published in the American Society of Civil Engineering (ASCE) Journal of Transportation Engineering, Part A: Systems as: Behnia, D., Hendry M.T., Abdulrazagh, P.H., and Wahba, A. “Railway Dynamic Load Factors Developed from Instrumented Wheelset Measurements”. DOI: 10.1061/JTEPBS.0000685.

Chapter 4 is submitted (on March 2024) for publication in the Journal of Vehicle System Dynamics (Taylor & Francis) as: Behnia, D. and Hendry, M.T. “Quantifying the Impact of Rail Profile Changes on the Magnitude of Dynamic Loads through Instrumented Wheelset Measurements,” (*in Revision*).

Chapter 5 is submitted (on March, 2024) for publication in the Journal of Civil Structural Health Monitoring (Springer) as: Behnia, D. and Hendry, M.T. “Impact of Subgrade Track Stiffness on Dynamic Loads: A Comprehensive Evaluation Using Instrumented Wheelset and MRail Measurements,” (*Under Review*).

Chapter 6 is submitted (on March, 2024) for publication in the Journal of Transportation Geotechnics (Elsevier) as Behnia, D. and Hendry, M.T. “Quantifying the Impact of Subgrade Stiffness Transition Directions on Railway Dynamic Load Factor,” (*Under Review*).

I was responsible for all work reported in the manuscript including the data collection, data analysis and interpretation, discussion of the results, and manuscript composition. Dr. M.T. Hendry was involved in the concept formation and manuscript composition and has reviewed all parts of the work as the supervisor.

To my parents,

beloved mom (Nasrin Mother), who lost her battle to cancer

may her beautiful soul rest in peace

and my father

&

To my wonderful wife (Alaleh)

Acknowledgment

I would like to express my deepest gratitude to my supervisor, Dr. Michael T. Hendry, the director of the Canadian Rail Research Laboratory (CaRRL), for giving me the opportunity to work in this group and for his constant guidance and encouragement throughout this research. The completion of this research would not have been possible without his tireless efforts.

Furthermore, this research would not have been possible without the support provided by CaRRL, which is funded by the Natural Sciences and Engineering Research Council of Canada (NSERC), Canadian Pacific Railway, Canadian National Railway, the Association of American Railways – Transportation Technology Center Inc., the National Research Council of Canada, Transport Canada and Alberta Innovates – Technology Futures. Thanks to Tom Edwards and Albert Wahba for their support during this research.

I am grateful to Dr. Mustafa Gül and Dr. Renato Macciotta Pulisci for providing several valuable suggestions for my thesis by putting their valuable time and effort into reviewing my work. I am also very thankful to Dr. Parisa Haji Abdulrazagh, a former postdoctoral fellow working with CaRRL, for her constructive comments and help.

And, of course, my parents, to whom I am forever grateful for their love, sacrifice, and hard work. Above all, I would like to express my sincere and unending gratitude to my wife, Alaleh. While you may only sometimes understand what I am doing, your support is fundamental to me seeing it through.

Table of Contents

Abstract.....	ii
Preface.....	iv
Acknowledgment.....	vi
Table of Contents.....	vii
List of Figures.....	xi
List of Tables.....	xxv
1. Introduction.....	1
1.1. Problem description.....	2
1.2. Research objectives.....	4
1.3. Description of study site.....	5
1.4. Scope and methodology.....	5
1.4.1. Quantifying the effect of observable track characteristics.....	6
1.4.2. Investigating the impact of track surface roughness.....	7
1.4.3. Evaluating the impact of track subgrade stiffness.....	8
1.4.4. Evaluating the impact of transition directions.....	9
1.5. Research limitations.....	10
1.6. Thesis outline.....	10
1.7. References.....	11
2. Literature Review.....	16
2.1. Track structure.....	16
2.1.1. Track superstructure.....	16
2.1.2. Track substructure.....	17
2.2. Characterization and loading environment in North America.....	18
2.2.1. Dynamic load factor (ϕ).....	19
2.2.2. Measurement systems.....	21
2.2.3. Instrumented wheelset (IWS) system.....	22
2.3. Track geometry.....	24
2.3.1. Fundamental measurements.....	24
2.3.2. Track roughness interpretation methods.....	25
2.3.2. Rail surface (profile).....	28
2.4. Effect of track substructure on track performance.....	29

2.4.1. Track stiffness.....	30
2.4.2. Measurement technologies for vertical track deflection.....	32
2.4.3. University of Nebraska rolling deflection system (MRail)	33
2.4.4. Quantifying track subgrade stiffness	34
2.5. References	36
3. Railway Dynamic Load Factors Developed from Instrumented Wheelset Measurements	48
3.1. Contribution of the Ph.D. candidate.....	48
3.2. Abstract	48
3.3. Introduction	49
3.4. Materials and methods	51
3.5. Presentation of results	53
3.6. Discussion	55
3.7. Conclusion.....	60
3.8. Acknowledgement.....	60
3.9. References	61
4. Quantifying the Impact of Rail Profile Changes on the Magnitude of Dynamic Loads through Instrumented Wheelset Measurements	64
4.1. Contribution of the Ph.D. candidate.....	64
4.2. Abstract	64
4.3. Introduction	65
4.4. Measured datasets	67
4.4.1. Dynamic load measurements.....	68
4.4.2. Rail profile measurements	70
4.5. Results	71
4.6. Data preparation and alignment	72
4.7. Discussion	74
4.8. Conclusion.....	81
4.9. Acknowledgement.....	82
4.10. References	82
5. Impact of Subgrade Track Stiffness on Dynamic Loads: A Comprehensive Evaluation Using Instrumented Wheelset and MRail Measurements	89
5.1. Contribution of the Ph.D. candidate.....	89
5.2. Abstract	89

5.3. Introduction	90
5.4. Study site and measurement systems	93
5.4.1. Study Site.....	94
5.4.2. Measuring wheel/rail dynamic interactions using the IWS system.....	94
5.4.3. Measuring <i>VTD</i> using the MRail system.....	95
5.5. Results	96
5.6. Discussion	100
5.6.1. Evaluation of the effect of VTD_{sub} on ϕ	102
5.6.2. Evaluation of the effect of VTD_{sub} and speed (S) on ϕ	105
5.7. Conclusion.....	110
5.8. Acknowledgement.....	112
5.9. References	112
6. Quantifying the Impact of Subgrade Stiffness Transition Directions on Railway Dynamic Load Factor	122
6.1. Contribution of the Ph.D. candidate.....	122
6.2. Abstract	122
6.3. Introduction	123
6.4. Study site	125
6.5. Measurement systems	126
6.5.1. Wheel-rail dynamic load measurement system.....	127
6.5.2. Vertical track deflection (<i>VTD</i>) measurement system.....	127
6.6. Quantifying the change of subgrade stiffness (ΔVTD_{sub}).....	128
6.7. Results	129
6.8. Discussion	132
6.8.1. Effect of transition direction (ΔVTD_{subR}) on ϕ	135
6.8.2. Effect of transition direction (ΔVTD_{subR}) and train speed (S) on ϕ	139
6.9. Conclusion.....	144
6.10. Acknowledgement.....	146
6.11. References	146
7. Conclusions & Recommendations.....	151
7.1. Quantifying the impact of observable track characteristics on dynamic load magnitudes	151
7.2. Quantifying the effect of surface track vertical deviation on dynamic load magnitudes.	152

7.3. Quantitative evaluation of subgrade track stiffness effects on dynamic load magnitudes	153
7.4. Quantitative evaluation of transition directions impacts on dynamic load magnitudes...	153
7.5. Contributions of track parameters to railway dynamic load factor	155
7.6. Implications of this study	155
7.7. Recommendations	156
8. References	159
A. Appendix A: Summary of the Dynamic Load Factors (ϕ) Equations Presented in the Literature for Passenger Railways	182
B. Appendix B: Developed Dynamic Load Factor (ϕ) Equations in Miles per Hour (m/h)	183
C. Appendix C: Supplemental Materials for Chapter 4	184
D. Appendix D: Supplemental Materials for Chapter 5	187
E. Appendix E: Supplemental Materials for Chapter 6	193

List of Figures

Figure 2-1. A typical cross-section of a ballasted track foundation shows the superstructure and substructure (<i>after</i> Loizos et al., 2017).	16
Figure 2-2. Photograph of the instrumented wheelsets (IWS) system installed on the Gondola railcar to collect the data used for this study. Wheatstone bridge strain gauges and connectors are covered in yellow epoxy coating, which is visible in the photograph (Images by Michael T. Hendry).	24
Figure 2-3. Definition of mid-chord offset (MCO) (<i>after</i> Li et al., 2015).	28
Figure 2-4. Schematic of the MRail system for measuring the relative VTD (Y_{rel}); (a) original system; (b) sensor system; (c) new MRail system (<i>after</i> Do et al., 2020; and Roghani and Hendry, 2015; photo credit Hendry, 2014).	35
Figure 3-1. Photograph of the instrumented wheelset (IWS) installed on the Gondola railcar to collect the data used for this study. Wheatstone bridge strain gauges and connectors covered in epoxy coating visible in the photograph. (Image by Michael T. Hendry.)	48
Figure 3-2. Example vertical load data from the IWS system including tangent track, a switch, a grade crossing, and a short bridge (steel span). These data are presented as (a) a satellite image of the section of track (image © Google, Image © 2022 CNES/Airbus); (b) measurements from two slower moving west-bound trains; and (c) measurements from two faster moving east-bound trains.	54
Figure 3-3. Probability distributions of vertical load measurements from the IWS: (a) on tangent track, grade crossings, and switches; and (b) on curves and bridges. Note that data includes all four instrumented wheels, and all four passes.	55

Figure 3-4. IWS measurements from tangent track as (a) dynamic load factor (ϕ) for 5 km/h increments of train speed; and (b) the number of measurements used to develop the ϕ for each increment of train speed..... 57

Figure 3-5. IWS measurements from curves as (a) dynamic load factor (ϕ) for 5 km/h increments of train speed; and (b) the number of measurements used to develop the ϕ for each increment of train speed. 57

Figure 3-6. IWS measurements from bridges as (a) dynamic load factor (ϕ) for 5 km/h increments of train speed; and (b) the number of measurements used to develop the ϕ for each increment of train speed. 58

Figure 3-7. IWS measurements from grade crossings as (a) dynamic load factor (ϕ) for 5 km/h increments of train speed; and (b) the number of measurements used to develop the ϕ for each increment of train speed..... 58

Figure 3-8. IWS measurements from switches as (a) dynamic load factor (ϕ) for 5 km/h increments of train speed; and (b) the number of measurements used to develop the ϕ for each increment of train speed. 54

Figure 3-9. IWS measurements from nontangent track (inclusive of curves, bridges, grade crossings, and switches) as (a) dynamic load factor (ϕ) for 5 km/h increments of train speed; and (b) the number of measurements used to develop the ϕ for each increment of train speed. 55

Figure 4-1. Photograph of the IWS system installed on a car used to collect data on the magnitude of dynamic loads along the track. Wheatstone bridge strain gauges and connectors are covered in yellow epoxy (Image by Michael T. Hendry)..... 69

Figure 4-2. Probability distributions of track geometry measurements (available datasets) from the track geometry car: (a) rail profile on tangent and curve tracks; and (b) rail profile on grade crossings, switches, and bridges. 73

Figure 4-3. IWS and rail profile measurements based on Grubbs' values of dynamic load factor (ϕ) for 5 km/h increments of train speed and 2 mm increments of rail profile: (a) tangent sections; (b) curves; and (c) track assets..... 77

Figure 4-4. IWS measurements derived from the maximum Grubbs' test values of dynamic load factor (ϕ) for 5 km/h increments of train speed regarding the statistical significance conditions for three different ranges of rail profile (in mm), including $0 \leq |RP|_{max} < 2$, $10 \leq |RP|_{max} < 12$, and $18 \leq |RP|_{max} < 20$, compared to AREMA (2021) (ϕ_{AREMA} (Equation 4-2)) and Behnia et al. (2022) ($\phi_{Behnia et al.}^{Tan}$ (Equation 4-3) and $\phi_{Behnia et al.}^{NTan}$ (Equation 4-4)) estimations, in: (a) tangent sections; (b) curves; and (c) track assets. (*Note: A solid line signifies high reliability zone, a dash dotted line represents moderate reliability zone, and a dotted line designates low reliability zone*)..... 78

Figure 4-5. A comparative evaluation of ϕ_{AREMA} estimations against measured values derived from the IWS system and computed via maximum Grubbs' test values in various track classes (1 through 4) and categories (tangent track, curve track, and track assets) regarding the considered range of rail profile changes. 80

Figure 4-6. IWS and rail profile measurements based on the maximum Grubbs' test values for ϕ for 2 mm increments of rail profile regarding the statistical significance conditions for four track classes, including Class 1 ($S_{max} = 15$ km/h [~ 10 mph], ϕ_{15}), Class 2 ($S_{max} = 40$ km/h [25 mph], ϕ_{25}), Class 3 ($S_{max} = 65$ km/h [~ 40 mph], ϕ_{65}), and Class 4 ($S_{max} = 95$ km/h [~ 60 mph], ϕ_{95}), compared to Behnia et al. (2022) ($\phi_{Behnia et al.}^{Tan}$ (Equation 4-3) and $\phi_{Behnia et al.}^{NTan}$ (Equation 4-4)) estimations, in: (a) tangent sections; (b) curves; and (c) track assets. 81

Figure 5-1. Photograph the train-mounted system with instrumented wheelset (IWS) and MRail systems installed on the Gondola railcar to collect the data used for this study (image credit: Michael T. Hendry)..... 94

Figure 5-2. An example compares an 800 m section of normalized VTD_{sub} (VTD_{sub}^{Normal}) MRail system data obtained using the Z_{score} technique for a tangent section of track. 98

Figure 5-3. Probability distributions of vertical load measurements from the IWS system: (a) on tangent and curve sections; and (b) on bridges, grade crossings, and switches. The data are from all four instrumented wheels and both passes. 99

Figure 5-4. Probability distributions of VTD_{sub} measurements from the MRail system: (a) on tangent and curve sections; and (b) on bridges, grade crossings, and switches. The data are from both rails and both passes. The graph is segregated into three sections by blue lines, indicating good ($VTD_{sub} \leq 3.1$), average ($3.1 < VTD_{sub} \leq 4.4$), and poor ($VTD_{sub} > 4.4$) tracks. 99

Figure 5-5. IWS and VTD_{sub} measurements based on the Grubbs values of dynamic load factor ($\phi \geq 1.1$) for 0.4 mm increments of subgrade track stiffness (VTD_{sub}) on: (a) tangent tracks; (b) low rail in curves; and (c) track assets. The horizontal lines are based on equations by Behnia et al. (2022), where the ϕ_{C1} line is for 15 km/h (~10 mph), the ϕ_{C2} line is for 40 km/h (25 mph), the ϕ_{C3} line is for 65 km/h (~40 mph), and the ϕ_{75} line (75 km/h or ~47 mph) is for the maximum speed with a reliable number of data points. The graph is segregated into three sections by blue lines, indicating good ($VTD_{sub} \leq 3.1$), average ($3.1 < VTD_{sub} \leq 4.4$), and poor ($VTD_{sub} > 4.4$) tracks. 104

Figure 5-6. Grubbs values of dynamic load factor ($\phi \geq 1.1$) values for 5 km/h increments of train speed and 0.4 mm increments of VTD_{sub} on: (a) tangent sections; (b) low rail in curves; and (c) track assets. 106

Figure 5-7. IWS and VTD_{sub} (measured by MRail) measurements based on the Grubbs values of the dynamic load factor ($\phi \geq 1.1$) for 0.4 mm increments of VTD_{sub} with respect to significance conditions for four specific train speeds on: (a) tangent tracks; (b) low rail in curves; and (c) track assets. Note the specific speeds include $S= 15$ km/h (~10 mph, in black), 40 km/h (25 mph, in magenta), 65 km/h (~40 mph, in grey), and 75 km/h (~47 mph, in red) and the shaded regions represent the ϕ value based on the specific speeds (ϕ_{C1} , ϕ_{C2} , ϕ_{C3} , and ϕ_{75}) and equations developed by Behnia et al. (2022). The solid, dash-dot, and dotted lines correspond to high, medium, and low reliability zones, respectively. The graph is segregated into three sections by blue lines, indicating good ($VTD_{sub} \leq 3.1$), average ($3.1 < VTD_{sub} \leq 4.4$), and poor ($VTD_{sub} > 4.4$) tracks. 107

Figure 5-8. Example of comparing the dynamic load factor (ϕ) obtained using the Grubbs test with the equations developed by Behnia et al. (2022) for 0.4 mm increments of VTD_{sub} in track Class 2 (40 km/h [25 mph]) on track assets. The graph is segregated into three sections by blue lines, indicating good ($VTD_{sub} \leq 3.1$), average ($3.1 < VTD_{sub} \leq 4.4$), and poor ($VTD_{sub} > 4.4$) tracks. 108

Figure 5-9. Fitted quadratic lines over dynamic load factor (ϕ) values measured through the IWS system based on three scenarios for subgrade stiffness conditions (good, average, and poor) for 5 km/h increments of train speed across: (a) tangent track; (b) curve sections; and (c) track assets. 110

Figure 6-1. Photographs of the instrumented railcar (train-mounted system) with instrumented wheelset (IWS) and MRail systems installed on the Gondola railcar to collect the data used for this study: (a) instrumented railcar; (b) IWS and MRail systems (images by Michael T. Hendry).. 127

Figure 6-2. (a) Satellite image of the section of track (image © Google, Image © 2023 CNES/Airbus); an example of vertical load and ΔVTD_{sub} data from the instrumented car along a

section of tangent track for (b) two slower-moving westbound trains and (c) two faster-moving eastbound trains; and (d) subgrade track stiffness changes along this section of track (in terms of ΔVTD_{sub}). 131

Figure 6-3. Probability distribution plots illustrating vertical load measurements acquired from the IWS system for: (a) tangent and curve sections; and (b) bridges, grade crossings, and switches. Note: The dataset encompasses data collected from all four instrumented wheels across both passes. 134

Figure 6-4. Probability distributions of variations in subgrade track stiffness, in terms of ΔVTD_{sub} , based on measurements from the MRail system for: (a) tangent track and curve sections; and (b) bridges, grade crossings, and switches. Note: the data include both rails and both passes. 134

Figure 6-5. Comparing the Behnia et al. (2022) line regarding track classes with ϕ value changes regarding the ΔVTD_{sub} with 0.01 mm/m increments for $\phi \geq 1.1$ on: (a) tangent track; (b) curve sections; and (c) track assets. Note the horizontal lines are based on equations from Behnia et al. (2022), where the ϕ_{C1} line is for 15 km/h (~10 mph), ϕ_{C2} line is for 40 km/h (25 mph), ϕ_{C3} line is for 65 km/h (~41 mph), and ϕ_{75} line (75 km/h or ~47 mph) is for the maximum speed with a reliable number of data points..... 137

Figure 6-6. Comparing the Behnia et al. (2022) line regarding the track classes and conditions (i.e., good-average and poor tracks) with ϕ value changes regarding the ΔVTD_{sub} with 0.01 mm/m increments for $\phi \geq 1.1$ on: (a) tangent track; (b) curve sections; and (c) track assets. Note the shaded areas are based on equations from Behnia et al. (2022), where ϕ_{C1} is for 15 km/h (~10 mph), ϕ_{C2} is for 40 km/h (25 mph), ϕ_{C3} is for 65 km/h (~41 mph), and ϕ_{75} is for the maximum speed with a reliable number of data points (75 km/h~ 47 mph). 138

Figure 6-7. IWS and MRail measurements for tangent track based on the Grubbs test values of the dynamic load factor (ϕ) for 0.01 mm/m increments of ΔVTD_{sub} regarding the estimated ϕ values by Behnia et al. (2022) for tangent track (Equation 6-7) and reliability (confidence level) conditions for four specific train speeds: (a) 15 km/h (~10 mph, as Class 1, ϕ_{C1}); (b) 40 km/h (25 mph, as Class 2, ϕ_{C2}); (c) 65 km/h (~40 mph, as Class 3, ϕ_{C3}); and (d) 75 km/h (~47 mph, as the maximum speed with appropriate number of data points, ϕ_{75}). Note: the solid, dash-dot, and dotted lines respectively correspond to zones of high, moderate, and low reliability. 140

Figure 6-8. IWS and MRail measurements for non-tangent track (inclusive of curve sections and track assets) based on the Grubbs test values of the dynamic load factor (ϕ) for 0.01 mm/m increments of ΔVTD_{sub} regarding the estimated ϕ values by Behnia et al. (2022) for non-tangent track (Equation 6-8) and reliability (confidence level) conditions for four specific train speeds: (a) 15 km/h (~10 mph, as Class 1, ϕ_{C1}); (b) 40 km/h (25 mph, as Class 2, ϕ_{C2}); (c) 65 km/h (~40 mph, as Class 3, ϕ_{C3}); and (d) 75 km/h (~47 mph, as the maximum speed with appropriate number of data points, ϕ_{75}). Note: the solid, dash-dot, and dotted lines respectively correspond to zones of high, moderate, and low reliability. 142

Figure 6-9. IWS and MRail measurements for track assets based on the Grubbs test values of the dynamic load factor (ϕ) for 0.01 mm/m increments of ΔVTD_{sub} regarding the estimated ϕ values by Behnia et al. (2022) (Equation 6-8) and reliability (confidence level) conditions and track conditions (i.e., good-average and poor subgrade conditions of track) for four specific train speeds: (a) 15 km/h (~10 mph, as Class 1, ϕ_{C1}); (b) 40 km/h (25 mph, as Class 2, ϕ_{C2}); (c) 65 km/h (~40 mph, as Class 3, ϕ_{C3}); and (d) 75 km/h (~47 mph, as the maximum speed with appropriate number of data points, ϕ_{75}). Note: the solid, dash-dot, and dotted lines respectively correspond to zones of high, moderate, and low reliability. 143

Figure C-1. IWS and rail surface measurements based on maximum values of dynamic load factor (ϕ) for 5 km/h increments of train speed and 2 mm increments of rail surface: (a) tangent sections; (b) curves; and (c) track assets..... 184

Figure C-2. IWS and rail surface measurements based on the maximum Grubbs’ test values of ϕ values for 2 mm increments of rail profile regarding the statistical significance conditions for four track classes, including Class 1 ($S_{max}= 15$ km/h [~ 10 mph], ϕ_{15}), Class 2 ($S_{max}= 40$ km/h [25 mph], ϕ_{40}), Class 3 ($S_{max}= 65$ km/h [~ 40 mph], ϕ_{65}), and Class 4 ($S_{max}= 95$ km/h [~ 60 mph], ϕ_{95}), compared to AREMA (2021) (ϕ_{AREMA} [Eq. (2)]) estimations, in: (a) tangent tracks; (b) curves; and (c) track assets. 184

Figure C-3. Fitted surfaces over dynamic loads (in terms of ϕ) from IWS, with train speed increments of 5 km/h and rail surface increments of 2 mm: (a) tangent tracks; (b) curves; and (c) track assets (i.e., grade crossings, bridges, and switches). Note: Dark grey, light grey, and white markers represent high-, moderate-, and low-reliability zones, respectively. Fitted surfaces are based on data from the high- and moderate-reliability zones. 185

Figure C-4. ϕ trends across North American track classes: Comparative analysis showcasing ϕ changes based on fitted surfaces for defined rail surface threshold values within each track class, in (a) tangent tracks, (b) curves, and (c) track assets. Note: The shaded areas represent estimated values for each track class, according to AREMA (2021) (Equation 4-2). 185

Figure C-5. ϕ trends across North American track classes: Comparative analysis showcasing ϕ changes based on fitted surfaces for defined rail surface threshold values within each track class, in (a) tangent tracks, (b) curves, and (c) track assets. Note: The shaded areas represent estimated values for each track class, according to Behnia et al. (2022) (Equations 4-3 and 4-4). 186

Figure D-1. IWS and VTD_{sub} measurements based on maximum values of the dynamic load factor ($\phi \geq 1.1$) for 0.4 mm increments of subgrade track stiffness (VTD_{sub}) on: (a) tangent sections; (b) curve sections; and (c) track assets. The graph is segregated into three sections by blue lines, indicating good ($VTD_{sub} \leq 3.1$), average ($3.1 < VTD_{sub} \leq 4.4$), and poor ($VTD_{sub} > 4.4$) tracks..... 171

Figure D-2. IWS and VTD_{sub} measurements based on maximum values of the dynamic load factor ($\phi \geq 1.1$) for 0.4 mm increments of subgrade track stiffness (VTD_{sub}) on curves: (a) low (inner) rail; and (b) high (outer) rail. The graph is segregated into three sections by blue lines, indicating good ($VTD_{sub} \leq 3.1$), average ($3.1 < VTD_{sub} \leq 4.4$), and poor ($VTD_{sub} > 4.4$) tracks..... 171

Figure D-3. IWS and VTD_{sub} measurements based on the Grubbs values of the dynamic load factor ($\phi \geq 1.1$) for 0.4 mm increments of subgrade track stiffness (VTD_{sub}) on: (a) curve sections; and (b) high (outer) rail in curve sections. Note the horizontal lines are based on equations provided by Behnia et al. (2022), where the ϕ_{C1} line is for 15 km/h (~10 mph), ϕ_{C2} line is for 40 km/h (~25 mph), ϕ_{C3} line is for 65 km/h (~40 mph), and ϕ_{75} line (75 km/h~ 47 mph) is for the maximum speed with a reliable number of data points. The graph is segregated into three sections by blue lines, indicating good ($VTD_{sub} \leq 3.1$), average ($3.1 < VTD_{sub} \leq 4.4$), and poor ($VTD_{sub} > 4.4$) tracks. 172

Figure D-4. IWS and VTD_{sub} measurements based on the Grubbs values of the dynamic load factor ($\phi \geq 1.1$) for 0.4 mm increments of subgrade track stiffness (VTD_{sub}) on: (a) tangent sections; (b) low (inner) rail in curve sections; and (c) track assets. Note the horizontal lines are based on the equation provided by AREMA (2021), where the ϕ_{C1} line is for 15 km/h (~10 mph), ϕ_{C2} line is for 40 km/h (~25 mph), ϕ_{C3} line is for 65 km/h (~40 mph), and ϕ_{75} line (75 km/h~ 47 mph) is for the maximum speed with a reliable number of data points. The graph is segregated into three

sections by blue lines, indicating good ($VTD_{sub} \leq 3.1$), average ($3.1 < VTD_{sub} \leq 4.4$), and poor ($VTD_{sub} > 4.4$) tracks..... 172

Figure D-5. IWS and VTD_{sub} measurements based on the Grubbs values of the dynamic load factor ($\phi \geq 1.1$) for 0.4 mm increments of subgrade track stiffness (VTD_{sub}) on: (a) curve sections; and (b) high (outer) rail in curve sections. Note the horizontal lines are based on the equation provided by AREMA (2021) [29], where the ϕ_{C1} line is for 15 km/h (~10 mph), ϕ_{C2} line is for 40 km/h (~25 mph), ϕ_{C3} line is for 65 km/h (~40 mph), and ϕ_{75} line (75 km/h~ 47 mph) is for the maximum speed with a reliable number of data points. The graph is segregated into three sections by blue lines, indicating good ($VTD_{sub} \leq 3.1$), average ($3.1 < VTD_{sub} \leq 4.4$), and poor ($VTD_{sub} > 4.4$) tracks. 173

Figure D-6. Effect of VTD_{subAvg} with increments of 0.4 mm on maximum values of $|RP|_{max}$ on: (a) tangent sections; (b) curve sections; and (c) track assets. The graph is segregated into three sections by blue lines, indicating good ($VTD_{sub} \leq 3.1$), average ($3.1 < VTD_{sub} \leq 4.4$), and poor ($VTD_{sub} > 4.4$) tracks..... 173

Figure D-7. Maximum values of the dynamic load factor ($\phi \geq 1.1$) values for 5 km/h increments of train speed and 0.4 mm increments of VTD_{sub} on: (a) tangent track; (b) low rail in curve sections; (c) high rail in curve sections; and (d) track assets. 174

Figure D-8. Grubbs values of the dynamic load factor ($\phi \geq 1.1$) for 5 km/h increments of train speed and 0.4 mm increments of VTD_{sub} for the high rail in curves..... 174

Figure D-9. IWS and VTD_{sub} (measured by MRail) measurements based on the Grubbs values of the dynamic load factor ($\phi \geq 1.1$) for 0.4 mm increments of VTD_{sub} with respect to statistical significance conditions for four specific train speeds on the high rail in curve sections. Note the specific speeds include S= 15 km/h (~10 mph, in black), 40 km/h (~25 mph, in magenta), 65 km/h

(~40 mph, in grey), and 75 km/h (~47 mph, in red); and the shaded regions represent the ϕ values based on the specific speeds (ϕ_{C1} , ϕ_{C2} , ϕ_{C3} , and ϕ_{75}) and equations developed by Behnia et al. (2022). The graph is segregated into three sections by blue lines, indicating good ($VTD_{sub} \leq 3.1$), average ($3.1 < VTD_{sub} \leq 4.4$), and poor ($VTD_{sub} > 4.4$) tracks. 175

Figure D-10. IWS and VTD_{sub} (measured by MRail) measurements based on the Grubbs values of the dynamic load factor ($\phi \geq 1.1$) for 0.4 mm increments of VTD_{sub} with respect to significance conditions for four specific train speeds on: (a) tangent track; (b) the low rail in curves; and (c) track assets. Note the specific speeds include S= 15 km/h (~10 mph, in black), 40 km/h (~25 mph, in magenta), 65 km/h (~40 mph, in grey), and 75 km/h (~47 mph, in red); and the shaded regions represent the ϕ values based on the specific speeds (ϕ_{C1} , ϕ_{C2} , ϕ_{C3} , and ϕ_{75}) and equations developed by AREMA (2021). The graph is segregated into three sections by blue lines, indicating good ($VTD_{sub} \leq 3.1$), average ($3.1 < VTD_{sub} \leq 4.4$), and poor ($VTD_{sub} > 4.4$) tracks. 175

Figure D-11. IWS and VTD_{sub} (measured by MRail) measurements based on the Grubbs values of the dynamic load factor ($\phi \geq 1.1$) for 0.4 mm increments of VTD_{sub} with respect to significance conditions for four specific train speeds on the high rail in curve sections. Note the specific speeds include S= 15 km/h (~10 mph, in black), 40 km/h (~25 mph, in magenta), 65 km/h (~40 mph, in grey), and 75 km/h (~47 mph, in red); and the shaded regions represent the ϕ values based on the specific speeds (ϕ_{C1} , ϕ_{C2} , ϕ_{C3} , and ϕ_{75}) and equations developed by AREMA (2021) [29]. The graph is segregated into three sections by blue lines, indicating good ($VTD_{sub} \leq 3.1$), average ($3.1 < VTD_{sub} \leq 4.4$), and poor ($VTD_{sub} > 4.4$) tracks. 176

Figure E-1. Maximum ϕ values for 5 km/h increments of train speed and 0.01 mm/m increments of ΔVTD_{sub} on tangent track for: (a) soft-to-stiff transitions; and (b) stiff-to-soft transitions. 177

Figure E-2. Maximum ϕ values for 5 km/h increments of train speed and 0.01 mm/m increments of ΔVTD_{sub} on curve sections for: (a) soft-to-stiff transitions; and (b) stiff-to-soft transitions. . 177

Figure E-3. Maximum ϕ values for 5 km/h increments of train speed and 0.01 mm/m increments of ΔVTD_{sub} on track assets for: (a) soft-to-stiff transitions; and (b) stiff-to-soft transitions..... 178

Figure E-4. Comparing the AREMA (2021) line regarding the track classes with ϕ value changes regarding the ΔVTD_{sub} with 0.01 mm/m increments for $\phi \geq 1.1$ for: (a) tangent track; (b) curve sections; and (c) track assets. 178

Figure E-5. Comparing the AREMA (2021) line regarding the track classes and conditions (i.e., good-average and poor tracks) with ϕ value changes regarding the ΔVTD_{sub} with 0.01 mm/m increments for $\phi \geq 1.1$ for: (a) tangent track; (b) curve sections; and (c) track assets..... 179

Figure E-6. The Grubbs test values of ϕ for 5 km/h increments of train speed and 0.01 mm/m increments of ΔVTD_{sub} on tangent track for: (a) soft-to-stiff transitions; and (b) stiff-to-soft transitions..... 179

Figure E-7. The Grubbs test values of ϕ for 5 km/h increments of train speed and 0.01 mm/m increments of ΔVTD_{sub} on curve sections for: (a) soft-to-stiff transitions; and (b) stiff-to-soft transitions..... 180

Figure E-8. The Grubbs test values of ϕ for 5 km/h increments of train speed and 0.01 mm/m increments of ΔVTD_{sub} on track assets for: (a) soft-to-stiff transitions; and (b) stiff-to-soft transitions..... 180

Figure E-9. IWS and MRail measurements for tangent track based on the Grubbs test values of dynamic load factor (ϕ) for 0.01 mm/m increments of ΔVTD_{sub} regarding the estimated ϕ values by AREMA (2021) (Equation 6-9) and reliability (confidence level) conditions for four specific train speeds: (a) 15 km/h (~10 mph, as Class 1, ϕ_{C1}); (b) 40 km/h (25 mph, as Class 2, ϕ_{C2}); (c)

65 km/h (~40 mph, as Class 3, ϕ_{C3}); and (d) 75 km/h (~47 mph, as the maximum speed with appropriate number of data points, ϕ_{75}). Note: the solid, dash-dot, and dotted lines respectively correspond to zones of high, moderate, and low reliability. 181

Figure E-10. IWS and MRail measurements for non-tangent track (inclusive of curve sections and track assets) based on the Grubbs test values of dynamic load factor (ϕ) for 0.01 mm/m increments of ΔVTD_{sub} regarding the estimated ϕ values by AREMA (2021) (Equation 6-9) and reliability (confidence level) conditions for four specific train speeds: (a) 15 km/h (~10 mph, as Class 1, ϕ_{C1}); (b) 40 km/h (25 mph, as Class 2, ϕ_{C2}); (c) 65 km/h (~40 mph, as Class 3, ϕ_{C3}); and (d) 75 km/h (~47 mph, as the maximum speed with appropriate number of data points, ϕ_{75}). Note: the solid, dash-dot, and dotted lines correspond to zones of high, moderate, and low reliability, respectively. 182

Figure E-11. IWS and MRail measurements in tangent track based on the Grubbs test values of dynamic load factor (ϕ) for 0.01 mm/m increments of ΔVTD_{sub} regarding the estimated ϕ values by Behnia et al. (2022) (Equation 6-7) and AREMA (2021) (Equation 6-9) and reliability (confidence level) conditions and track conditions (i.e., good-average and poor subgrade conditions of track) for four specific train speeds: (a) 15 km/h (~10 mph, as Class 1, ϕ_{C1}); (b) 40 km/h (25 mph, as Class 2, ϕ_{C2}); (c) 65 km/h (~40 mph, as Class 3, ϕ_{C3}); and (d) 75 km/h (~47 mph, as the maximum speed with appropriate number of data points, ϕ_{75}). Note: the solid, dash-dot, and dotted lines respectively correspond to zones of high, moderate, and low reliability. . 183

Figure E-12. IWS and MRail measurements in curve sections based on the Grubbs test values of dynamic load factor (ϕ) for 0.01 mm/m increments of ΔVTD_{sub} regarding the estimated ϕ values by Behnia et al. (2022) (Equation 6-8) and AREMA (2021) (Equation 6-9) and reliability (confidence level) conditions and track conditions (i.e., good-average and poor subgrade

conditions of track) for four specific train speeds: (a) 15 km/h (~10 mph, as Class 1, ϕ_{C1}); (b) 40 km/h (25 mph, as Class 2, ϕ_{C2}); (c) 65 km/h (~40 mph, as Class 3, ϕ_{C3}); and (d) 75 km/h (~47 mph, as the maximum speed with appropriate number of data points, ϕ_{75}). Note: the solid, dash-dot, and dotted lines respectively correspond to zones of high, moderate, and low reliability. . 184

Figure E-13. IWS and MRail measurements in track assets based on the Grubbs test values of dynamic load factor (ϕ) for 0.01 mm/m increments of ΔVTD_{sub} regarding the estimated ϕ values by AREMA (2021) (Equation 6-9) and reliability (confidence level) conditions and track conditions (i.e., good-average and poor subgrade conditions of track) for four specific train speeds: (a) 15 km/h (~10 mph, as Class 1, ϕ_{C1}); (b) 40 km/h (25 mph, as Class 2, ϕ_{C2}); (c) 65 km/h (~40 mph, as Class 3, ϕ_{C3}); and (d) 75 km/h (~47 mph, as the maximum speed with appropriate number of data points, ϕ_{75}). Note: the solid, dash-dot, and dotted lines respectively correspond to zones of high, moderate, and low reliability. 185

List of Tables

Table 2-1. Summary of the dynamic load factor (ϕ) equations presented in literature divided by intended use for passenger and freight railways.	19
Table 2-2. Definitions of variables used in Table 2-1 (<i>after</i> Van Dyke et al. 2017)	20
Table 2-3. comparison of load measurement systems (<i>after</i> Van Dyk, 2015).	23
Table 2-4. A brief overview of key track geometry measurement descriptions (AREMA, 2012; FRA, 2007; TC, 2011; Hyslip, 2002).	25
Table 2-5. The main interpretation types for track geometry (FRA, 2007; TC, 2011).	26
Table 2-6. Regulated Threshold Values for Defining Geometry Defects for Freight Service Tracks (Data from TC 2011).	27
Table 2-7. Operator threshold values for defining priority deometry defects for freight service tracks (Roghani and Hendry, 2017).	27
Table 3-1. Summary of the dynamic load factor (ϕ) equations presented in literature for freight railways.	50
Table 3-2. Definitions of variables used in Table 3-1.	50
Table 3-3. Statistical measures from probability distributions of dynamic vertical load measurements from the IWSs.	54
Table 3-4. Dynamic load factors (ϕ) derived from the Grubb’s test values from the IWS data up to the maximum allowable freight train speed within each North American class of track.....	58
Table 4-1. Dynamic load factor (ϕ) equations for North American freight railways.	67
Table 4-2. Regulated threshold values for defining geometry defects for freight service tracks (TC, 2011).	70

Table 4-3. Statistical measures from probability distributions of dynamic vertical load and rail profile measurements from the IWS and track geometry car.	73
Table 4-4. Comparative evaluation of measured load trends against the provided estimations by AREMA (2021) and Behnia et al. (2022) regarding the threshold values for rail profile changes in different classes of freight service tracks.	80
Table 5-1. The widely used and recent dynamic load factor (ϕ) equations presented in the literature for freight railways.	Error! Bookmark not defined.
Table 5-2. Comparison of measured ϕ values derived from the Grubbs test and ϕ_{75} line developed by AREMA (2021).	104
Table 6-1. Mathematical equations to calculate the conversion of VTD to VTD_{sub} and ΔVTD_{sub}	129
Table 6-2. Dynamic load factor (ϕ) equations under consideration for assessing the impact of transition direction in freight railways.	135
Table 6-3. Comparing the maximum dynamic load factor derived from the Grubbs test values of IWS data with the ϕ_{75} values developed by Behnia et al. (2022) and AREMA (2021) with regard to the transition direction.	136
Table 6-4. Comparing the effect of subgrade track conditions (inclusive of good-average and poor tracks) on ϕ values for both transition directions.	142
Table D-1. Statistical measures from probability distributions of dynamic vertical load measurements from the IWS system.	192
Table D-2. Statistical measures from probability distributions of VTD_{sub} measurements from the MRail system.	192

Table E-1. Comparison of ϕ_{75} line developed by AREMA (Equation 6-9) and the maximum Grubbs test values from the IWS system based on transition direction and track conditions (derived from Figure E10)..... 201

1. Introduction

Canada has one of the largest railway networks globally, with more than 48,000 route kilometers of track. In recent decades, the reliance on rail for transporting goods in Canada has surged. The Canadian railway predominantly operates as a heavy freight network, responsible for moving over 70% of the nation's goods, highlighting its vital role in the economy and the necessity for its efficient and safe operation (Fallah Nafari, 2017). These aspects underscore the critical role of the railway industry in the Canadian economy and the indispensable need for its efficient and safe operation. The increased demand for railway infrastructures in recent years has subjected track superstructure and substructure components to greater loads than their original designs, dating back to the early 20th century. The associated dynamic loads pose a significant risk of damage to both the railway track and vehicles, potentially leading to component failures, fatigue crack development (Guan et al., 2014; Holder et al., 2017), and uneven settlement (Olofsson and Telliskivi, 2003).

The escalation of dynamic loads can accelerate track degradation and lead to rail breaks. Rail breaks are critical safety concerns, often causing service disruptions and derailments with potentially disastrous outcomes. Rail breaks and failures of track components are the most frequent causes of derailment in Canada (Leishman et al., 2017). Liu et al. (2012) also identified physical rail breaks and track geometry defects as the primary causes of train derailments in the United States' Class 1 freight railroads. Data from the Federal Railroad Administration (FRA) and the Railroad Accident and Incident Reporting System (RAIRS) indicate that a significant number of train incidents in North America stem from track-related issues and deviations in track geometry (Lasisi, 2019; TSB, 2016).

The steel rail is a key component of the railway track, responsible for bearing and transmitting loads to the substructure (Sadeghi and Barati, 2010b). Rail failures are often linked to track degradation, which is influenced by changes in track geometry and stiffness. These changes can induce and amplify dynamic wheel/rail interaction forces, increasing the probability of fatigue fractures and rail breaks. The FRA recognizes rail failures as a significant factor in train accidents. Therefore, a thorough understanding of dynamic loads along the track is crucial for the railway industry, especially given the recent trends of increasing axle loads and speeds on freight lines. This research aims to achieve three primary objectives: firstly, to reassess our current understanding of dynamic load variations along the track in relation to different track structures; secondly, to determine the influence of track surface roughness- a key factor in rail fatigue life- on dynamic load magnitudes; and thirdly, to evaluate the importance and effects of subgrade stiffness conditions and their variations on dynamic loads. Addressing these objectives presents a significant opportunity to improve railway design and maintenance practices.

1.1. Problem description

North America's rail network, established over a century ago, was primarily designed to minimize earthwork and the number of bridges and tunnels, with little consideration for terrain or soil characteristics (Li et al., 2015). Railway track owners face growing commercial pressures to optimize track performance without experiencing rail and track component failures. To enhance performance, track owners increase operational speeds and capacities. However, the precise track capacity remains to be discovered due to a lack of understanding regarding the dynamic loads' spectrum on the track. Insight into how track characteristics, especially in freight lines, influence the magnitude of dynamic loads is also limited.

Recent increases in dynamic load have been linked to reduced rail fatigue life, leading to more frequent maintenance cycles (Leong et al., 2007; Leong and Murray, 2008). In Canada, rail breaks and failures of track components are the leading causes of train derailments (Leishman et al., 2017). These derailments tend to happen at faster train speeds than other causes, making them higher in energy and resulting in a greater number of cars derailing. This also makes the cars contents more likely to be released. Given the ongoing rail failures, revisiting our understanding of the magnitude of dynamic loads exerted on the rail is valuable. This is crucial for ensuring the safety of train operations and preventing accidents caused by rail malfunctions and fractures.

The dynamic train-track interaction is influenced by two major factors: changes in track geometry and variations in track subgrade stiffness (Sussman et al., 2001; Lundqvist and Dahlberg, 2005; Dahlberg, 2010). Track geometry refers to the three-dimensional spatial orientation of railway tracks (Selig and Waters, 1994; Hyslip, 2002; Li et al., 2015), while track subgrade stiffness refers to the rigidity of the track's underlying foundation. These factors contribute to the increasing and fluctuating nature of the dynamic interaction between trains and tracks. The track structures, such as bridges, grade crossings, and switches, also affect the dynamic loads along the track. However, the extent of track structures' influence on the magnitude of dynamic loads is not yet fully comprehended.

The use of an Instrumented Wheelset (IWS) and MRail systems provides numerous advantages in railway engineering. The IWS system can capture the wheel-rail dynamic forces under varying operating conditions, facilitating a deeper understanding of the railway track behavior (Higgins et al., 1992; Bracciali et al., 2014; Ren and Chen, 2019). Under different operating conditions, the MRail system also offers extensive possibilities for acquiring information on subgrade track conditions, fostering an enhanced comprehension of substructure behavior. The MRail system,

developed in Sweden (Berggren et al., 2005) and at the University of Nebraska (McVey et al., 2005; Lu, 2008; Greisen, 2010), offers significant opportunities for gathering data on subgrade track conditions (Roghani and Hendry, 2016; Roghani and Hendry, 2017). The MRail system contributes to an improved understanding of the behavior of the railway substructure in various operational scenarios. Continuous readings from across the network from track geometry cars have the potential to provide a quantitative evaluation of surface track roughness (variability).

During this research, a comprehensive evaluation of the IWS and MRail measurements was conducted over more than 340 km of Canadian freight railway track. The surface track geometry variability was available as a regular measurement. This extensive database was used to develop and evaluate the influence of track structures, surface roughness, and subgrade conditions on the dynamic load magnitudes. Quantifying the effect of subgrade conditions on dynamic load magnitudes has presented the opportunity to investigate the impact of travel direction (i.e., transition direction: soft-to-stiff and stiff-to-soft).

1.2. Research objectives

The primary objective of this research is to enhance understanding of how track characteristics and substructure- including track structures (assets), track surface roughness, and stiffness variations- affect dynamic load magnitudes.

The specific research objectives of this PhD program are as follows:

- I. To evaluate the in-service wheel-rail contact forces from the instrumented wheelset (IWS) measurements to determine the relation with observable track characteristics (e.g., switches and grade crossings).
- II. To quantify the effect of track surface roughness (i.e., rail pro) on the magnitude of dynamic loads.

- III. To examine the impact of track subgrade stiffness on wheel-rail contact forces, and quantify how subgrade stiffness conditions affect the magnitude of dynamic loads.
- IV. To evaluate the impact of transition directions (i.e., soft-to-stiff and stiff-to-soft) on dynamic load magnitudes.

1.3. Description of study site

Data for Objectives I-IV were exclusively sourced from a 340 km section of a Class 1 North American freight railway track in the Canadian Prairies. This track section includes over 30 bridges, one tunnel, 100 grade crossings, and 50 switches. Of this, 230 km is tangent track, and 83 km consists of curves. The track supports over 50 million gross tonnes of annual freight and predominantly features concrete ties and continuously welded rail (CWR).

1.4. Scope and methodology

The aim of this research is to analyze load data to assess the magnitude of dynamic loads, represented by ϕ values. The study focuses on three key aspects: observable track structures (e.g., switches and grade crossings), track surface roughness, and variations in subgrade stiffness. The impact of speed on these parameters is also evaluated.

The research utilizes two types of data: commercial data from IWS and MRail measurements, and regular data from track geometry measurements. The IWS system, used for measuring dynamic forces at the wheel-rail interface of moving railway vehicles, and the MRail system, used for capturing vertical track deflection (*VTD*) measurements, provide valuable insights for railway engineers. The *VTD* measurements are used to derive indices that reflect the magnitude and variability of subgrade stiffness. Track geometry data, routinely collected by rail companies to assess track structure performance, is also used. Additionally, various sources such as aerial

photographs, GPS, and Google Earth are used to establish the spatial coordinates of track characteristics.

The dynamic load factor (ϕ) is a ratio of the vertical loads exerted on the rail by a moving railway vehicle (dynamic loads, P_d) to the static loads (P_s) resulting from the combined weight of the railcar and its contents (Van Dyke et al., 2017). The ϕ value is crucial in the design of track structures and the selection of rail steel and cross-section (weight) (Peters, 2010; Sadeghi, 2012; AREMA, 2021). Therefore, this research primarily focuses on the ϕ value along the track.

1.4.1. Quantifying the effect of observable track characteristics

This section describes the methodology used to achieve the first objective of the research: evaluating the magnitude of dynamic loads along the track from the instrumented wheelset (IWS) measurements to quantify the effect of the observable track characteristics on dynamic load magnitudes.

The study emphasizes the dynamic load factor (ϕ) due to its critical role in railway design, particularly in the selection of rail steel and cross-sectional (weight) properties. IWS measurements are a valuable resource for re-evaluating the equations used by engineers in track design. The dynamic load factor (ϕ) correlates the magnitude of vertical wheel-to-rail loads (dynamic loads) with the static loads from the weight of the railcar and its contents, considering the effect of travel speed. Equations for ϕ have been put forth by the American Railway Engineering and Maintenance-of-Way Association (AREMA) and others. However, a significant limitation of the current ϕ equations is that they are based on loads measured at instrumented track sections under constant track conditions, without accounting for the variability of wheel loads.

Dynamic load measurements were obtained using two IWSs over four passes along a 340 km section of track operated by a North American Class 1 freight railway in the Canadian Prairies.

The goal was to compare the measured dynamic load magnitudes with the established ϕ equations for freight railways and to develop new ϕ equations that are applicable to both tangent and non-tangent tracks, including bridges, grade crossings, curves, and switches.

1.4.2. Investigating the impact of track surface roughness

This section delineates the methodology used to achieve the second objective of this research: understanding and quantifying the influence of track surface roughness on the dynamic loads along the track. Track geometry defects, a significant factor in mainline freight derailments in the United States and Canada, can lead to rail wear, rolling contact fatigue (RCF), and rail welding, which in turn can cause rail breaks (Liu et al., 2012; TSB, 2013). These defects, such as rail surface changes, can influence the initiation and propagation of RCF defects. The challenge lies in interpreting the effectiveness of changes in surface track geometry into dynamic load magnitudes. Therefore, this section concentrates on evaluating the impact of rail profile (surface) changes, representing surface roughness, on dynamic load magnitudes.

The rail profile (surface) is a key parameter in evaluating track geometry, and changes in this parameter are crucial for the railway industry, especially concerning dynamic interactions between wheels and rails. It is imperative for engineers to carefully monitor and manage rail profile changes to improve track performance and ensure the safety and reliability of railway operations. The methodology to achieve this includes: (1) data alignment; (2) determination of analysis parameters, such as window length and overlap ratio; (3) preliminary data analysis, such as outlier detection and track characteristics behaviour; (4) quantification of the impact of rail profile changes on dynamic load magnitudes; and (5) evaluation of the impact of the train speed. This objective was conducted under a specific feature, as it considered the impact of both speed and surface geometry changes simultaneously.

1.4.3. Evaluating the impact of track subgrade stiffness

This section outlines the methodology used to achieve the third objective of this research: evaluating the impact of track subgrade stiffness on dynamic load magnitudes. This involves using and combining vertical track deflection (VTD) and wheel-rail force measurements from the MRail and IWS systems.

The MRail system offers several advantages, making it an effective tool for this objective: (1) it allows for continuous measurement of the entire track, enabling large-scale comparisons; (2) it can be integrated into revenue service trains, operating at normal track speed without requiring track downtime, thus providing cost benefits for the railway industry; and (3) measurements are conducted under heavy axle loads, implying the impact of subgrade conditions within the measurements. Variations in track stiffness, both high and low, significantly affect dynamic loads and rail behavior, leading to rail breaks and defects (Li and Berggren, 2010). Soft sections with significant vertical deflection can accelerate rail defects and disturb ballast, while stiff sections can increase rolling contact fatigue and wear of ties and ballast. Therefore, continuous monitoring of maximum vertical deflection along the track using the MRail system provides valuable insights into evaluating rail integrity and determining acceptable ranges of track subgrade stiffness. This objective aims to evaluate the impact of stiffness changes on vertical load magnitudes using data from MRail and IWS. A key part of this objective is to provide new insights into the correlation between stiffness variations and the magnitude of vertical loads in relation to train speed. The methodology includes (1) deriving subgrade stiffness from *VTD* measurements from MRail, (2) evaluating data based on track characteristics, (3) conducting preliminary data analysis to identify threshold values, (4) aligning the location of IWS and MRail measurements due to different frequencies, (5) analyzing data, such as outlier detection and ideal sample size, (6) evaluating the

impact of subgrade stiffness conditions (i.e., good, average, and poor tracks) on dynamic load magnitudes, and (7) evaluating the impact of train speed.

1.4.4. Evaluating the impact of transition directions

This section details the methodology used to address the fourth objective of the research, which is to quantify the effect of variations in track subgrade stiffness on wheel-rail dynamic interactions, with a particular focus on the impact of transition directions (from soft to stiff track and vice versa) on dynamic load magnitudes. Transition zones, such as those before and after bridges and grade crossings, are known for accelerated degradation, which can lead to increased maintenance costs, operational delays, and a higher risk of derailments. Therefore, understanding how changes in subgrade stiffness affect dynamic load magnitudes is essential, especially at these critical transition points.

The work involves integrating the results of mapping subgrade stiffness with wheel-rail dynamic force measurements to enhance our understanding of transitions between soft and stiff track conditions. The goal is to quantify how dynamic load magnitudes are amplified or attenuated due to transition directions. The methodology includes: (1) calculating subgrade stiffness from MRail measurements, (2) determining changes in subgrade stiffness using the secant slope value, (3) conducting preliminary data analysis to identify threshold values, (4) aligning the location of IWS and MRail measurements due to different frequencies, (5) analyzing data, such as outlier detection and ideal sample size, (6) evaluating the impact of transition directions on dynamic load magnitudes, (7) considering the effect of subgrade stiffness conditions (good, average, and poor) on the effectiveness of transition directions, and (8) evaluating the influence of train speed on these dynamics.

1.5. Research limitations

While this research has provided valuable insights into the relationship between track structures, surface profile roughness, and stiffness variations on dynamic load magnitudes, some limitations should be acknowledged. The measurement conditions were limited to dynamic loads from a single car and suspension type, wheel diameter, and static load. This study was conducted without explicitly correlating the dynamic load factor (ϕ) with specific waveforms generated at the wheel-rail interface, such as P₁, P₂, and R-waves, which could provide additional insights into potential impact damage and vibration propagation. Additionally, this investigation did not consider the impact forces generated by rail corrugations. Regarding the track subgrade stiffness conditions, the study did not fully account for the effects of initial tamping and particle breakage during early loading cycles. Moreover, the evolution of track stiffness over time due to factors such as particle size reduction and changes in shear strength was not captured. These limitations present opportunities for future research to develop a more comprehensive understanding of track behaviour under dynamic loading conditions.

1.6. Thesis outline

This thesis has been prepared in a paper-based format. The thesis comprises seven chapters, including this first introductory chapter and six appendices.

Chapter Two provides the necessary literature review for this study.

In *Chapter Three* (manuscript #1), focuses on quantifying the impact of observable track characteristics on dynamic load magnitudes and compares these findings with previously established equations.

Chapter Four (manuscript #2) evaluates how track surface roughness impacts dynamic load magnitudes. The results are compared with the dynamic load factor estimated by AREMA and the estimation from the first objective to quantify the effect of surface roughness.

In *Chapter Five* (manuscript #3) evaluates the impact of subgrade stiffness beneath rail tracks on the magnitude of dynamic loads. The results are compared with the dynamic load factor estimated by AREMA and the estimation from the first objective to quantify the effect of subgrade stiffness.

Chapter Six (manuscript #4) evaluates how transition directions, in relation to changes in subgrade stiffness, affect the magnitude of dynamic loads under varying subgrade conditions. The findings are compared with the dynamic load factor estimated by AREMA and the estimation from the first objective to quantify the impact of transition directions on dynamic load magnitudes.

Chapter Seven presents the conclusions and recommendations derived from this study.

Appendices A to E provide supplementary materials and detailed analysis information related to the procedures used in the various objectives.

1.7. References

American Railway Engineering and Maintenance of Way Association. (2021). *Manual for Railway Engineering*. Lanham, MD: AREMA.

Berggren, E., Jahlenius, A., Bengtsson, B., & Berg, M. (2005). Simulation development, and field testing of track stiffness measurement vehicle. In *Proceedings of the 8th International Heavy Haul Conference*, Rio de Janeiro, Brazil, June 14-16 (pp. 763-771).

Bracciali, A., Cavaliere, F., & Macherelli, M. (2014, April). Review of instrumented wheelset technology and applications. In *Proceedings of the 2nd International Conference on Railway Technology: Research, Development and Maintenance* (pp. 1-16).

- Fallah Nafari, S. (2017). Quantifying the Distribution of Rail Bending Stresses along the Track using Train-Mounted Deflection Measurements.
- Greisen, C.J. (2010). *Measurement, simulation, and analysis of the mechanical response of railroad track*. (M.Sc. Thesis). University of Nebraska–Lincoln, Department of Mechanical Engineering.
- Guan, Q., Zeng, J., & Jin, X. (2014). An angle of attack-based derailment criterion for wheel flange climbing. *Proceedings of the Institution of Mechanical Engineers, Part F: Journal of Rail and Rapid Transit*, 228(7), 719-729.
- Higgins, R. L., Otter, D. E., & Martin, R. W. (1992, January). High accuracy load measuring wheelset. In *Tenth International Wheelset Congress: Sharing the Latest Wheelset Technology in Order to Reduce Costs and Improve Railway Productivity; Preprints of Papers* (pp. 181-188). Barton, ACT: Institution of Engineers, Australia.
- Holder, D. E., Csenge, M. V., Qian, Y., Dersch, M. S., Edwards, J. R., & Van Dyk, B. J. (2017). Laboratory investigation of the Sk1-style fastening system's lateral load performance under heavy haul freight railroad loads. *Engineering Structures*, 139, 71-80.
- Hyslip, J. P. (2002). Fractal analysis of track geometry data. *Transportation research record*, 1785(1), 50-57.
- Lasisi, A. (2019). *Dimension reduction techniques in track geometry quality analysis and safety*. University of Delaware.
- Leishman, E. M., Hendry, M. T., & Martin, C. D. (2017). Canadian main track derailment trends, 2001 to 2014. *Canadian Journal of Civil Engineering*, 44(11), 927-934.
- Leong, J., & Murray, M. H. (2008, February). Probabilistic analysis of train–track vertical impact forces. In *Proceedings of the Institution of Civil Engineers-Transport*, 161(1), 15-21.

- Leong, J., Murray, M., & Steffens, D. (2007). Examination of railway track dynamic models capabilities against measured field data. In *Proceedings International Heavy Haul Conference Specialist Technical Session* (pp. 257-267). International Heavy Haul Association.
- Li, D., Hyslip, J., Sussmann, T., Chrismer, S. (2015). *Railway Geotechnics*. CRC Press, Taylor & Francis Group.
- Li, M. X. D., & Berggren, E. G. (2010). A study of the effect of global track stiffness and its variations on track performance: simulation and measurement. *Proceedings of the Institution of Mechanical Engineers, Part F: Journal of Rail and Rapid Transit*, 224(5), 375-382.
- Lundqvist, A., & Dahlberg, T. (2005). Load impact on railway track due to unsupported sleepers. *Proceedings of the Institution of Mechanical Engineers, Part F: Journal of Rail and Rapid Transit*, 219(2), 67-77.
- Liu, X., Saat, M. R., & Barkan, C. P. L. (2012). Analysis of causes of major train derailment and their effect on accident rates. *Transportation Research Record*, 2289, 154–163.
- Lu, S. (2008). *Real-time vertical track deflection measurement system*. (Ph.D. Thesis). University of Nebraska at Lincoln, Department of Mechanical Engineering.
- McVey, B., Farritor, S., Norman, C., Wood, N., Arnold, R., Fetei, M., & El-Sibaie, M. (2005). Track modulus measurement from a moving railcar. In *Proceedings of the Annual Conference, American Railway Engineering and Maintenance of Way Association*, Chicago, IL, Sept. 25-28.
- Olofsson, U., & Telliskivi, T. (2003). Wear, plastic deformation and friction of two rail steels—a full-scale test and a laboratory study. *Wear*, 254(1-2), 80-93.
- Peters, N. (2010). *CN Railway Engineering Course*. Montreal: McGill University.

- Ren, Y., & Chen, J. (2019). A new method for wheel–rail contact force continuous measurement using instrumented wheelset. *Vehicle System Dynamics*, 57(2), 269-285.
- Roghani, A., & Hendry, M. T. (2016). Continuous vertical track deflection measurements to map subgrade condition along a railway line: Methodology and case studies. *Journal of Transportation Engineering*, 142(12), 04016059.
- Roghani, A., & Hendry, M. T. (2017). Quantifying the impact of subgrade stiffness on track quality and the development of geometry defects. *Journal of Transportation Engineering, Part A: Systems*, 143(7), 04017029.
- Sadeghi, J. (2012). New advances in analysis and design of the railway track system. *Journal of Reliability and Safety of Railway*, 30(3), 75–100.
- Sadeghi, J., & Barati, P. (2010). Evaluation of conventional methods in analysis and design of railway track system. *International Journal of Civil Engineering*, 8(1), 44–56.
- Selig, E. T., & Waters, J. M. (1994). *Track Geotechnology and Substructure Management*. Thomas Telford ISBN: 0-07277-2013-9.
- Sussmann, T. R., O’Hara, K. R., Kutrubes, D., Heyns, F. J., & Selig, E. T. (March 2001). Development of ground penetrating radar for railway infrastructure condition detection. *Proceedings of the Symposium on the Application of Geophysics to Engineering and Environmental Problems, Denver, CO*.
- Transportation Safety Board of Canada. (2016). *Statistical Summary - Railway Occurrences 2015 - Data Tables*. Retrieved from <http://www.bst-tsb.gc.ca/eng/stats/rail/2015/sser-ssro-2015-tbls.asp> [cited 11/12 2023].
- Transportation Safety Board of Canada. (2013). *Statistical Summary Railway Occurrences*. Cat. No. TU1-2/2013, Gatineau, Canada.

Van Dyk, B. J., Edwards, J. R., Dersch, M. S., Ruppert, J. C. J., & Barkan, C. P. (2017). Evaluation of dynamic and impact wheel load factors and their application in design processes. *Proceedings of the Institution of Mechanical Engineers, Part F: Journal of Rail and Rapid Transit*, 231(1), 33–43.

2. Literature Review

2.1. Track structure

The major purpose of a rail track is to furnish a durable, smooth surface for train movement and to distribute wheel loads with minimal pressure on the subgrade, recognized as the weakest element (Kerr, 2003). A standard railway track construction comprises a superstructure and substructure (Selig and Waters, 1994). The cross-section of a typical ballasted railway track foundation is presented in Figure 2-1. The superstructure encompasses rails, the fastening system (which holds on the rail in place on the ties), and ties, while the substructure includes ballast, subballast, and subgrade. The subsequent sections delineate the primary functions of a railway track's superstructure and substructure components.

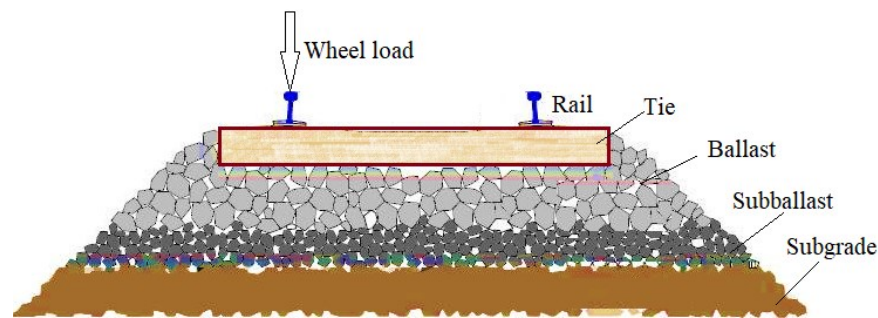


Figure 2-1. A typical cross-section of a ballasted track foundation shows the superstructure and substructure (*after* Loizos et al., 2017).

2.1.1. Track superstructure

The railway superstructure encompasses the fundamental elements constituting the framework of a railway track, guaranteeing its stability, safety, and functionality. Comprising diverse components that collaborate harmoniously, it sustains the load of trains, furnishes a resilient and even running surface, and facilitates the safe passing of rolling stock. The superstructure constitutes the visible portion above the subgrade and is discernible to the naked eye. Its constituent elements encompass rails, sleepers, and fastening systems (Esveld, 2001).

Rails constitute long steel beams serving as the running surface for train wheels. They are meticulously designed to endure the forces imposed by rolling stock while ensuring a smooth and consistent ride. Sleepers, typically constructed from materials such as wood or concrete, are strategically positioned at consistent intervals along the track to provide support and secure the rails in place. Fastening components, such as clips or spikes, affix the rails to the sleepers, thereby preserving their alignment and stability (Bianculli, 2001).

The railway superstructure incorporates additional elements to optimize safety and operational efficiency. These encompass switches and grade crossings, facilitating track changes, junctions enabling train divergence or merging, and level crossings where railways intersect with roads, necessitating specialized safety measures. The superstructure also encompasses bridges, tunnels, walls, and various engineering structures (Wei, 2018).

2.1.2. Track substructure

The substructure comprises layers, including ballast, subballast, and subgrade, which support the track superstructure components. The ballast constitutes granular crushed rock material beneath and around the ties, positioned between the track structure and the underlying foundation. The preferred composition for the ballast layer involves angular crushed rock aggregate, such as limestone, granite, or basalt, with diameters falling within the range of 10 to 75 mm (Li et al., 2015). The ballast fulfills various roles, such as drainage, load spreading, and maintaining track geometry (Selig and Waters, 1994)). The subballast layer is a transitional material between the ballast and subgrade. It is ideally a well-graded material to enhance load distribution, facilitate efficient drainage, and prevent the migration of subgrade material into the ballast.

Ballast and subballast collectively constitute the granular layer beneath the tie and above the subgrade. The thickness of the granular layer should be sufficient to mitigate stress on the subgrade

to a tolerable level, preventing subgrade failure due to excessive deformation (plastic strain) or progressive soil shearing (Selig and Waters, 1994). Additionally, the thickness of the granular layer influences the track modulus and, consequently, the vertical deflection of the track. The thickness of the ballast depends on various factors, including ballast quality and the maximum axle load of the line. A minimum thickness of 0.3 m (12 in) is typically considered satisfactory based on industry experience (Raymond, 1978).

The subgrade is the foundational support for a railway track, and its quality significantly influences the performance of all track components. The subgrade, constituting the base of a railway track, directly impacts the effectiveness of all track components due to its quality. Inadequate bearing capacity within the subgrade poses challenges in maintaining track geometry, requiring more frequent maintenance. Insufficient bearing capacity in the subgrade makes it challenging to maintain track geometry, necessitating frequent maintenance. Soft subgrades have been associated with heightened wear and degradation of track and ballast, stemming from significant movements linked to their soft nature (Selig and Waters, 1994; TSB, 1999; Hendry et al., 2008, 2011). Soft subgrade materials are also prone to continual settlement and plastic deformation, posing risks of sudden failure and safety issues in rail operations (Konrad et al., 2007; TSB, 2008). Despite its pivotal role, the substructure, especially the subgrade, has historically been considered less than the superstructure (Selig and Waters, 1994). The stiffness of the subgrade beneath a railway track is commonly evaluated through its resilient modulus (Li et al., 2015).

2.2. Characterization and loading environment in North America

The components in the track superstructure in North America have been designed based on practical experience, lacking a comprehensive comprehension of the specific loading environment responsible for distinct failure mechanisms. The design methodology enhancements for track

superstructure components could lead to a more resilient track structure, provided the loading environment can be thoroughly characterized (Caughron et al., 2012; Van Dyk, 2015). The operational conditions in North America stand out from those in many other parts of the world, primarily due to the prevalence of heavy axle-load rail freight transport and the sharing of infrastructure between heavy axle-load freight and intercity passenger rail traffic. One of the challenges arising from this operational scenario is the design of essential infrastructure components under a diverse range of loading conditions. To effectively characterize the loads impacting the track structure, it is essential to investigate potential sources of variation. A fundamental aspect of the design process is establishing relations between loading conditions and factors that amplify the magnitude of dynamic loads. This analysis can provide a better insight into the conditions that increase the frequency of rail breaks and failures.

2.2.1. Dynamic load factor (ϕ)

Rail steel structure performance is mainly dependent on the magnitude of dynamic loads. In designing ballasted track structures, particular emphasis is always given to steel rails to ensure the rail can withstand and transfer all applied loads to the substructure (Doyle, 1980; Sadeghi and Barati, 2010a). Since the applied loads can intensify for different reasons, such as variation in track stiffness, rail surface roughness, and rail corrugation (Sadeghi, 2012; Kerr, 2003), the magnitude of dynamic loads along the track must be reassessed.

The main approaches to railway track design and analysis are allowable stress design (ASD) and limit state design (LSD) (Sadeghi, 2012). The magnitude of dynamic loads is essential in both approaches. Numerous parameters influence the car body's actual load on the track structure. In the design phase, specific parameters are incorporated, utilizing a dynamic factor or impact factor to improve the accuracy of load estimation. It is commonly recognized that the forces exerted at

the wheel-rail interface by moving loads are greater than those generated by the same wheel loads at rest (Kerr, 2003).

Consequently, the design wheel load is typically set higher than the static wheel load to accommodate this augmentation due to speed. In the design approaches, the magnitude of the static wheel load is amplified using a dynamic load factor (ϕ) to consider the effect of dynamic loads in the design of track components (Van Dyk et al., 2013; Van Dyk, 2015). The dynamic wheel load factor is commonly derived empirically through the analysis of field data and is formulated concerning train speed. The number of elements involved in its formulation may vary based on the sophistication of track instrumentation and underlying assumptions (Doyle, 1980).

The dynamic load factor (ϕ) is the ratio of the vertical wheel-to-rail loads from a moving railway vehicle (dynamic loads, P_d) to static loads (P_s) resulting from the weight of the rail car and its contents (Van Dyke et al., 2017), often developed as a function of train speed. These equations for ϕ and the evaluated dynamic loads are often used to design track structures or select rail steel and cross-sections (weight) (Peters, 2010; Sadeghi, 2012; AREMA, 2021). Examples of equations to estimate the upper envelope of ϕ and dynamic loads are presented in Table 2-1, and the variables for these equations are defined in Table 2-2. These equations range from relatively simple linear functions of train speed to more complex functions that include parameters such as wheel diameters, track modulus, and empirical factors.

$$P_d = \phi P_s \qquad \text{Equation 2-1}$$

A limitation of the existing ϕ equations is that they have been derived from measured dynamic loads from trains as they pass over an instrumented section of track (Dybala and Radkowski, 2013; Van Dyk et al., 2017; Yu and Hendry, 2019). For example, the relationship between ϕ and train speed developed for North American freight operations by Van Dyk et al. (2017) was derived from

wheel impact load detector (WILD) data. While dynamic loads measured from instrumented track capture the range of loads from differing rolling stock types (locomotives and variety of cars), axle loads, and wheel conditions, it is limited to a single configuration of the track, which is often well-supported and well-maintained tangent track which is unlikely to be representative of either the average or worst-case conditions for the generation of dynamic loads (Van Dyk et al., 2017).

Table 2-1. Summary of the dynamic load factor (ϕ) equations presented in literature divided by intended use for passenger and freight railways.

Type	Expression for ϕ	Equation	Reference
Passenger lines	$1 + \frac{4.5S^2}{10^5} - \frac{1.5S^3}{10^7}$	(2-2)	German Railways $\{V \leq 200\}$ (Schramm, 1961)
	$(1 + 3.86 \times 10^{-5}S^2)^{\frac{2}{3}}$	(2-3)	WMATA (Prause et al., 1974)
	$1.098 + 8 \times 10^{-4}S + 10^{-6}S^2$	(2-4)	Iran Railways (Sadeghi, 2012)
	$1 + 0.021 \frac{S}{D}$	(2-5)	Talbot (Hay, 1982)
	$1 + 4.92 \frac{S}{D}$	(2-6)	South African Railways (Doyle, 1980)
	$1 + \frac{S}{58.14\sqrt{U}}$	(2-7)	Indian Railways (Srinivasan, 1969)
	$1 + \frac{19.65S}{D\sqrt{U}}$	(2-8)	Clark formula (Doyle, 1980)
	$1 + \delta\eta t$	(2-9)	Eisenmann formula (Esveld, 2001)
	$\frac{8.784(\alpha_1 + \alpha_2)S}{P_S} \sqrt{\frac{D_j P_u}{g}}$	(2-10)	British Railways (Doyle, 1980)
	Freight lines	$1 + \alpha + \beta + \gamma$	(2-11)
$1 + 5.21 \frac{S}{D}$		(2-12)	(AREMA, 2021)
$1.099 + 0.00621S$		(2-13)	(Van Dyk et al., 2017)
$1 + 0.00466S$		(2-14)	Used by track operator (Peters, 2010)

2.2.2. Measurement systems

The rail industry has access to various technologies, systems, and instrumentation strategies for quantifying the performance of vehicles and tracks. Specifically, technologies such as instrumented wheelsets (IWS), truck performance detectors (TPD), and wheel impact load detectors (WILD) are employed to monitor forces at the wheel-rail interface (Wiley and Elsaleiby, 2011; CN Railway, 2011). A comparison of load measurement technologies is outlined in Table

2-3. These systems are crucial in monitoring rolling stock performance, evaluating wheel and vehicle functionality, and enhancing predictive and reactive maintenance strategies. Railway infrastructure engineers can also utilize these systems to gain insights into the magnitude and distribution of loads impacting the track structure. A comprehensive understanding of this loading environment forms the basis for analyzing and designing critical infrastructure components.

Table 2-2. Definitions of variables used in Table 2-1 (*after* Van Dyke et al. 2017)

Variable	Definition
S	Train speed (km/h)
D	Wheel diameter (mm)
U	Track modulus
δ	Track maintenance condition
η	Speed factor
t	Upper confidence limits regarding the probability of exceedance
P_s	Static load (kN)
$\alpha_1 + \alpha_2$	Total rail joint dip angle (radians)
D_j	Track stiffness at joints (kN/mm)
P_u	Unsprung load on one wheel (kN)
g	Acceleration due to gravity (m/s^2)
α, β, γ	Empirical coefficients derived from train speed, vehicle, and other track parameters

2.2.3. Instrumented wheelset (IWS) system

The National Research Council Canada (NRCC) has been a leading designer and developer of IWS for rail cars in North America for over 20 years. The NRC's IWS system is based on proven technology implemented globally in over 800 instrumented wheelsets on passenger and freight rolling stock (Woelfle, 2016). The NRC's verified IWS technology provides direct, accurate measurements of the dynamic vertical, lateral, and longitudinal forces at the wheel/rail interface. The IWS data collection was conducted as part of a more extensive investigation of on-track performance, which included an instrumented 15.8 m (52 ft) gondola car (Roghani et al., 2015; Roghani and Hendry, 2016; 2017; Fallah Nafari et al., 2018a; 2018b). The car was loaded with gravel to a total weight of 1175 kN (264 kips). One end of the instrumented car was fitted with two IWS, each consisting of one axle with two-wheel plates (as shown in Figure 2-2). Each IWS

wheel plate is 915 mm (36") diameter Class F and instrumented with 16 full-bridge Wheatstone strain gauge circuits, which are interpreted to forces applied to the wheels from the rail and resolve these forces into vertical, lateral and traction forces for each of the four wheels (Woelfle, 2016).

Table 2-3. comparison of load measurement systems (*after Van Dyk, 2015*).

Specifications	Measurement system		
	Instrumented wheelset (IWS)	Truck performance detector (TPD)	Wheel impact load detector (WILD)
Implementation location	Vehicle mounted	Wayside	Wayside
Continuous data regarding	Vehicle	Track	Track
Speed measurement	✓	✓	✓
Nominal vertical load measurements	✓	✓	✓
Measures in tangent track	✓	✓	✓
Measures in curves	✓	✓	×

The IWS was measured at a 200 Hz frequency and filtered with a 20 Hz low-pass filter applied to the data during acquisition (Higgins et al., 1992; Bracciali et al., 2014; Barbosa, 2016; Ren and Chen, 2019). A Garmin GPS18X global positioning system (GPS) determined each measurement's latitude, longitude, time, and speed. Each wheel of the IWS was calibrated individually in the laboratory before installation. The IWS load measurements accuracy was not provided with instruments; however, the end of the car with IWS had a 576.2 kN static load measured by a scale after the system installation, and this compares very favorably with the sum of the static loads from the four IWS wheels at 574.6 kN, a difference of 0.3 %. The wheels had very little wear and were free of defects that would increase dynamic loads. In this investigation, the available IWS data is recorded between July and August 2015 and includes around 60 million data points from four different runs, two runs in each direction with a maximum operating speed of 95 km/h. The main reason for choosing this method to measure the load data is to record the wheel/rail contact forces along the track when passing over various structures.



Figure 2-2. Photograph of the instrumented wheelsets (IWS) system installed on the Gondola railcar to collect the data used for this study. Wheatstone bridge strain gauges and connectors are covered in yellow epoxy coating, which is visible in the photograph (Images by Michael T. Hendry).

2.3. Track geometry

Ensuring the optimal operational state of railway tracks is a paramount responsibility for railway owners (Hsu et al., 2017). Consequently, railway companies must undertake periodic track inspections, incurring cost and time. Active maintenance of track quality is imperative, relying on consistent track geometry inspections (Berggren et al., 2008).

The spatial arrangement of railway tracks in three dimensions, namely 'track geometry,' is a fundamental indicator of track performance and ride quality (Selig and Waters, 1994; Hyslip, 2002; Li et al., 2015; UIC, 2008). Significant deviations in track geometry can lead to irregularities, impacting operational safety, train speed, and the magnitude of dynamic loads (Odashima et al., 2017). Hence, conducting track geometry surveys at regular intervals throughout the year enables the identification and improvement of track geometry issues before they reach a point of posing a potential risk for vehicle derailments.

2.3.1. Fundamental measurements

Major Canadian railway operators, including Canadian National (CN) and Canadian Pacific (CP), continuously employ specially designed rail vehicles to monitor track geometry across their networks. Track geometry measurements detail the spatial location of each rail. They are utilized

in the railway industry to confirm that the rail’s shape enables trains to safely traverse the track at their designated maximum speed (AREMA, 2012). Track geometry measurements are typically taken at 0.30 m (1ft.) intervals along the railway. Numerous variables are utilized to assess track geometry in a single survey, categorized based on whether the orientation of one or both rails is considered in the calculation. Variables associated with track geometry, such as track gauge, crosslevel, and twist, encompass the evaluation of deviations between the two rails, producing a singular value at each point in track geometry measurements.

Conversely, track geometry variables such as alignment and surface measure the absolute orientation of each rail relative to a distinct datum. These measurements are defined individually for each rail at every measurement position. A detailed description of these typical track geometry measures is presented in Table 2-4 (AREMA, 2012; FRA, 2007; TC, 2011; Hyslip, 2002).

Table 2-4. A brief overview of common track geometry measurement descriptions (AREMA, 2012; FRA, 2007; TC, 2011; Hyslip, 2002).

Track geometry parameter	Description
Gauge	The horizontal distance between the two rails measured 16 mm below the top of the rail (standard gauge= 1435.1 mm)
Crosslevel	The difference in elevation between both rails on a tangent track
Warp (Twist)	The difference in crosslevel values between two points located 18.9 m (62 ft) or 9.5 m (31 ft) apart along the track
Surface (profile)	The mid-chord offset (MCO) measured vertically on the surface of the rail
Alignment	The horizontal deviation of the rail relative to a straight-line reference chord after projecting both the rail and the chord onto the horizontal plane

2.3.2. Track roughness interpretation methods

After collecting track geometry data, various methods can be employed to interpret the data and differentiate between well-performing track sections and those requiring intervention or realignment. The three primary types of track geometry interpretations encompass threshold

exceedance analysis, running roughness analysis, and track quality index (TQI) analysis. The main types of track geometry interpretation are presented in Table 2-5.

Table 2-5. The main interpretation types for track geometry (FRA, 2007; TC, 2011).

Interpretation type	Definition
Threshold exceedance	Evaluation of track geometry based on predefined threshold values
Running roughness	Smoothed squares of individual track geometry variables
Track quality indices (TQI)	Combinations of individual or statistical threshold exceedances or standard deviations calculated from multiple track geometry variables within a given track section, either individually or collectively.

Analyzing track geometry data based on threshold exceedances is a straightforward procedure. Maximum thresholds are established, and when surpassed, they indicate the necessity for corrective maintenance (Rail Safety and Standard Board Limited, 2011; TC, 2012; FRA, 2014). In simpler terms, a track geometry defect is identified when the measured values exceed the predefined threshold values specified in regulations (FRA, 2007; TC, 2011). These threshold values are determined based on the assigned track class to ensure that each class aligns train speeds with the specific track conditions. Table 2-6 shows the regulated (i.e., predefined) threshold values regarding track classes (TC, 2011). According to both Transport Canada and the FRA, Class 1, with the lowest maximum track speed of 16 km/h (10 mph), has the highest geometry thresholds, while Class 5, with the highest maximum track speed of 129 km/h (80 mph), has the lowest geometry thresholds. Thus, a track section is maintained to meet the requirements of its assigned class and the corresponding maximum allowable speed.

Defects surpassing the limits set by regulators are classified as urgent due to their safety implications, necessitating immediate action. Beyond safety limits, there exists a second category with more stringent threshold values defined by the operator (typically 66 to 75% of the safety limits (Li et al., 2015)), designating them as priority defects and establishing them as the maintenance limit for the track (see also Table 2-7). These defects require monitoring until repaired to prevent escalation beyond safety limits, transitioning into urgent defects. Notably, track sections

with higher operating speeds often have more stringent thresholds. In Canada, major railway operators (CN and CP) adhere to tighter track geometry thresholds than those mandated by Transport Canada. This practice aims to avoid mandatory track closure in case of threshold exceedance, ensuring timely correction should Transport Canada's minimum thresholds ever be breached.

Table 2-6. Regulated Threshold Values for Defining Geometry Defects for Freight Service Tracks (Data from TC 2011).

Track classification	Max. allowable speed [km/h (mph)]	Gauge		Profile (surface) [mm (in.)]	Crosslevel (tangents & curves) [mm (in.)]	Warp [over 18.9 m (62 ft)] [mm (in.)]	Alignment (tangent) [mm (in.)]
		not less than [mm (in.)]	not more than [mm (in.)]				
Class 1	16 (10)	1416.1 (55.75)	1473.2 (58)	76.2 (3)	76.2 (3)	76.2 (3)	127.0 (5.0)
Class 2	40 (25)	1416.1 (55.75)	1466.9 (57.75)	69.9 (2.75)	50.8 (2)	57.2 (2.25)	76.2 (3)
Class 3	64 (40)	1422.4 (56)	1466.9 (57.75)	57.2 (2.25)	44.5 (1.75)	50.8 (2)	44.5 (1.75)
Class 4	97 (60)	1422.4 (56)	1460.5 (57.5)	50.8 (2)	31.8 (1.25)	44.5 (1.75)	38.1 (1.5)
Class 5	129 (80)	1422.4 (56)	1460.5 (57.5)	31.8 (1.25)	25.4 (1)	38.1 (1.5)	19.1 (0.75)

Table 2-7. Operator threshold values for defining priority geometry defects for freight service tracks (Roghani and Hendry, 2017).

Track classification	Max. allowable speed [km/h (mph)]	Gauge		Profile (surface) [mm (in.)]	Crosslevel (tangents & curves) [mm (in.)]	Warp [over 18.9 m (62 ft)] [mm (in.)]	Alignment (tangent) [mm (in.)]
		not less than [mm (in.)]	not more than [mm (in.)]				
Class 1	16 (10)	1416.1 (55.75)	1463.7 (57.62)	50.8 (2)	25.4 (1)	57.2 (2.25)	95.3 (3.75)
Class 2	40 (25)	1416.1 (55.75)	1454.2 (57.25)	38.1 (1.5)	25.4 (1)	44.5 (1.75)	57.2 (2.25)
Class 3	64 (40)	1422.4 (56)	1454.2 (57.25)	32.7 (1.25)	25.4 (1)	38.1 (1.5)	34.9 (1.375)
Class 4	97 (60)	1422.4 (56)	1454.2 (57.25)	25.4 (1)	25.4 (1)	34.9 (1.375)	28.6 (1.125)
Class 5	129 (80)	1422.4 (56)	1454.2 (57.25)	19.1 (0.75)	17.5 (0.6875)	28.6 (1.125)	9.5 (0.375)

2.3.2. Rail surface (profile)

In the North American context, the surface track geometry parameter is assessed through mid-chord offsets (MCO) (Hyslip, 2002; Li et al., 2015). The chord is conceptualized as an imaginary straight-line beam with a fixed length (i.e., the chord length), linking two points on the rail. When utilized to define the surface MCO, the reference datum becomes either the horizontal or vertical projection of the three-dimensional beam. The chord, conceptualized as an imaginary straight-line beam with a fixed length connecting two points on the rail, is the basis for defining surface MCO. The reference datum for this measurement is the vertical projection of the three-dimensional beam. Vertical deviations between these chord projections and the corresponding projection of the track at the mid-chord position are considered surface measurements (see also Figure 2-3). Chord lengths commonly utilized are 24.1 meters (79 feet), 18.9 meters (62 feet), and 9.5 meters (31 feet).

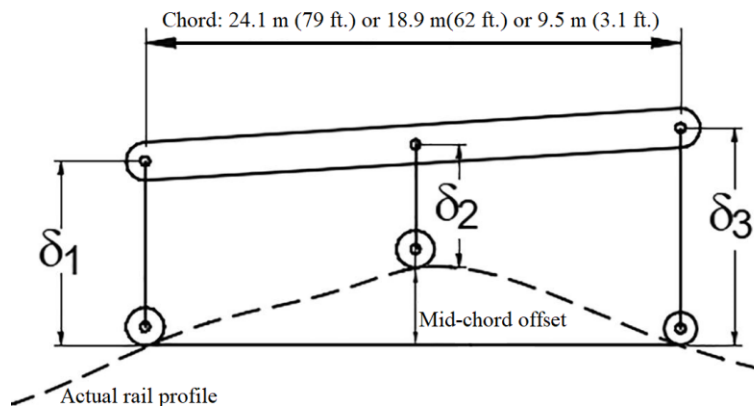


Figure 2-3. Definition of mid-chord offset (MCO) (after Li et al., 2015).

Track surface deviations assessed at identical track positions but employing different chord lengths seldom exhibit equal results. Using distinct fixed chord lengths gives rise to varied reference datums in MCO measurements. Consistent MCO discrepancies arise only when the reference chords intersect at their midpoints. It is noteworthy that MCO measurements may not align with geodetic measurements conducted using a theodolite positioned off the track, as the orientation of

the reference chord changes at each measurement position along the railway based on the rail geometry. Quantifying track surface roughness through MCO measurements introduces a mechanical filtering effect, eliminating long-wavelength features in track geometry (Hyslip, 2002; Li et al., 2015).

The examination of the probability of derailment showed a direct correlation between rail profile (i.e., surface roughness) variations and derailment occurrences, particularly in curved tracks (Mohammadzadeh and Ghahremani, 2012). Srivastava et al. (2014) demonstrated the substantial impact of rail and wheel surface profiles on the design of fatigue-resistant railroads and the planning of inspections. Therefore, the rail profile diagnosis system can determine faults in railway tracks since deviation in this parameter can significantly change wheel-rail interaction (Karaduman, 2012) and affect rail fatigue life (i.e., rail breaks). The characteristics of typical impact loads arising from irregularities in wheel and rail, such as rail corrugation and variations in rail and wheel profiles, can intensify dynamic load magnitudes (Remennikov and Kaewunruen, 2008). This intensification leads to fatigue-related issues, such as rolling contact fatigue (RCF). Railway operators often employ grinding to address this concern as a preventive measure against RCF (Cannon et al., 2003; Kumar, 2006). Illustratively, an example demonstrates that elevating the axle load from 25 to 30 tonnes results in a 27% increase in vertical profile change and a 10% rise in the rolling contact fatigue index (Zerbst et al., 2009).

2.4. Effect of track substructure on track performance

Track substructure problems can appear on the surface through geometric defects and rough track geometry. The track substructure quality plays a crucial role in influencing the performance of the superstructure, as these two components are mutually dependent; a deterioration in one component can impede the performance of the other. Various studies have emphasized the critical role of track

stiffness in railway performance and maintenance requirements and highlighted its effect on optimizing track design for improved performance and reduced maintenance needs (Sajjad et al., 2023; Shi et al., 2023; Tong et al., 2022; Indraratna et al. 2019; Powrie and Le Pen, 2016; Indraratna et al. 2012; Puzavac et al., 2012; Berggren, 2009; Hawari et al., 2008). As an example, Indraratna et al. (2012) discuss the high maintenance costs associated with track stiffness issues in coastal Australia, aggravated by poor drainage and ballast degradation. To provide a concrete example, substantial deformations caused by soft foundations can lead to the wear and deterioration of substructure and track elements (Hendry et al., 2008, 2011; Selig and Waters, 1994; TSB, 1999, 2008). Similarly, the effects arising from flaws on the rail surface can amplify dynamic loads, with more substantial impacts potentially triggering rail breaks (through the rail fatigue life) and failures in track components. Impacts resulting from imperfections on the rail surface may cause the displacement of fine-grained soils from the subgrade, contaminating the ballast; more severe impacts can induce plastic deformation in the weak subgrade soil. Therefore, gaining a comprehensive understanding of the condition of the track substructure is essential for ensuring the safe and reliable operation of the railway system.

2.4.1. Track stiffness

The track stiffness represents the effects of all track components under the rail, including subgrade, ballast, sub-ballast, and tie fasteners (Cai et al., 1994). The serviceability of a track section highly depends on track stiffness and roughness (Scanlan et al., 2016). Vertical track stiffness (vertical track load divided by track deflection) is a fundamental parameter of track design that influences the bearing capacity dynamic behaviour of passing vehicles, specifically track geometry quality and track components life (Cai et al., 1994; Lundqvist and Dahlberg, 2010). Since the track stiffness can significantly impact the magnitude of dynamic load and vertical geometrical defects

(longitudinal level and corrugation/roughness), this parameter can provide further information about the scheduling of corrective and preventive maintenance actions (Cai et al., 1994; Selig and Li, 1994; Lundqvist and Dahlberg, 2010). Selig and Li (1994) showed that the significant contribution of track stiffness is from the subgrade conditions.

High and low track stiffness have their pros and cons. Relatively high track stiffness is beneficial since it can provide sufficient track resistance to applied loads and decrease track deflection (reduce track deterioration). While excessively high stiffness can lead to excessive vibration, fatigue, and fracture, low track modulus may lead to large deformations that increase maintenance activities. Significant variations in track modulus (e.g., transition zones) can increase dynamic loading (Read et al., 1994; Selig and Li, 1994; Zarembski and Palese, 2003). Heelis et al. (1999) suggested that a track with high and consistent modulus will allow for higher train speeds and increase performance and revenue. However, Powrie and Le Pen (2016) demonstrated that while high track stiffness reduces track displacements and rail bending stresses, it also concentrates loads on fewer sleepers, highlighting the need for optimized track stiffness to balance performance and maintenance requirements.

Designing and constructing a railway foundation on peat and organic soils presents a heightened challenge for geotechnical engineers (Hendry, 2011; Ibrahim et al., 2014). Muskeg, characterized by peat, poses a distinct challenge for railway foundations, particularly within the Canadian rail network. The prevailing perspective in geotechnical engineering suggests avoiding muskeg as a foundation material whenever possible. However, due to the extensive muskeg-covered terrain in Canada, avoidance is not always feasible, especially for continuous linear structures like railways (Hendry and Roghani, 2015). Muskeg exhibits significant deformations under loading, with

observations of track displacements exceeding 25 mm (1 in) from cyclic train loading. The assessment of structural stability on this type of soil also proves to be an intricate challenge.

2.4.2. Measurement technologies for vertical track deflection

The railway industry employs various systems for measuring vertical track deflection (VTD). These methods mainly aim to evaluate the railway line's potential for accommodating increases in axle load or traffic levels. These measurement approaches are categorized into two groups: standstill and continuous methods. Standstill methods involve measurements taken at specific locations, requiring the measurement system to stop to take measurements. In contrast, continuous methods allow continuous measurement of VTD while the system moves along the track.

Standstill techniques have historically seen broader usage, whereas rolling measurement methods have been more recently devised and continue to be a subject of ongoing research (Berggren et al., 2008). In standstill methodologies, the stiffness of a track segment is computed by installing transducers or accelerometers on either the ties and rails and monitoring their response to a known load. Various techniques, including the falling weight deflectometer (FWD) and the impact hammer, have been developed based on static loads (Zarembski and Choros, 1979; Kerr, 1983; Ebersohn and Selig, 1994; Read et al., 1994), and they are classified as standstill devices for measuring track stiffness. The FWD is commonly utilized to evaluate the stiffness of the track structure, excluding the rails. This apparatus involves a mass dropped from a predetermined height onto rubber buffers affixed to a footplate (Burrow et al., 2007).

The continual assessment of track support across extensive distances holds significant potential as a valuable addition to the maintenance tools accessible to railway personnel (Sussman et al., 2001; Ebersöhn et al., 1993; Carr, 1999). Continuous methods allow measuring the stiffness while moving along the track, such as TTCI's track loading vehicle (TLV) (Li et al., 2004; FRA, 2004;

Norman et al., 2004), vibrating masses (Wangqing et al., 1997; Berggren et al., 2002), and MRail rolling deflection. The latter approach is being developed and tested for use on North American railroads (Zarembski and Choros, 1979; Kerr, 1983; Ebersohn and Selig, 1994; Read et al., 1994; Sussman et al., 2001; Berggren et al., 2002; Li et al., 2002; Li et al., 2004; Norman et al., 2004; Arnold et al., 2006; Berggren, 2009). The Transportation Technology Center Inc. (TTCI) developed the TLV for continuous track stiffness measurement to enhance track maintenance efficiency and railroad operations' safety (Thompson et al., 2001; Li et al., 2002, 2004). The measurement approach involves one instrumented coach (the TLV) and an additional empty tanker car for measuring the unloaded vertical rail profile. The coach axle is capable of bearing a load ranging from 4 to 245 kN (1 to 55 kip), while the tanker car (acting as the reference axle) applies loads from 0 to 13 kN (0 to 3 kip). Laser-based systems on each vehicle measure track deflections in response to the applied loads.

2.4.3. University of Nebraska rolling deflection system (MRail)

In a collaborative effort with the Federal Railroad Administration, the University of Nebraska at Lincoln (UNL) has devised a continuous track vertical deflection measurement system (Norman, 2004; Norman et al., 2004; McVey et al., 2005; Farritor, 2006; McVey, 2006; Arnold et al., 2006; Greisen, 2010; Farritor and Fateh, 2013). This system is employed in the present research to measure vertical track deflections (*VTD*) and is known as the MRail system. The original configuration of the MRail system comprises two enclosures positioned over the rails on either side of the car, each equipped with two-line lasers and cameras (as shown in Figure 2-4).

The implemented MRail system measured the relative deflection (Y_{rel}) between the rail surface and the rail-wheel contact plane at a distance of 1.22 m (4 ft) from the nearest wheel to the sensor system (Figure 2-4a). This system included two-line lasers and a camera attached to a rigid bracket

(Figure 2-4b). Since the distance between the wheel/rail contact plane and the camera ($h + Y_{rel}$) was always constant due to the rigidity of the bracket, Y_{rel} was calculated by subtracting (h) from ($h + Y_{rel}$) (Norman et al., 2004; Lu, 2008). Figure 2-4c shows a newer system implemented in this study that uses one laser beam to shine a line on the head of the rail at the camera's field of view (Roghani and Hendry, 2017; Roghani et al., 2015). The only difference between the old and the new system is the method used to calculate the distance between the rail surface and the camera (h). The obtained datasets include latitude and longitude coordinates of measurements, the calculated milepost (MP), and Y_{rel} values for both the right and left rail at intervals of 0.305 meters (1 ft.). The field data analyses have represented the ability of the system to map the relative stiffness of the subgrade (Roghani and Hendry, 2016; Roghani et al., 2015; 2017). Previous studies showed the correlation between the statistical properties of Y_{rel} data (i.e., average and standard deviation) and track structural performance (Roghani and Hendry, 2016; Roghani et al., 2015; 2017). Numerous studies have indicated the consistency and repeatability of MRail measurements (Norman, 2004; McVey, 2006; Hendry and Roghani, 2015). Anomalies occur in the positions of defects and joints, increasing up to 25% as train speed rises. This rise is attributed to increased train dynamics (Lu, 2008; Griesen, 2010).

2.4.4. Quantifying track subgrade stiffness

Roghani and Hendry (2016) introduced a methodology for quantifying track subgrade stiffness (VTD_{sub}) through the application of a moving average to filter MRail measurements (VTD) (Equation 2-15). The resulting VTD_{sub} value predominantly represents vertical track deflection attributable to subgrade conditions. In Equation 2-15, the parameter L (in meters) signifies a crucial threshold length that governs the filtering process, aiming to eliminate lower wavelengths caused by surface imperfections such as rail profile changes and joints. An appropriate resolution (L)

selection depends on the specific dimensions of the features under study. Roghani and Hendry (2016) emphasized that opting for $L=20$ m yields the highest precision when assessing subgrade characteristics.

$$VTD_{sub}(i) = \left(0.305/L\right)^{L/(2)(0.305)} \sum_{-L/(2)(0.305)}^{L/(2)(0.305)} VTD[i+j] \quad \text{Equation 2-15}$$

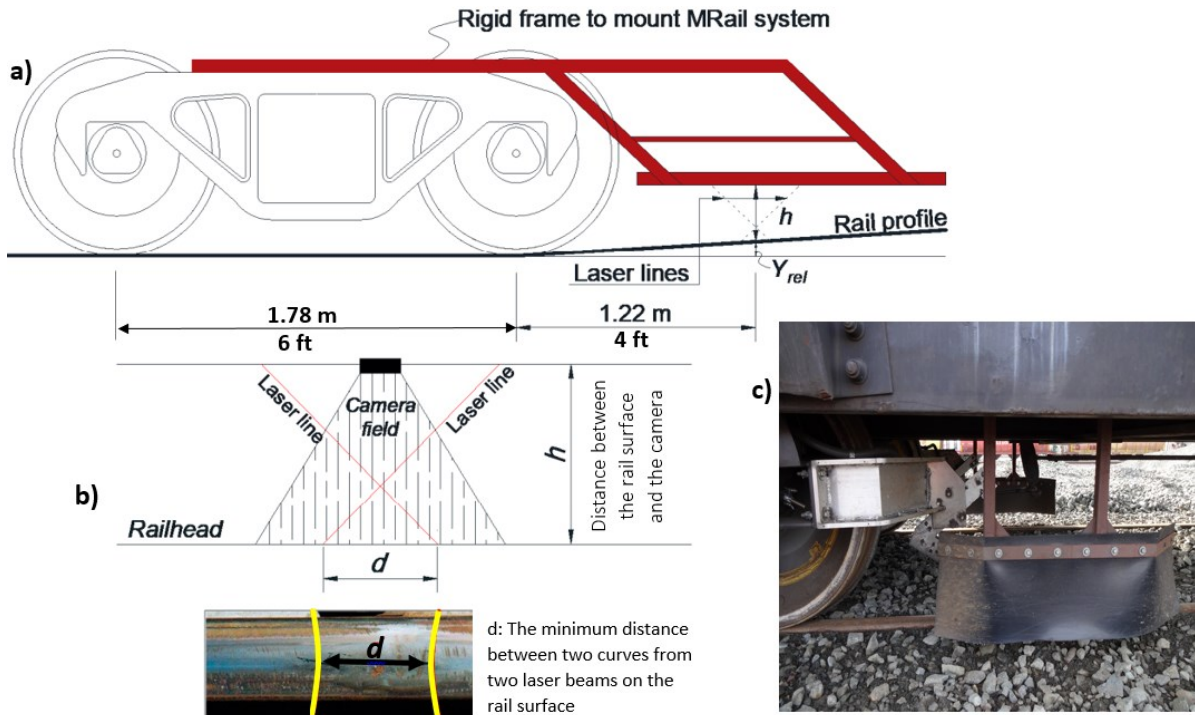


Figure 2-4. Schematic of the MRail system for measuring the relative VTD (Y_{rel}); (a) original system; (b) sensor system; (c) new MRail system (after Do et al., 2020; and Roghani and Hendry, 2015; photo credit Hendry, 2014).

This filtering method provided the maximum resolution of subgrade features while minimizing the influence of track surface conditions. The conversion of MRail measurements (VTD or Y_{rel}) to subgrade track stiffness (VTD_{sub}) was validated using a comprehensive 3D finite element model and multiple field validation methods, including comparisons with known subgrade conditions and other investigative techniques like Ground Penetrating Radar surveys. The validation demonstrated that the conversion method offers a reliable representation of subgrade stiffness, suitable for practical applications in railway engineering and maintenance planning (Fallah Nafari

et al., 2018a, b; Judge et al., 2018; Roghani and Hendry, 2017). Hence, this approach allows for a more accurate assessment of subgrade stiffness over extensive track lengths, enabling further investigation into the impact of track modulus and its variation on track geometry performance. Furthermore, Roghani and Hendry (2017) introduced a method for quantifying changes in VTD_{sub} , designated as ΔVTD_{sub} . ΔVTD_{sub} is calculated by assessing the slope of VTD_{sub} concerning distance, serving as a transparent and straightforward metric. The computation of ΔVTD_{sub} entails determining the absolute value of the secant slope of VTD_{sub} , with distance (d) representing the track length over which this slope is evaluated (Equation 2-2). In line with the applied approach and filtering procedures for VTD measurements, Roghani and Hendry (2017) proposed the adoption of a fixed d value set at 20 meters to maintain methodological consistency in the analysis.

$$\Delta VTD_{sub}(x_i) = \frac{|VTD_{sub}(x_i + d/2) - VTD_{sub}(x_i - d/2)|}{d} \quad \text{Equation 2-16}$$

2.5. References

- AREMA. (2012). *Manual for railway engineering*. American Railway Engineering and Maintenance of Way Association. Lanham, MD, USA.
- AREMA. (2021). *Manual for railway engineering*. American Railway Engineering and Maintenance of Way Association. Lanham, MD: AREMA.
- Arnold, R., Lu, S., Hogan, C., Farritor, S., Fateh, M., & El-Sibaie, M. (2006, September). Measurement of vertical track modulus from a moving railcar. In *Proceedings of the AREMA Annual Conference*, Louisville, KY.
- Barbosa, R. S. (2016). Evaluation of railway track safety with a new method for track quality identification. *Journal of Transportation Engineering*, 142(11), 04016053.

- Berggren, E. (2009). Railway track stiffness: dynamic measurements and evaluation for efficient maintenance. (Ph.D. thesis, KTH).
- Berggren, E. G., Li, M. X., & Spännar, J. (2008). A new approach to the analysis and presentation of vertical track geometry quality and rail roughness. *Journal of Wear*, 265(9-10), 1488-1496.
- Berggren, E., Jahlénus, Å., & Bengtsson, B. E. (2002). Continuous track stiffness measurement: An effective method to investigate the structural condition of a track. *Proc. Int. Conf. of Railway Engineering*, Engineering Technics Press, London.
- Bianculli, A. J. (2001). *Trains and Technology: Track and Structures* (Vol. 1). University of Delaware Press.
- Birmann, F. (1965, June). Paper 5: Track parameters, static and dynamic. In *Proceedings of the Institution of Mechanical Engineers, Conference Proceedings*, 180(6), 73-85. Sage UK: London, England: SAGE Publications.
- Bracciali, A., Cavaliere, F., & Macherelli, M. (2014, April). Review of instrumented wheelset technology and applications. In: *Proceeding of the 2nd International Conference of Railway Technology, Res., Develop. Maintenance* (pp. 1-16).
- Burrow, M., Chan, A., & Shein, A. (2007). Falling weight deflectometer based inverse analysis of ballasted railway tracks. *Geotechnical Engineering, Proceedings of the Institution of Civil Engineers, Issue GE3*, pp 169–177, July.
- Cai, Z., Raymond, G. P., & Bathurst, R. J. (1994). Estimate of Static Track Modulus Using Elastic Foundation Models. *Transportation Research Record 1470*, pp. 65-72.
- Canadian National (CN) Railway. (2011). Wheel Impact Load Detectors: The Early History on CN. In: *Proceedings of the 31st Annual North American Rail Mechanical Operations Seminar*, St. Louis, Missouri, March.

- Cannon, D. F., Edel, K. O., Grassie, S. L., & Sawley, K. (2003). Rail defects: an overview. *Fatigue and Fracture of Engineering Materials and Structures*, 26(10), 865-886.
- Carr, G. A. (1999, September). Dynamic response of railroad track induced by high speed trains and vertical stiffness transitions with proposed method of measurement. *Tufts University*.
- Caughron, B. M., Saat, M. R., & Barkan, C. P. L. (2012). Identifying and Prioritizing Shared Rail Corridor Technical Challenge. In: *Proceedings of the 2012 Annual AREMA Conference*, Chicago, Illinois, September.
- Do, N. T., Gül, M., & Nafari, S. F. (2020). Continuous evaluation of track modulus from a moving railcar using ANN-based techniques. *Vibration*, 3(2), 149-161.
- Doyle, N. F. (1980). Railway track design: a review of current practice (No. UIC Cat 54 0 12).
- Dybała, J., & Radkowski, S. (2013). Reduction of Doppler effect for the needs of wayside condition monitoring system of railway vehicles. *Mechanical Systems and Signal Processing*, 38(1), 125-136.
- Ebersöhn, W., & Selig, E. T. (1994). Track modulus measurements on a heavy haul line. *Transportation Research Record (1470)*, 73–82.
- Ebersöhn, W., Trevizo, M. C., & Selig, E. T. (1993). Effect of low track modulus on track performance. In *Proceedings of Fifth International Heavy Haul Conference* (pp. 379-388).
- Esveld, C. (2001). *Modern Railway Track* (2nd ed.). MRT-Productions, Delft 2001.
- Fallah Nafari, S., Gül, M., Hendry, M. T., & Cheng, J. R. (2018a). Estimation of vertical bending stress in rails using train-mounted vertical track deflection measurement systems. *Proceedings of the Institution of Mechanical Engineers, Part F: Journal of Rail and Rapid Transit*, 232(5), 1528-1538.

- Fallah Nafari, S., Gül, M., Hendry, M. T., Otter, D., & Roger Cheng, J. J. (2018b). Operational vertical bending stresses in rail: Real-life case study. *Journal of Transportation Engineering, Part A: Systems*, 144(3), 05017012.
- Farritor, S. (2006). Real-time measurement of track modulus from a moving car. *U.S. Department of Transportation*.
- Farritor, S., & Fateh, M. (2013). Measurement of vertical track deflection from a moving rail car. *U.S. Department of Transportation*.
- Federal Railroad Administration (FRA). (2004). A preliminary design of a system to measure vertical track modulus from a moving railcar (Rep. No. RR04-03). *U.S. Department of Transportation, Federal Railroad Administration, Washington, D.C., August 20, 2009*.
- Federal Railroad Administration (FRA). (2007). Track Safety Standard Compliance Manual. *U.S. Dept. of Transportation, Washington, DC*.
- Federal Railroad Administration (FRA). (2014). Track and rail and infrastructure integrity compliance manual. *Federal Railroad Administration, Washington DC, USA*.
- Greisen, C. J. (2010). Measurement, Simulation, and Analysis of the Mechanical Response of Railroad Track. *M.Sc. Thesis, Department of Mechanical Engineering, University of Nebraska at Lincoln*.
- Hawari, H. M., & Murray, M. H. (2008, January). Deterioration of railway track on heavy haul lines. In *Conference on Railway Engineering* (pp. 7-10).
- Hay, W. W. (1982). *Railroad engineering*. John Wiley & Sons.
- Heelis, M. E., Collop, A. C., Dawson, A. R., Chapman, D. R., & Krylov, V. V. (1999). Predicting and measuring vertical track displacements on soft subgrades. *Loughborough University. [Conference contribution](#)*.

- Hendry, M. T. (2011). The geomechanical behaviour of peat foundations below rail-track structures. Ph.D. Thesis, *University of Saskatchewan, Saskatoon, Canada*.
- Hendry, M., & Roghani, A. (2015). Rolling Measurement of Vertical Deflection: Assessing a technology for the measurement of the deflection of track structure and its use to map poor subgrade locations. *Technical Report prepared for the Transportation Development Centre of Transport Canada*, 30 pp.
- Hendry, M., Martin, D., Barbour, S., & Edwards, T. (2008). Monitoring cyclic strain below a railway embankment overlying a peaty foundation using novel instrumentation. In *61st Canadian Geotechnical Conference*, Edmonton, Alberta, September 21-24, Paper No. 443.
- Hendry, M. T., Edwards, T., Martin, C. D., & Barbour, S. (2011). Assessing the Condition of Peat Subgrades Subjected to Heavy Axle Loads: Effectiveness of the use of Piles to Strengthen Embankment. *2011 International Heavy Haul Association Conference - Railroading in Extreme Conditions*, Calgary, AB, June 19-22.
- Higgins, R. L., Otter, D. E., & Martin, R. W. (1992, January). High accuracy load measuring wheelset. In *Tenth International Wheelset Congress: Sharing the Latest Wheelset Technology in Order to Reduce Costs and Improve Railway Productivity*. Preprints of Papers (pp. 181-188). Barton, ACT: Institution of Engineers, Australia.
- Hsu, H. H., Chang, C. Y., & Hsu, C. H. (Eds.). (2017). *Big data analytics for sensor-network collected intelligence*. Morgan Kaufmann.
- Hyslip, J. P. (2002). *Fractal Analysis of Geometry Data for Railway Track Condition Assessment*. Ph.D. Thesis, Department of Civil Engineering, University of Massachusetts, Amherst, MA.

- Ibrahim, A., Huat, B. B., Asadi, A., & Nahazanan, H. (2014). Foundation and embankment construction in peat: An overview. *Electronic Journal of Geotechnical Engineering*, 19(2014), 10079-10094.
- Indraratna, B., Nimbalkar, S., & Rujikiatkamjorn, C. (2012). "Future of Australian rail tracks capturing higher speeds with heavier freight." Australian Geomechanics Society Sydney Chapter Symposium, (October 2012).
- Indraratna, B., Sajjad, M. B., Ngo, T., Correia, A. G., & Kelly, R. (2019). Improved performance of ballasted tracks at transition zones: A review of experimental and modelling approaches. *Transportation Geotechnics*, 21, 100260.
- Judge, A., Ho, C., Huang, H., Hyslip, J., & Gao, Y. (2018). *Field Investigation and Modeling of Track Substructure Performance Under Trains Moving at Critical Speed* (No. DOT/FRA/ORD-18/21).
- Karaduman, G., Karaköse, M., & Akin, E. (2012, December). Experimental fuzzy diagnosis algorithm based on image processing for rail profile measurement. In *Proceedings of 15th International Conference Mechatronika* (pp. 1-6). IEEE.
- Kerr, A. D. (1983). A method for determining the track modulus using a locomotive or car on multi-axle trucks. *Proceedings AREA*, 84, 269-286.
- Kerr, A. D. (2003). *Fundamentals of Railway Track Engineering*. Omaha, NE: Simmons-Boardman Books, Inc.
- Konrad, J.-M., Grenier, S., & Garnier, P. (2007). Influence of repeated heavy axle loading on peat bearing capacity. In: *60th Canadian Geotechnical Conference*, Ottawa, ON, pp. 1551-1558.
- Kumar, S. (2006). A study of the rail degradation process to predict rail breaks. Ph.D. thesis, Luleå tekniska universitet.

- Li, D., Hass, K., & Meddah, A. (2002, June). Moving closer to performance-based track geometry inspection. *Railway Track and Structures*, 15-17.
- Li, D., Hyslip, J.P., Sussmann, T.R., & Chrismer, S.M. (2015). *Railway geotechnics*. Taylor and Francis Group LLC, Boca Raton, FL, USA.
- Li, D., Thompson, R., Marquez, P., & Kalay, S. (2004). Development and Implementation of a Continuous Vertical Track-Support Testing Technique. *Transportation Research Record: Journal of the Transportation Research Board*, No. 1863, TRB, National Research Council, Washington, D.C., 2004, pp. 68–73.
- Lu, S. (2008). Real-Time Vertical Track Deflection Measurement System. M.Sc. Thesis, Department of Mechanical Engineering, University of Nebraska at Lincoln.
- Lundqvist, A., & Dahlberg, T. (2005). Railway track stiffness variation-consequences and countermeasures. In: 19th IAVSD Symposium of Dynamics of Vehicles on Roads and Tracks, Milano, August 29-September 2, 2005. Dept Mech Eng, Politecnico di Milano.
- McVey, B. (2006). A Nonlinear Approach to Measurement of Vertical Track Deflection from a Moving Railcar. M.Sc. Thesis, Department of Mechanical Engineering, University of Nebraska, at Lincoln, NE.
- McVey, B., Norman, C., Wood, N., Farritor, S., Arnold, R., Fateh, M., & El-Sibaie, M. (2005, September). Track modulus measurement from a moving railcar. In: *Proceedings of the AREMA Annual Conference*, Chicago, IL.
- Mohammadzadeh, S., & Ghahremani, S. (2012). Estimation of train derailment probability using rail profile alterations. *Structure and Infrastructure Engineering*, 8(11), 1034-1053.
- Norman, C. (2004). Measurement of track modulus from a moving railcar. *M.Sc. Thesis, Department of Mechanical Engineering, University of Nebraska at Lincoln*.

- Norman, C., Farritor, S., Arnold, R., Elias, S.E.G., Fateh, M., Sibaie, M. E. (2004). Design of a System to Measure Track Modulus from a Moving Railcar. *Proceedings from Railway Engineering, London 2004*.
- Odashima, M., Azami, S., Naganuma, Y., Mori, H., & Tsunashima, H. (2017). Track geometry estimation of a conventional railway from car-body acceleration measurement. *Mechanical Engineering Journal*, 4(1), 16-00498. [DOI: <https://dx.doi.org/10.1299/mej.16-00498>]
- Peters N. (2010). CN Railway Engineering Course. Retrieved from McGill University Civil Engineering Graduate Studies class.
- Powrie, W., & Le Pen, L. (Ed.). (2016). *A Guide to Track Stiffness: August 2016*. University of Southampton Department of Civil & Environmental Engineering.
- Prause, R. H., Meacham, H. C., Harrison, H. D., Johns, T. G., & Glaeser, W. A. (1974). Assessment of design tools and criteria for urban rail track structures. *Washington, DC: Urban Mass Transportation Administration. Department of Transportation*.
- Puzavac, L., Popović, Z., & Lazarević, L. (2012). Influence of track stiffness on track behaviour under vertical load. *Promet-Traffic&Transportation*, 24(5), 405-412.
- Rail Safety and Standard Board Limited. (2011). Track system requirements. *United Kingdom, London*.
- Raymond, G.P. (1978). Design for railroad ballast and subgrade support. *Journal of the Geotechnical Engineering Division, ASCE*, 104, 45-59.
- Read, D., Chrismer, S., Ebersöhn, W., & Selig, E.T. (1994). Track modulus measurements at the Pueblo soft subgrade site. *Transportation Research Record*, 1470, 55.
- Remennikov, A. M., & Kaewunruen, S. (2008). A review of loading conditions for railway track structures due to train and track vertical interaction. *Structural Control and Health Monitoring*:

The Official Journal of the International Association for Structural Control and Monitoring and of the European Association for the Control of Structures, 15(2), 207-234.

Ren, Y., & Chen, J. (2019). A new method for wheel–rail contact force continuous measurement using instrumented wheelset. *Vehicle System Dynamics*, 57(2), 269-285.

Roghani, A., Macciotta, R., & Hendry, M. T. (2017). Quantifying the effectiveness of methods used to improve railway track performance over soft subgrades: methodology and case study. *Journal of Transportation Engineering, Part A: Systems*, 143(9), 04017043.

Roghani, A., & Hendry, M. T. (2016). Continuous vertical track deflection measurements to map subgrade condition along a railway line: Methodology and case studies. *Journal of Transportation Engineering*, 142(12), 04016059.

Roghani, A., & Hendry, M. T. (2017). Quantifying the impact of subgrade stiffness on track quality and the development of geometry defects. *Journal of Transportation Engineering, Part A: Systems*, 143(7), 04017029.

Roghani, A., Macciotta, R., & Hendry, M. (2015, March). Combining track quality and performance measures to assess track maintenance requirements. In *ASME/IEEE Joint Rail Conference (Vol. 56451, p. V001T01A009)*. American Society of Mechanical Engineers.

Sadeghi, J. (2012). New advances in analysis and design of railway track system. *Journal of Reliability and Safety Railway*, 30(3), 75-100.

Sadeghi, J., & Barati, P. (2010a). Evaluation of conventional methods in analysis and design of railway track system. *International Journal of Civil Engineering*, 8(1), 44-56.

Sadeghi, J., & Barati, P. (2010b). Improvements of conventional methods in railway track analysis and design. *Canadian Journal of Civil Engineering*, 37(5), 675-683.

- Sajjad, M. B., Indraratna, B., Ngo, T., Kelly, R., & Rujikiatkamjorn, C. (2023). A computational approach to smoothen the abrupt stiffness variation along railway transitions. *Journal of Geotechnical and Geoenvironmental Engineering*, 149(8), 04023063.
- Scanlan, K. M., Hendry, M. T., & Martin, C. D. (2016, April). Evaluating the Equivalency Between Track Quality Indices and the Minimum Track Geometry Threshold Exceedances Along a Canadian Freight Railway. In *ASME/IEEE Joint Rail Conference (Vol. 49675, p. V001T01A012)*. American Society of Mechanical Engineers.
- Schramm, G. (1961). Permanent way technique and permanent way economy. *Darmstadt, Germany: Otto Elsner Verlagsgesellschaft, Elsner*.
- Selig, E. T., & Li, D. (1994). Track modulus: its meaning and factors influencing it. *Transportation Research Record 1470*, 47-54.
- Selig, E. T., & Waters, J. M. (1994). Track Geotechnology and Substructure Management. *Thomas Telford ISBN: 0-07277-2013-9*.
- Shi, C., Zhou, Y., Xu, L., Zhang, X., & Guo, Y. (2023). A critical review on the vertical stiffness irregularity of railway ballasted track. *Construction and Building Materials*, 400, 132715.
- Srinivasan M. (1969). Modern permanent way. *Mumbai, India: Somaiya Publications*.
- Srivastava, J. P., Sarkar, P. K., & Ranjan, V. (2014). Contact stress analysis in wheel–rail by Hertzian method and finite element method. *Journal of The Institution of Engineers (India): Series C*, 95, 319-325.
- Sussmann, T. R., O'Hara, K. R., Kutrubes, D., Heyns, F. J., & Selig, E. T. (March 2001). Development of ground penetrating radar for railway infrastructure condition detection. *Proceedings of the Symposium on the Application of Geophysics to Engineering and Environmental Problems, Denver, CO*.

- TC (Transport Canada). (2011). *Rules respecting track safety*. Ottawa, ON, Canada: TC.
- TC (Transport Canada). (2012). *Rules respecting track safety*. Canada, Ottawa.
- Thompson, R., & Li, D. (2002, February). Automated Vertical Track Strength Testing Using TTCI's Track Loading Vehicle. *Technology Digest*. 1489, 17–25.
- Tong, Y., Liu, G., Yousefian, K., & Jing, G. (2022). Track vertical stiffness–value, measurement methods, effective parameters and challenges: A review. *Transportation Geotechnics*, 37, 100833.
- TSB (Transportation Safety Board of Canada). (1999). *Railway Investigation Report R99Q0019*. The Transportation Safety Board of Canada (TSB).
- TSB (Transportation Safety Board of Canada). (2008). *Railway Investigation Report R04Q0040*. Cat. No. TU3-6/04-2E, ISBN 978-0-662-47573-6.
- UIC (International Union of Railways). (2008). *Best Practice Guide for Optimum*. Proceedings of the Edition Techniques Ferroviaires; UIC: Paris, France.
- Van Dyk, B. J., Dersch, M. S., Edwards, J. R., Ruppert Jr, C., & Barkan, C. P. (2013, April). Quantifying shared corridor wheel loading variation using wheel impact load detectors. In *ASME/IEEE Joint Rail Conference (Vol. 55300, p. V001T01A002)*. American Society of Mechanical Engineers.
- Van Dyk, B. (2015). Characterization of the loading environment for shared-use railway superstructure in North America. *M.Sc. thesis, University of Illinois at Urbana-Champaign*.
- Van Dyk, B. J., Edwards, J. R., Dersch, M. S., Ruppert Jr, C. J., & Barkan, C. P. (2017). Evaluation of dynamic and impact wheel load factors and their application in design processes. *Proceedings of the Institution of Mechanical Engineers, Part F: Journal of Rail and Rapid Transit*, 231(1), 33-43.

- Wangqing, W., Geming, Z., Kaiming, Z., & Lin, L. (1997). Development of inspection car for measuring railway track elasticity. *Proc., 6th Heavy Haul Conf., International Heavy Haul Association, Cape Town, South Africa.*
- Wei, Z. (2018). Modelling and monitoring of dynamic wheel-rail interaction at railway crossing. *Ph.D. thesis, Ph.D. thesis, Delft Technical University, Delft.*
- Wiley, R., & Elsalebby, A. (2011). A Review of Wheel Impact Measurement Variation. *TD-11-007. Transportation Technology Center, Incorporated, Pueblo, Colorado.*
- Woelfle A. (2016). Analysis of Wheel-Rail Forces during (MRail) Rolling Deflection Tests. *Technical Report, National Research Council, Canada.*
- Yu, F., & Hendry, M. T. (2019). A new strain gauge configuration on the rail web to decouple the wheel–rail lateral contact force from wayside measurement. *Proceedings of the Institution of Mechanical Engineers, Part F: Journal of Rail and Rapid Transit, 233(9), 951-960.*
- Zarembski, A. M., & Choros, J. (1979). On the measurement and calculation of vertical track modulus. *Association of American Railroads.*
- Zarembski, A. M., & Palese, J. (2003). Transitions eliminate impact at crossings. *Railway track and structures, 99(8).*
- Zerbst, U., Lundén, R., Edel, K. O., & Smith, R. A. (2009). Introduction to the damage tolerance behaviour of railway rails—a review. *Engineering fracture mechanics, 76(17), 2563-2601.*

3. Railway Dynamic Load Factors Developed from Instrumented Wheelset Measurements

3.1. Contribution of the Ph.D. candidate

All the work presented in this chapter, including the data processing, review of literature, analysis, discussion of the results, and writing of the text, is carried out by the Ph.D. candidate. As a supervisor, Dr. M.T. Hendry has reviewed all parts of the work. This chapter has been published with the following citation:

Behnia, D., Hendry, M. T., Haji Abdulrazagh, P., & Wahba, A. (2022). "Railway Dynamic Load Factors Developed from Instrumented Wheelset Measurements." *Journal of Transportation Engineering, Part A: Systems*, 148(7), 04022042.

3.2. Abstract

Dynamic load factors (ϕ) relate the magnitude of vertical wheel-to-rail loads in operation (dynamic loads) to static loads resulting from the weight of the rail car and its contents, as a function of train speed. The ϕ equations are often used in the selection of rail steel and cross-sections (weight). Equations for ϕ have been put forth by the American Railway Engineering and Maintenance-of-Way Association (AREMA) and others. A limitation of the existing ϕ equations is that they have been derived from loads measured at instrumented sections of track and observe the many wheel loads but with constant track conditions. For this study, measurements of dynamic loads from two instrumented wheelset (IWS) as it conducted four passes over a 340 km section of track operated by a North American Class 1 freight railway through the Canadian Prairies. These measurements provided dynamic loads from one loaded freight car over various track structures at differing train speeds. This paper presents the IWS data sets and the variation of dynamic loads between multiple passes of the section of track studied, and the statistical distribution of dynamic

loads. New ϕ equations are developed for tangent track and nontangent track (inclusive of bridges, grade crossings, curves, and switches).

3.3. Introduction

Rail breaks and failures of rail components are the most frequent causes of derailment in Canada (Leishman et al., 2017); the resulting derailments occur at higher train speeds, on average, than other derailment causes and thus are higher energy, result in a greater number of derailed cars, and have a greater potential to result in the release the contents of rail cars (Leishman et al., 2017). In light of continuing rail failures, it is worth revisiting the understanding of the magnitude of loads that the rail is subjected to.

The dynamic load factor (ϕ) is the ratio of the vertical wheel-to-rail loads from a moving railway vehicle (dynamic loads, P_d) to static loads (P_s) resulting from the weight of the rail car and its contents (Equation 3-1) (Van Dyke et al., 2017), often developed as a function of train speed. These equations for ϕ , and the evaluated dynamics loads, are often used in the design of track structures or the selection of rail steel and cross-sections (weight) (Peters, 2010; Sadeghi, 2012; AREMA 2021). Examples of equations for the upper envelope of ϕ and dynamic loads for freight railways are presented in Table 3-1, and the variables for these equations are defined within Table 3-2. The dynamic load factors for passenger lines are presented in the Appendix A. These equations range from relatively simple linear functions of train speed to more complex functions that include parameters such as wheel diameters, track modulus, and empirical factors

$$P_d = \phi P_s \qquad \text{Equation 3-1}$$

A limitation of the existing ϕ equations is that they have been derived from measured dynamic loads from trains as they pass over an instrumented section of track (Dybala and Radkowski, 2013; Van Dyk et al., 2017; Yu and Hendry, 2019). For example, the development of a relationship

between ϕ and train speed developed for the North American freight operations by Van Dyk et al. (2017) was derived from wheel impact load detector (WILD) data. While dynamic loads measured from instrumented track capture the range of loads from differing rolling stock types (locomotives, and variety of cars), axle loads, and wheel conditions it is limited to a single configuration of track that is often well-supported and well-maintained tangent track, which is unlikely to be representative of either the average or worst-case conditions for the generation of dynamic loads (Van Dyk et al., 2017).

Table 3-1. Summary of the dynamic load factor (ϕ) equations presented in literature for freight railways.

Expression for ϕ	Reference
$1 + \alpha + \beta + \gamma$	ORE; Birmann (1965)
$1 + 5.21 \frac{S}{D}$	AREMA (2021)
$1.099 + 0.00621S$	Van Dyk et al. (2017)
$1 + 0.00466S$	Peters (2010); used by track operator

Table 3-2. Definitions of variables used in Table 3-1.

Variable	Definition
S	Train speed (km/h)
D	Wheel diameter (mm)
α, β, γ	Empirical coefficients derived from train speed, vehicle, and other track parameters

In this paper, data from an instrumented wheelset (IWS) that measures vertical dynamic loads and other forces while moving was used to take measurements along a 340 km section of a North American Class 1 freight railway line. These measurements are limited to dynamic loads from a single car and suspension type, wheel diameter, and static load; they do provide dynamic loads generated from the range of track conditions, track assets (bridges, grade crossings, curves, and switches), and operational train speeds encountered on a Class 1 freight railway main line.

This paper presents the IWS data sets and the variation of dynamic loads between multiple passes of the section of track studied, the statistical distribution of dynamic loads, a comparison of ϕ derived from the IWS measurements to others for North American freight railways (Peters, 2010;

Van Dyk et al., 2017; AREMA, 2021). The ϕ are evaluated versus train speed for differing track conditions and track assets (tangent, curved, bridges, grade crossings, and switches) develop ϕ equations. The data is also tabulated to provide ϕ values representative of the loading conditions generated within the range of speeds permissible on North American classes of track (1 through 4). To the best of the authors' knowledge, this is the first published ϕ derived from the IWS measurements on a Class 1 North American freight railway.

3.4. Materials and methods

The IWS data collection was conducted as part of a larger investigation on track performance that included the instrumentation of a 15.8 m (52 ft.) gondola car (Roghani et al., 2015, 2016, 2017a, b; Fallah Nafari et al., 2018a, b). The car was loaded with gravel to a total weight of 1,175 kN (264 kips). One end of the instrumented car was fitted with two IWS, each of which consist of one axle with two-wheel plates (Figure 3-1). Each IWS wheel plate is 915 mm (36 in.) diameter Class F and instrumented with 16 full-bridge Wheatstone strain gauge circuits, which are interpreted to forces applied to the wheels from the rail and resolve these forces into vertical, lateral, and traction forces for each of the four wheels (only vertical forces, i.e., dynamic loads are presented within this paper) (Woelfle, 2016). The IWS was measured at a 200 Hz frequency and filtered with a 20 Hz low-pass filter was applied to the data during acquisition (Higgins et al., 1992; Bracciali, 2014; Cakdi, 2015; Barbosa, 2016; Ren and Chen, 2019). The latitude, longitude, time, and speed for each measurement was determined with a Garmin GPS18X global positioning system (GPS).

Each wheel of the IWS was calibrated individually in the laboratory before installation. Accuracy of the load measurements from the IWS are not provided with the instruments; however, the end of the car with the IWS had a static load of 576.2 kN measured by a scale after the installation of the IWS system, and this compares very favorably with the sum of the static loads from the four

IWS wheels at 574.6 kN, a difference of 0.3%. The wheels had very little wear and were free of defects that would increase dynamic loads.

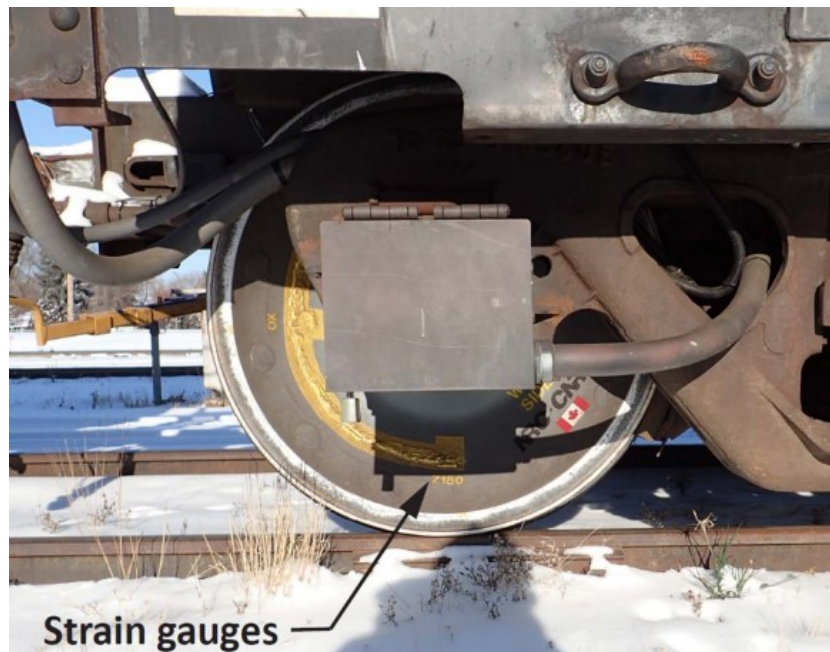


Figure 3-1. Photograph of the instrumented wheelset (IWS) installed on the Gondola railcar to collect the data used for this study. Wheatstone bridge strain gauges and connectors covered in epoxy coating visible in the photograph. (Image by Michael T. Hendry.)

The section of track included in this study is operated by a Class 1 railway and is part of a high traffic subdivision [>50 Gross million tonne (GMT)/year] through the Canadian Prairies. The studied section of track includes 30 bridges and overpasses, 50 switches, more than 100 grade crossings and approximately 83 km of curves. The rail is continuously welded and is supported primarily by concrete ties.

The IWS data used in this study was recorded over four passes of the study site, two in each direction, between July 2015 and August 2015, with maximum train speeds of 95 km/h. The passes were conducted with the car in revenue service (inserted within a freight train), thus without control over the type or weight of adjacent cars, or of the speed of travel. These limitations are common when conducting measurements on the track of a Class 1 North American freight railway. In total,

the data base collected and evaluated within this study consisted of more than 56×10^6 vertical dynamic load measurements.

3.5. Presentation of results

Examples of the resulting data are presented in Figure 3-2 for an 800 m section of track that includes a switch, grade crossing, and a relatively short bridge (Figure 3-2a). This includes four passes of the instrumented car, two at slower speeds (24 and 50 km/h) in the west-bound direction (Figure 3-2b), and two at higher speeds (77 and 88 km/h) in the eastbound direction (Figure 3-2c). The track features (switch, crossing, and bridge) initiate oscillations in dynamic loads that are clearly evident for the higher speed passes (Figure 3-2c). The magnitudes and pattern of dynamic loads are also remarkably similar and repeatable between the two higher speed passes in the same direction (Figure 3-2c).

The distribution of the magnitude of measured vertical dynamic loads by track type (tangent and curve) and features (switch, crossing, and bridge) are presented in Figure 3-3. This distribution was developed from all four IWS wheels and all four passes. There is a large disparity in the amount of data collected on each type of track, where tangent track comprised 69.9% of the measured data, curves comprised 24.7%, bridges comprised 1.6%, grade crossings comprised 2.2%, and switches comprised 1.6%. The statistical values that represent this distribution are presented in Table 3-3. These distributions are normal in nature and have mean and median values that are very close to the static load (144 kN) (Table 3-3). Tangent track has the narrowest distribution and thus the least number of extreme values (Figure 3-3a); this is followed by the curved track and bridges with very similar distributions (Figure 3-3b), and grade crossings and switches, also with very similar distributions. The largest measured dynamic loads are measured on tangent track; however, the authors attribute this disproportionately greater data collection on

tangent track. The highest 99.9th percentile dynamic vertical load occurs for switches, which is attributed the presence of the switch point.

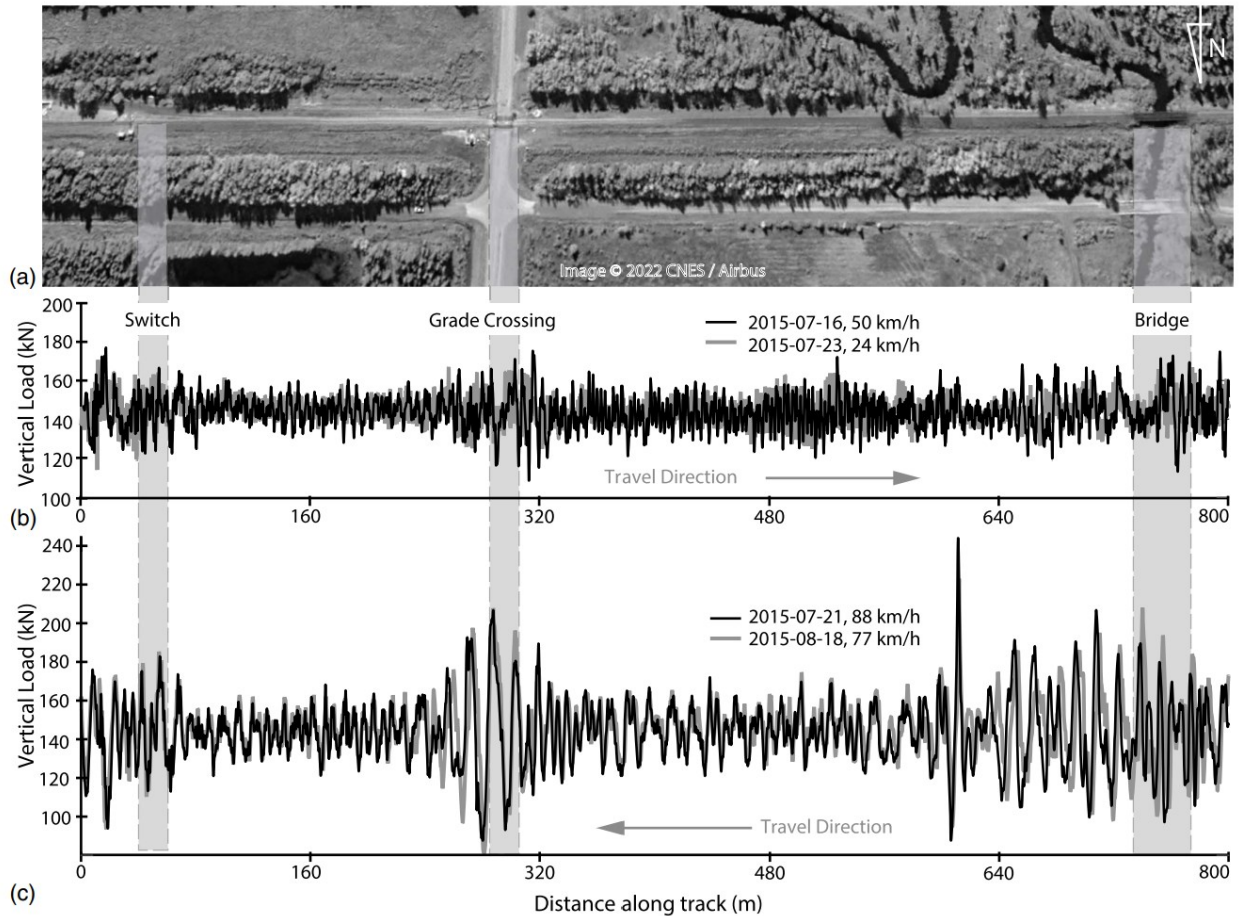


Figure 3-2. Example vertical load data from the IWS system including tangent track, a switch, a grade crossing, and a short bridge (steel span). These data are presented as (a) a satellite image of the section of track (image © Google, Image © 2022 CNES/Airbus); (b) measurements from two slower moving west-bound trains; and (c) measurements from two faster moving east-bound trains.

Table 3-3. Statistical measures from probability distributions of dynamic vertical load measurements from the IWSs.

Track type	μ (kN)	Median (kN)	σ (kN)	Maximum (kN)	99.9 th (kN)
All	143.9	144.1	11.3	384.4	177.9
Tangent track	143.9	144.2	10.9	384.4	176.5
Curved section	143.7	143.6	12.2	292.8	180.2
Bridge	144.6	144.6	12.4	288.9	181.9
Grade crossing	144.2	144.1	13.1	264.2	183.4
Switch	144.1	144.1	14.4	302.5	187.2

Note: Data includes all four instrumented wheels, ad all four passes; μ = mean; σ =standard deviation; and 99th= 99.9th percentile

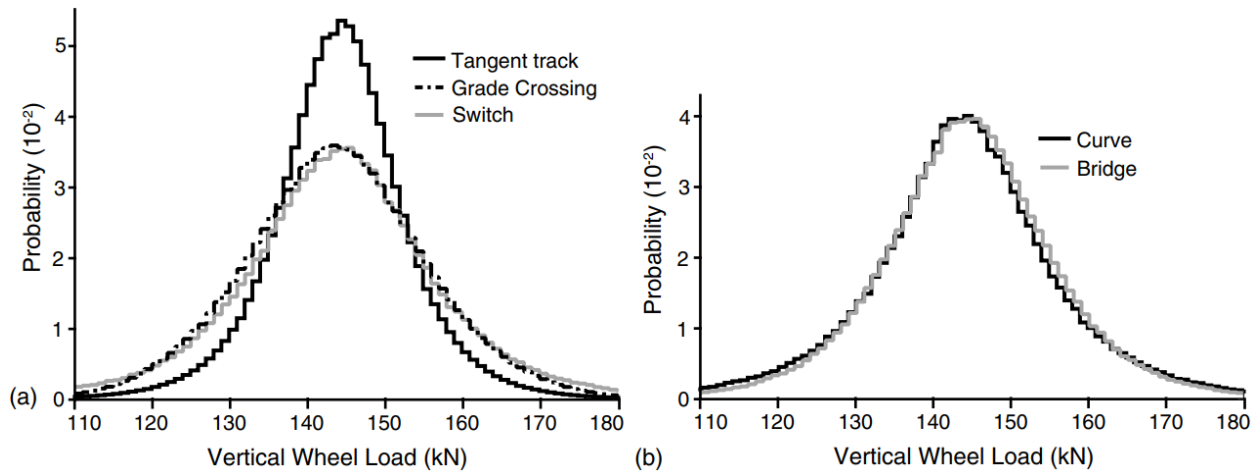


Figure 3-3. Probability distributions of vertical load measurements from the IWS: (a) on tangent track, grade crossings, and switches; and (b) on curves and bridges. Note that data includes all four instrumented wheels, and all four passes.

3.6. Discussion

The ϕ equations are generated using the upper envelope of measured dynamic loads, such that they can be used as design loads. Using the maximum measured dynamic loads from the IWS system results in very high ϕ values (>2.6), significantly higher than predicted by any of the other ϕ equations (a Grubbs' value (G) at which μ is the mean value of the sample, σ is the standard deviation, x_i is the value of the i^{th} element of the data set (Equation 3-2)

$$G = \max_{i=1, \dots, n} |x_i - \mu| / \sigma \quad \text{Equation 3-2}$$

Figure 3-4 presents the ϕ derived from the IWS measurements over tangent track, evaluated for 5 km/h increments for the maximum measured dynamic loads (inclusive of outliers), the 99.9th percentile value, and G from the Grubbs' test. The ϕ values in Figure 3-4 are compared to Equation 3-3 from AREMA (2021) and evaluated with the diameter of the IWS wheel, and Equation 3-4 from Van Dyk et al. (2017)

$$1 + 5.21 \frac{S}{D} \quad \text{Equation 3-3}$$

$$1.099 + 0.00621S \quad \text{Equation 3-4}$$

From Figure 3-4 the ϕ evaluated from the Grubbs' test for the removal of outliers consistently increases with increasing speed, whereas the ϕ evaluated from the 99.9th percentile is more variable. Also from Figure 3-4, the AREMA (2021) equation (Equation 3-3) provides a close representation of the ϕ derived from the Grubbs' test applied to IWS data from tangent track and train speeds in excess of 60 km/h. Equation 3-3 increasingly underestimates ϕ with decreasing train speed below 60 km/h, approaching an underestimation of 0.2 below 5 km/h. The ϕ versus train speed plots similar to Figure 3-4 were also generated for curved track (Figure 3-5), bridges (Figure 3-6), grade crossings (Figure 3-7), and switches (Figure 3-8), with poor representation by Equation 3-3, which significantly underestimates the magnitude of dynamic loads on nontangent track. The data contained within each 5 km/h increment plotted in Figures 3-4, 3-5, 3-6, 3-7, 3-8, and 3-9 is normally distributed with a mean and median value at $\phi = 1.0$ (at static load). The trend in the σ is illustrated Figures 3-4, 3-5, 3-6, 3-7, 3-8, and 3-9 as the 99th percentile magnitudes as this is 3σ . Qualitatively, Figure 3-4 shows a strong consistent relationship between train speed and ϕ , suggesting a high reliability of ϕ threshold value, where each 5 km/h increment consisted of more than 6×10^6 data points. The trends became less consistent, implying a lower reliability of ϕ threshold value, when the number of data point were below 4×10^4 ; for example, Figure 3-6 for speeds <30 km/h.

A quadratic equation fit to the ϕ values for tangent track derived using the Grubbs' test, as a function of train speed, and is presented subsequently as Equation 3-5. Thus, Equation 3-5 defines the range of ϕ that tangent track may experience in service. Equation 3-5 provides a close fit with an R^2 value of 0.97 also evident in Figure 3-4. Equations developed for the other track types provided much poorer fits, the authors propose that the lesser amount of data at some speeds resulted in a greater variability. However, due to the similar statistical distributions of the

measurements collected for grade crossings, switches, curves, and bridges in Figure 3-3, all of these nontangent track data were grouped together and plotted in Figure 3-9, and a quadratic equation fit to ϕ values derived using the Grubbs' test was generated (Equation 3-6). Equation 3-6 provides a close fit with an R^2 value of 0.91 also evident in Figure 3-9. Thus, Equation 3-6 defines the range of ϕ that nontangent track may experience in service

$$\phi_{Tan} = 3 \times 10^{-5}S^2 + 1.4 \times 10^{-3}S + 1.19 \quad \text{Equation 3-5}$$

$$\phi_{NTan} = 3 \times 10^{-5}S^2 + 2.5 \times 10^{-3}S + 1.27 \quad \text{Equation 3-6}$$

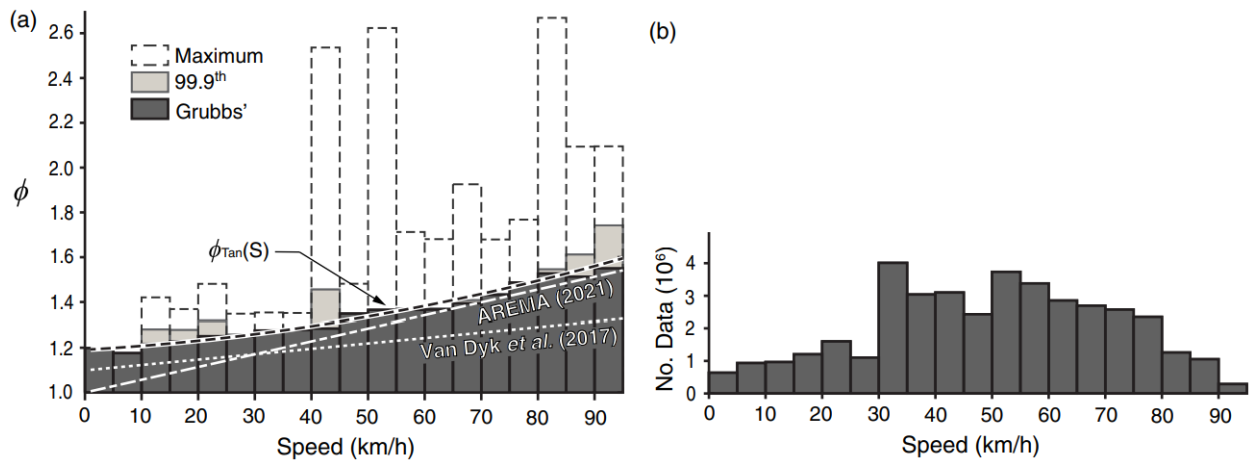


Figure 3-4. IWS measurements from tangent track as (a) dynamic load factor (ϕ) for 5 km/h increments of train speed; and (b) the number of measurements used to develop the ϕ for each increment of train speed.

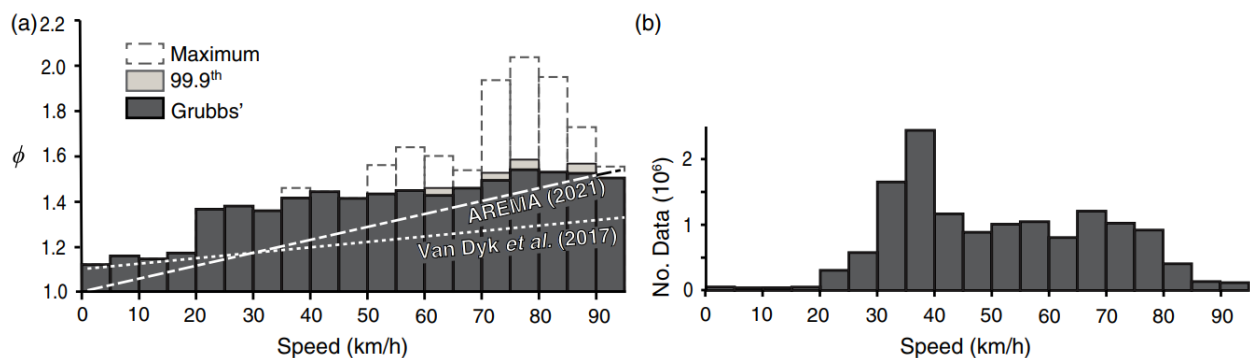


Figure 3-5. IWS measurements from curves as (a) dynamic load factor (ϕ) for 5 km/h increments of train speed; and (b) the number of measurements used to develop the ϕ for each increment of train speed.

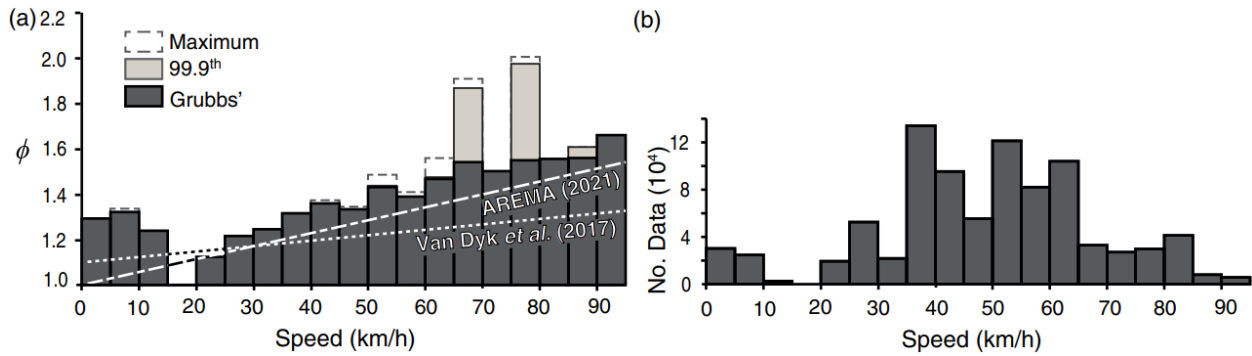


Figure 3-6. IWS measurements from bridges as (a) dynamic load factor (ϕ) for 5 km/h increments of train speed; and (b) the number of measurements used to develop the ϕ for each increment of train speed.

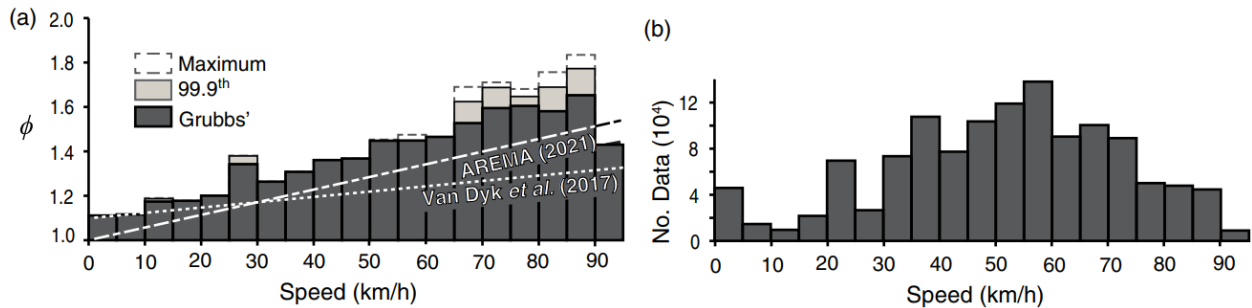


Figure 3-7. IWS measurements from grade crossings as (a) dynamic load factor (ϕ) for 5 km/h increments of train speed; and (b) the number of measurements used to develop the ϕ for each increment of train speed.

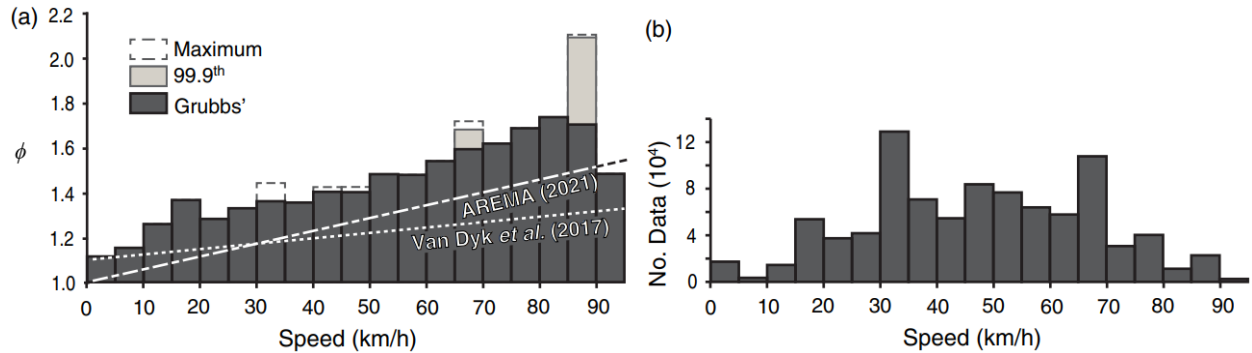


Figure 3-8. IWS measurements from switches as (a) dynamic load factor (ϕ) for 5 km/h increments of train speed; and (b) the number of measurements used to develop the ϕ for each increment of train speed.

Table 3-4. Dynamic load factors (ϕ) derived from the Grubb's test values from the IWS data up to the maximum allowable freight train speed within each North American class of track

Class	Max. Speed km/h (mph)	AREMA (Equation 3-12)	Tangent	Curve	Bridge	Grade Crossing	Switch	All non-Tangent
1	16 (10)	1.09	1.22	1.17	1.32	1.18	1.36	1.36
2	40 (25)	1.23	1.28	1.41	1.32	1.34	1.36	1.41
3	64 (40)	1.36	1.37	1.44	1.43	1.46	1.54	1.54
4	97 (60)	1.55	1.55	1.54	1.66	1.65	1.73	1.73

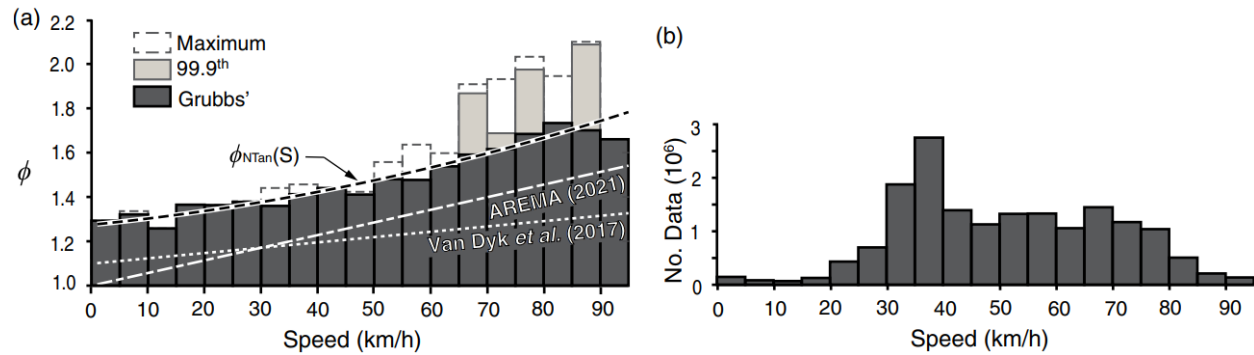


Figure 3-9. IWS measurements from nontangent track (inclusive of curves, bridges, grade crossings, and switches) as (a) dynamic load factor (ϕ) for 5 km/h increments of train speed; and (b) the number of measurements used to develop the ϕ for each increment of train speed.

As an alternative, and arguably more useful, presentation of ϕ the data was re-evaluated over the ranges of permissible train speeds within a given class of track (e.g., Class 2 track allows for train speeds from 0 to 40 km/h) for each track type and presented within Table 3-4. The values in Table 3-4 then define the range of ϕ that class of track may experience in service.

The IWS data and the presentation of the data within Figures 3-4, 3-5, 3-6, 3-7, 3-8, and 3-9 provide a measure of ϕ as a function of speed. As the IWS wheelsets are of very low wear and free of defects, the dynamic loads measured from the IWS are a result of speed, the variation of track conditions and the dynamic characteristics of the car. Thus, as evident in the magnitudes of maximum ϕ and Equations 3-5 and 3-6 that define the range of ϕ that track may be subjected to, that the effect of track conditions is clearly substantial and exceed previous estimates [as provided by AREMA (2021)].

These measurements differ significantly from the data obtained from the measurements of instrumented track [such as those presented in Van Dyk et al. (2017) from WILD sites] in that those results were representative of the loads caused by different locomotives and car types, and differing conditions of wheels on a consistent track section; whereas the results presented within this paper are primarily a result of different track conditions encountered by the IWS system. The authors propose that the two studies are complementary; that neither the data obtained from the

measurements of instrumented track or within this study wholly represent the dynamic loads imparted on the rails; the combined effect is anticipated to further increase the range of ϕ ; and future studies should combine these two measurement types.

3.7. Conclusion

This study analysed dynamic loads, in terms of ϕ , derived from data collected from IWS. This differs from past studies that have relied on instrumented sections of track. The instrumented sections of track capturing the magnitudes of dynamic loads from all car types and conditions that pass over the site, but under constant track conditions. The IWS provided measurements of dynamics loads under constant car type and conditions, but on the variety of track conditions found over 340 km of in-service track. The results of this study demonstrated that the impact of track conditions is significant, resulting in ranges of dynamic loads and ϕ that track may experience well in excess of that provided by common means of estimating, especially for nontangent track (inclusive of curves, switches, crossings and bridges). Equations of ϕ as a function of speed (Equations 3-5 and 3-6) were developed to quantify this range. However, the authors propose that further work is yet required to develop ranges of dynamic loads and ϕ that incorporate both track conditions and variations in car type and condition.

3.8. Acknowledgement

The authors would like to thank the Canadian National Railway for their support and facilitation of this project. Specifically, Tom Edwards for facilitating the collection of these data sets. This research was made possible through the Canadian Rail Research Laboratory (www.carrl.ca). Funding was provided by the Natural Sciences and Engineering Research Council of Canada (NSERCIRC 523369-18), Canadian National Railway, the National Research Council of Canada, and Transport Canada.

3.9. References

- AREMA (American Railway Engineering and Maintenance of Way Association). (2021). *Manual for railway engineering*. Lanham, MD: AREMA.
- ASTM. (2021). *Standard practice for dealing with outlying observations*. ASTM E178-02. West Conshohocken, PA: ASTM.
- Barbosa, R. S. (2016). Evaluation of railway track safety with a new method for track quality identification. *Journal of Transportation Engineering Part A: Systems*, 142(11), 04016053. [https://doi.org/10.1061/\(ASCE\)TE.1943-5436.0000855](https://doi.org/10.1061/(ASCE)TE.1943-5436.0000855).
- Birmann, F. (1965). Paper 5: Track parameters, static and dynamic. In *Proc., Institution of Mechanical Engineers*, 73–85. London: SAGE.
- Bracciali, A., F. Cavaliere, and M. Macherelli. (2014). Review of instrumented wheelset technology and applications. In *Proceeding, 2nd International Conference on Railway Technology: Research, Development and Maintenance*, 1–16. Stirlingshire, Scotland: Civil-Comp Press.
- Cakdi, S., S. Cummings, and J. Punwani. (2015). Heavy haul coal car wheel load environment: Rolling contact fatigue investigation. In *Proceeding, Joint Rail Conference, American Society of Mechanical Engineers Digital Collection*. Washington, DC: ASME.
- Doyle, N. F. (1980). *Railway track design: A review of current practice*. Canberra, WA: Australian Government Publishing Service.
- Dybala, J., and S. Radkowski. (2013). Reduction of Doppler effect for the needs of wayside condition monitoring system of railway vehicles. *Mechanical Systems and Signal Processing*, 38(1), 125–136. <https://doi.org/10.1016/j.ymssp.2012.03.003>.
- Esveld, C. (2001). *Modern railway track*. Zaltbommel, Netherlands: MRT-Productions.

- Fallah Nafari, S., M. Gül, M. T. Hendry, and J. R. Cheng. (2018a). Estimation of vertical bending stress in rails using train-mounted vertical track deflection measurement systems. *Proc. Inst. Mech. Eng., Part F: J. Rail Rapid Transit*, 232(5), 1528–1538. <https://doi.org/10.1177/0954409717738444>.
- Fallah Nafari, S., M. Gül, M. T. Hendry, D. Otter, and J. J. Roger Cheng. (2018b). Operational vertical bending stresses in rail: Real-life case study. *Journal of Transportation Engineering Part A: Systems*, 144(3), 05017012. <https://doi.org/10.1061/JTEPBS.0000116>.
- FRA (Federal Railroad Administration). (2007). *Track safety standard compliance manual*. Washington, DC: USDOT.
- Grubbs, F. E. (1969). Procedures for detecting outlying observations in samples. *Technometrics*, 11(1), 1–21. <https://doi.org/10.1080/00401706.1969.10490657>.
- Hay, W. W. (1982). *Railroad engineering*. New York: Wiley.
- Higgins, R. L., D. E. Otter, and R. W. Martin. (1992). High accuracy load measuring wheelset. In *Proc., 10th Int. Wheelset Congress: Sharing the Latest Wheelset Technology in Order to Reduce Costs and Improve Railway Productivity, 181–187*. Barton, ACT, Australia: Institution of Engineers.
- Leishman, E. M., M. T. Hendry, and C. D. Martin. (2017). Canadian main track derailment trends, 2001 to 2014. *Can. J. Civ. Eng.*, 44(11), 927–934. <https://doi.org/10.1139/cjce-2017-0076>.
- Pearson, R. K. (2005). *Mining imperfect data: Dealing with contamination and incomplete records*. Philadelphia, PA: Society for Industrial and Applied Mathematics.
- Peters, N. (2010). *CN railway engineering course*. Montreal: McGill Univ.
- Prause, R. H., H. C. Meacham, H. D. Harrison, T. G. John, and W. A. Glaeser. (1974). *Assessment of design tools and criteria for urban rail track structures: Volume I. At-grade tie-ballast track*.

Washington, DC: DOT, Urban Mass Transportation Administration Office of Research and Development.

Ren, Y., and J. Chen. (2019). A new method for wheel–rail contact force continuous measurement using instrumented wheelset. *Vehicle System Dynamics*, 57(2), 269–285. <https://doi.org/10.1080/00423114.2018.1460853>.

Roghani, A., and M. T. Hendry. (2016). Continuous vertical track deflection measurements to map subgrade condition along a railway line: Methodology and case studies. *Journal of Transportation Engineering Part A: Systems*, 142(12), 04016059. [https://doi.org/10.1061/\(ASCE\)TE.1943-5436.0000892](https://doi.org/10.1061/(ASCE)TE.1943-5436.0000892).

Roghani, A., and M. T. Hendry. (2017a). Quantifying the impact of subgrade stiffness on track quality and the development of geometry defects. *Journal of Transportation Engineering Part A: Systems*, 143(7), 04017029. <https://doi.org/10.1061/JTEPBS.0000043>.

Roghani, A., R. Macciotta, and M. Hendry. (2015). Combining track quality and performance measures to assess track maintenance requirements. In *Proceeding, ASME/IEEE Joint Rail Conf.* Washington, DC: ASME.

Roghani, A., R. Macciotta, and M. T. Hendry. (2017b). Quantifying the effectiveness of methods used to improve railway track performance over soft subgrades: Methodology and case study. *Journal of Transportation Engineering Part A: Systems*, 143(9), 04017043. <https://doi.org/10.1061/JTEPBS.0000071>.

Sadeghi, J. (2012). New advances in analysis and design of railway track system. *Journal of Reliability and Safety Railway*, 30(3), 75–100.

Sadeghi, J., and P. Barati. (2010). Evaluation of conventional methods in analysis and design of railway track system. *International Journal of Civil Engineering*, 8(1), 44–56.

4. Quantifying the Impact of Rail Profile Changes on the Magnitude of Dynamic Loads through Instrumented Wheelset Measurements

4.1. Contribution of the Ph.D. candidate

All of the work presented in this chapter was performed by the Ph.D. candidate, including literature review, data modelling, processing, analysis, and interpretation, as well as manuscript preparation. As a supervisor, Dr. M.T. Hendry, reviewed all parts of the work. This chapter is submitted (March, 2024) for publication in the Journal of Vehicle System Dynamics:

Behnia, D., and Hendry, M.T. (2024). “Quantifying the impact of rail profile changes on the magnitude of dynamic loads through instrumented wheelset measurements.” Journal of Vehicle System Dynamics (Taylor & Francis).

4.2. Abstract

Track geometry significantly influences train-track dynamic interactions, primarily due to irregularities at the wheel-rail interface. These irregularities generate dynamic load excitations, leading to defects and damage. This study evaluates how track surface longitudinal level vertical changes affect vertical wheel-to-rail loads, quantified by the dynamic load factor (ϕ), due to the importance of ϕ in track design. A limitation of the existing studies is their focus on instrumented sections and numerical modellings without considering different track structures. This study conducted dynamic load measurements using two instrumented wheelsets (IWS) over a 340 km section operated by a North American Class 1 freight railway in the Canadian Prairies under various track structures and train speeds. Rail profile measurements were obtained as routine measurements through a track geometry car. The paper presents statistical distributions of rail profile characteristics across different track structures and evaluates two widely used and recently developed ϕ equations within the context of North American freight railways to quantify the

impact of rail surface changes on dynamic load magnitudes. The study also evaluates regulated threshold values by considering observed trends in the measured data, which aims to quantify and compare these values with our current understanding.

4.3. Introduction

The occurrence of derailments brings about notable financial burdens and substantial service disturbances (Wang and Li, 2012). The primary causes of derailments in Canada are rail breaks and track component failures (Leishman et al., 2017). These derailments occur at higher speeds than those resulting from other causes, contributing to increased energy levels, a more significant number of derailed cars, and a heightened risk of releasing the contents of rail cars (Leishman et al., 2017). Given the continuing occurrences of rail failures, it is crucial to revisit our understanding of the intensity of loads experienced by the rail.

One of the major influential factors in variability and increasing train-track dynamic interactions is track geometry (Sussman et al., 2001; Lundqvist and Dahlberg, 2005; Dahlberg, 2010). The majority of dynamic excitations experienced by the track and vehicle are attributed to irregularities at the wheel-rail interface (Lestoille et al., 2016; Panunzio et al., 2017; Dingqing and Selig, 2018; Milne et al., 2021). Track surface irregularities are pivotal in generating these load excitations (Karttunen et al., 2012; Andersson et al., 2015). These dynamic load excitations can lead to many defects with different damage mechanisms (Nielsen et al., 2003; Naeimi et al., 2015) and are considered a significant concern for railway companies due to safety issues (Dingqing and Selig, 2018). Wear, cyclic plasticity, and rolling contact fatigue (RCF) represent the primary mechanisms of damage observed on both wheels and rails, potentially leading to the occurrence of rail breaks (Johnson, 1989; Asplund and Soderstrom, 2022; Maglio et al., 2024).

Many design guidelines for track components in North America incorporate historical wheel loads and various evaluation factors (Van Dyk et al., 2017). Several factors influence the actual load imparted into the track structure from the car body. A dynamic load factor (ϕ) is applied in designs for a more accurate load estimation. The ϕ is defined as the ratio of dynamic wheel-to-rail loads (P_d) from a moving vehicle at the wheel-rail interface to the static load (P_s) caused by the vehicle's weight and its contents [Equation (1)] (Van Dyk et al., 2017). Equations for the dynamic load factor, ϕ , and the associated dynamic loads are commonly applied in the design of track structures and in selecting appropriate rail steel and cross-section (weights) (Peters, 2010; Sadeghi, 2012; AREMA, 2021).

$$\phi = \frac{P_d}{P_s} \quad (1)$$

Existing understanding of the impact of rail profile (also referred to as the rail surface or longitudinal level of the rail) changes on dynamic load magnitudes is limited, as it primarily focuses on specific track sections, known as instrumented sections (Tong et al., 1979; Sun et al., 2004; Nemeth and Schleinzer, 2008; Zhao and Li, 2012; Agh, 2023), or relies on numerical analysis (Dimasi and Weinstock, 1978; El-Sibaie, 2000; Karttunen et al., 2012; Wang and Li, 2012; Andersson et al., 2015; Naeimi et al., 2015; Dung et al., 2022; Zhang et al., 2024). Instrumented sections can capture a range of loads from different types of rolling stock (such as locomotives and various cars), wheel conditions, and axle loads. However, these sections typically represent a single configuration of track, often well-supported and well-maintained, which is unlikely to represent average or worst-case conditions for dynamic load generation (Behnia et al., 2022).

This investigation was conducted based on ϕ value as a representative of the magnitude of dynamic train-track interaction, which plays a crucial role in the design process. The ϕ values and

rail profile changes were derived from measurements of an instrumented wheelset (IWS) and a track geometry car. These measurements were collected along a 340 km section of a Class 1 freight railway line in North America, encompassing a variety of track structures such as tangent tracks, curves, grade crossings, bridges, and switches. Dynamic load measurements are limited to a single car and suspension type, wheel diameter, static load, and the range of operational train speeds experienced on a Class 1 freight railway main line. According to the significant impact of rail profile changes on wheel-rail dynamic interactions, track geometry data are limited to rail profile records.

This paper comprehensively evaluates how rail profile changes affect the dynamic loads on Class 1 North American freight railways. The study compares ϕ values obtained from IWS measurements with established standards (AREMA, 2021) and recent findings (Behnia et al., 2022), evaluating their implications for rail profile conditions (Table 4-1). Surfaces have also been fitted over the data to quantify the influence of rail profile changes and train speeds on ϕ . The data are also tabulated to provide ϕ values representative of the loading conditions generated within the range of speeds permissible on North American classes of track (1 through 4) and regulated threshold values for rail profile changes regarding the estimated values.

Table 4-1. Dynamic load factor (ϕ) equations for North American freight railways.

Expression for ϕ	Equation	Reference
$\phi_{AREMA} = 1 + 5.21 \frac{S}{D}$	(4-2)	(AREMA 2021)
$\phi_{Behnia et al.}^{Tan} = 3 \times 10^{-5} S^2 + 1.4 \times 10^{-3} + 1.19$ (for tangent track)	(4-3)	(Behnia et al. 2022)
$\phi_{Behnia et al.}^{NTan} = 3 \times 10^{-5} S^2 + 2.5 \times 10^{-3} + 1.27$ (for non-tangent track)	(4-4)	

Note: (S): Train speed (km/h); (D): wheel diameter (mm).

4.4. Measured datasets

This study utilizes two datasets, one representing dynamic loads at the wheel-rail interface and the other capturing track surface longitudinal-level geometry. The latter was measured using a track

geometry car, while the former was recorded via the IWS system. The investigation focuses on a high-traffic subdivision operated by a Class 1 railway, with an annual gross tonnage (GMT) exceeding 50 million tons, traversing the Canadian Prairies. The rail is continuously welded in the studied section, predominantly supported by concrete ties. This section includes 30 bridges, 50 switches, over 100 grade crossings, and approximately 83 km of curves. Since the track traverses diverse surface geologies, it likely requires varying curve radii to adapt to the terrain (Scanlan, 2018). Mainline railroads typically feature curves ranging from 1 to 2 degrees, with sharper curves of 5 to 10 degrees in mountainous or challenging terrain (AREMA, 2021).

4.4.1. Dynamic load measurements

As part of a comprehensive track performance study, data were collected using the IWS installed on a 15.8 m (52 ft) gondola car (Roghani and Hendry, 2016, 2017; Roghani et al., 2017; Fallah Nafari et al., 2018a, b; Behnia et al., 2022). The car was equipped with two IWSs, each consisting of an axle with two Class F wheel plates of 915 mm (36 in.) diameter (Figure 4-1). Each wheel plate was equipped with 16 full-bridge Wheatstone strain gauge circuits, interpreting the rail forces on the wheels into vertical, lateral, and traction forces for each wheel (only vertical forces, i.e., dynamic loads are presented within this investigation). In practice, a minimum value of 200 Hz is recommended to capture the essential dynamics of the wheelset (Bracciali et al, 2014). However, according to Shannon's theorem, anti-aliasing and practical constraints often compromise ideal sampling rates and data quality. Consequently, lower rates are frequently used due to limitations in data processing and storage (Pires et al., 2021; Salvador et al., 2016; Ahlbeck et al., 1980). Low-pass filtering also positively affects anti-aliasing (Bracciali et al, 2014). The IWS measurements were taken at a 200 Hz frequency and subjected to a 20 Hz low-pass filter (Woelfle, 2016).

A Garmin GPS18X global positioning system (GPS) was used to record each measurement's

latitude, longitude, time, and speed. Prior to installation, each IWS wheel was calibrated in the lab. The IWS system is a high-precision device for measuring wheel-rail forces. Its test accuracy is typically maintained within 5% during bench calibration and line verification processes (Wu et al., 2023; Higgs et al., 1992). Behnia et al. (2022) also demonstrated the accuracy and repeatability of IWS measurements across different runs and directions. The accuracy of the IWS measurements was evaluated by comparing the static load measured by scale (576.2 kN) with that measured by IWS (574.6 kN), revealing a negligible discrepancy of 0.3%. The wheels had minimal wear and were free of defects that could amplify dynamic loads. The IWS data were recorded between July 2015 and August 2015, encompassing four passes of the study site (two in each direction), with a maximum train speed of 95 km/h (59 mph). As the study was conducted during revenue service, the measurements were taken without control over the type or weight of adjacent cars or travel speed. This study's collected and evaluated vertical dynamic load included more than 56×10^6 measurements.

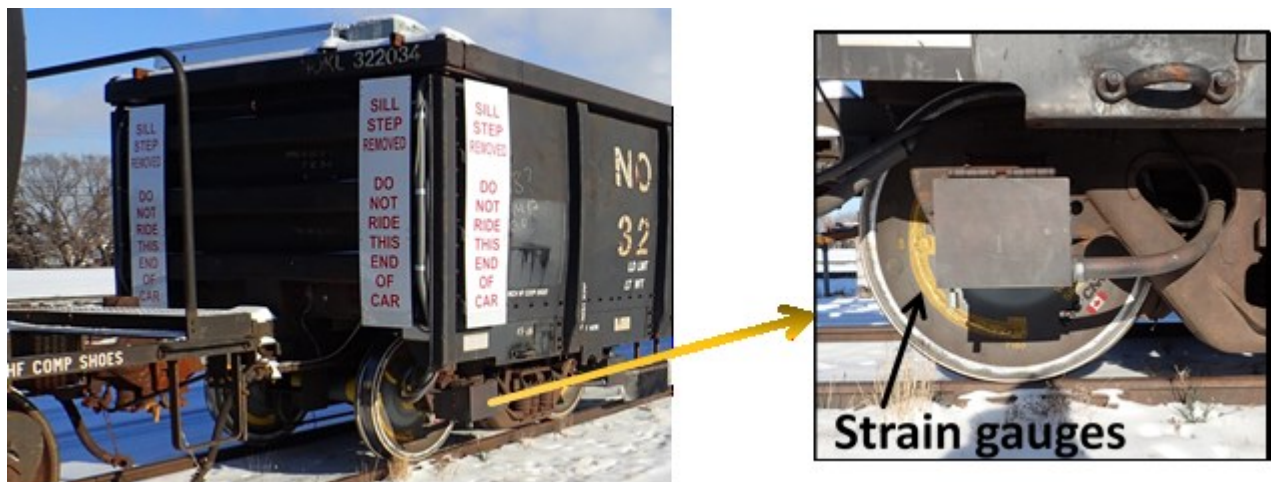


Figure 4-1. Photograph of the IWS system installed on a car used to collect data on the magnitude of dynamic loads along the track. Wheatstone bridge strain gauges and connectors are covered in yellow epoxy (Image by Michael T. Hendry).

4.4.2. Rail profile measurements

Railway operators use track geometry measurements to ensure safe and efficient train operations by monitoring the rail's shape and ride quality at the designated maximum speed of the track (AREMA 2021). Major Canadian railway operators routinely monitor track geometry using specialized vehicles that collect data at intervals of 0.30 m (1 ft.) (Scanlan et al., 2016). These measurements are essential for assessing track performance and identifying sections that may be defective based on established threshold values (Hyslip, 2002; Scanlan et al., 2016). Geometry defects that exceed regulatory thresholds can significantly impact wheel-rail dynamic interactions. Table 4-2 presents the regulated threshold values for freight tracks, where the track class determines speed limits for trains to align with the track condition (FRA, 2007; Transport Canada, 2011).

Table 4-2. Regulated threshold values for defining geometry defects for freight service tracks (TC, 2011).

Class	Maximum allowable speed [km/h (mph)]	Gauge [mm (in.)]	Profile (surface) [mm (in.)]	Crosslevel (tangents & curves) [mm (in.)]	Warp (over 18.9 m distance) [mm (in.)]	Alignment (tangent) [mm (in.)]
1	16 (10)	1416.1-1473.2 (55.75-57.62)	76.2 (2)	76.2 (3)	76.2 (3)	127.0 (5)
2	40 (25)	1416.1-1466.9 (55.75-57.25)	69.9 (1.5)	50.8 (2)	57.2 (2.25)	76.2 (3)
3	64 (40)	1422.4-1466.9 (56-57.25)	57.2 (1.25)	44.5 (1.75)	50.8 (2)	44.5 (1.75)
4	97 (60)	1422.4-1460.5 (56-57.25)	50.8 (1)	31.8 (1.25)	44.5 (1.75)	38.1 (1.5)
5	129 (80)	1422.4-1460.5 (56-57.25)	31.8 (0.75)	25.4 (1)	38.1 (1.5)	19.1 (0.75)

The longitudinal level of the rail (aka the rail profile or rail surface), a key track geometry parameter, plays a significant role in wheel-rail dynamic interaction. It represents the vertical deviation of the rail relative to a straight-line reference chord (18.9 m or 62 ft.) after projecting both the rail and the chord onto the vertical plane. The track longitudinal level geometry variable

in North America is quantified as mid-chord offsets (MCO) (Hyslip, 2002; Li et al., 2015). The longitudinal level of the rail is typically characterized by two parameters: hump (i.e., lifted zone; positive values) and dip (i.e., fall-off or depression zone; negative values) (FRA, 2007). The rail profile data were recorded in April 2015. This study collected and evaluated more than 1.23×10^6 rail profile measurements.

4.5. Results

Given the four passes of the IWS measurements, an initial assessment of the repeatability of load measurements was essential. Behnia et al. (2022) highlighted the remarkable consistency in the magnitude and pattern of dynamic loads across different runs. Their study examined the dynamic load magnitudes across various track conditions and classified them into two groups based on their statistical distributions, including tangent track and non-tangent track (i.e., curves, bridges, grade crossings, and switches). The statistical distributions showed the narrowest distribution for tangent tracks, indicating fewer extreme values than other track characteristics. Likewise, the statistical distributions of vertical dynamic load magnitudes in track assets (i.e., grade crossings, bridges, and switches) and curves were remarkably similar. The measured load data distribution varied widely by track characteristics, with tangent sections comprising 69.9% of the dataset, followed by curves (24.7%), grade crossings (2.2%), bridges (1.6%), and switches (1.6%). Table 4-3 details the statistical values for vertical dynamic loads by track type, where the mean and median values closely approximated the static load (144 kN), indicating normal distributions in nature.

The analysis of rail profile changes across different track characteristics, as shown in Figure 4-2, reveals that curves and tangent tracks exhibit similar statistical distributions, as do other track assets such as grade crossings, bridges, and switches. All these distributions exhibit the characteristics of a normal distribution. The mean (μ) values for rail profile changes are close to

zero across all track types, indicating minimal average deviations in the rail profile. However, the standard deviation (σ) values vary significantly among track types. The statistical distributions of the rail profile measurements in tangent tracks and curves exhibit narrower standard deviations compared to other track assets, indicating more consistent rail profile conditions and fewer extreme values. Conversely, grade crossings, switches, and bridges show broader distributions (i.e., higher variability), reflecting more diverse rail profile conditions. Table 4-3 presents the statistical parameters of rail profile changes for various track assets, indicating that tangent tracks and curves have comparable and narrower standard deviations than other assets.

4.6. Data preparation and alignment

The data preparation phase, critical for evaluating the impact of rail profile on dynamic loads, focused on two main aspects: determining the appropriate window length and overlap ratio for data alignment and choosing a suitable function to characterize the rail profile. Since track longitudinal level geometry was recorded at 0.3 m (1 ft) intervals and load measurements were taken every 0.005 seconds (i.e., the interval value is speed-dependent), aligning these datasets was imperative for further analysis. Data alignment typically employs sliding windows with a specific length for detailed examination. The window length and overlap ratio are vital parameters in this process. Following standard maintenance and geometry measurement practices, a 20-meter window length was chosen (FRA, 2007; Transport Canada, 2011). Since these datasets were measured using two different global positioning system (GPS) formats, it was essential to evaluate data accuracy. The evaluation revealed that data accuracy was approximately 5 m. Therefore, to ensure the integrity of data alignment, the overlap ratio was determined to be less than this threshold (<5 m). Accordingly, four overlap ratios- 75% (15 m), 80% (16 m), 90% (18 m), and 95% (19 m)- were considered. Sensitivity analysis indicated that a 95% overlap ratio provided

high-quality results for investigating the effect of rail profile on dynamic load magnitudes. The selected window length and overlap ratio were also justified by measuring rail profile variation using mid-chord offsets (MCO) of equivalent length (Ebersohn, 1998; Sadeghi, 2010).

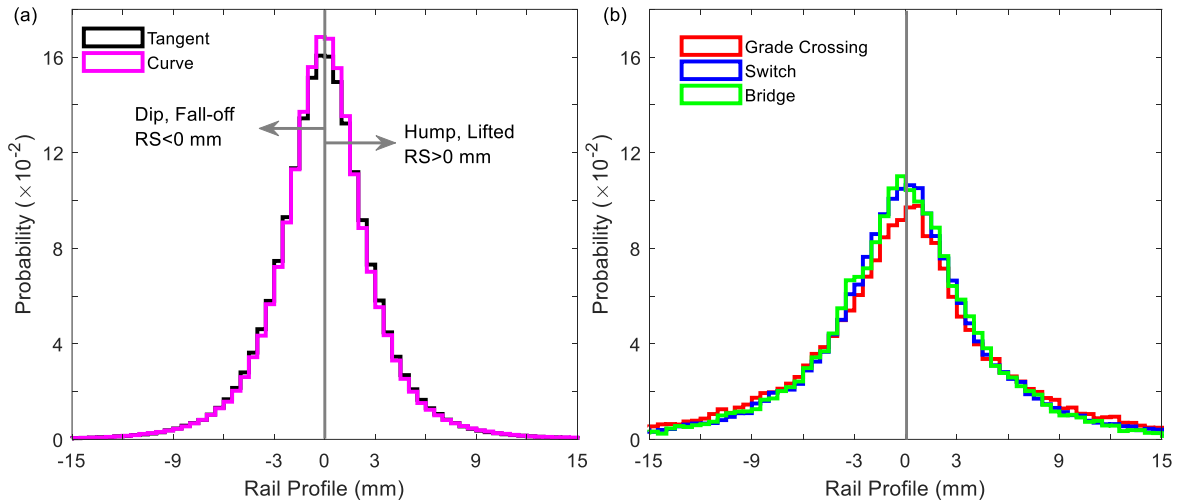


Figure 4-2. Probability distributions of track geometry measurements (available datasets) from the track geometry car: (a) rail profile on tangent and curve tracks; and (b) rail profile on grade crossings, switches, and bridges.

Table 4-3. Statistical measures from probability distributions of dynamic vertical load and rail profile measurements from the IWS and track geometry car.

Track Type		μ	Median	σ	Maximum	99.9th
Vertical Load	All	143.9 (kN)	144.1 (kN)	11.3 (kN)	384.4 (kN)	177.9 (kN)
	Tangent	143.9 (kN)	144.2 (kN)	10.9 (kN)	384.4 (kN)	176.5 (kN)
	Curve	143.7 (kN)	143.6 (kN)	12.2 (kN)	292.8 (kN)	180.2(kN)
	Bridge	144.6 (kN)	144.6 (kN)	12.4 (kN)	288.9 (kN)	181.9 (kN)
	Grade crossing	144.2 (kN)	144.1 (kN)	13.1 (kN)	264.2 (kN)	183.4 (kN)
	Switch	144.1 (kN)	144.1 (kN)	14.4 (kN)	302.5 (kN)	187.2 (kN)
Rail Profile	All	-0.00 (mm)	-0.02 (mm)	3.64 (mm)	H: 58.11 (mm) D: -46.85 (mm)	H: 20.14 (mm) D: -17.80 (mm)
	Tangent	0.00 (mm)	-0.02 (mm)	3.42 (mm)	H: 41.66 (mm) D: -32.17 (mm)	H: 18.60 (mm) D: -15.95 (mm)
	Curve	0.00 (mm)	-0.02 (mm)	3.44 (mm)	H: 58.11 (mm) D: -46.85 (mm)	H: 18.92 (mm) D: -17.03 (mm)
	Bridge	-0.01 (mm)	-0.06 (mm)	5.47 (mm)	H: 31.53 (mm) D: -32.52 (mm)	H: 25.39 (mm) D: -20.64 (mm)
	Grade crossing	-0.03 (mm)	-0.01 (mm)	6.58 (mm)	H: 38.51 (mm) D: -31.87 (mm)	H: 28.16 (mm) D: -24.93 (mm)
	Switch	0.00 (mm)	-0.02 (mm)	5.74 (mm)	H: 39.87 (mm) D: -31.98 (mm)	H: 27.42 (mm) D: -23.09 (mm)

Note: Load data include all four instrumented wheels and all four passes: μ = mean; σ = standard deviation; *H*= Hump; *D*= Dip; and 99.9th = 99.9 percentile.

As previously mentioned, rail profile measurements can be categorized into two types based on the signage (\pm) used: hump ($RP > 0$) and dip ($RP < 0$) (Figure 4-2). The distributions of these track characteristics, whether humps or dips, appear to be normally distributed around the mean for each type of track characteristics, as suggested by their similar shapes (Figure 4-2). Also, given the high degree of correlation between hump and dip values ($R^2 = 0.75$) across the studied section, this study focuses on the absolute value of the rail profile in each window ($|RP|$). As the study aims to evaluate the impact of rail profile on the magnitude of dynamic load, the maximum of $|RP|$ values ($|RP|_{\max}$) are used to represent the rail profile along the considered window.

4.7. Discussion

Statistical distribution analysis of dynamic loads and rail profile conditions identified three distinct categories: tangent tracks, curves, and track assets (e.g., grade crossings, bridges, and switches). The ϕ value is derived from the upper envelope of dynamic load measurements, underscoring the necessity of considering the influence of outliers. Recent research by Behnia et al. (2022) highlights the Grubbs' test as an effective method for identifying and removing outliers in dynamic load magnitudes within railway engineering. This technique employs the Grubbs' value (G) to determine if a data point is an outlier (Grubbs, 1969):

$$G = \frac{\max_{i=1, \dots, n} |x_i - \mu|}{\sigma} \quad \text{Equation 4-5}$$

where μ and σ are the mean and standard deviation of the sample, respectively, and x_i represents the value of the i^{th} element in the dataset. Figure 4-3 illustrates the maximum Grubbs' values for ϕ derived from IWS measurements conducted on tangent tracks, curves, and track assets, with the data evaluated at 5 km/h increments in train speed and 2 mm in rail profile. The figure indicates a more consistent increase trend in the Grubbs' values, in contrast to the higher degree of inconsistency observed when using the original dataset values (see also Figure C-1).

This study employed a statistical approach to determine the ideal sample size for each bin to achieve statistical significance. The ideal sample size (n) was determined using three parameters: the Z_{score} (Equation 4-6), standard deviation (σ), and margin of error (λ) (Equation 4-7) (x : represents the individual measurements or data points) (Kotrlik and Higgins, 2001).

$$Z_{score} = \frac{x - \mu}{\sigma} \quad \text{Equation 4-6}$$

$$n = \frac{Z_{score}^2 \cdot \sigma \cdot (1 - \sigma)}{\lambda^2} \quad \text{Equation 4-7}$$

The Z_{score} is linked to the desired confidence level, typically between 90% and 99% (Crow, 1956), and is frequently set at 95% (Bury, 1999). As it is common in modelling and simulation to accept a margin of error of 10% (Oberkampf et al., 2002), this study adopted confidence levels of 95% (dark grey) and 90% (light grey) (as shown in Figures 4-3 and C-1).

Based on the number of data points in each bin (sample size), the bars in the graphs were categorized into high-reliability (represented by dark grey, with $n \geq 97$ samples and a 95% confidence level), moderate-reliability (represented by light grey, with $68 < n < 97$ samples and a 90% confidence level), and low-reliability (represented by white, with $n \leq 67$ samples and a 90% confidence level) zones (see Figure 4-3). Although rail profile changes varied from 0 to 58.1, the subsequent analysis was confined to the 0-24 mm range, determined by the number of data points and sections defined for statistical significance. This study evaluated the impact of longitudinal level vertical deviations of the rail (also termed rail profile or surface variations within track geometry parameters) on the magnitude of dynamic loads, as quantified by the ϕ . This study considered two reference values for this purpose, including the estimations provided by AREMA (2021) (Equation 4-2) and Behnia et al. (2022) (Equations 4-3 and 4-4).

Sadeghi (2010) notes that rail profile tolerances may range from ± 6 to ± 20 mm across various track classes. Therefore, this study assessed rail profile ($|RP|_{\max}$) variations from two perspectives: by examining three distinct values within the typical range of rail profile variations (0-2 mm, 10-12 mm, and 18-20 mm) and by considering the maximum allowable speeds for different track classes (1 through 4).

Figure 4-4 illustrates the influence of rail profile changes on ϕ values, compared to previous estimates (Equations 4-2, 4-3, and 4-4), at varying train speeds. Across all categories, when rail profile changes exceeded 12 mm ($|RP|_{\max} \geq 12$ mm), the estimated values consistently underestimated the ϕ values. For rail profile variations within the range of 0-2 mm, ϕ_{AREMA} values tended to underestimate the dynamic load magnitudes, particularly at lower speeds (i.e., ≤ 40 km/h for tangent tracks, ≤ 65 km/h for curves, and ≤ 75 km/h for track assets). In contrast, within the same range, the $\phi_{Behnia et al.}^{Tan}$ and $\phi_{Behnia et al.}^{NTan}$ values effectively captured dynamic load magnitudes, providing accurate ϕ estimations.

Figure 4-4(a) shows that the estimation of ϕ_{AREMA} values becomes challenging primarily at lower speeds (≤ 35 km/h) or with significant rail profile changes ($|RP|_{\max} > 10$ mm). Conversely, for $\phi_{Behnia et al.}^{Tan}$ values, the difficulty arises when the rail profile values are high ($|RP|_{\max} > 10$ mm), as the measured values exceed the estimated ones.

In curves, the ϕ_{AREMA} values consistently underestimated the measured load by 1 to 25%, with greater underestimations associated with more significant rail profile changes. Figure 4-4(b) illustrates that these underestimations by ϕ_{AREMA} values are more pronounced at lower speeds (below 65 km/h: classes 1, 2, and 3) in curves. Conversely, the $\phi_{Behnia et al.}^{NTan}$ values provided reliable estimates for rail profile variations up to 12 mm. When rail profile changes fluctuated

between 18 and 20 mm, the measured load values exhibited a slight discrepancy of less than 5% above the $\phi_{Behnia\ et\ al.}^{NTan}$ values.

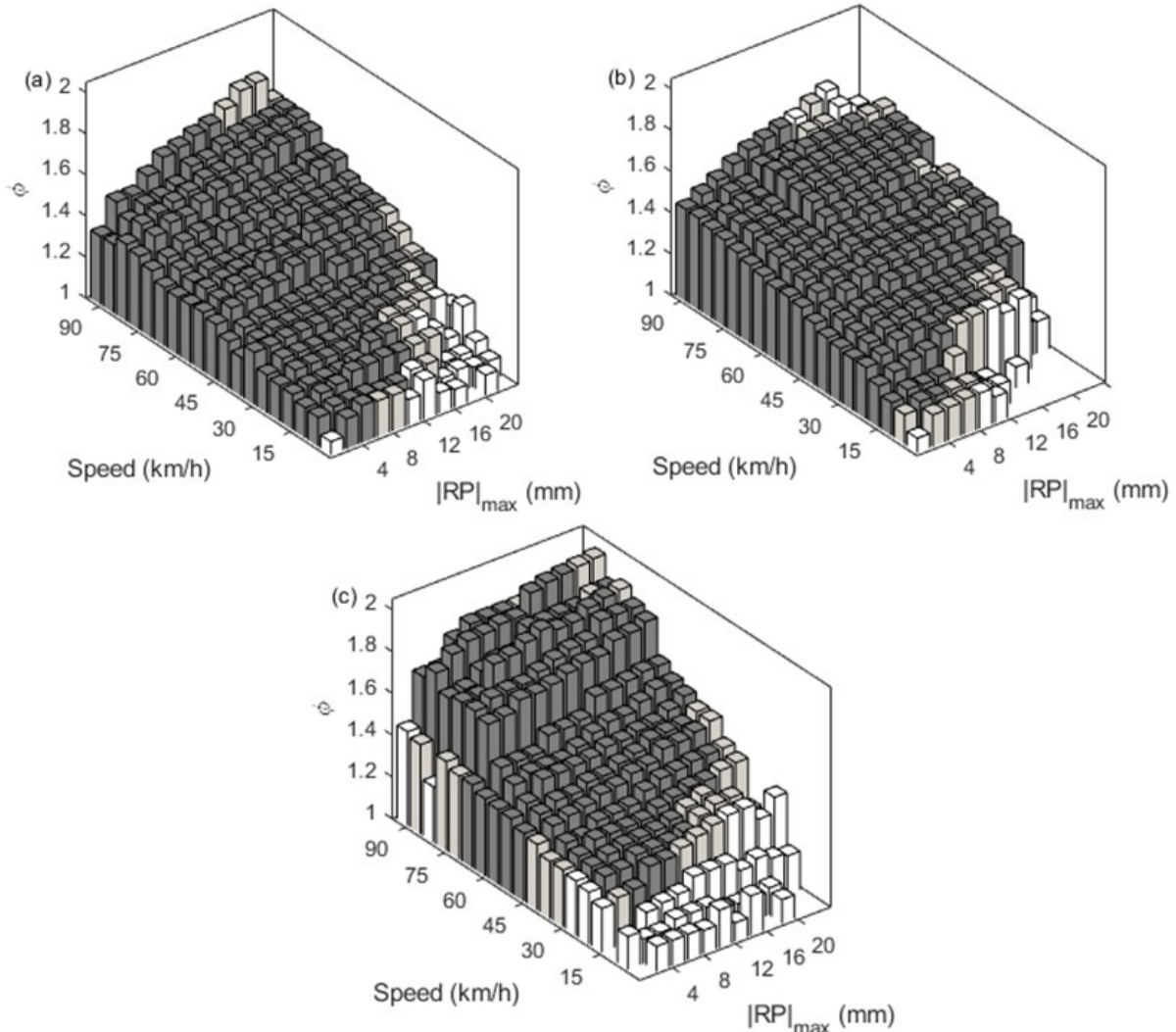


Figure 4-3. IWS and rail profile measurements based on Grubbs' values of dynamic load factor (ϕ) for 5 km/h increments of train speed and 2 mm increments of rail profile: (a) tangent sections; (b) curves; and (c) track assets.

In track assets, the ϕ_{AREMA} values underestimated the measured load by 10% when rail profile changes were between 0-2 mm. This underestimation increased to 32% when rail profile changes were 18-20 mm (Figure 4-4(c)). The $\phi_{Behnia\ et\ al.}^{NTan}$ values accurately captured dynamic load magnitudes for rail profile changes less than 12 mm and train speeds below 65 km/h. However,

for train speeds exceeding 65 km/h and higher rail profile values, the actual values surpassed the $\phi_{Behnia et al.}^{NTan}$ estimates by approximately 15%.

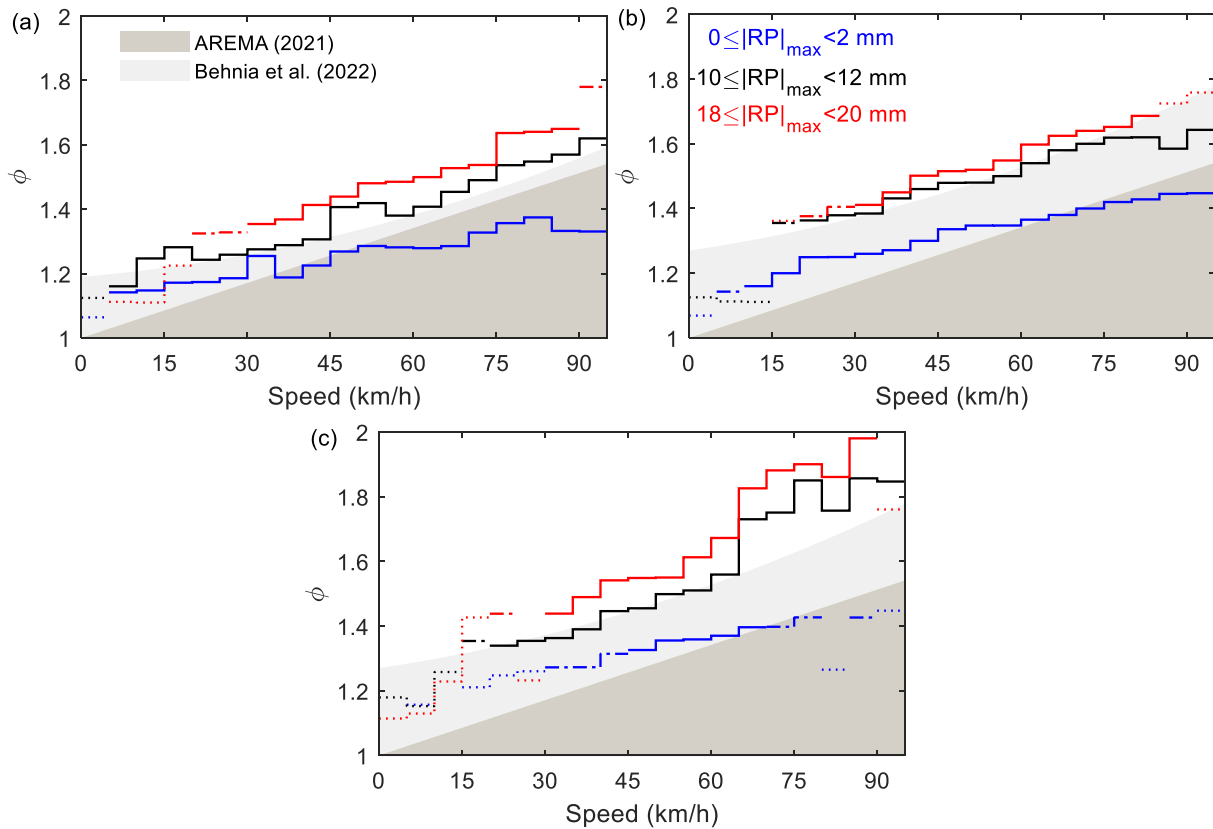


Figure 4-4. IWS measurements derived from the maximum Grubbs’ test values of dynamic load factor (ϕ) for 5 km/h increments of train speed regarding the statistical significance conditions for three different ranges of rail profile (in mm), including $0 \leq |RP|_{max} < 2$, $10 \leq |RP|_{max} < 12$, and $18 \leq |RP|_{max} < 20$, compared to AREMA (2021) (ϕ_{AREMA} (Equation 4-2)) and Behnia et al. (2022) ($\phi_{Behnia et al.}^{Tan}$ (Equation 4-3) and $\phi_{Behnia et al.}^{NTan}$ (Equation 4-4)) estimations, in: (a) tangent sections; (b) curves; and (c) track assets. (Note: A solid line signifies high reliability zone, a dash dotted line represents moderate reliability zone, and a dotted line designates low reliability zone).

For the majority of track classes and corresponding categories, ϕ_{AREMA} estimations consistently underestimated the measured ϕ values within a range of 1% to 36% (also refer to Figure C-2).

Figure 4-5 illustrates the results of a comparative analysis between ϕ_{AREMA} values and measured values obtained from various track classes and categories. Figure 4-6 indicates that the measured loads exceeded the $\phi_{Behnia et al.}^{Tan}$ and $\phi_{Behnia et al.}^{NTan}$ values across all categories when rail profile variations surpassed 8-10 mm in track class 1 ($S \leq 15$ km/h, ϕ_{15}). In tangent tracks, Figure 4-6(a)

shows that $\phi_{Behnia\ et\ al.}^{Tan}$ may underestimate the measured loads across all track classes (1-4). In curves (Figure 4-6(b)), the measured loads were approximately 10% higher than $\phi_{Behnia\ et\ al.}^{NTan}$ values when rail profile variations were above 8 mm at lower speeds (Classes 1 (ϕ_{15}) and 2 (ϕ_{40})). Also, for Class 3 (ϕ_{65}), with rail profile changes over 12 mm, $\phi_{Behnia\ et\ al.}^{NTan}$ underestimated the measured loads by about 10%. However, at higher speeds (Class 4, ϕ_{95}) in curves, $\phi_{Behnia\ et\ al.}^{NTan}$ provided accurate estimations within the range of rail profile variations considered in this study. Regarding track assets (Figure 4-6(c)), for rail profile changes more significant than 8 mm, the measured loads exceeded the $\phi_{Behnia\ et\ al.}^{NTan}$ values by 10%, 15%, 20%, and 5% for Classes 1, 2, 3, and 4, respectively. The more minor increase in Class 4 is attributed to limitations in rail profile data (<16 mm).

Figure 4-3 qualitatively demonstrates a strong correlation between train speed, rail profile changes, and ϕ . Thus, the subsequent step focuses on fitting a surface over the data with high and moderate reliability (refer to Figure C-3). Table 4-4 evaluates the trends in the measured loads concerning predefined threshold values for each track class (i.e., classes 1-4). This evaluation is compared to the reference values considered (i.e., AREMA (2021) and Behnia et al. (2022)) concerning train speed (i.e., track classes) and rail profile changes. Table 4-4 reveals that in tangent tracks, the ϕ_{AREMA} values underestimate the dynamic loads by 50% across all classes, while the underestimation by $\phi_{Behnia\ et\ al.}^{NTan}$ ranges from 31% to 48%. In non-tangent sections (i.e., curves and track assets), the underestimation by ϕ_{AREMA} and $\phi_{Behnia\ et\ al.}^{NTan}$ generally increases with higher track classes (i.e., higher train speeds). The most significant discrepancy is observed in class 4, where ϕ_{AREMA} underestimates by 161% and $\phi_{Behnia\ et\ al.}^{NTan}$ by 115% for track assets (see also Figures C-4 and C-5).

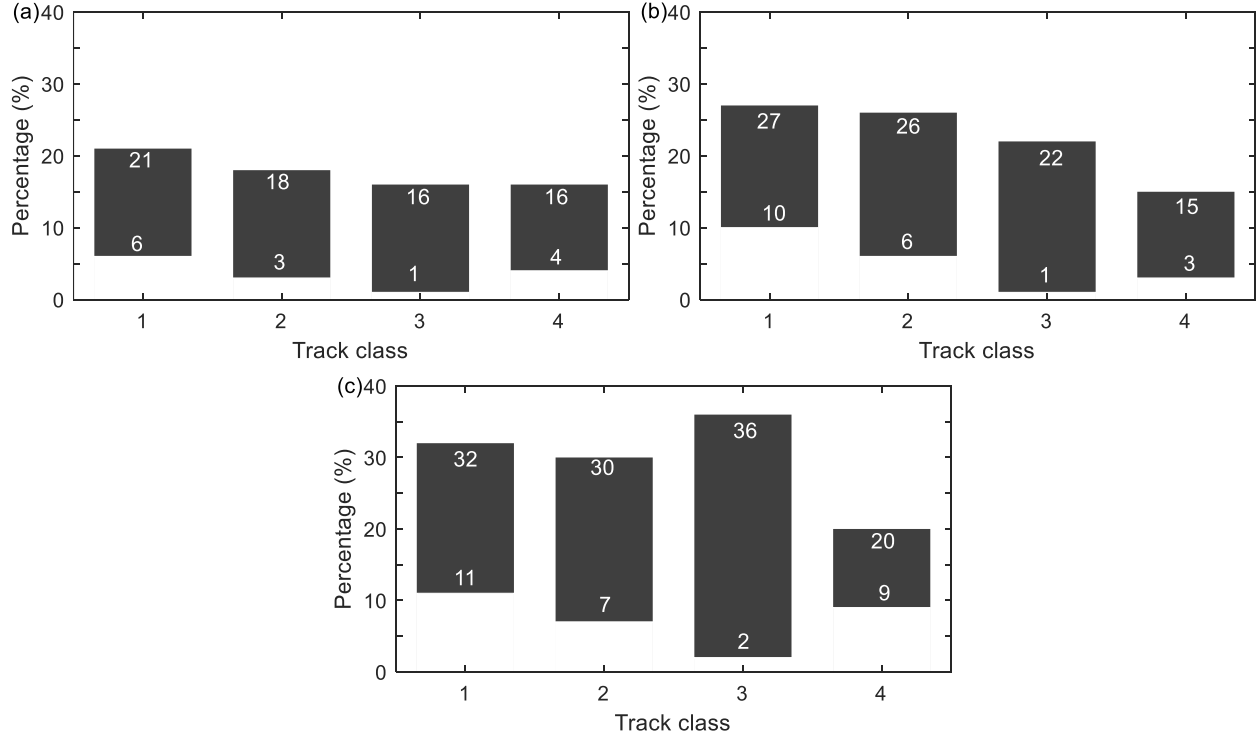


Figure 4-5. A comparative evaluation of ϕ_{AREMA} estimations against measured values derived from the IWS system and computed via maximum Grubbs' test values in various track classes (1 through 4) and categories (tangent track, curve track, and track assets) regarding the considered range of rail profile changes.

Table 4-4. Comparative evaluation of measured load trends against the provided estimations by AREMA (2021) and Behnia et al. (2022) regarding the threshold values for rail profile changes in different classes of freight service tracks.

class	Tangent track compared to		Curve track compared to		Track assets compared to	
	ϕ_{AREMA} (Equation 4-2)	$\phi_{Behnia et al.}^{Tan}$ (Equation 4-3)	ϕ_{AREMA} (Equation 4-2)	$\phi_{Behnia et al.}^{NTan}$ (Equation 4-4)	ϕ_{AREMA} (Equation 4-2)	$\phi_{Behnia et al.}^{NTan}$ (Equation 4-4)
1	50%	31%	42%	23%	48%	28%
2	55%	48%	46%	29%	56%	37%
3	50%	45%	70%	47%	95%	69%
4	50%	45%	113%	76%	161%	115%

Note: All percentage values show the increment regarded the corresponding values based on the provided equations, including AREMA (2021) (ϕ_{AREMA}) (Equation 4-2) and Behnia et al. (2022) ($\phi_{Behnia et al.}^{Tan}$ and $\phi_{Behnia et al.}^{NTan}$) (Equations 4-3 and 4-4). The $\phi_{Rail profile (mm) / Speed (km/h)}$ values are developed based on the increment trend of measured ϕ values, maximum allowable train speed, and defined threshold values in each class.

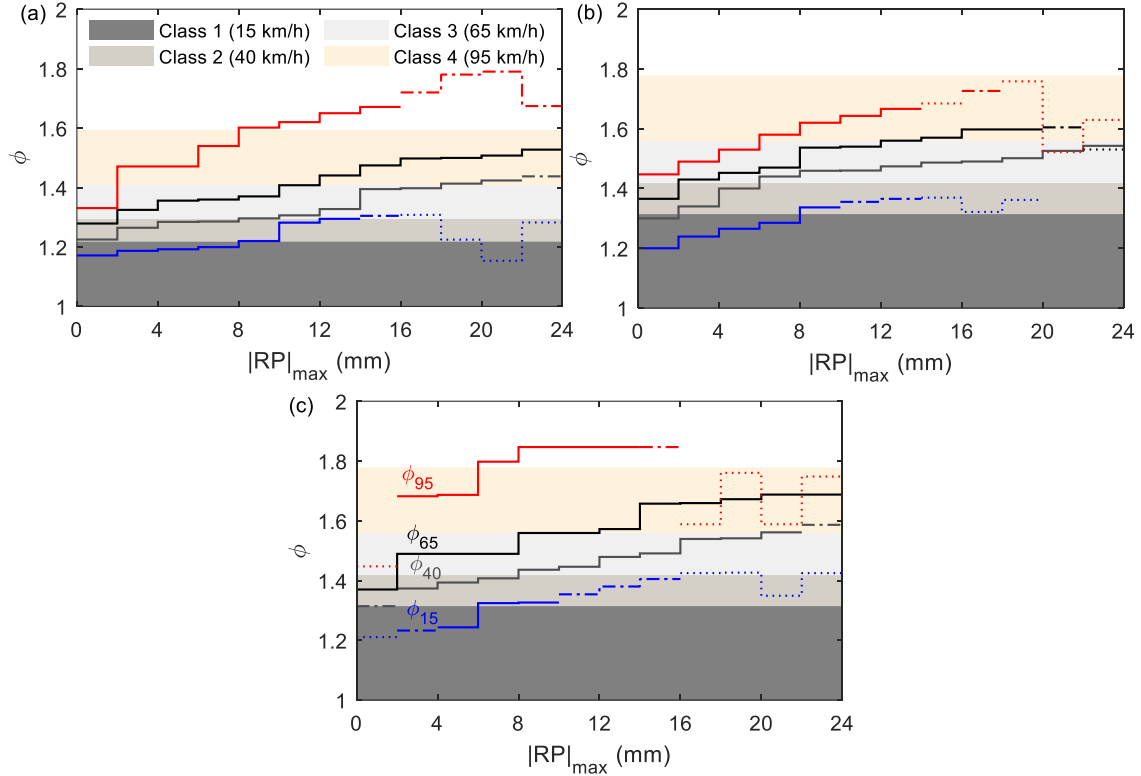


Figure 4-6. IWS and rail profile measurements based on the maximum Grubbs' test values for ϕ for 2 mm increments of rail profile regarding the statistical significance conditions for four track classes, including Class 1 ($S_{max} = 15$ km/h [~ 10 mph], ϕ_{15}), Class 2 ($S_{max} = 40$ km/h [25 mph], ϕ_{25}), Class 3 ($S_{max} = 65$ km/h [~ 40 mph], ϕ_{65}), and Class 4 ($S_{max} = 95$ km/h [~ 60 mph], ϕ_{95}), compared to Behnia et al. (2022) (ϕ_{Behnia}^{Tan} et al. (Equation 4-3) and ϕ_{Behnia}^{NTan} et al. (Equation 4-4)) estimations, in: (a) tangent sections; (b) curves; and (c) track assets.

4.8. Conclusion

This study investigated the influence of track longitudinal level vertical variations (also known as rail profile or surface changes) on dynamic loads, as indicated by dynamic load factor (ϕ), using data from instrumented wheelset (IWS) measurements. In contrast to previous research that primarily relied on instrumented track sections and numerical modeling, this study considered diverse track structures and evaluated the effect of the track longitudinal level changes on the magnitude of dynamic loads across various track structures. The IWS provided measurements of dynamic loads across a 340 km section of track under constant car type and conditions but on various track conditions. The results of this study revealed that changes in rail profile significantly affect dynamic load magnitudes, particularly evident in non-tangent tracks, including curve

sections and track assets (i.e., grade crossings, bridges, and switches). Commonly used methods for estimating ϕ tend to underestimate dynamic loads, particularly when the maximum rail profile irregularity exceeds 10 mm. Analysis of statistical distributions and observed trends in rail profile and dynamic loads across different track structures suggests the requisite of considering distinct threshold values for tangent and non-tangent sections (i.e., curve sections and track assets). This investigation potentially offers valuable insights for quantifying surface fatigue and modelling surface damage by highlighting the correlation between rail profile changes and dynamic load magnitudes. However, further research is needed to establish comprehensive dynamic load and track surface longitudinal level deviation ranges considering track conditions and vehicle type variations. Investigating the impact of frequencies above 20 Hz on loads at distinct rail irregularities may also demonstrate substantial increases and offer fresh insights into the consequences of longitudinal rail level variations.

4.9. Acknowledgement

The authors thank Canadian National Railway for supporting and facilitating this project, specifically *Albert Wahba* and *Tom Edwards* for facilitating the collection of these datasets. This research was made possible through the *Canadian Rail Research Laboratory* (www.carrl.ca).

4.10. References

- Ágh, C. (2023). Connection between track geometry quality and dynamic vehicle response at various speeds. *The Baltic Journal of Road and Bridge Engineering*, 18(3), 169-187.
- Andersson, R., Torstensson, P. T., Kabo, E., & Larsson, F. (2015). The influence of rail surface irregularities on contact forces and local stresses. *Vehicle System Dynamics*, 53(1), 68-87.
- American Railway Engineering and Maintenance of Way Association (AREMA). (2021). *Manual for Railway Engineering*. Lanham, MD: AREMA.

- Asplund, M., & Söderström, P. (2022). Field validation of force response from defective wheel. In *12th International Conference on Contact Mechanics and Wear of Rail/Wheel Systems*, 4-7 September 2022, Melbourne, Victoria, Australia.
- Behnia, D., Hendry, M. T., Haji Abdulrazagh, P., & Wahba, A. (2022). Railway Dynamic Load Factors Developed from Instrumented Wheelset Measurements. *Journal of Transportation Engineering, Part A: Systems*, 148(7), 04022042.
- Bury, K. V. (1999). *Statistical Distributions in Engineering*. Cambridge University Press.
- Crow, E. L. (1956). "Confidence intervals for a proportion." *Biometrika*, 43(3/4), 423–35. <https://doi.org/10.2307/2332920>.
- Dahlberg, T. (2010). Railway Track Stiffness Variations-Consequences and Countermeasures. *International Journal of Civil Engineering*, 8(1).
- Dimasi, F., & Weinstock, H. (1978). A parametric study to relate railcar speed to permissible combinations of track geometry deviations.
- Dingqing, L., & Selig, E. T. (2018). "Wheel/track dynamic interaction: track substructure perspective." In E. Schiehlen (Ed.), *Interaction of Railway Vehicles with the Track and Its Substructure* (pp. 183-196). Routledge.
- Dung, T. A., Van Tham, M., & Le Hai, H. A. (2022). A Study on Derailment at Railway Turnout Using Multi-body Dynamics Simulation. *Journal of Materials and Engineering Structures (JMES)*, 9(4), 499-505.
- Ebersohn, W. (1998). "Implementing a railway infrastructure maintenance system." In *Conference on Railway Engineering Proceedings: Engineering Innovation for a Competitive Edge* (pp. 395-402). Rockhampton, Qld: Central Queensland University.

- El-Sibaie, M. (2000). Computer model developed to predict rail passenger car response to track geometry (No. RR000-04). Washington, DC: United States. Federal Railroad Administration.
- Fallah Nafari, S., Gül, M., Hendry, M. T., & Cheng, J. R. (2018). Estimation of vertical bending stress in rails using train-mounted vertical track deflection measurement systems. *Proceedings of the Institution of Mechanical Engineers, Part F: Journal of Rail and Rapid Transit*, 232(5), 1528-1538.
- Fallah Nafari, S., Gül, M., Hendry, M. T., Otter, D., & Roger Cheng, J. J. (2018). Operational vertical bending stresses in rail: Real-life case study. *Journal of Transportation Engineering, Part A: Systems*, 144(3), 05017012.
- Federal Railroad Administration (FRA). (2007). *Track Safety Standard Compliance Manual*. Washington, DC: USDOT.
- Grubbs, F. E. (1969). Procedures for detecting outlying observations in samples. *Technometrics*, 11(1), 1-21.
- Hyslip, J. P. (2002). *Fractal Analysis of Geometry Data for Railway Track Condition Assessment* (Doctoral dissertation). Department of Civil Engineering, University of Massachusetts, Amherst, MA.
- Johnson, K. L. (1989). The strength of surfaces in rolling contact. *Proceedings of the Institution of Mechanical Engineers, Part C: Mechanical Engineering Science*, 203(3), 151-163.
- Karttunen, K., Kabo, E., & Ekberg, A. (2012). A numerical study of the influence of lateral geometry irregularities on mechanical deterioration of freight tracks. *Proceedings of the Institution of Mechanical Engineers, Part F: Journal of Rail and Rapid Transit*, 226(6), 575-586.

- Kotrlik, J. W., & Higgins, C. C. (2001). "Organizational research: Determining appropriate sample size in survey research." *Journal of Information Technology, Learning, and Performance*, 19(1), 43.
- Leishman, E. M., Hendry, M. T., & Martin, C. D. (2017). Canadian main track derailment trends, 2001 to 2014. *Canadian Journal of Civil Engineering*, 44(11), 927-934.
- Lestoille, N., Soize, C., & Funfschilling, C. (2016). "Sensitivity of train stochastic dynamics to long-term evolution of track irregularities." *Vehicle System Dynamics*, 54(5), 545-567.
- Li, D., Hyslip, J. P., Sussmann, T. R., & Chrismer, S. M. (2016). *Railway Geotechnics*. Taylor & Francis Group LLC, Boca Raton, FL, USA.
- Lundqvist, A., & Dahlberg, T. (2005). "Railway Track Stiffness Variation-Consequences and Countermeasures." In *19th IAVSD Symposium of Dynamics of Vehicles on Roads and Tracks*, Milano, August 29-September 2, 2005. Department of Mechanical Engineering, Politecnico di Milano.
- Maglio, M., Vernersson, T., Nielsen, J. C., Ekberg, A., & Kabo, E. (2024). Influence of railway wheel tread damage on wheel-rail impact loads and the durability of wheelsets. *Railway Engineering Science*, 32(1), 20-35.
- Milne, D., Harkness, J., Le Pen, L., & Powrie, W. (2021). "The influence of variation in track level and support system stiffness over longer lengths of track for track performance and vehicle track interaction." *Vehicle System Dynamics*, 59(2), 245-268.
- Naeimi, M., Zakeri, J. A., Esmacili, M., & Shadfar, M. (2015). Influence of uneven rail irregularities on the dynamic response of the railway track using a three-dimensional model of the vehicle-track system. *Vehicle System Dynamics*, 53(1), 88-111.

- Nemeth, I., & Schleinzer, G. (2008). Investigation into the indirect determination of wheel-rail surface roughness. In *Proceedings of the 11th Mini Conference on Vehicle System Dynamics, Budapest* (pp. 135-146).
- Nielsen, J. C., Lundén, R., Johansson, A., & Vernersson, T. (2003). Train-track interaction and mechanisms of irregular wear on wheel and rail surfaces. *Vehicle System Dynamics*, 40(1-3), 3-54.
- Oberkampf, W. L., DeLand, S. M., Rutherford, B. M., Diegert, K. V., & Alvin, K. F. (2002). "Error and uncertainty in modeling and simulation." *Journal of Reliability Engineering and System Safety*, 75(3), 333-357.
- Panunzio, A. M., Puel, G., Cottreau, R., Simon, S., & Quost, X. (2017). "Construction of a stochastic model of track geometry irregularities and validation through experimental measurements of dynamic loading." *Vehicle System Dynamics*, 55(3), 399-426.
- Peters, N. (2010). *CN Railway Engineering Course*. Retrieved from McGill University Civil Engineering Graduate Studies class.
- Roghani, A., & Hendry, M. T. (2016). Continuous vertical track deflection measurements to map subgrade condition along a railway line: Methodology and case studies. *Journal of Transportation Engineering*, 142(12), 04016059.
- Roghani, A., & Hendry, M. T. (2017a). Quantifying the impact of subgrade stiffness on track quality and the development of geometry defects. *Journal of Transportation Engineering, Part A: Systems*, 143(7), 04017029.
- Roghani, A., Macciotta, R., & Hendry, M. T. (2017). Quantifying the effectiveness of methods used to improve railway track performance over soft subgrades: methodology and case study. *Journal of Transportation Engineering, Part A: Systems*, 143(9), 04017043.

- Sadeghi, J. (2010). Development of railway track geometry indexes based on statistical distribution of geometry data. *Journal of Transportation Engineering*, 136(8), 693-700.
- Scanlan, K. M., Hendry, M. T., & Martin, C. D. (2016). "Evaluating the Equivalency Between Track Quality Indices and the Minimum Track Geometry Threshold Exceedances Along a Canadian Freight Railway." In: *ASME/IEEE Joint Rail Conference* (Vol. 49675, p. V001T01A012). American Society of Mechanical Engineers.
- Sun, Y., Dhanasekar, M., & Roach, D. (2004). Effect of track geometry irregularities on wheel-rail impact forces.
- Sussman, T. R., Ebersöhn, W., & Selig, E. T. (2001). Fundamental nonlinear track load-deflection behavior for condition evaluation. *Transportation Research Record*, 1742(1), 61-67.
- Transport Canada (TC). (2011). *Rules Respecting Track Safety*. Ottawa, ON, Canada: TC.
- Tong, P., Brantman, R., Greif, R., & Mirabella, J. (1979). *Tests of the Amtrak SDP-40F Train Consist Conducted on Chessie System Track* (No. DOT-TSC-FRA-79-14). United States. Federal Railroad Administration. Office of Research and Development.
- Van Dyk, B. J., Edwards, J. R., Dersch, M. S., Ruppert Jr, C. J., & Barkan, C. P. (2017). "Evaluation of dynamic and impact wheel load factors and their application in design processes." In: *Proceedings of the Institution of Mechanical Engineers, Part F: Journal of Rail and Rapid Transit*, 231(1), 33-43.
- Wang, W., & Li, G. X. (2012). Development of high-speed railway vehicle derailment simulation—Part I: A new wheel/rail contact method using the vehicle/rail coupled model. *Engineering Failure Analysis*, 24, 77-92.

Woelfle, A. (2016). "Report for the National Research Council. In Analysis of wheel-rail forces during (MRail) rolling deflection tests." Gloucester, ON, Canada: National Research Council Canada, Automotive and Surface Transportation.

Zhang, P., He, C., Shen, C., Dollevoet, R., & Li, Z. (2024). Comprehensive validation of three-dimensional finite element modeling of wheel-rail high-frequency interaction via the V-Track test rig. *Vehicle System Dynamics*, 1-25.

Zhao, X., Li, Z., & Liu, J. (2012). Wheel-rail impact and the dynamic forces at discrete supports of rails in the presence of singular rail surface defects. *Proceedings of the Institution of Mechanical Engineers, Part F: Journal of Rail and Rapid Transit*, 226(2), 124-139.

5. Impact of Subgrade Track Stiffness on Dynamic Loads: A Comprehensive Evaluation Using Instrumented Wheelset and MRail Measurements

5.1. Contribution of the Ph.D. candidate

All the work presented in this chapter, which includes data processing, review of literature, analysis and discussion of the results, and writing of the text, is carried out by the Ph.D. candidate. As a supervisor, Dr. M.T. Hendry has reviewed all parts of the work. This chapter is submitted (January, 2024) for publication in the Journal of Civil Structural Health Monitoring with the following citation:

Behnia, D., Hendry, M.T. (2023). “Impact of subgrade track stiffness on dynamic loads: a comprehensive evaluation using instrumented wheelset and MRail measurements.” Journal of Civil Structural Health Monitoring (Springer).

5.2. Abstract

This paper evaluates the influence of subgrade track stiffness on the magnitude of dynamic loads. Quantifying the impact of subgrade stiffness on dynamic loads is crucial for enhancing railway design and ensuring the safety and durability of track components. This study focused on dynamic load factor (ϕ), given the pivotal role of this parameter in the design of railway track structures and the selection of rail steel and cross-sections (weight). Despite extensive studies evaluating the impact of subgrade stiffness on dynamic loads, existing research has primarily relied on measurements from instrumented track sections with constant conditions, neglecting the effects of various track structures. This study combined two datasets collected from a 340 km track operated by a North American Class 1 freight railway through the Canadian Prairies: the instrumented wheelset (IWS) measured the magnitude of dynamic loads and subgrade track stiffness (VTD_{sub}) acquired through MRail measurements. These measurements provided the dynamic loads and

vertical track deflections resulting from a loaded freight car traveling at various speeds over various track structures. This paper evaluates the IWS and MRail datasets to discuss how subgrade track stiffness influences ϕ values and presents the statistical distributions of dynamic loads and subgrade track stiffness values. New ϕ lines are developed based on subgrade stiffness conditions (good, average, and poor) for the tangent track, curve section, and track assets (including bridges, grade crossings, and switches). This study also reveals that worsening subgrade conditions can increase the ϕ values by up to 9% in tangent sections and 15% in non-tangent sections compared to good subgrade conditions.

5.3. Introduction

Inconsistencies in subgrade stiffness can lead to uneven load distribution and subsequent track degradation, posing significant safety risks (Punetha and Nimbalkar, 2023; Cai et al., 2022; Indraratna et al., 2019; Li et al., 2003); thereby, understanding the impact of subgrade stiffness on dynamic load magnitudes is vital for railway engineers to ensure track safety and performance, optimize track component design, and plan effective maintenance strategies (Faizi et al., 2023; Heydari, 2023; Guo et al., 2022; Grossoni et al., 2019; Judge et al., 2018; Wang et al., 2016; Raymond, 1985). Track stiffness is closely linked to intensified safety concerns, such as rail squat, increased risk of structural flaws, uneven settlement, early deterioration, and increased dynamic stresses (UIC, 2008; Lundqvist and Dahlberg, 2005; Liu and Wang, 2002; Esveld, 2001; Sussman et al., 2001; Selig and Li, 1994). Also, considering that rail breaks and track component failures are leading causes of derailments in Canada (Leishman et al., 2017), a deeper comprehension of the relationship between subgrade stiffness and dynamic loading is essential.

The railway industry uses various vertical track deflection (*VTD*) measurement systems to evaluate track stiffness, categorized into standstill methods and rolling measurement techniques (Berggren,

2009). Standstill methods involve calculating the stiffness of a track section by instrumenting ties or rails with transducers or accelerometers and monitoring their response under a known load, such as a falling weight deflectometer (FWD) or impact hammer (Ebersöhn and Selig, 1994; Read et al, 1994; Kerr, 1983; Zarembski and Choros, 1979). Conversely, rolling measurement techniques, employing devices such as a track loading vehicle (TLV), rolling stiffness measurement vehicle (RSMV), or the University of Nebraska's rolling deflection system (commercially known as MRail), measure *VTD* as the system moves along the track, offering the advantage of continuous, *real-time* monitoring (Greisen, 2010; McVey, 2006; Sussman et al., 2001). The MRail system offers a significant advantage by enabling continuous, in-service measurement of vertical track deflection (Farritor and Fateh, 2013; Greisen et al., 2009; Lu et al., 2007). This capability facilitates the identification of localized stiffness variations, complements existing inspection data, and provides quantitative inputs for maintenance planning- all without disrupting revenue service (Roghani and Hendry, 2017; Roghni et al., 2017; Roghani and Hendry, 2016). The MRail system empowers railroads with a more comprehensive subgrade and overall track structure health assessment than traditional and discrete measurement methods (Tong et al., 2022; Farritor and Fateh, 2013; Greisen, 2010; Li et al., 2004).

Evaluating dynamic loads is important to ensuring railway safety and functionality in practice and academic research (Remennikov and Kaewunruen, 2008). The instrumented wheelset (IWS) system is a practical method for measuring dynamic loads at the wheel-rail interface while moving (Behnia et al., 2022). The IWS system offers valuable insights into the dynamic responses of railway tracks, the influence of track structures on load distribution, and the interaction between vehicles and infrastructure (Behnia et al., 2022).

One limitation of current research into the impact of subgrade track stiffness on dynamic loading conditions is that they have been derived from measured dynamic loads from trains as they pass over an instrumented section of track (Ngamkhanong et al., 2020; Mei et al., 2019; Zhang et al., 2017; Puzavac et al., 2012; Li et al., 2004). Despite previous research, real-time measurements have yet to be used to analyze how track stiffness influences dynamic loads. Understanding the influence of track stiffness on dynamic load magnitudes is crucial for ensuring the structural integrity of railway tracks and minimizing the risk of failures, such as rail squats and excessive wear (Tong et al., 2022; Berggren, 2009; Remennikov and Kaewunruen, 2008; Li et al., 2004). This understanding, in turn, can lead to reduced risk of failures and increased operational efficiency.

In this paper, the collected data comes from the train-mounted measurement system, including IWS data, which captures the variations in dynamic loads, and MRail data, which records vertical track deflections (*VTD*). These measurements were recorded during two passes along a section of 340 km of North American Class 1 freight railway line while the train was moving. Despite their initial association with a particular railcar featuring a specific suspension design, wheel size, and static load, these measurements offer practical insights into the dynamic loads induced by diverse track conditions. Track conditions comprise various track structures, including tangent tracks, curve sections, bridges, grade crossings, and switches, and must be considered alongside different train speeds. Since the dynamic load factor ($\phi = P_d/P_s$, where P_d is the dynamic load and P_s is the static load, Eq. (1)) is vital in railway design for designing track structures and selecting rail steel and cross-sections (weight) (AREMA, 2021; Sadeghi, 2012; Peters, 2010), this study considered ϕ values to evaluate the impact of subgrade stiffness on dynamic load magnitudes.

This paper presents the IWS and MRail data sets, the variation of subgrade stiffness between two passes of the studied track section, the statistical distribution of dynamic loads and subgrade stiffness, and a comparison of ϕ derived from the IWS measurements regarding subgrade stiffness conditions to others for North American freight railways (provided by AREMA (2021) as the most common value and the developed equations by Behnia et al. (2022) as the most recent value). The ϕ values are evaluated versus train speed and subgrade stiffness conditions (calculated through MRail measurements: VTD_{sub}) for differing track conditions and track assets (tangent, curved, bridges, grade crossings, and switches) to develop ϕ lines. The findings are further evaluated with ϕ values corresponding to allowable speeds on North American track classes 1 through 3. To the best of the authors' knowledge, this study is the first published attempt to examine the effects of subgrade track stiffness on the dynamic load magnitudes (in terms of ϕ) recorded from IWS and MRail measurement systems on North American Class 1 freight railways.

5.4. Study site and measurement systems

The data employed in this study were gathered using two accurate and reliable measurement systems installed on the train: the IWS and MRail systems. The data-gathering efforts were part of a more extensive investigation focused on evaluating track performance (Behnia et al., 2022; Fallah Nafari et al., 2018a, b; Roghani and Hendry, 2017; Roghani et al., 2017; Roghani and Hendry, 2016; Roghani et al., 2015). The measurement systems were installed over a 15.8 m (52 ft.) gondola car (Figure 5-1) that was loaded with gravel, reaching a total weight of 1,175 kN (264 kips). The IWS system was utilized to measure the dynamic interaction between the wheel and rail interface, and the MRail system was applied to record the vertical deflection of the loaded track under the moving car (VTD). The data utilized in this investigation were recorded during two passes of the study site, both conducted in the same direction, in July 2015.

5.4.1. Study Site

The section of track examined in this study is operated by a Class 1 freight railway. It constitutes a vital part of a heavily used railway division, with an annual traffic volume exceeding 50 million gross tonnes (MGT), traversing the Canadian Prairies. The measurements were conducted along a 340 km track section that included 30 bridges and overpasses, more than 100 grade crossings, 50 switches, and approximately 83 km of curves. The continuously welded rail (CWR) was predominantly supported by concrete ties. The maximum operational train speed was 82 km/h (51 mph). The measurements were undertaken with the car in revenue service; hence, there was no control over the adjacent cars' type, weight, and travel speed; such limitations are typical when acquiring measurements on a Class 1 North American freight railway track.



Figure 5-1. Photograph the train-mounted system with instrumented wheelset (IWS) and MRail systems installed on the Gondola railcar to collect the data used for this study (image credit: Michael T. Hendry).

5.4.2. Measuring wheel/rail dynamic interactions using the IWS system

The IWS system was applied to quantify dynamic load magnitudes at the wheel-rail interface. Two IWS systems were installed on one end of the instrumented car, each consisting of a single axle with two type F (915 mm or 36 in. in diameter) wheel plates (Figure 5-1). These wheel plates were instrumented with 16 full-bridge Wheatstone strain gauge circuits, each dedicated to assessing forces exerted upon the wheels by the rail (Woelfle, 2016). This system aids in analyzing and

interpreting forces, including vertical, lateral, and traction components, for all four wheels; however, this investigation is limited to the vertical load data (in terms of ϕ). The data acquisition process involved continuously monitoring the IWS system at a sampling frequency of 200 Hz. A 20 Hz low-pass filter was subsequently applied (Ren and Chen, 2019; Barbosa, 2016; Cakdi et al., 2015; Bracciali et al., 2014; Higgins et al., 1992). Location (latitude and longitude), time, and speed for each measurement were ascertained using a Garmin GPS18X global positioning system (GPS). Before installation, each wheel was calibrated in the laboratory. Because the IWS system did not provide data regarding measurement accuracy, the measured static load obtained by the scale was compared with the data from the IWS; the difference was only 3%, indicating the high accuracy of the IWS measurements. The wheels had very little wear and were free of defects capable of increasing dynamic loads.

5.4.3. Measuring *VTD* using the MRail system

The MRail rolling deflection measurement system (Figure 5-1) was collaboratively developed by the University of Nebraska and the Federal Railroad Administration (FRA) (Farritor and Fateh, 2013; Greisen, 2010; Lu, 2008; Arnold et al., 2006; Farritor, 2006; McVey, 2006; McVey et al., 2005; Norman et al., 2004). This system measured the *VTD* values along the section of track under study. The MRail system comprises laser and camera sensors designed to assess track deflection at a distance of 1.22 m relative to the center of the railcar's inboard wheel with respect to a point positioned at the base of that wheel. The *VTD* measurements were recorded every 0.305 m (1 ft.) along both track rails. The accuracy of MRail measurements was assessed through trackside measurements involving cameras and linear variable differential transducers (LVDT); a comparison of the *VTD* values predicted by this method with those measured by the MRail system indicated the measurements were accurate within 10% (Farritor and Fateh, 2013).

Roghani and Hendry (2016) conducted an extensive investigation into the capabilities of the MRail system for mapping subgrade variations and conditions. Their study proposed a process to measure the stiffness of the subgrade and embankment construction (VTD_{sub}) through the measurement of VTD . The VTD data were filtered to reduce lower wavelength data originating from track surface structural conditions and imperfections; this refinement can thus allow the data to represent the stiffness of the subgrade and embankment construction. This filtering process was implemented using a moving average technique chosen for its simplicity and capability in noise reduction while preserving the integrity of sharp step responses (Smith, 1997). This filtering procedure results in the filtered version of the VTD dataset denoted as VTD_{sub} . The VTD_{sub} values indicate vertical track deflection predominantly attributed to subgrade conditions (Equation 5-2) (Roghani and Hendry, 2016):

$$VTD_{sub}(i) = \frac{0.305}{L} \sum_{-L/(2)(0.305)}^{L/(2)(0.305)} VTD[i + j], \quad \text{Equation 5-2}$$

where L (in m) signifies a critical threshold length dictating the filtration of lower wavelengths. The appropriate resolution (L) selection depends on the characteristic dimensions of the investigated features. Using $L= 20$ m to investigate subgrade features provides the highest attainable resolution (Roghani and Hendry, 2016).

5.5. Results

This research aimed to determine the impact of subgrade track stiffness (VTD_{sub}) on the magnitude of dynamic loads along railway tracks. The first step involved assessing the repeatability of the MRail system measurements. For this purpose, data from the MRail system for an 800 m section of tangent track were considered to evaluate the repeatability of the measurements (Figure 5-2). The MRail measurements comprised two separate runs, each characterized by distinct speeds and without adjacent car-derived data for comparison. Hence, the VTD_{sub} values were normalized

(VTD_{sub}^{Normal}) by the Z-score technique to remove any influence of these factors and enable a meaningful comparison. Figure 5-2 demonstrates a notably similar and consistent pattern in the VTD_{sub} measurements, confirming the repeatability of the data collected.

Research conducted by Behnia et al. (2022) demonstrates the uniformity and consistency in the magnitude and pattern of dynamic loads across different test runs. Figure 5-3 presents the distribution of measured vertical dynamic loads along track characteristics, including tangent tracks, curves, grade crossings, bridges, and switches, based on data from the present study for all four wheels of the IWS system and two passes. Behnia et al. (2022) also examined dynamic load magnitudes for different track conditions and categorized the results into two groups based on statistical distributions: tangent and nontangent tracks. As seen in Figure 5-3, the narrowest distribution for data from the present study is associated with tangent tracks, indicating a relatively lower occurrence of extreme values than for other track characteristics. The statistical distributions for vertical dynamic loads in nontangent tracks (track assets and curve) also show remarkable similarities. A review of statistical metrics for these data, including mean (μ), median, and standard deviation (σ), across all categories indicates normal distributions (Table D-1).

The data preparation procedure was implemented to derive the subgrade stiffness (VTD_{sub}) from the measured vertical track deflection (VTD) collected via the MRail system. This procedure, utilizing moving average methodology, aims to mitigate the impact of surface irregularities and imperfections, thereby minimizing noise within the dataset. In this evaluation, consistent with earlier studies (Roghani and Hendry, 2017; Roghani and Hendry, 2016), a moving average technique was used, conducted at regular intervals of 20 meters, chosen for its ability to offer the highest resolution in discerning subgrade features. Subsequently, the subgrade stiffness can be classified into three distinct categories based on the thresholds outlined in AREMA (2021): “good”

($VTD_{sub} \leq 3.1$ mm), “average” ($3.1 < VTD_{sub} \leq 4.4$ mm), and “poor” ($VTD_{sub} > 4.4$ mm). Figure 5-4 illustrates the statistical distributions of VTD_{sub} across various track characteristics, highlighting the predominant measurements under average track conditions. Tangent and curve tracks exhibit similar statistical distributions (Figure 5-4(a)). The preliminary evaluation of curve sections reveals that good track conditions ($VTD_{sub} \leq 3.1$ mm) are predominantly linked to the high (outer) rail, which experiences lower loads. Grade crossings, bridges, and switches show comparable statistical distributions. Therefore, in light of the VTD_{sub} values for various track characteristics and statistical distributions, a discerning classification emerged, organizing the data into two groups: (1) tangent and curve tracks and (2) track assets (inclusive of grade crossings, bridges, and switches) (Table D-2).

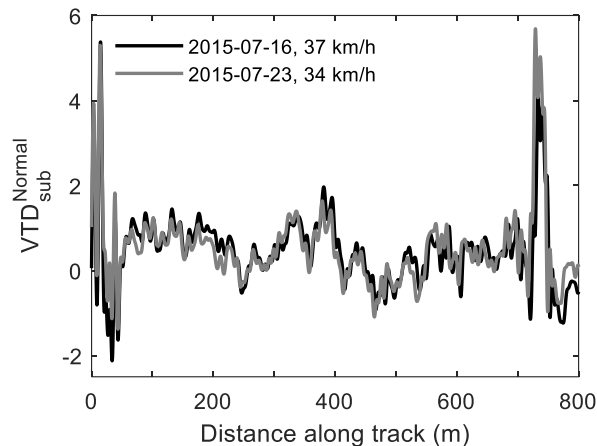


Figure 5-2. An example compares an 800 m section of normalized VTD_{sub} (VTD_{sub}^{Normal}) MRail system data obtained using the Z-score technique for a tangent section of track.

This study required setting a specific threshold value for the rest of the analysis to evaluate how VTD_{sub} affects the magnitude of dynamic loads. Setting an appropriate threshold for ϕ values also enables this study to isolate the effect of subgrade stiffness (VTD_{sub}), increase statistical power, address the limitations posed by the relatively small sample size, and enhance the overall reliability and validity of the findings (Sendra et al., 2023; Di and Sardanelli, 2020; Collell et al., 2018; Taber, 2018; Balasubramanian et al., 2014). Subsequently, for the evaluation, considering the established

ϕ threshold value and the spatial location of each measurement, the corresponding subgrade stiffness (VTD_{sub}) value is allocated to each ϕ value. Therefore, an evaluation was conducted involving three distinct threshold values: 1.3, 1.2, and 1.1 (Figure 5-3). Based on the number of available datasets and the observed statistical distributions for the magnitude of dynamic loads, as shown in Figure 5-3, $\phi \geq 1.1$ was regarded as an appropriate threshold value for the later evaluations.

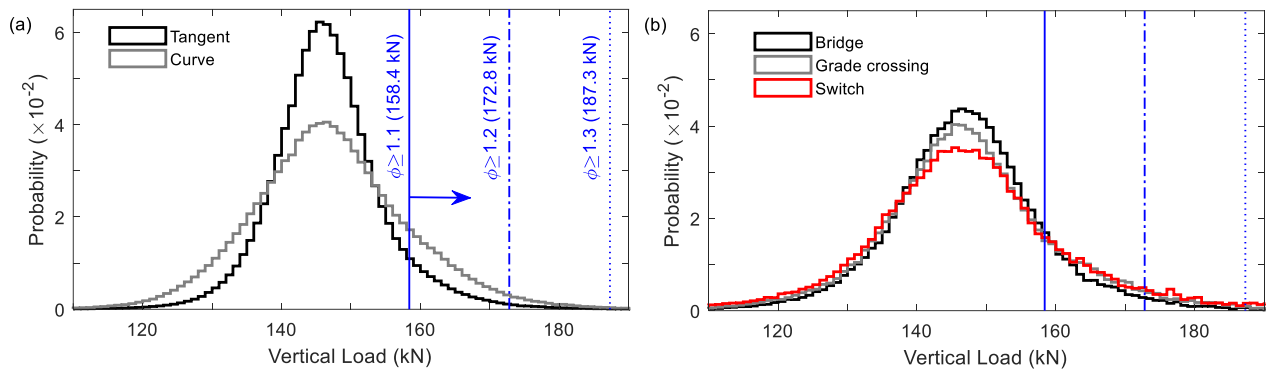


Figure 5-3. Probability distributions of vertical load measurements from the IWS system: (a) on tangent and curve sections; and (b) on bridges, grade crossings, and switches. The data are from all four instrumented wheels and both passes.

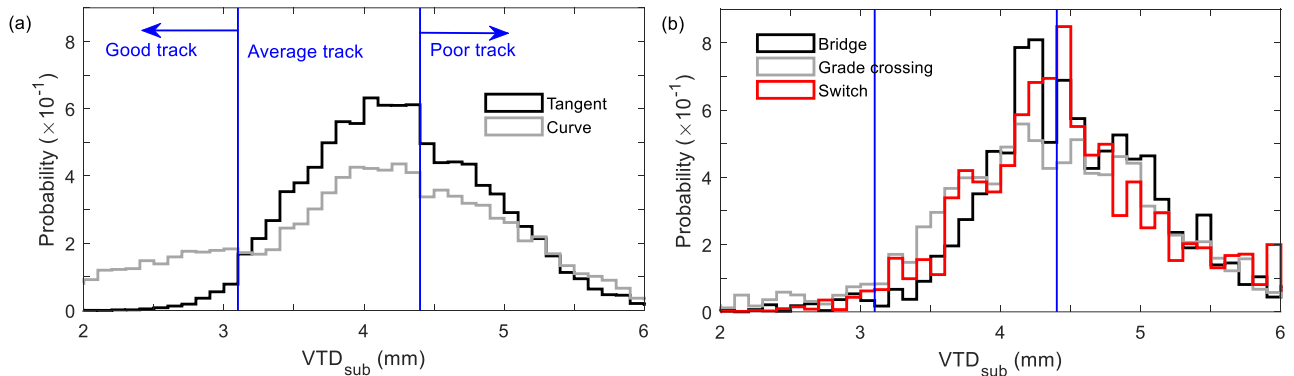


Figure 5-4. Probability distributions of VTD_{sub} measurements from the MRail system: (a) on tangent and curve sections; and (b) on bridges, grade crossings, and switches. The data are from both rails and both passes. The graph is segregated into three sections by blue lines, indicating good ($VTD_{sub} \leq 3.1$), average ($3.1 < VTD_{sub} \leq 4.4$), and poor ($VTD_{sub} > 4.4$) tracks.

Given the statistical measures of dynamic loads and VTD_{sub} measurements, a reliable approach involved classifying the data into three distinct groups: tangent track, curve, and track assets (grade crossings, bridges, and switches). After applying these criteria (data classification and $\phi \geq 1.1$), it

became apparent that most of the dataset (60%) was concentrated within curves. In contrast, tangent tracks contributed 31% of the dataset, with the remaining 9% attributable to track assets.

5.6. Discussion

Achieving accurate estimates with minimal uncertainty necessitates larger sample sizes (Cochran,1997). As the desired confidence level increases and the acceptable margin of error decreases, the requisite sample size grows to maintain the validity and reliability of results (Krejcie and Morgan, 1970). In engineering applications, confidence levels and margins of error serve as guiding principles for selecting appropriate sample sizes for simulations and modelling studies. An ideal sample size balances the need for precision and reliability against practical constraints such as computational costs and data availability (Lenth, 2001). Careful consideration of this balance ensures robust and defensible findings from engineering analyses (Nanjundeswaraswamy and Divakar, 2021; Memon et al., 2020). Hence, choosing the ideal sample size is crucial to ensure statistical analyses are valid and accurately represent the data. Properly determining a sample size also enhances the probability of identifying meaningful effects, thus reinforcing the study's reliability. Determination of the ideal sample size (n), as guided by mathematical formulation (Equation 5-3), depends on four parameters: the Z_{score} (Equation 5-4), standard deviation (σ), mean value (μ), and margin of error (λ) (Bartlett et al., 2001):

$$n = \frac{Z_{score}^2 \cdot \sigma \cdot (1-\sigma)}{\lambda^2} \quad \text{Equation 5-3}$$

$$Z_{score} = \frac{x-\mu}{\sigma} \quad \text{Equation 5-4}$$

The Z -score indicates the intended confidence level, often selected as 90, 95, or 99%. In modelling and simulation, a margin of error of 10% and a confidence level of 90-95% have been deemed reasonable (Oberkampff et al., 2002). However, balancing the confidence level with the practical constraints of obtaining a large sample size is essential. According to the typical range (90-99%)

and widely used (95%) confidence level, this study determined three reliability zones: high (for 95% confidence level), moderate (for 90% confidence level), and low (for <90% confidence level). Thus, in terms of the minimum sample size required for reliability, this study considered three scenarios: high reliability (95%, $n \geq 96$: represented by dark grey), moderate reliability (90%, $96 < n \leq 68$: shown as light grey), and low reliability (<90%, $n < 68$: displayed as white) zones (Figures 5-5 and 5-6).

The dynamic load factor (ϕ) is determined using the upper envelope approach for measured dynamic loads; thus, the evaluation procedure should be developed based on the maximum load values (Figures D-1, D-2, and D-7). Recognizing and eliminating outliers is crucial as this plays a significant role in ensuring the robustness and reliability of subsequent data analysis (ASTM, 2021). Behnia et al. (2022) showed the Grubbs test represents an optimal approach for identifying and removing outliers in railway engineering. In the Grubbs test, a specific metric denoted as the Grubbs value (G) is employed to assess the aberrant nature of individual data points. The equation for calculating G (Equation 5-5) considers the μ and σ of the dataset, with x_i representing the value of the i^{th} element within the dataset:

$$G = \frac{\max_{i=1, \dots, n} |x_i - \mu|}{\sigma} \quad \text{Equation 5-5}$$

The current investigation considered three equations (Equations 5-6, 5-7, and 5-8; Table 5-1) used to estimate ϕ values to evaluate how subgrade stiffness (in terms of VTD_{sub}) influences the magnitude of dynamic load (in terms of ϕ). These formulations were developed by Behnia et al. (2022) (Equations 5-6 and 5-7), signifying a recent development in the area of ϕ values, and by AREMA (2021) (Equation 5-8)), representing the most accepted ϕ value within the field. In light of the study by Behnia et al. (2022), wherein Equation 5-6 (on tangent track) and Equation 5-7 (on

nontangent track) were developed using the same study site and datasets, the ensuing evaluation primarily used these equations.

Table 5-1. The widely used and recent dynamic load factor (ϕ) equations presented in the literature for freight railways.

Equation for ϕ		Equation (#)	Reference
$\phi_{Tan} = 3 \times 10^{-5} S^2 + 1.4 \times 10^{-3} S + 1.19$	(for tangent track)	[5-6]	Behnia et al. (2022)
$\phi_{NTan} = 3 \times 10^{-5} S^2 + 2.5 \times 10^{-3} S + 1.27$	(for nontangent track)	[5-7]	
$\phi = 1 + 5.21 \frac{S}{D}$		[5-8]	AREMA (2021)

Notably, the negative VTD values observed in the measurements indicate temporary rises in the rail height, primarily caused by localized reductions in track support near rail joints or soft locations and on CWR sections positioned over bridge abutments. Because these high and negative values (inconsistency) occurred infrequently, this study only focused on the positive values (>0). Technically, two aspects can be considered to study how the track stiffness conditions (VTD_{sub}) affect the dynamic load factor (ϕ). The first was how VTD_{sub} influences ϕ values, and the second was how speed (S) and VTD_{sub} affect ϕ values. This study also considered four specific train speeds related to different track classes (maximum allowable speeds) and the number of data points to evaluate train speed, including the corresponding lines for 15 km/h (~10 mph) as Class 1, 40 km/h (25 mph) as Class 2, 65 km/h (~40 mph) as Class 3, and 75 km/h (~47 mph) as the maximum speed with an appropriate number of data points (Figure D-6).

5.6.1. Evaluation of the effect of VTD_{sub} on ϕ

As noted above, the available datasets were categorized into three groups based on the statistical distributions: tangent track, curve sections, and track assets. Figure 5-5 presents ϕ values derived from the IWS measurements over various categories, evaluated for 0.4 mm increments of VTD_{sub} collected from the MRail system for the maximum Grubbs values of dynamic load. Figure 5-5(a)

indicates the critical range for ϕ increases for tangent track falls between VTD_{sub} values of 2 and 4.4 mm.

Commonly, the higher ϕ values on the low rail than the high rail arise because the super-elevation difference between the low and high rails generates a centrifugal force that transfers a more significant portion of the vehicle's weight onto the low rail, resulting in higher dynamic loads (AREMA, 2021; Soleimani and Moavenian, 2017; Kish and Samavedam, 2013). The statistical distribution of ϕ values revealed a compelling pattern in the curve sections (Figure D-3). The ϕ values exceeding 1.1 were mainly observed on the low rail. These findings also imply that the discrepancy between the load experienced by the high and low rails grows under average and poor track conditions; thereby, the low rail in curve sections experiences higher dynamic loads with worsening subgrade stiffness (i.e., increasing VTD_{sub}).

Given this study aim to consider maximum dynamic load (ϕ) values, the later analysis on curve sections focused on the low rail. Figures 5-5(b) and (c) demonstrate VTD_{sub} values ranging from 2 to 5 mm and exceeding 2 mm can be critical with respect to increasing the ϕ value in curve and track assets, respectively. Figure 5-5 also presents a comparative analysis of ϕ values with the estimated values by Behnia et al. (2022) at four specific speeds as mentioned above (based on the shaded areas). Based on the number of data points where $\phi \geq 1.1$ (Figure D-6), the highest train speed with a sufficient number of measurements was 75 km/h (with a maximum train speed of 82 km/h). Hence, to evaluate the influence of VTD_{sub} on the dynamic load factor, the ϕ value associated with the 75 km/h speed (highlighted in red in Figure 5-5) was considered the reference value for the later evaluation.

According to Equation 5-6 (for tangent track), the ϕ values surpass the ϕ_{75} -line when $VTD_{sub} \geq 3.2$ mm. Equation 5-6 tends to underestimate the measured values by approximately 5% in cases where

$VTD_{sub} \geq 3.2$ mm. This underestimation indicates the equation has some limitations in such situations. Equation 5-7 (for nontangent track) underestimates ϕ values for curve when $VTD_{sub} \geq 4.4$ mm; more specifically, Equation 5-7 demonstrates an underestimation of around 7% for the low rail while effectively capturing ϕ values for the high rail. For track assets, ϕ values exceed the Equation 5-7 estimation by approximately 8% when VTD_{sub} surpasses 3.6 mm.

Table 5-2. Comparison of measured ϕ values derived from the Grubbs test and ϕ_{75} line developed by AREMA (2021).

Category	Critical Value for VTD_{sub} (mm)	Underestimation (%)
Tangent track	2.8	8
Curve section	2.4	13
Track assets	1.2	22

Note: These values are derived by comparing the ϕ value calculated using the Grubbs test with estimated values based on AREMA (2021) guidelines, considering the maximum speed and sufficient data points (ϕ_{75} -line). The critical VTD_{sub} value indicates the subgrade vertical track deflection that intensifies dynamic loads to the extent that they exceed the ϕ_{75} threshold, signifying a heightened influence of these loads on the track structure.

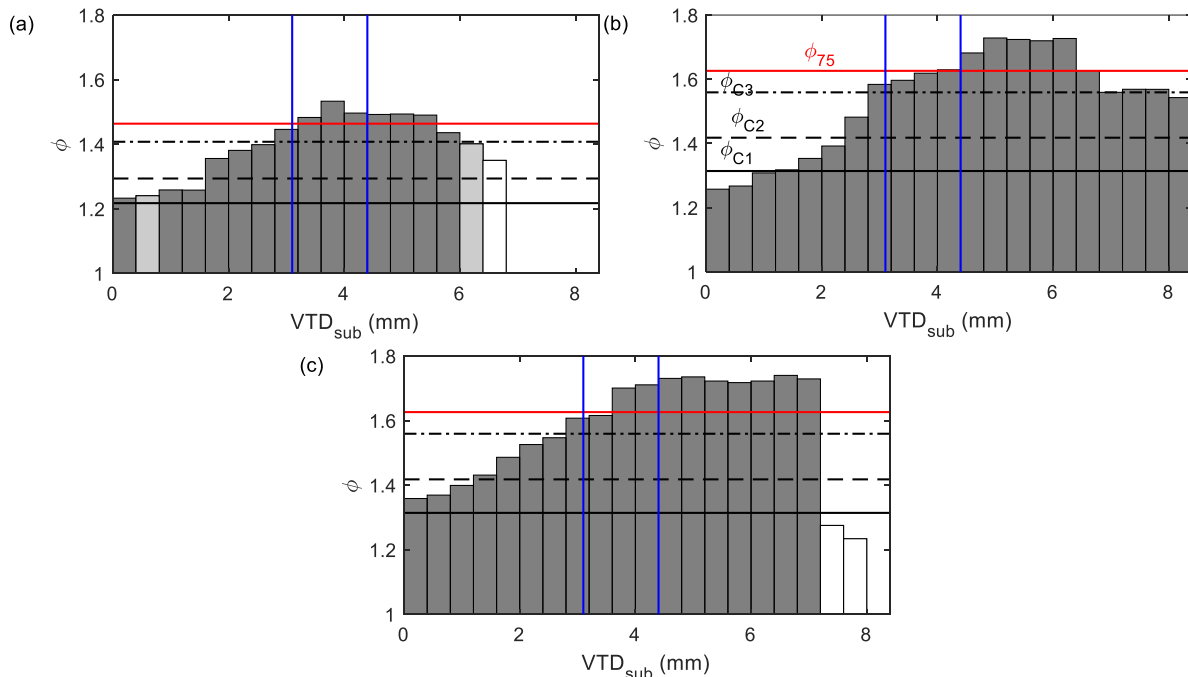


Figure 5-5. IWS and VTD_{sub} measurements based on the Grubbs values of dynamic load factor ($\phi \geq 1.1$) for 0.4 mm increments of subgrade track stiffness (VTD_{sub}) on: (a) tangent tracks; (b) low rail in curves; and (c) track assets. The horizontal lines are based on equations by Behnia et al. (2022), where the ϕ_{C1} line is for 15 km/h (~10 mph), the ϕ_{C2} line is for 40 km/h (25 mph), the ϕ_{C3} line is for 65 km/h (~40 mph), and the ϕ_{75} line (75 km/h or ~47 mph) is for the maximum speed with a reliable number of data points. The graph is segregated into three sections by blue lines, indicating good ($VTD_{sub} \leq 3.1$), average ($3.1 < VTD_{sub} \leq 4.4$), and poor ($VTD_{sub} > 4.4$) tracks.

The estimations provided by Behnia et al. (2022) (Equations 5-6 and 5-7) consistently exceed the values presented by AREMA (2021) (Equation 5-8). These differences are especially pronounced in cases involving nontangent tracks, inclusive of curves and track assets. Table 5-2 presents a comparison of the values derived from the Grubbs test and the ϕ_{75} -line developed by AREMA (2021) (Equation 5-8) (see also Figures D-4 and D-5).

Roghani and Hendry (2017) showed defect locations correspond to areas with low modulus (indicative of higher VTD) and high variability in track modulus. Furthermore, Behnia and Hendry (2024) demonstrated that rail surface alterations amplify the magnitude of dynamic loads. Upon assessing the impact of VTD_{sub} on rail surface changes, a direct correlation is apparent between increasing VTD_{sub} and rail surface values for good and average track conditions. Conversely, a gradual decrease (and even a steady state trend) in rail surface with increasing VTD_{sub} values is evident for poor track conditions. This relationship explains the gradual decrease in ϕ values at higher VTD_{sub} values, particularly for poor track conditions.

Dynamic load measurements, recorded in-service, depend on a range of train speeds. As shown in Figure 5-5 (see also Figures D-4 and D-5), these representations accentuate the importance of accounting for speed-related variations. Thus, the later phase of this research was dedicated to exploring the combined influence of speed and VTD_{sub} on ϕ values.

5.6.2. Evaluation of the effect of VTD_{sub} and speed (S) on ϕ

Given the well-established dependence of ϕ on train speed (S), this research investigates the combined effect of S and subgrade stiffness (VTD_{sub}) on ϕ values. Figure 5-6 shows the maximum Grubbs values of ϕ measured by the IWS system based on 5 km/h increments of train speed and 0.4 mm increments of VTD_{sub} from the MRail system measurements, conducted on data for tangent track, the low rail in curve, and track assets (see also Figure D-8 for the high rail in curve). This

figure offers valuable insight into how changes in train speed impact the influence of VTD_{sub} on ϕ values. As previously noted, this study focuses on four distinct train speeds corresponding to different track classes and the maximum train speed with an appropriate number of data points. Figure 5-7 (see also Figure D-9) shows increasing train speed amplifies the influence of VTD_{sub} variations on ϕ values. In addition, Figures 5-6 and 5-7 highlight that ϕ values tend to increase more for average track than for good track across all track categories.

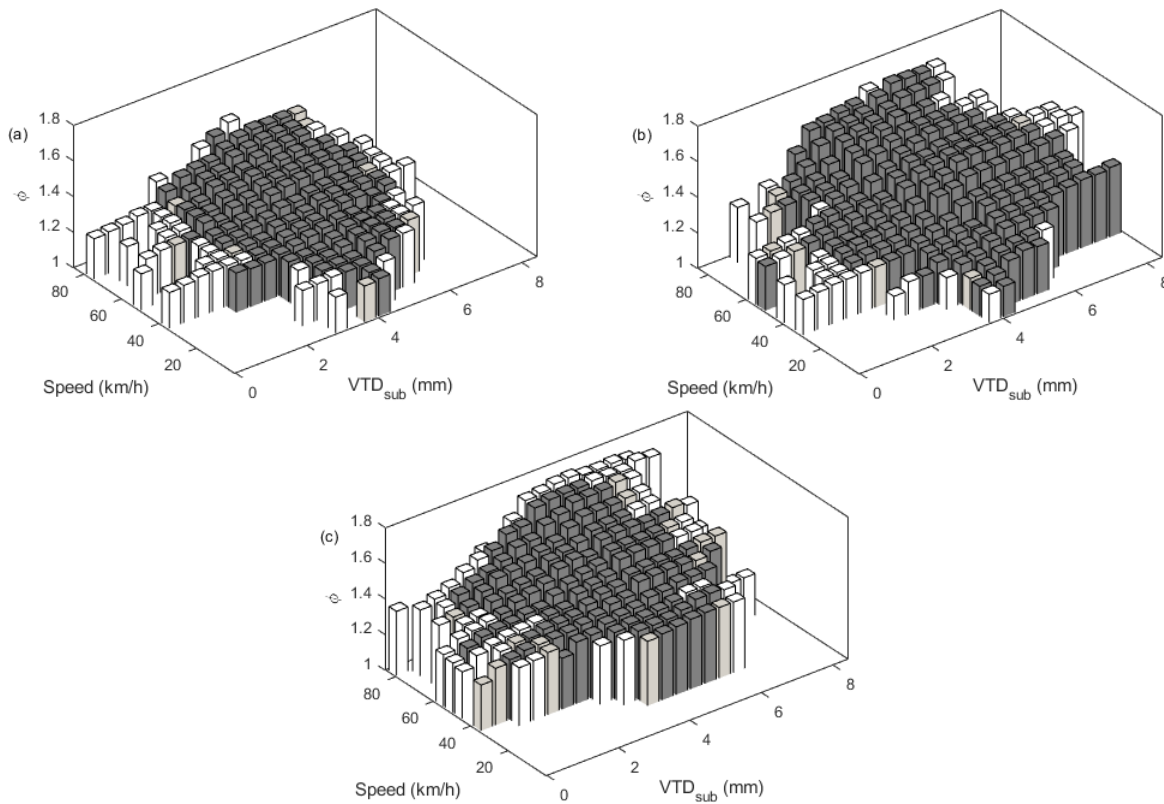


Figure 5-6. Grubbs values of dynamic load factor ($\phi \geq 1.1$) values for 5 km/h increments of train speed and 0.4 mm increments of VTD_{sub} on: (a) tangent sections; (b) low rail in curves; and (c) track assets.

For tangent track, the measured ϕ values exceed the values estimated by Equation 5-6 for VTD_{sub} values >4 mm (Figure 5-7(a)). Specifically, Equation 5-6 underestimates ϕ values by less than 10% for average and poor track but provides accurate estimations for good track. For the low rail on curve, the measured ϕ values exceed the estimates developed by Equation 5-7 (for nontangent track) for VTD_{sub} values greater than 4 mm by around 10% (Figure 5-7(b)). Nevertheless, for the

high rail in curve sections, Equation (5-7) more accurately captures the magnitude of dynamic loads (Figure D-9). These observations highlight how critical VTD_{sub} values (> 4 mm) leading to elevated loads primarily occur for the low rail on curve. When VTD_{sub} values surpass 3.6 mm in track assets, the estimates provided by Equation (5-7) for nontangent track tend to underestimate the dynamic load by around 10%.

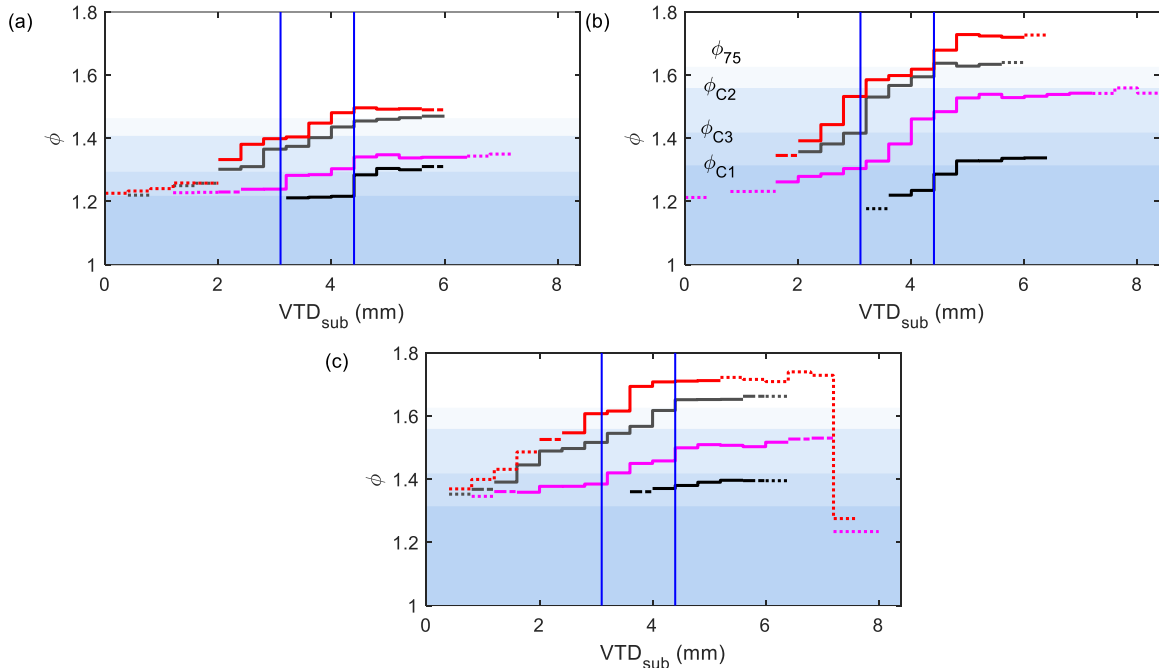


Figure 5-7. IWS and VTD_{sub} (measured by MRail) measurements based on the Grubbs values of the dynamic load factor ($\phi \geq 1.1$) for 0.4 mm increments of VTD_{sub} with respect to significance conditions for four specific train speeds on: (a) tangent tracks; (b) low rail in curves; and (c) track assets. Note the specific speeds include $S= 15$ km/h (~ 10 mph, in black), 40 km/h (25 mph, in magenta), 65 km/h (~ 40 mph, in grey), and 75 km/h (~ 47 mph, in red) and the shaded regions represent the ϕ value based on the specific speeds (ϕ_{C1} , ϕ_{C2} , ϕ_{C3} , and ϕ_{75}) and equations developed by Behnia et al. (2022). The solid, dash-dot, and dotted lines correspond to high, medium, and low reliability zones, respectively. The graph is segregated into three sections by blue lines, indicating good ($VTD_{sub} \leq 3.1$), average ($3.1 < VTD_{sub} \leq 4.4$), and poor ($VTD_{sub} > 4.4$) tracks.

The ϕ values provided by Equation 5-8 closely align with the estimates reported by Behnia et al. (2022) for tangent track at higher speeds, differing by around 10% (see also Figure D-10). However, Equation 5-8 underestimates ϕ values by more than 20% at lower speeds. Additionally, ϕ values for the low rail in curves when VTD_{sub} is greater than 2.4 mm exceed the estimates provided by Equation 5-8 by more than 20%. For the high rail, critical values of VTD_{sub} greater

than 3.2 mm result in an underestimation by Equation 5-8 of around 15% (Figure D-11). For track assets, the estimates provided by Equation 5-8 tend to be 25 to 30% lower than the measured loads when VTD_{sub} values exceed 1.2 mm.

Furthermore, the data were evaluated using the delta approach ($\Delta\phi$), subtracting estimated values ($\phi_{estimated}$) from measured values ($\phi_{measured}$) (Equation 5-9). The Δ -procedure compares measured ϕ values with those calculated from previously established equations (Equations 5-6, 5-7, and 5-8), helping identify discrepancies. The delta (Δ) method systematically identifies uncertainties from input parameters, such as train speed (S) and track stiffness (VTD_{sub}), to the output quantity of interest - the ϕ values (Kasy, 2019; Serfling, 2009; Kurowicka and Cooke, 2006; Lehmann and Casella, 2006). Accordingly, this method quantitatively evaluates how individual parameters (S , VTD_{sub}) and combined effects from various track structures influence the output ϕ values.

$$\Delta\phi = \phi_{estimated} - \phi_{measured}$$

Equation 5-9

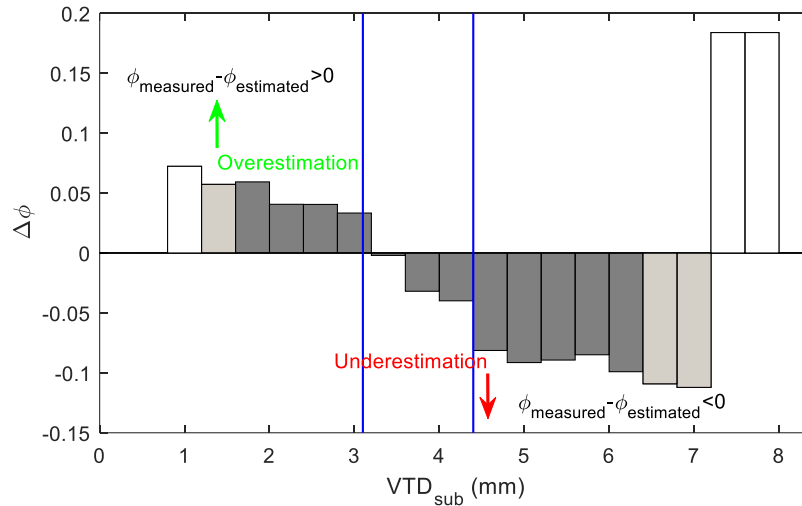


Figure 5-8. Example of comparing the dynamic load factor (ϕ) obtained using the Grubbs test with the equations developed by Behnia et al. (2022) for 0.4 mm increments of VTD_{sub} in track Class 2 (40 km/h [25 mph]) on track assets. The graph is segregated into three sections by blue lines, indicating good ($VTD_{sub} \leq 3.1$), average ($3.1 < VTD_{sub} \leq 4.4$), and poor ($VTD_{sub} > 4.4$) tracks.

A resulting delta value below zero indicates a problem with underestimation. This approach shows the $\phi_{estimated}$ values from Equations 5-6 and 5-7 underestimate measured values by less than 10% across both tangent and nontangent tracks. These underestimations mainly occur for average and poor tracks. In contrast, the $\phi_{estimated}$ values from Equation 5-8 have more substantial underestimations, exceeding 20% for the tangent track and are approximately 30% for the nontangent sections. Figure 5-8 shows an example of this delta approach.

For the final evaluation of the influence of subgrade stiffness on ϕ values along various track structures, this study considered three loading scenarios (tangent tracks, curve sections, and track assets) and three subgrade stiffness conditions (good, average, and poor). Quadratic equations fit the ϕ values derived using Grubbs' test as a function of train speed regarding subgrade stiffness conditions. Figure 5-9 visually shows these equations. The curves reveal increasing trends of ϕ values with increasing train speeds, which becomes more pronounced with worsening subgrade stiffness conditions. These findings establish the range of ϕ values for different track structures that may experience in service, dependent upon the subgrade stiffness conditions. Table 5-3 quantitatively compares the impact of worsening subgrade conditions on ϕ values across different track structures. Worsening subgrade conditions can increase the ϕ values by up to 9% in tangent sections and 15% in non-tangent sections compared to good subgrade conditions. The ϕ values provided by AREMA (2021) tend to underestimate the measured values, even for good subgrade conditions. However, the estimations by Behnia et al. (2022) can capture the ϕ values along good subgrade conditions, while the measured loads surpass estimations in average and poor subgrade scenarios.

The measurements used in this paper significantly differ from those obtained from instrumented tracks (such as Ngamkhanong et al. (2022) from a specific transition zone). The latter captured the

loads induced by various locomotives, car types, and wheel conditions on a consistent track section. In contrast, the current study's results primarily reflect the diverse track conditions (structures) encountered by the IWS system. The authors suggest these two approaches are complementary, as neither dataset fully captures the dynamic loads exerted on the rails. The combined insights are expected to further increase the range of ϕ based on the subgrade stiffness conditions. Future research should integrate these measurement methodologies to provide a more detailed analysis.

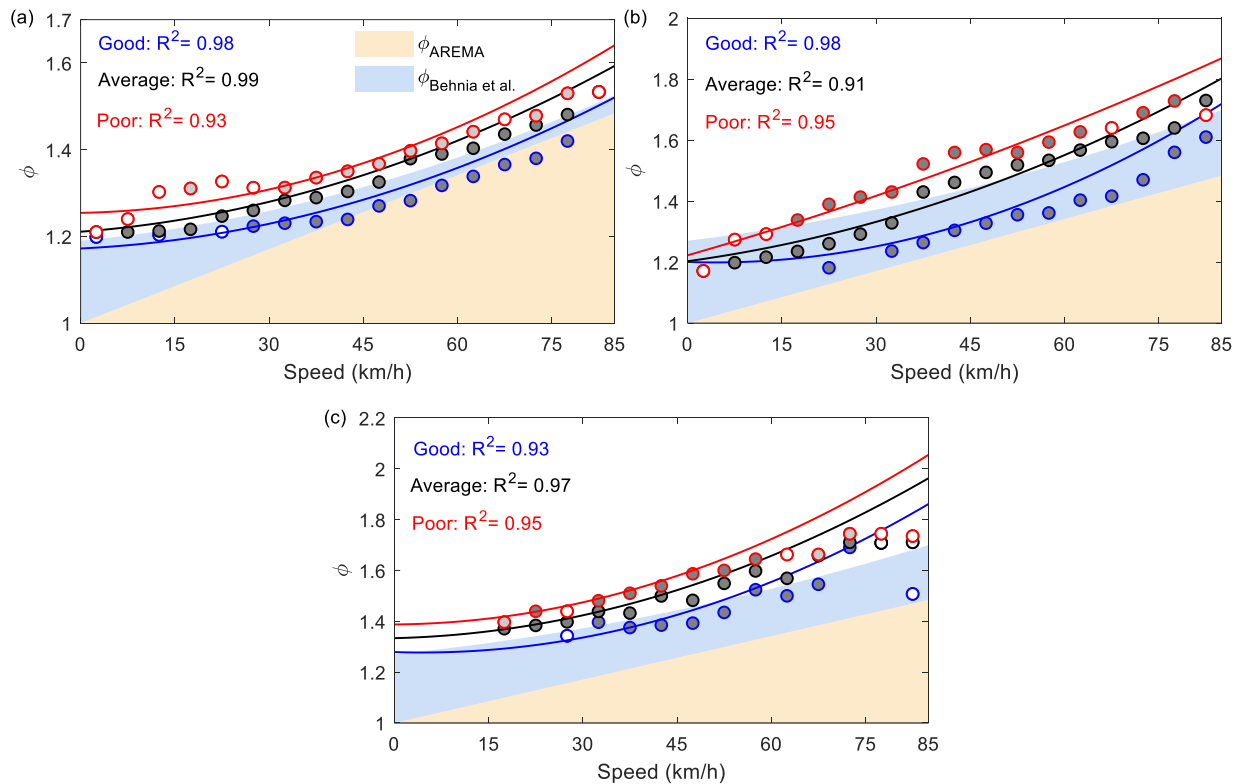


Figure 5-9. Fitted quadratic lines over dynamic load factor (ϕ) values measured through the IWS system based on three scenarios for subgrade stiffness conditions (good, average, and poor) for 5 km/h increments of train speed across: (a) tangent track; (b) curve sections; and (c) track assets.

5.7. Conclusion

This study analyzed the impact of subgrade stiffness (VTD_{sub}) conditions on dynamic load magnitudes, in terms of ϕ , through the measurements derived from IWS and MRail systems. This study differs from previous investigations that have relied on instrumented track sections for

evaluation. The instrumented sections of the track record the dynamic load magnitudes of all types of cars and conditions passing over the site while under constant track conditions. For this study, the measured data were collected from a single car type under constant conditions across a diverse range of track conditions over 340 km of in-service track. The findings of this study demonstrated the significant impact of subgrade stiffness, track structures, and variations in train speed on dynamic loads. The observed loads exceeded previous estimations, particularly for track assets (inclusive of crossings, switches, and bridges), and under average or poor subgrade conditions. VTD_{sub} values exceeding 3.6 mm (i.e., average and poor subgrade conditions) are critical, resulting in elevated loads compared to previous estimations. This understanding could enable the development of targeted monitoring and maintenance strategies for vulnerable track sections exhibiting such defects, leading to more effective and efficient maintenance practices. The estimations proposed by Behnia et al. (2022) (Equations 5-6 and 5-7) demonstrated better performance compared to the AREMA (2021) (Equation 5-8) estimations. Equations of ϕ as functions of speed and subgrade conditions were developed to quantify this range. These equations revealed that worsening subgrade conditions can amplify the ϕ values, with increases of up to 9% observed in tangent tracks and up to 15% in nontangent sections compared to good subgrade conditions. Further research is recommended to evaluate the impact of subgrade track stiffness (VTD_{sub}) on ϕ values while incorporating track conditions and variations in car types and conditions. Additionally, future investigation should consider the directional aspects of transitions (i.e., from soft to stiff or vice versa) to gain a more comprehensive understanding of dynamic loads along railway tracks.

5.8. Acknowledgement

The authors thank the Canadian National Railway for their support and facilitation of this project and specifically Tom Edwards for facilitating the collection of these datasets. This research was made possible through the Canadian Rail Research Laboratory (www.carri.ca). Funding was provided by the Natural Sciences and Engineering Research Council of Canada (NSERC IRC 523369-18), Canadian National Railway, the National Research Council Canada, and Transport Canada.

5.9. References

- AREMA (American Railway Engineering and Maintenance of Way Association). (2021). *Manual for railway engineering*. Lanham, MD: AREMA.
- Arnold, R., Lu, S., Hogan, C., Farritor, S., Fateh, M., & El-Sibaie, M. (2006, September). Measurement of vertical track modulus from a moving railcar. In: *Proceedings of the AREMA Annual Conference, Louisville, KY*.
- ASTM. (2021). *Standard practice for dealing with outlying observations. ASTM E178-02*. West Conshohocken, PA: ASTM.
- Balasubramanian, V., Ho, S. S., & Vovk, V. (Eds.). (2014). *Conformal prediction for reliable machine learning: theory, adaptations and applications*. Newnes.
- Barbosa, R. S. (2016). Evaluation of railway track safety with a new method for track quality identification. *Journal of Transportation Engineering*, 142(11), 04016053.
- Bartlett II, J.E., Kotrlik, J.W., and Higgins, C.C. (2001). Organizational research: Determining appropriate sample size in survey research. *Information Technology, Learning, and Performance Journal*, 19(1), 43.

- Behnia, D., & Hendry, M. T. (2023, Submitted). Quantifying the impact of rail profile changes on the magnitude of dynamic loads through instrumented wheelset measurements. *Journal of Vehicle System Dynamics*, Taylor & Francis.
- Behnia, D., Hendry, M. T., Haji Abdulrazagh, P., & Wahba, A. (2022). Railway dynamic load factors developed from instrumented wheelset measurements. *Journal of Transportation Engineering, Part A: Systems*, 148(7), 04022042.
- Berggren, E. (2009). Railway Track Stiffness – Dynamic Measurements and Evaluation for Efficient Maintenance. Doctoral Thesis, Rail Vehicles, KTH, TRITA AVE 2009:17, ISBN 978-91-7415-293-7, Stockholm, Sweden, 2009.
- Bracciali, A., Cavaliere, F., & Macherelli, M. (2014, April). Review of instrumented wheelset technology and applications. In *Proc. 2nd Int. Conf. Railway Technol., Res., Develop. Maintenance (pp. 1-16)*.
- Cai, X., Zhang, Q., Wang, Q., Cui, X., & Dong, B. (2022). Effects of the subgrade differential arch on damage characteristics of CRTS III slab track and vehicle dynamic response. *Construction and Building Materials*, 327, 126982.
- Cakdi, S., Cummings, S., & Punwani, J. (2015, March). Heavy haul coal car wheel load environment: Rolling contact fatigue investigation. In *ASME/IEEE Joint Rail Conference (Vol. 56451, p. V001T02A005)*. American Society of Mechanical Engineers.
- Cochran, W. G. (1977). *Sampling techniques*. John Wiley & Sons.
- Code, U. I. C. (2008). *719R Earthworks and track bed for railway lines*. Paris: Union Internationale des Chemins de Fer, 117.

- Collell, G., Prelec, D., & Patil, K. R. (2018). A simple plug-in bagging ensemble based on threshold-moving for classifying binary and multiclass imbalanced data. *Neurocomputing*, 275, 330-340.
- Di Leo, G., & Sardanelli, F. (2020). Statistical significance: p value, 0.05 threshold, and applications to radiomics—reasons for a conservative approach. *European radiology experimental*, 4, 1-8.
- Ebersöhn, W., & Selig, E. T. (1994). Track modulus measurements on a heavy haul line. *Transportation Research Record*, 1470, 73.
- Esveld, C. (2001). *Modern railway track*. (Vol. 385). Zaltbommel: MRT-productions.
- Faizi, K., Beetham, P., & Kromanis, R. (2023). Performance evaluation of rail track bed stiffness: pre and post stabilisation. *Construction and Building Materials*, 407, 133452.
- Fallah Nafari, S., Gül, M., Hendry, M. T., & Cheng, J. R. (2018a). Estimation of vertical bending stress in rails using train-mounted vertical track deflection measurement systems. *Proceedings of the Institution of Mechanical Engineers, Part F: Journal of Rail and Rapid Transit*, 232(5), 1528-1538.
- Fallah Nafari, S., Gül, M., Hendry, M. T., Otter, D., & Roger Cheng, J. J. (2018b). Operational vertical bending stresses in rail: Real-life case study. *Journal of Transportation Engineering, Part A: Systems*, 144(3), 05017012.
- Farritor, S. (2006). Real-time measurement of track modulus from a moving car. (No. DOT/FRA/ORD-05/05), U.S. Dept. of Transportation, Washington, DC.
- Farritor, S., & Fateh, M. (2013). Measurement of vertical track deflection from a moving rail car. (No. DOT/FRA/ORD-13/08). United States. Federal Railroad Administration. Office of Research and Development.

- Greisen, C. J. (2010). Measurement, simulation, and analysis of the mechanical response of railroad track. M.Sc. dissertation, Dept. of Mechanical Engineering, Univ. of Nebraska, Lincoln, NE.
- Greisen, C., Lu, S., Duan, H., Farritor, S., Arnold, R., GeMeiner, B., ... & Carr, G. (2009, January). Estimation of rail bending stress from real-time vertical track deflection measurement. In *Joint Rail Conference (Vol. 43383, pp. 175-182)*.
- Grossoni, I., Andrade, A. R., Bezin, Y., & Neves, S. (2019). The role of track stiffness and its spatial variability on long-term track quality deterioration. *Proceedings of the Institution of Mechanical Engineers, Part F: Journal of Rail and Rapid Transit*, 233(1), 16-32.
- Guo, Y., Shi, C., Zhao, C., Markine, V., & Jing, G. (2022). Numerical analysis of train-track-subgrade dynamic performance with crumb rubber in ballast layer. *Construction and Building Materials*, 336, 127559.
- Heydari, H. (2023). Evaluating the dynamic behavior of railway-bridge transition zone: numerical and field measurements. *Canadian Journal of Civil Engineering*.
- Higgins, R. L., Otter, D. E., & Martin, R. W. (1992, January). High accuracy load measuring wheelset. In *Tenth International Wheelset Congress: Sharing the Latest Wheelset Technology in Order to Reduce Costs and Improve Railway Productivity*. Preprints of Papers (pp. 181-188). Barton, ACT: Institution of Engineers, Australia.
- Indraratna, B., Sajjad, M. B., Ngo, T., Correia, A. G., & Kelly, R. (2019). Improved performance of ballasted tracks at transition zones: A review of experimental and modelling approaches. *Transportation Geotechnics*, 21, 100260.

- Judge, A., Ho, C., Huang, H., Hyslip, J., & Gao, Y. (2018). Field investigation and modeling of track substructure performance under trains moving at critical speed (Report No. DOT/FRA/ORD-18/21).
- Kasy, M. (2019). Uniformity and the delta method. *Journal of Econometric Methods*, 8(1), 20180001.
- Kerr, A. D. (1983). A Method for Determining the Track Modulus Using A Locomotive Or Car On Multi-Axle Trucks. *Proceedings of the American Railway Engineering Association*, 84, 269-286.
- Kish, A., & Samavedam, G. (2013). *Track buckling prevention: theory, safety concepts, and applications* (No. DOT/FRA/ORD-13/16). John A. Volpe National Transportation Systems Center (US).
- Krejcie, R. V., & Morgan, D. W. (1970). Determining sample size for research activities. *Educational and psychological measurement*, 30(3), 607-610.
- Kurowicka, D., & Cooke, R. M. (2006). *Uncertainty analysis with high dimensional dependence modelling*. John Wiley & Sons.
- Lehmann, E. L., & Casella, G. (2006). *Theory of point estimation*. Springer Science & Business Media.
- Leishman, E. M., Hendry, M. T., & Martin, C. D. (2017). Canadian main track derailment trends, 2001 to 2014. *Canadian Journal of Civil Engineering*, 44(11), 927-934.
- Lenth, R. V. (2001). Some practical guidelines for effective sample size determination. *The American Statistician*, 55(3), 187-193.
- Smith, L., Doe, B., Li, D., Otter, D., & Uppal, S. (2003). Study of bridge approach and track transition degradation: Factors and mitigation.

- Li, D., Thompson, R., Marquez, P., and Kalay, S. (2004). Development and Implementation of a Continuous Vertical Track-Support Testing Technique. *Transportation Research Record: Journal of the Transportation Research Board*, 1863, 68–73.
- Liu, W., & Wang, W. (2002). Study on dynamic stiffness and damp measurement of railway crushed stone ballast. *Journal of the China Railway Society*, 24(6), 99-104.
- Lu, S. (2008). Real-time vertical track deflection measurement system. *Ph.D. dissertation, Dept. of Mechanical Engineering, Univ. of Nebraska, Lincoln, NE.*
- Lu, S., Hogan, C., Minert, B., Arnold, R., Farritor, S., GeMeiner, W., & Clark, D. (2007, January). Exception criteria in vertical track deflection and modulus. In *ASME/IEEE Joint Rail Conference (Vol. 4787, pp. 191-198).*
- Lundqvist, A., & Dahlberg, T. (2005). Railway track stiffness variation-consequences and countermeasures. In *19th IAVSD Symposium of Dynamics of Vehicles on Roads and Tracks, Milano, August 29-September 2, 2005.* Department of Mechanical Engineering, Politecnico di Milano.
- McVey, B. (2006). A nonlinear approach to measurement of vertical track deflection from a moving railcar. *M.Sc. dissertation, Department of Mechanical Engineering, University of Nebraska-Lincoln, Lincoln, NE.*
- McVey, B., Norman, C., Wood, N., Farritor, S., Arnold, R., Fateh, M., & El-Sibaie, M. (2005, September). Track modulus measurement from a moving railcar. In *Proceedings of the AREMA Annual Conference, Chicago, IL.*
- Mei, H., Leng, W., Nie, R., Tu, R., Li, Y., & Dong, J. (2019). Experimental research on the dynamic response characteristics of the transition subgrade induced by heavy-haul train

- passage. *Proceedings of the Institution of Mechanical Engineers, Part F: Journal of Rail and Rapid Transit*, 233(9), 974-987.
- Memon, M. A., Ting, H., Cheah, J. H., Thurasamy, R., Chuah, F., & Cham, T. H. (2020). Sample size for survey research: Review and recommendations. *Journal of Applied Structural Equation Modeling*, 4(2):1-20.
- Nanjundeswaraswamy, T. S., & Divakar, S. (2021). Determination of sample size and sampling methods in applied research. *Proceedings on engineering sciences*, 3(1), 25-32.
- Ngamkhanong, C., Ming, Q. Y., Li, T., & Kaewunruen, S. (2020). Dynamic train-track interactions over railway track stiffness transition zones using baseplate fastening systems. *Engineering Failure Analysis*, 118, 104866.
- Norman, C., Farritor, S., Arnold, R., Elias, S. E. G., Fateh, M., and Sibaie, M. E. (2004). Design of a system to measure track modulus from a moving railcar. In: *Proceeding of Railway Engineering, Engineering Technics Press, Edinburgh, U.K.*
- Oberkampf, W. L., DeLand, S. M., Rutherford, B. M., Diegert, K. V., & Alvin, K. F. (2002). Error and uncertainty in modeling and simulation. *Reliability Engineering & System Safety*, 75(3), 333-357.
- Peters, N. (2010). *CN railway engineering course*. Montreal: McGill Univ.
- Punetha, P., & Nimbalkar, S. (2023). An innovative rheological approach for predicting the behaviour of critical zones in a railway track. *Acta Geotechnica*, 18(10), 5457-5483.
- Puzavac, L., Popović, Z., & Lazarević, L. (2012). Influence of track stiffness on track behaviour under vertical load. *Promet- Traffic & Transportation*, 24(5), 405-412.
- Raymond, G. P. (1985). Analysis of track support and determination of track modulus. *Transportation Research Record*, 1022, 80-90.

- Read, D., Chrismer, S., Ebersöhn, W., and Selig, E. T. (1994). Track modulus measurements at the Pueblo soft subgrade site. *Transportation Research Record*, 1470, 55–64.
- Remennikov, A. M., & Kaewunruen, S. (2008). A review of loading conditions for railway track structures due to train and track vertical interaction. *Structural Control and Health Monitoring: The Official Journal of the International Association for Structural Control and Monitoring and of the European Association for the Control of Structures*, 15(2), 207-234.
- Ren, Y., & Chen, J. (2019). A new method for wheel–rail contact force continuous measurement using instrumented wheelset. *Vehicle System Dynamics*, 57(2), 269-285.
- Roghani, A., & Hendry, M. T. (2016). Continuous vertical track deflection measurements to map subgrade condition along a railway line: Methodology and case studies. *Journal of Transportation Engineering*, 142(12), 04016059.
- Roghani, A., & Hendry, M. T. (2017). Quantifying the impact of subgrade stiffness on track quality and the development of geometry defects. *Journal of Transportation Engineering, Part A: Systems*, 143(7), 04017029.
- Roghani, A., Macciotta, R., & Hendry, M. (2015, March). Combining track quality and performance measures to assess track maintenance requirements. In *ASME/IEEE Joint Rail Conference (Vol. 56451, p. V001T01A009)*. American Society of Mechanical Engineers.
- Roghani, A., Macciotta, R., & Hendry, M. T. (2017). Quantifying the effectiveness of methods used to improve railway track performance over soft subgrades: methodology and case study. *Journal of Transportation Engineering, Part A: Systems*, 143(9), 04017043.
- Sadeghi, J. (2012). New advances in analysis and design of railway track system. *Journal of Reliability and Safety in Railway*, 30(3), 75-100.

- Selig, E. T., & Li, D. (1994). Track modulus: Its meaning and factors influencing it. *Transportation Research Record, 1470*, 47-54.
- Sendra-Perez, C., Sanchez-Jimenez, J. L., Marzano-Felisatti, J. M., Encarnacion-Martinez, A., Salvador-Palmer, R., & Priego-Quesada, J. I. (2023). Reliability of threshold determination using portable muscle oxygenation monitors during exercise testing: a systematic review and meta-analysis. *Scientific Reports, 13*(1), 12649.
- Serfling, R. J. (2009). *Approximation theorems of mathematical statistics*. John Wiley & Sons; September 25.
- Smith, S. W. (1997). *The scientist and engineer's guide to digital signal processing*. California Technical Publication, San Diego.
- Soleimani, H., & Moavenian, M. (2017). Tribological aspects of wheel–rail contact: a review of wear mechanisms and effective factors on rolling contact fatigue. *Urban Rail Transit, 3*(4), 227-237.
- Sussman, T. R., Ebersöhn, W., & Selig, E. T. (2001). Fundamental nonlinear track load-deflection behavior for condition evaluation. *Transportation Research Record, 1742*(1), 61-67.
- Taber, K. S. (2018). The use of Cronbach's alpha when developing and reporting research instruments in science education. *Research in science education, 48*, 1273-1296.
- Tong, Y., Liu, G., Yousefian, K., & Jing, G. (2022). Track vertical stiffness–value, measurement methods, effective parameters and challenges: A review. *Transportation Geotechnics, 100833*.
- Wang, P., Wang, L., Chen, R., Xu, J., Xu, J., & Gao, M. (2016). Overview and outlook on railway track stiffness measurement. *Journal of Modern Transportation, 24*, 89-102.

- Woelfle, A. (2016). In *Analysis of wheel-rail forces during (MRail) rolling deflection tests*. Report for the National Research Council. Gloucester, ON, Canada: National Research Council Canada, Automotive and Surface Transportation.
- Zarembski, A. M. & Choros, J. (1979). On the measurement and calculation of vertical track modulus. *Proceedings of the American Railway Engineering Association*, 81, 156-173.
- Zhang, D., Zhai, W., & Wang, K. (2017). Dynamic interaction between heavy haul train and track structure due to increasing axle load. *Australian Journal of Structural Engineering*, 18(3), 190–203. <https://doi.org/10.1080/13287982.2017.1363126>.

6. Quantifying the Impact of Subgrade Stiffness Transition Directions on Railway Dynamic Load Factor

6.1. Contribution of the Ph.D. candidate

All the work presented in this chapter, which includes data processing, review of literature, analysis and discussion of the results, and writing of the text, is carried out by the Ph.D. candidate. As a supervisor, Dr. M.T. Hendry has reviewed all parts of the work. This chapter is submitted (March, 2024) for publication in the Journal of Transportation Geotechnics with the following citation:

Behnia, D., Hendry, M.T. (2024). “Quantifying the impact of subgrade stiffness transition directions on railway dynamic load factor.” Journal of Transportation Geotechnics (Elsevier).

6.2. Abstract

This study comprehensively evaluated how the transition direction (i.e., *soft-to-stiff* and *stiff-to-soft*) affects the magnitude of dynamic loads in terms of the dynamic load factor (ϕ). The datasets for this study were obtained from a 340 km railway track operated by a North American Class 1 freight railway that traverses the Canadian Prairies. The analysis integrated two primary datasets: dynamic load magnitudes collected via an instrumented wheelset (IWS) system and subgrade stiffness changes (ΔVTD_{sub}) calculated through MRail measurements. Given the pivotal role of ϕ values in railway design, particularly in decisions related to design of track structures, rail steel selection, and cross-sectional specifications, this investigation focused on evaluating ϕ values. The findings revealed that *soft-to-stiff* transitions amplify the magnitude of dynamic loads, whereas the reverse transition attenuates these loads. In particular, *soft-to-stiff* transitions can lead to an approximate 10% rise in ϕ values compared to the opposite transition. Furthermore, the study

underscored the substantial impact of subgrade conditions (VTD_{sub}) on dynamic load variations concerning transition direction.

6.3. Introduction

Variations in track stiffness can yield diverse effects on wheel-rail interactions, causing uneven settlement and potential amplification of dynamic loads (Behnia and Hendry, 2024a; Roghani and Hendry, 2017; Li and Berggren, 2010; Berggren, 2009; Burrow et al., 2009; UIC Code, 2008; Hunt and Wood, 2005). Significant variations in track stiffness have been pinpointed as a factor contributing to the accelerated deterioration of track geometry and later development of track geometry defects, which in turn can amplify the magnitude of dynamic loads (Behnia and Hendry, 2024b; Davis et al., 2003; Zaremski and Palese, 2003; Esveld, 2001; Sussman et al., 2001; Li and Selig, 1995; Cai et al., 1994; Read et al., 1994; Ebersohn et al., 1993) and lead to an increase in the probability of rail breaks.

Transition zones in railway infrastructure, such as locations adjacent to bridges, are critical areas where track stiffness varies significantly. These stiffness variations are a crucial factor influencing dynamic loads in such zones. As a train traverses a track with varying stiffness, the resulting uneven deflections in the track structure can lead to increased dynamic wheel loads (Heydari, 2023; Kurhan et al., 2020; Ngamkhanong et al., 2020; Wang et al., 2018). Rail breaks, failure of track components, and track geometry defects are the leading causes of derailment in both the United States and Canada (Leishman et al., 2017; Liu et al., 2012; TSB, 2013). In light of continuing rail failures, it is worth evaluating the impact of subgrade stiffness variations on the dynamic loading magnitudes along the railway track.

Assessing dynamic loads along railway tracks is paramount for effectively designing superstructures and subgrades (Chen et al., 2013). The dynamic load factor (ϕ), along with the

evaluated dynamic loads, is commonly used to design railway track structures or the selection of rail steel and cross-section (weight) (AREMA, 2021; Sadeghi, 2012; Peters, 2010). The ϕ signifies the ratio between the vertical loads caused by a moving railway vehicle (dynamic loads, P_d) and the static loads (P_s) resulting from the weight of the railcar and its contents (Behnia et al., 2022):

$$P_d = \phi \cdot P_s \quad \text{Equation 6-1}$$

Increasing dynamic loads can lead to accelerated wear and failure of track components, increased maintenance costs, and possible safety risks. Track subgrade stiffness is recognized to significantly influence dynamic load magnitudes (Roghani and Hendry, 2017; Li et al., 2015; Chen et al., 2013), but a specific gap exists in terms of evaluating how transition direction (i.e., *soft-to-stiff* or *stiff-to-soft*) impacts the magnitude of dynamic loads along the track despite this being critical for the design and maintenance of railway tracks. Another limitation of the existing studies on the effect of track stiffness on dynamic load magnitudes is that they have been focused on specific locations, known as instrumented sections of track (Grossoni et al., 2019; Burrow et al., 2009; Burrow et al., 2007; Jimenez, 2003; Thompson and Marquez, 2001; Ebersohn, 1996; Kerr, 1987; Kerr and Shenton, 1985; Kerr, 1983; Choros and Zarembski, 1981; Chang et al., 1980; Esveld, 1980), or those developed through numerical modelling (Lamprea et al., 2021; Quirke et al., 2017; Le et al., 2016; Sadeghi and Hashemi, 2008). It is also essential to comprehend how transition direction affects dynamic loads for the stability and safety of railway operations. The thorough analysis conducted herein can provide a data-driven evaluation of the effect of transition direction on the magnitude of dynamic loads (in terms of ϕ).

This investigation utilizes data collected by train-mounted instrumented wheelset (IWS) and MRail systems, respectively designed to measure dynamic loads and vertical track deflection (*VTD*) during movement. The data reflect dynamic loads and *VTD* values originating from a singular railcar and specific suspension characteristics, wheel diameter, and static load. The measured data encompass a comprehensive range of dynamic load scenarios from diverse track structures (including bridges, grade crossings, curves, and switches) and operational train speeds experienced on a Class 1 freight railway main line.

This paper presents two datasets [dynamic load (ϕ) from the IWS system and subgrade stiffness changes (ΔVTD_{sub}) calculated through the MRail data] and explores how dynamic load magnitudes vary with transition direction within the section of track studied. It also evaluates the statistical distributions of dynamic loads and ΔVTD_{sub} , evaluating the influence of the transition direction in comparison to other ϕ values considered for North American freight railways. The ϕ values obtained from IWS measurements are subject to evaluation based on the transition direction across various track structures, including tangent tracks, curve sections, bridges, grade crossings, and switches. The data are further evaluated to derive ϕ values representing the loading scenarios occurring within the allowable speed ranges on North American track classes (1 through 3), taking transition direction into account. To the best of the authors' knowledge, this study represents the first published research focusing on the influence of transition direction on the magnitude of dynamic loads on a Class 1 North American freight railway based on IWS and MRail datasets.

6.4. Study site

The section of railway track under investigation is operated by a Class 1 North American freight railway. This track is a crucial part of a widely used railway network that traverses the Canadian Prairies with an annual traffic volume of over 50 million gross tonnes (MGT). The study section

is 340 km of track featuring 30 bridges, over 100 grade crossings, 50 switches, and around 83 km of curve sections. The amount of data collected varied for different track structures: tangent sections constituted the majority of the dataset (53.2%), followed by curves (41.5%), grade crossings (2.6%), bridges (1.6%), and switches (1.1%). The track along this section is continuously welded rail (CWR), mainly supported by concrete ties. The maximum recorded train speed along the studied section was 82 km/h (51 mph). The measurements were conducted using a revenue-service railway car and, as a result, there was no control over the type, weight, or travel speed of adjacent railway cars. Such limitations are common when collecting data on Class 1 North American freight railway track.

6.5. Measurement systems

Figure 6-1 shows the instrumented train equipped with the IWS and MRail systems installed on one end of the rail car. These data collection efforts were part of a larger research project focused on the comprehensive evaluation of track performance (Behnia et al., 2024a, 2024b; Behnia et al., 2022; Falla Nafari et al., 2018a, 2018b; Roghani and Hendry, 2016, 2017; Roghani et al., 2017). These instrumentation systems were installed on a gondola car with a length of 15.8 m (52 ft). The gondola car was loaded with gravel, resulting in a total weight of 1,175 kN (264 kips). The IWS system was employed to capture and quantify the dynamic interaction at the interface between the wheel and the rail, and the MRail system was employed to measure the *VTD* of the track when subjected to the movement of the loaded railcar. The gathering of load data along the designated section, facilitated through IWS, comprised four runs (two in each direction). Among these, two runs involved MRail measurements. Hence, this study relied on the two runs encompassing IWS and MRail measurements.

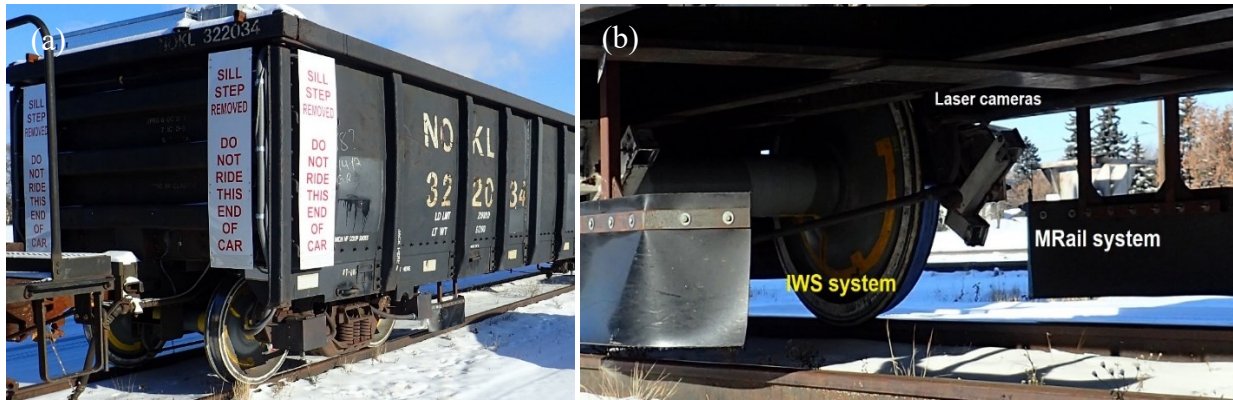


Figure 6-1. Photographs of the instrumented railcar (train-mounted system) with instrumented wheelset (IWS) and MRail systems installed on the Gondola railcar to collect the data used for this study: (a) instrumented railcar; (b) IWS and MRail systems (images by Michael T. Hendry).

6.5.1. Wheel-rail dynamic load measurement system

The gondola car was instrumented with two IWS systems. A single axle was fitted within each system, accommodating two class F wheel plates (915 mm or 36 in. in diameter) equipped with 16 full-bridge Wheatstone strain gauge circuits (Woelfle, 2016). The IWS system measured various force elements, encompassing vertical, lateral, and traction forces, for all four wheels. However, this study primarily considers data on vertical loads in terms of ϕ . The data acquisition process involved continuously monitoring the IWS system at a high sampling frequency of 200 Hz. A 20 Hz low-pass filter was then applied to the measured data during the measurement process (Behnia et al., 2022). During the measurements, a Garmin GPS18X was used to determine the latitude, longitude, time, and speed. Comparing the static load obtained through the system and the scale showed a discrepancy of only 3%, indicating a high level of accuracy in the measurements provided by the IWS system (Behnia et al., 2022). The instrumented wheels exhibited very little wear and were free of defects that could amplify dynamic loads.

6.5.2. Vertical track deflection (VTD) measurement system

The other part of the instrumented car was the MRail system as a rolling deflection measurement system (Figure 6-1). This measurement system represents a notable technological advancement

achieved through collaborative efforts between the University of Nebraska and the Federal Railroad Administration (FRA) (Arnold et al., 2006; Farritor, 2006; Farritor and Fateh, 2013; Griesen, 2010; Lu, 2008; McVey et al., 2005; Norman et al., 2004). The MRail system incorporates laser and camera sensors designed to measure the *VTD* from a distance of 1.22 m relative to the center of the railcar's inboard wheel. The 1.22-meter distance from the nearest wheel represents a trade-off between maximizing measurement distance from the wheel and mitigating increased vibration caused by a longer and heavier beam (Norman, 2004). The laser system mounted above the rails projects a continuous line onto the rail head while an accompanying camera captures images at 90 frames per second. This imaging frequency allows for calculating distances between consecutive measurements, which vary according to the train's speed. Subsequently, the collected data undergo post-processing to yield vertical track deflection (VTD) values at 0.305 m (1 ft.) intervals, ensuring compatibility with other railway industry datasets (e.g., track geometry). The calculation of VTD assumes that the unloaded rail profile is straight and level. The accuracy of VTD measurements was assessed using trackside measurements, which demonstrated an accuracy of 10% (Farritor and Fateh, 2013). The sensor tests demonstrated that the system effectively captures the correct trend in track stiffness (Norman, 2004).

6.6. Quantifying the change of subgrade stiffness (ΔVTD_{sub})

Roghani and Hendry (2016) proposed a procedure to quantify the track subgrade stiffness (VTD_{sub}) by filtering MRail measurements (*VTD*) using a moving average (Equation 6-2; Table 6-1). The calculated VTD_{sub} value primarily reflects vertical track deflection due to subgrade conditions. In Equation 6-2, L (in m) represents a crucial threshold length that governs the filtration process for eliminating lower wavelengths due to surface imperfections, such as rail surface (profile) changes and joints. An appropriate resolution (L) selection depends on the particular dimensions of the

studied features. As Roghani and Hendry (2016) highlighted, adopting $L=20$ m provides the highest accuracy when examining subgrade attributes.

Roghani and Hendry (2017) proposed a procedure to quantify the changes of VTD_{sub} , denoted as ΔVTD_{sub} . ΔVTD_{sub} is determined by evaluating the slope of VTD_{sub} with respect to distance as a transparent and straightforward metric. The calculation of ΔVTD_{sub} involves determining the absolute value of the secant slope of VTD_{sub} , with distance (d) representing the track length over which this slope is evaluated (Equation 6-3; Table 6-1). To maintain methodological consistency with the considered approach and filtering protocols employed for VTD measurements (Roghani and Hendry, 2017), this study set a fixed value of d equal to 20 m for this analysis.

Table 6-1. Mathematical equations to calculate the conversion of VTD to VTD_{sub} and ΔVTD_{sub} .

Expression	Equation (No.)
$VTD_{sub}(i) = \left(0.305 \frac{\sqrt{L}}{L}\right)^{L/(2)(0.305)} \sum_{-L/(2)(0.305)}^{L/(2)(0.305)} VTD[i + j]$	(6-2)
$\Delta VTD_{sub}(x_i) = \left VTD_{sub}(x_i + d/2) - VTD_{sub}(x_i - d/2) \right / d$	(6-3)

Sources: Roghani and Hendry, 2016, 2017.

6.7. Results

This research investigated how subgrade track stiffness (ΔVTD_{sub}) changes regarding transition directions influence dynamic load magnitudes. This investigation applied the procedure delineated in Equation 6-3 to identify the transition direction without considering the absolute function. It indicates that determining the transition direction regarding stiffness variations relies on the real value ($x_i \in R$) of ΔVTD_{sub} , referred to as ΔVTD_{subR} in Equation 6-4.

$$\Delta VTD_{subR}(x_i) = \left(VTD_{sub}(x_i + d/2) - VTD_{sub}(x_i - d/2) \right) / d \quad \text{Equation 6-4}$$

A positive delta value ($\Delta VTD_{subR} > 0$) indicates a *stiff-to-soft* transition, while a negative delta value ($\Delta VTD_{subR} < 0$) signifies a *soft-to-stiff* transition. Behnia and Hendry (2024a) demonstrated the

repeatability and consistency of VTD_{sub} measurements using the MRail system. Figure 6-2 represents a dataset sample from an 80 m tangent track section highlighting the implications of transition direction. The rationale for selecting a tangent track was to minimize the influence of track structures on dynamic load magnitudes. Figure 6-2 includes four passes of the instrumented car, two at lower speeds (45 and 37 km/h) in the westbound direction (Figure 6-2(b)) and two at higher speeds (51 and 55 km/h) in the eastbound direction (Figure 6-2(c)). A comparative analysis of Figures 6-2(b) and 6-2(c) shows soft-to-stiff transitioning (Figure 6-2(b)) amplifies the dynamic load magnitude, whereas the reverse transition (stiff-to-soft) (Figure 6-2(c)) leads to load attenuation. Thus, this study was designed to evaluate the impact of transition direction. The data in Figure 6-2(d) also demonstrate the repeatability of the measurements regarding ΔVTD_{sub} values. In a repeatability analysis of load measurements from the IWS system, Behnia et al. (2022) demonstrated consistency and uniformity in the magnitude and pattern of dynamic loads across multiple test runs. Figure 6-3 displays the statistical distributions of the data collected for various track structures, encompassing tangent tracks, curve sections, grade crossings, bridges, and switches. As mentioned earlier, the datasets used in this study came from two runs incorporating measurements from both IWS and MRail. Behnia et al. (2022) investigated dynamic load magnitudes in diverse track structures, classifying them into two groups based on statistical distributions: tangent and nontangent tracks (inclusive of curve sections, crossings, bridges, and switches). Figure 6-3 also highlights that the narrowest distribution of dynamic loads is observed for tangent tracks, indicating a relatively less frequent occurrence of extreme values than other track structures. The statistical distributions for vertical dynamic loads in track assets and curves, which fall under nontangent sections, exhibit similarities.

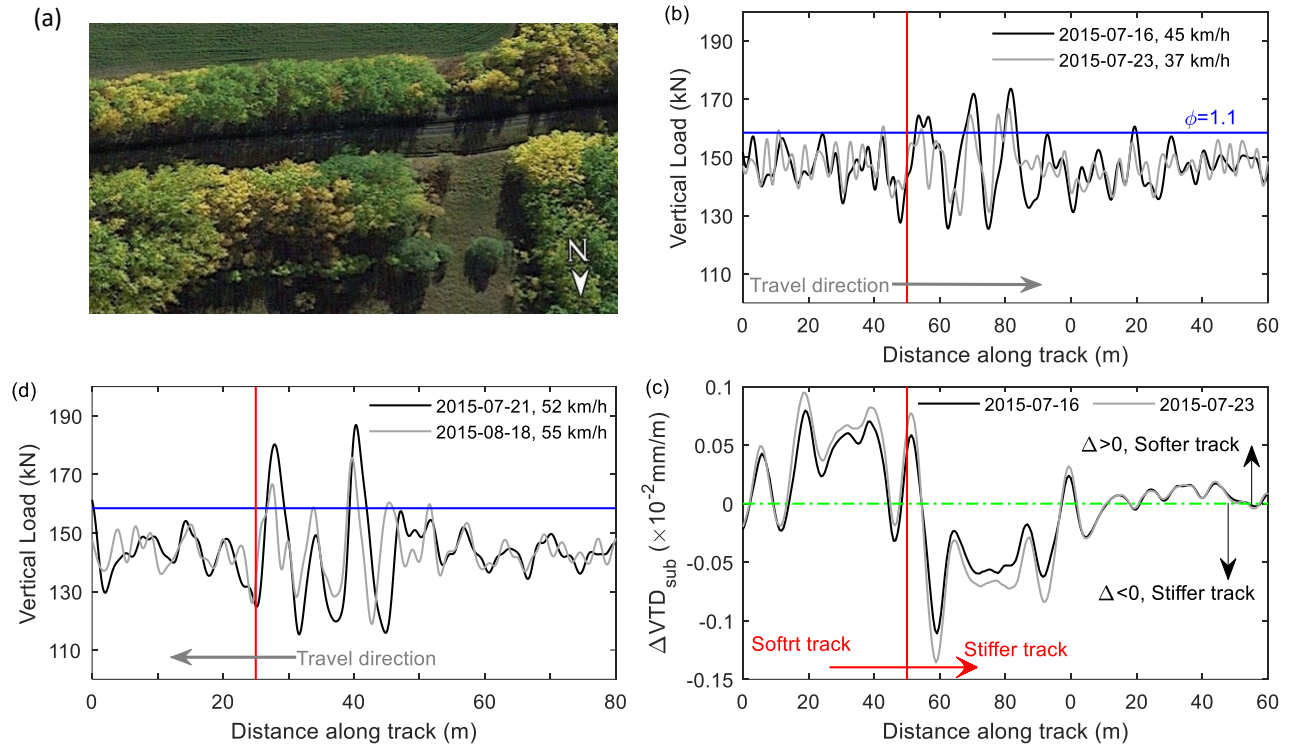


Figure 6-2. (a) Satellite image of the section of track (image © Google, Image © 2023 CNES/Airbus); an example of vertical load and ΔVTD_{sub} data from the instrumented car along a section of tangent track for (b) two slower-moving westbound trains and (c) two faster-moving eastbound trains; and (d) subgrade track stiffness changes along this section of track (in terms of ΔVTD_{sub}).

An approach comprising two key phases was employed to prepare the data. The initial step involved the computation of subgrade track stiffness (VTD_{sub}) through MRail measurements (VTD) in conjunction with Equation 6-2. Subsequently, Equation 6-4 was applied to quantify the changes in subgrade stiffness (ΔVTD_{subR}). Figure 6-4 presents the probability distribution of ΔVTD_{subR} across various track structures, including tangent tracks, curves, grade crossings, bridges, and switches. Figure 6-4(a) demonstrates that tangent tracks and curves share a similar distribution pattern. Grade crossings, bridges, and switches exhibit statistically comparable distributions (Figure 6-4(b)). Given the discerned values of ΔVTD_{subR} across diverse track structures and their respective statistical distributions, a distinctive classification scheme emerged that categorized the

data into 1) tangent and curve tracks and 2) track assets, including grade crossings, bridges, and switches.

It is essential to set a specific threshold value for later analyses to investigate how transition direction influences the magnitude of dynamic loads. To achieve this objective, the authors evaluated three distinct threshold values of 1.3, 1.2, and 1.1 (Figure 6-3). The evaluation of the available dataset and the statistical distributions observed in dynamic loads (Figure 6-3) shows that $\phi \geq 1.1$ is appropriate for later analyses. Given the statistical characteristics of dynamic loads and ΔVTD_{subR} values, a dependable approach involved classifying the available data into three categories: tangent track, curve section, and track assets (inclusive of grade crossings, bridges, and switches).

6.8. Discussion

The ideal sample size (n) was calculated using:

$$n = \frac{Z_{score}^2 \cdot \sigma \cdot (1 - \sigma)}{\lambda^2} \quad \text{Equation 6-5}$$

where n relies on three key parameters (Bartlett et al., 2001), including the standard deviation (σ), the margin of error (λ), and Z_{score} :

$$Z_{score} = \frac{(x - \mu)}{\sigma} \quad \text{Equation 6-6}$$

The Z-score indicates the confidence level, typically 90, 95, or 99%. Within modelling and simulation, a 10% margin of error and a confidence level ranging from 90% to 95% have been considered reasonable (Behnia et al., 2024a, b; Oberkamp et al., 2002). However, achieving a balance between the confidence level and the practical limitations in acquiring a sample size is essential. Thus, in modelling and simulations based on the measured data, a 10% margin of error combined with a confidence level ranging from 90 to 95% was considered reasonable (Behnia and Hendry, 2024a, b; Oberkamp et al., 2002).

The minimum sample size is necessary to obtain reliable results within the typical confidence level range (90-95%) of engineering modeling (Behnia and Hendry, 2024a, b; Oberkamp et al., 2002). Accordingly, this analysis considered three distinct scenarios that represented zones of high reliability (represented by a 95% confidence level, $n \geq 96$, and displayed in dark grey), moderate reliability (associated with a 90% confidence level, $96 < n \leq 68$ and shown in light grey), and low reliability (characterized by a confidence level below 90%, $n < 68$ and denoted in white) (as shown in Figure 6-5).

Because the dynamic load factors (ϕ) are determined using the upper envelope method, the evaluation procedure relied on the maximum load values (see also Figures E-1, E-2, and E-3). Identifying and removing outliers is of utmost importance, as this substantially enhances the dependability of subsequent data analysis (Behnia et al., 2022; ASTM, 2021). Behnia et al. (2022) showed that the Grubbs test is optimal for detecting and eliminating outliers in railway engineering. The Grubbs test value (G) is based on the mean value (μ) and standard deviation (σ) of the dataset, wherein x_i signifies the value of the i^{th} element contained within the dataset:

$$G = \max_{i=1, \dots, n} |x_i - \mu| / \sigma \quad \text{Equation 6-7}$$

This study centers on evaluating the influence of transition direction on the magnitude of dynamic loads, as quantified by the dynamic load factor (ϕ). Three equations were examined for this purpose. These equations were introduced by Behnia et al. (2022) (Equations 6-8 and 6-9), representing a recent advancement in the realm of ϕ calculations, and AREMA (2021) (Equation 6-10), as the widely accepted ϕ values (Table 6-2). This research was conducted over the same study site investigated by Behnia et al. (2022); thus, further analysis primarily relied on Equations 6-8 and 6-9.

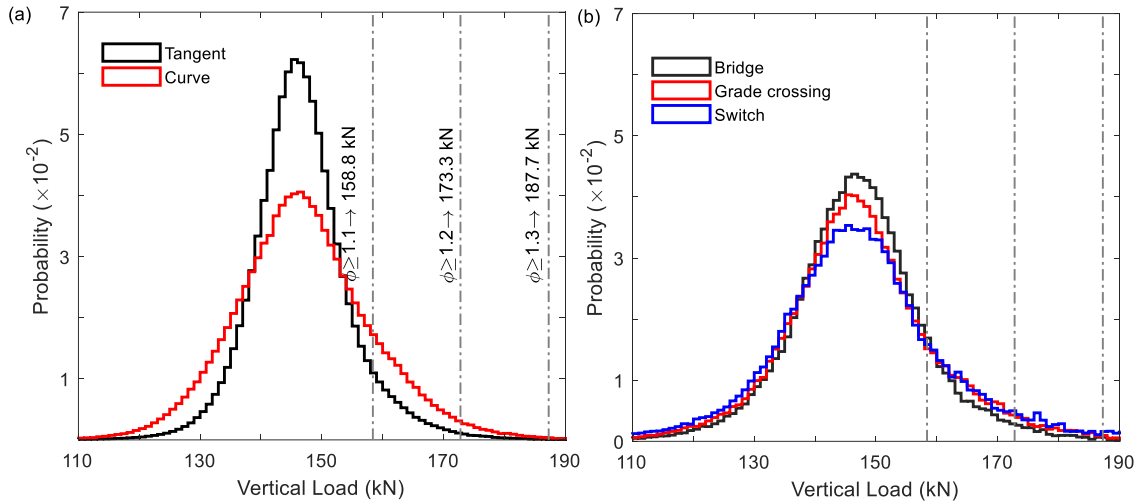


Figure 6-3. Probability distribution plots illustrating vertical load measurements acquired from the IWS system for: (a) tangent and curve sections; and (b) bridges, grade crossings, and switches. Note: The dataset encompasses data collected from all four instrumented wheels across both passes.

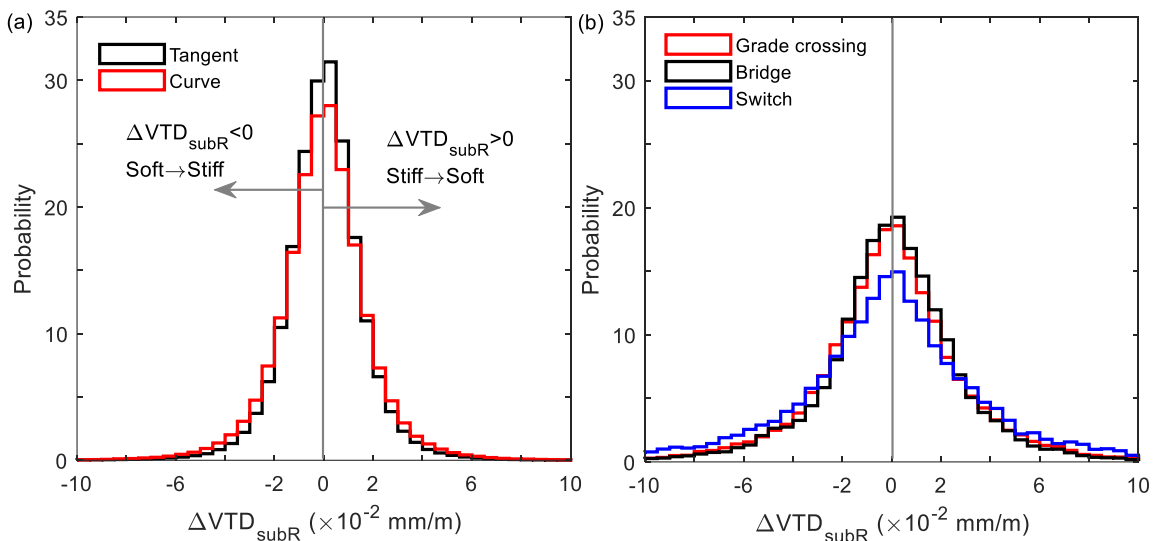


Figure 6-4. Probability distributions of variations in subgrade track stiffness, in terms of ΔVTD_{subR} , based on measurements from the MRail system for: (a) tangent track and curve sections; and (b) bridges, grade crossings, and switches. Note: the data includes both rails and both passes.

The study examines the influence of transition direction on the dynamic load factor (ϕ) through two distinct approaches. The first analysis focuses on the effect of transition direction (ΔVTD_{subR}) on the magnitude of dynamic loads (in terms of ϕ), and the second analysis considers the joint impact of speed (S) and transition direction (ΔVTD_{subR}) on the dynamic loading conditions. The impact of subgrade stiffness conditions (VTD_{sub}) was also considered, given their importance with

respect to the magnitude of dynamic load (Behnia and Hendry, 2024a). Four specific train speeds associated with different track classes and the available datasets were considered. These speeds included 15 km/h (~ 10 mph, Class 1), 40 km/h (25 mph, Class 2), 65 km/h (~ 40 mph, Class 3), and 75 km/h (~ 47 mph) identified as the maximum speed with a reasonable number of data points. Given the size of the dataset, the evaluation approach primarily concentrated on ΔVTD_{sub} values below 0.13.

Table 6-2. Dynamic load factor (ϕ) equations under consideration for assessing the impact of transition direction in freight railways.

Equation for ϕ	Equation (#)	Reference
$\phi_{Tan} = 3 \times 10^{-5} S^2 + 1.4 \times 10^{-3} S + 1.19$ (for tangent track)	(6-8)	Behnia et al. (2022)
$\phi_{NTan} = 3 \times 10^{-5} S^2 + 2.5 \times 10^{-3} S + 1.27$ (for non-tangent track)	(6-9)	
$\phi = 1 + 5.21S/D$	(6-10)	AREMA (2021)

6.8.1. Effect of transition direction (ΔVTD_{subR}) on ϕ

Figure 6-5 presents a comparative analysis of the maximum ϕ values derived from the Grubbs test on IWS measurements across various categories. These comparisons were conducted for 0.01 mm/m increments of ΔVTD_{sub} in both transition directions (ΔVTD_{subR}). Across all categories, the magnitude of dynamic loads during the soft-to-stiff ($\Delta VTD_{subR} < 0$) transition surpassed those observed for the stiff-to-soft ($\Delta VTD_{subR} > 0$) transition. These observations underscore that soft-to-stiff transitions amplify dynamic load magnitudes while stiff-to-soft transitions attenuate dynamic loads. The extent of these amplifications and attenuations falls within 5 to 10%.

The highest attainable train speed (S) with a reasonable number of data points was 75 km/h (while S_{max} was 82 km/h). Therefore, the estimated value by Behnia et al. (2022) at $S=75$ km/h was regarded as the reference value (ϕ_{75}) for the maximum ϕ in this evaluation. In tangent sections, the measured values closely align with the ϕ_{75} line (Equation 6-8) for both transition directions (Figure 6-5(a)). However, in curve sections, the ϕ_{75} line (Equation 6-9) provides appropriate

values for stiff-to-soft transitions but underestimates values for soft-to-stiff transitions, particularly when ΔVTD_{sub} exceeds 0.06 mm/m (Figure 6-5(b)). Both scenarios are of utmost significance when considering the magnitude of dynamic loads over track assets. Dynamic load values surpass the ϕ_{75} line when ΔVTD_{sub} exceeds 0.06 mm/m during stiff-to-soft transitions and 0.01 mm/m during soft-to-stiff transitions (Figure 6-5(c)). According to the ϕ_{75} value developed by AREMA (2021) (Equation 6-10), all values consistently exceed this threshold across all scenarios and categories (see also Figure E-4). Table 6-3 provides a comparative analysis of the impact of the transition direction on dynamic load magnitudes, considering the ϕ_{75} lines developed by Behnia et al. (2022) (Equations 6-8 and 6-9) and AREMA (2021) (Equation 6-10) across all relevant categories. Table 6-3 reveals that the soft-to-stiff transition is more critical than the stiff-to-soft transition, and the equations developed by Behnia et al. (2022) offer more reasonable estimations in this context.

Table 6-3. Comparing the maximum dynamic load factor derived from the Grubbs test values of IWS data with the ϕ_{75} values developed by Behnia et al. (2022) and AREMA (2021) with regard to the transition direction.

Track type	According to Behnia et al. (2022)		According to AREMA (2021)	
	Soft→Stiff	Stiff→Soft	Soft→Stiff	Stiff→Soft
	Δ (%)	Δ (%)	Δ (%)	Δ (%)
Tangent	10	5	12	7
Curve	6	Capture all	20	15
Track assets	8	3	22	17

Note: Δ values are the difference between the ϕ_{75} line determined by the two main studies considered for evaluation and the maximum Grubbs test values of ϕ derived from IWS measurements.

Roghani and Hendry (2017) classified the conditions of subgrade track stiffness into three distinct categories based on AREMA thresholds, including good track ($VTD_{sub} \leq 3.1$), average track ($3.1 < VTD_{sub} \leq 4.4$), and poor track ($VTD_{sub} > 4.4$). Behnia and Hendry (2024b) showed the impact of subgrade track conditions on the magnitude of dynamic loads; thus, this step is focused on the combined effects of subgrade conditions and transition direction on ϕ values. According to the threshold value ($\phi \geq 1.1$), few data points are associated with good tracks. For this reason, this

study consolidated subgrade stiffness conditions into two broader groups, namely good-average (comprising both conditions) and poor.

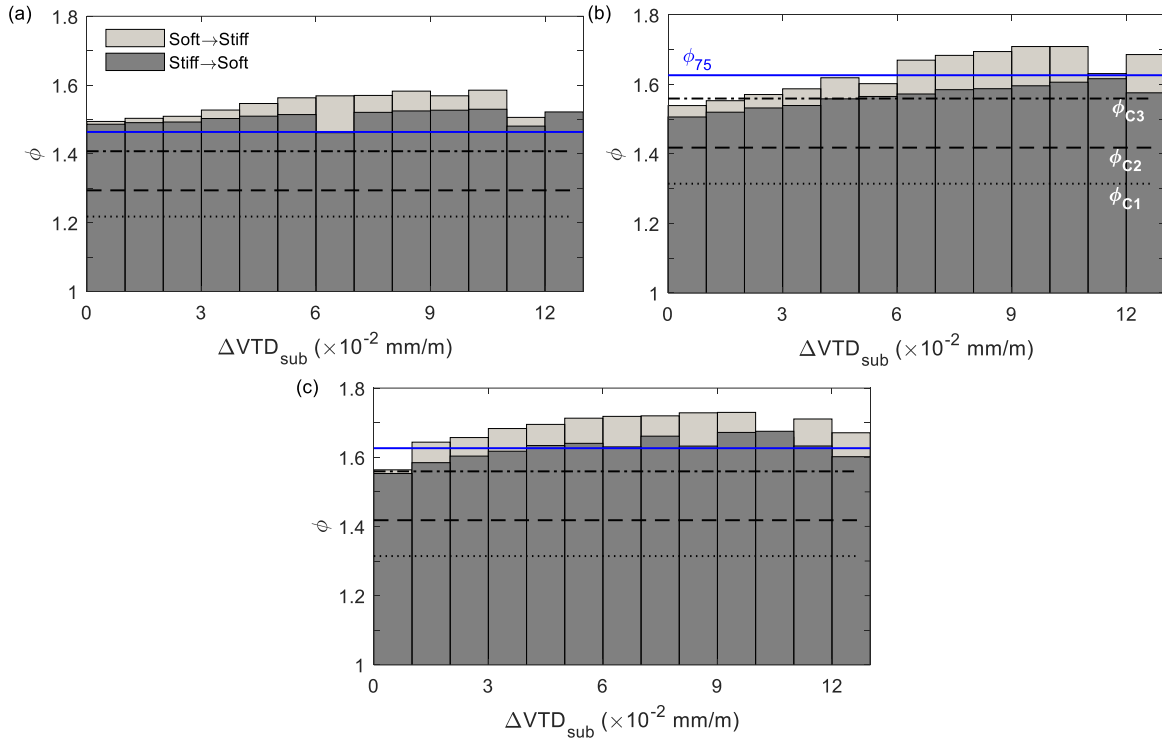


Figure 6-5. Comparing the Behnia et al. (2022) line regarding track classes with ϕ value changes regarding the ΔVTD_{sub} with 0.01 mm/m increments for $\phi \geq 1.1$ on: (a) tangent track; (b) curve sections; and (c) track assets. Note the horizontal lines are based on equations from Behnia et al. (2022), where the ϕ_{C1} line is for 15 km/h (~10 mph), ϕ_{C2} line is for 40 km/h (25 mph), ϕ_{C3} line is for 65 km/h (~41 mph), and ϕ_{75} line (75 km/h or ~47 mph) is for the maximum speed with a reliable number of data points.

Figure 6-6 illustrates the impact of subgrade conditions on ϕ values concerning transition directions and stiffness variations. It shows that subgrade track conditions intensify dynamic load magnitudes in both transitions and across all categories. Subgrade track conditions in tangent and curve sections lead to an approximate 15% increase in dynamic loads in both transition directions. For track assets, this amplification ranges between 20 and 25%. From a technical perspective, a poor track leads to a more substantial increase in dynamic loads than a good-average track. The impact of transition direction on dynamic loads is less significant for poor subgrade conditions than for good-average subgrade conditions. For good-average tracks, soft-to-stiff transitions result

in a 10% increase in dynamic loads. This effect for stiff-to-soft transitions fluctuates between 5 and 10% in poor subgrade conditions. Comparing these findings to the ϕ_{75} line developed by Behnia et al. (2022) shows that the critical situation is observed for poor subgrade conditions, with a 10% underestimation. The ϕ_{75} line provided by AREMA (2021) consistently underestimates dynamic loads across all categories and subgrade track conditions (Figure E-5 and Table E-1).

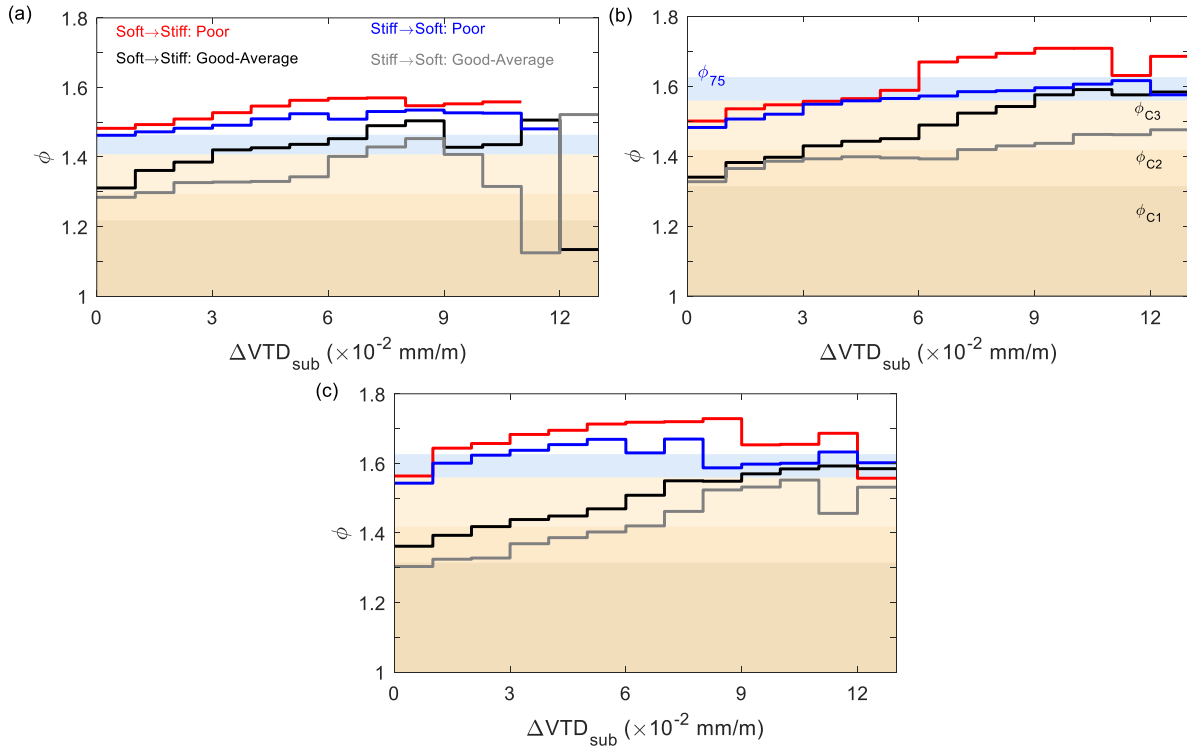


Figure 6-6. Comparing the Behnia et al. (2022) line regarding the track classes and conditions (i.e., good-average and poor tracks) with ϕ value changes regarding the ΔVTD_{sub} with 0.01 mm/m increments for $\phi \geq 1.1$ on: (a) tangent track; (b) curve sections; and (c) track assets. Note that the shaded areas are based on equations from Behnia et al. (2022), where ϕ_{C1} is for 15 km/h (~10 mph), ϕ_{C2} is for 40 km/h (25 mph), ϕ_{C3} is for 65 km/h (~41 mph), and ϕ_{75} is for the maximum speed with a reliable number of data points (75 km/h~ 47 mph).

Dynamic load magnitudes were measured during in-service operations, so the recorded values were contingent on different train speeds. These observations become evident when examining the graphical representations in Figures 6-5 and 6-6 (see also Figures E-4 and E-5), underscoring the significance of considering variations associated with train speed. Hence, the forthcoming phase

of this study was devoted to investigating the collective impact of speed (S) and ΔVTD_{subR} on ϕ values.

6.8.2. Effect of transition direction (ΔVTD_{subR}) and train speed (S) on ϕ

The evaluation of maximum Grubbs test values of ϕ based on 5 km/h increments of train speed and 0.01 mm/m increments of ΔVTD_{sub} over various track categories (inclusive of tangent, curve, and assets) and both transition directions ($\pm\Delta VTD_{subR}$) shows these parameters have a considerable influence on the magnitude of dynamic loads (see Figures E-6, E-7, and E-8). This analysis highlights that incremental changes in train speed intensify the impact of transition directions on dynamic load magnitudes. This evaluation also provides better insight into how changes in train speed influence the interplay between ΔVTD_{sub} and transition direction (ΔVTD_{subR}) in ϕ values. As mentioned, this study concentrated on four specific train speeds corresponding to track classes (1 through 3) and the maximum train speed with a reasonable number of data points (75 km/h).

Figures 6-7 and 6-8 present a comparative analysis of the influence of variations in ΔVTD_{sub} and train speed on changes in the ϕ value concerning transition direction across different categories. This examination across various categories reveals that transition direction can result in an approximate 10% variance in dynamic load factor values. Soft-to-stiff transitions yield higher values of ϕ than stiff-to-soft transitions. In tangent sections, the derived ϕ values from the equation proposed by Behnia et al. (2022) (Equation 6-8) underestimate the measured values by more than 10% during the soft-to-stiff transition; this underestimation decreases to less than 5% when transitioning from a stiffer section to a softer section (Figure 6-7). A critical threshold¹ is noted at ΔVTD_{sub} values beyond the 0.02 to 0.04 mm/m range, as measured values of ϕ exceed the values estimated by Equation 6-8. In comparison, the estimates provided by AREMA (2021) (Equation

¹ Critical thresholds are defined based on situations where the measured ϕ values exceed the predictions made by earlier equations.

6-10) exhibit a 16% underestimation during the soft-to-stiff transition and a 14% underestimation during the stiff-to-soft transition. The discrepancy in tangent sections between the estimations developed by Equation 6-10 and Equation 6-8 is primarily associated with lower speeds. Thus, the divergence in these estimations was predominantly attributed to lower train speeds (Figure E-9).

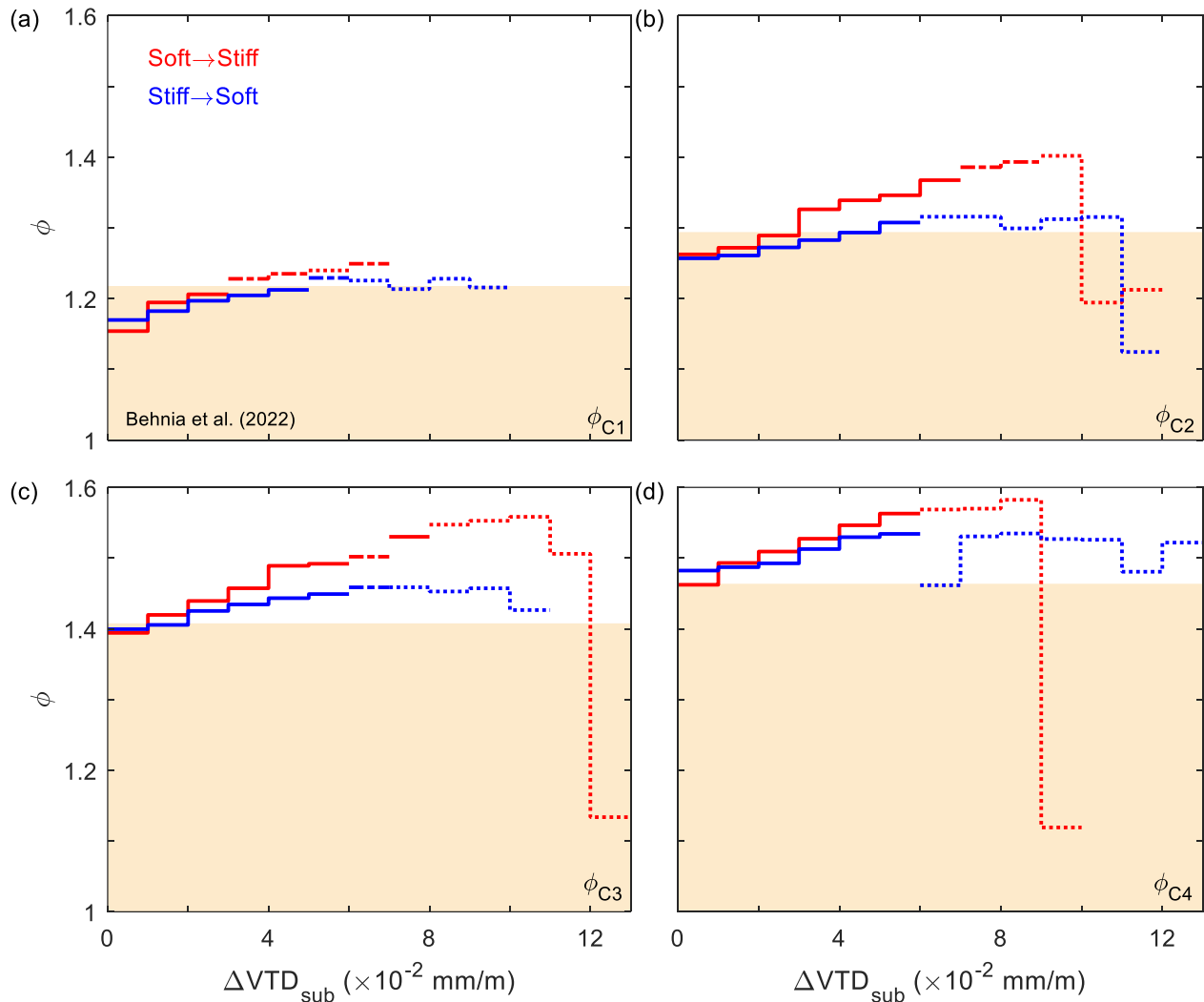


Figure 6-7. IWS and MRail measurements for tangent track based on the Grubbs test values of the dynamic load factor (ϕ) for 0.01 mm/m increments of ΔVTD_{sub} regarding the estimated ϕ values by Behnia et al. (2022) for tangent track (Equation 6-8) and reliability (confidence level) conditions for four specific train speeds: (a) 15 km/h (~10 mph, as Class 1, ϕ_{C1}); (b) 40 km/h (25 mph, as Class 2, ϕ_{C2}); (c) 65 km/h (~40 mph, as Class 3, ϕ_{C3}); and (d) 75 km/h (~47 mph, as the maximum speed with appropriate number of data points, ϕ_{75}). Note: the solid, dash-dot, and dotted lines, respectively, correspond to zones of high, moderate, and low reliability.

In nontangent sections (inclusive of curves and track assets), the ϕ values provided by Behnia et al. (2022) (Equation 6-9) underestimate measured ϕ values by over 10% for soft-to-stiff transitions. When transitioning in the opposite direction (stiff-to-soft), this underestimation decreases to less than 5% (Figure 6-8). When ΔVTD_{sub} values exceed 0.04-0.05 mm/m in curves and 0.02-0.04 mm/m in track assets, the observed ϕ values surpass the values estimated by Equation 6-9 (Figure 6-8). Therefore, these values are identified as the critical thresholds within these categories. In stiff-to-soft transitions, Equation 6-9 provides more dependable estimates with an underestimation of less than 4%, particularly in curves (Figure 6-8). In nontangent tracks, the estimates provided by AREMA (2021) (Equation 6-10) significantly underestimate ϕ values by 20-30%. The higher underestimations are primarily associated with the soft-to-stiff transition (see also Figure E-10).

To gain a deeper understanding of how transition direction (ΔVTD_{subR}) impacts ϕ values, the data were evaluated within the framework of subgrade track conditions (VTD_{sub}). Table 6-4 compares ϕ values under good-average and poor subgrade conditions, considering transition direction and track categories. Soft-to-stiff transitions in poor subgrade conditions exhibit a smaller increase in ϕ values than stiff-to-soft transitions in good-average subgrade conditions (see also Figures 6-9, E-11, E-12, and E-13). This difference is primarily due to the subgrade track condition. During the soft-to-stiff transition in the poor subgrade conditions, the train moves from a more unfavorable condition track to a better one, and the gradual augmentation in ϕ values is smaller than for the stiff-to-soft transition. Figure 6-9 provides an illustrative example of the comparative evaluation of changes in ϕ values regarding the considered train speeds, ΔVTD_{sub} variations, and transition directions (ΔVTD_{subR}) in track assets.

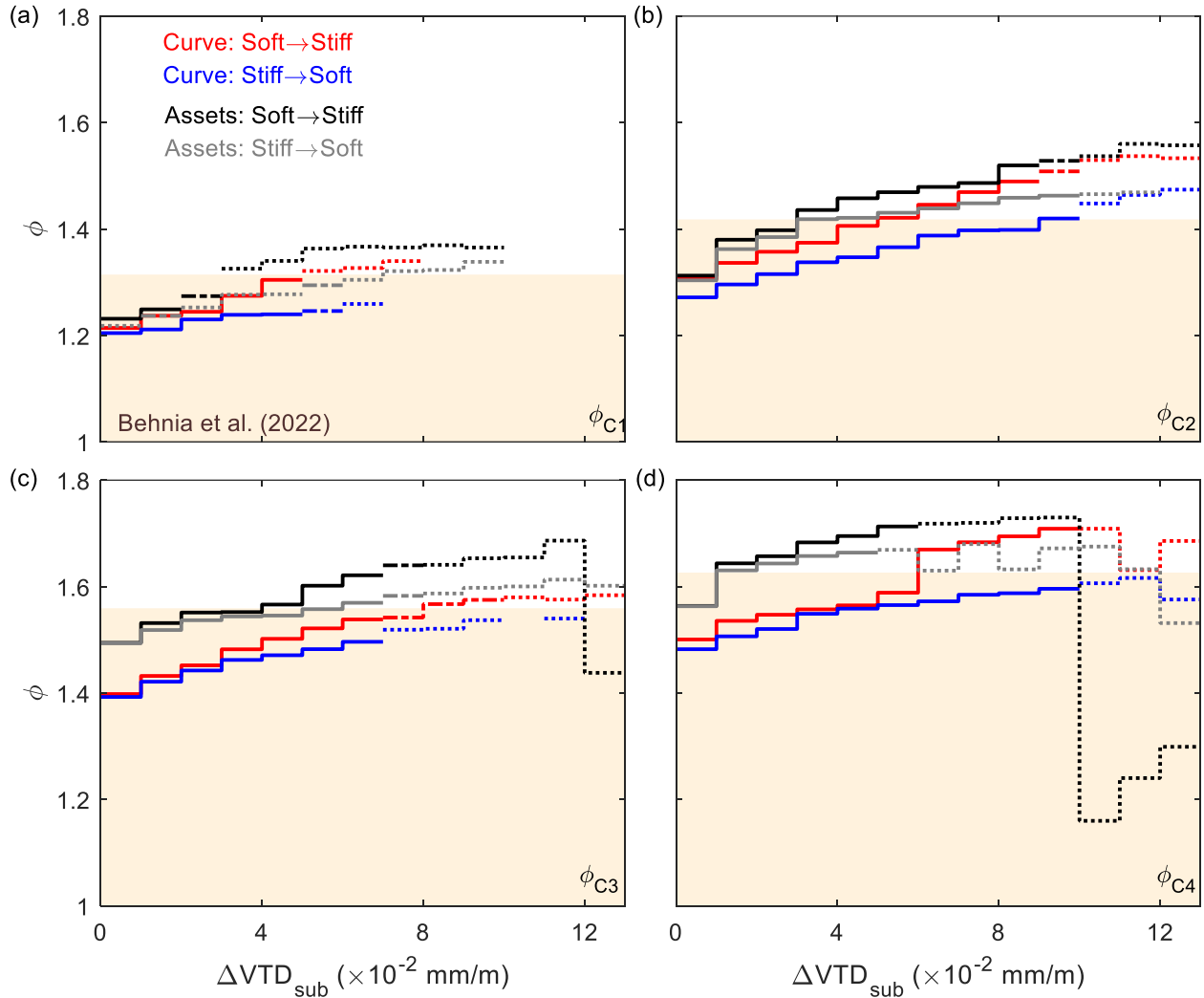


Figure 6-8. IWS and MRail measurements for non-tangent track (inclusive of curve sections and track assets) based on the Grubbs test values of the dynamic load factor (ϕ) for 0.01 mm/m increments of ΔVTD_{sub} regarding the estimated ϕ values by Behnia et al. (2022) for non-tangent track (Equation 6-9) and reliability (confidence level) conditions for four specific train speeds: (a) 15 km/h (~10 mph, as Class 1, ϕ_{C1}); (b) 40 km/h (25 mph, as Class 2, ϕ_{C2}); (c) 65 km/h (~40 mph, as Class 3, ϕ_{C3}); and (d) 75 km/h (~47 mph, as the maximum speed with appropriate number of data points, ϕ_{75}). Note: the solid, dash-dot, and dotted lines, respectively, correspond to zones of high, moderate, and low reliability.

Table 6-4. Comparing the effect of subgrade track conditions (inclusive of good-average and poor tracks) on ϕ values for both transition directions.

Track type	$\delta_{\text{Soft} \rightarrow \text{Stiff}}$ (%)	$\delta_{\text{Stiff} \rightarrow \text{Soft}}$ (%)
Tangent	4-11	4-14
Curve	5-11	4-12
Track assets	5-16	5-20

Note: δ value represents the difference between good-average and poor subgrade conditions with the same transition direction in percentage.

The findings demonstrate that the equations proposed by Behnia et al. (2022) (Equation 6-8 and 6-9) effectively capture the dynamic load magnitudes for stiff-to-soft transitions under good-average conditions. In the soft-to-stiff transition, Equations 6-8 and 6-9 underestimate observed values by less than 6% in cases of good-average tracks. Based on Equations 6-8 and 6-9, the critical thresholds for ΔVTD_{sub} are defined by a range from 0.05 to 0.06 mm/m in tangent sections and values exceeding 0.09 mm/m in curves.

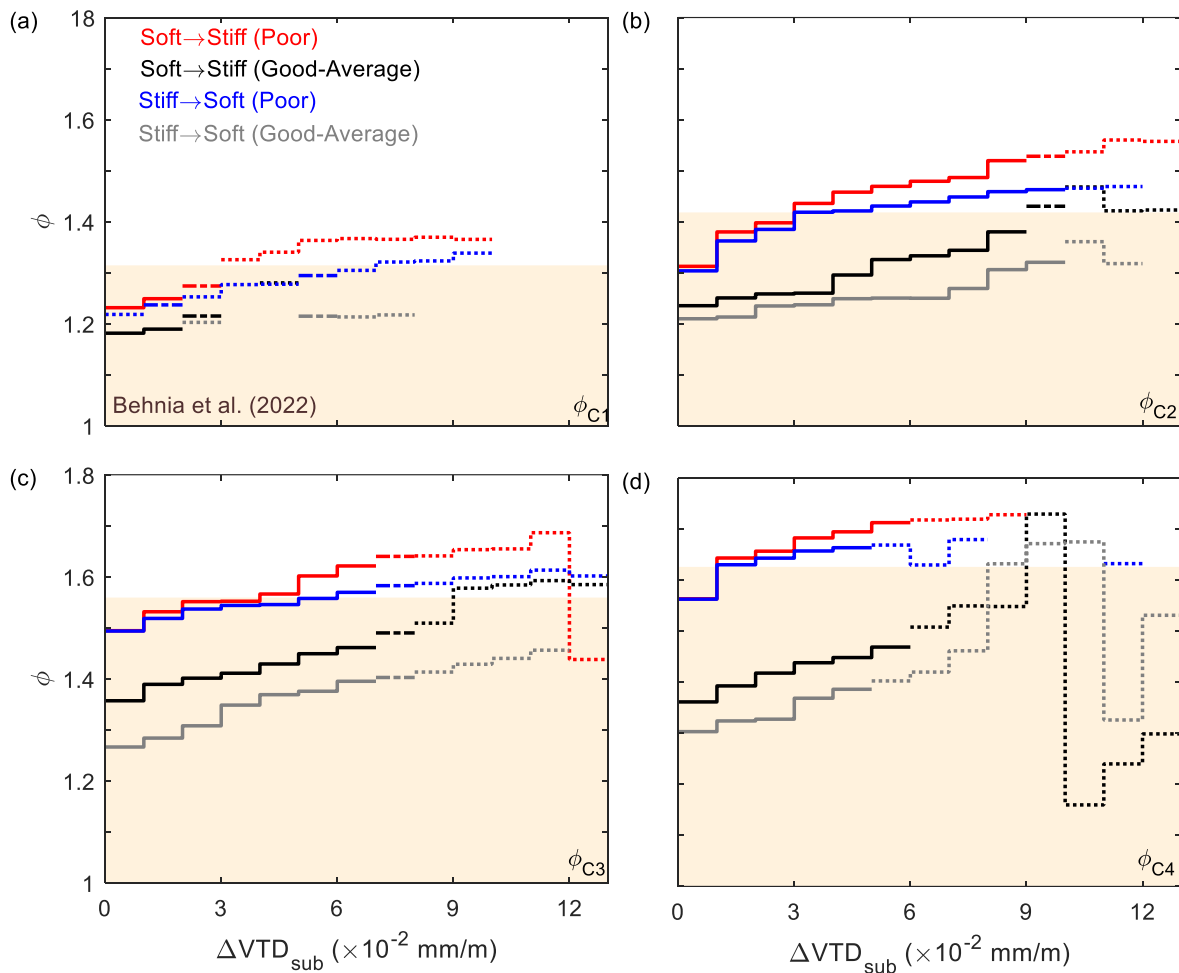


Figure 6-9. IWS and M-Rail measurements for track assets based on the Grubbs test values of the dynamic load factor (ϕ) for 0.01 mm/m increments of ΔVTD_{sub} regarding the estimated ϕ values by Behnia et al. (2022) (Equation 6-9) and reliability (confidence level) conditions and track conditions (i.e., good-average and poor subgrade conditions of track) for four specific train speeds: (a) 15 km/h (~10 mph, as Class 1, ϕ_{C1}); (b) 40 km/h (25 mph, as Class 2, ϕ_{C2}); (c) 65 km/h (~40 mph, as Class 3, ϕ_{C3}); and (d) 75 km/h (~47 mph, as the maximum speed with appropriate number of data points, ϕ_{75}). Note: the solid, dash-dot, and dotted lines, respectively, correspond to zones of high, moderate, and low reliability.

For soft-to-stiff transitions with poor subgrade conditions, the degree of underestimation exceeds 10% across all categories. In this scenario, the critical thresholds for ΔVTD_{sub} decrease to 0.01-0.03 mm/m for tangent tracks and 0.04-0.05 mm/m for nontangent sections. For stiff-to-soft transitions over poor subgrade conditions, the values estimated by Equations 6-8 and 6-9 result in an underestimation of approximately 5%. In this context, the critical thresholds for ΔVTD_{sub} fluctuate between 0.02-0.05 mm/m for tangent tracks and 0.03-0.06 mm/m for nontangent sections (see also Figures 6-9, E-11, and E-12). Comparatively, the ϕ values provided by Equation 6-10 predominantly lead to an underestimation ranging from 10 to 30% for transition scenarios and subgrade track conditions (Figures E-11, E-12, and E-13). For good-average tracks, Equation 6-10 underestimates ϕ values by 5-12% for tangent tracks and by 5-20% for nontangent sections. In poor subgrade conditions, the degree of underestimation increases to 7-15% for tangent tracks and 15-30% for nontangent sections.

6.9. Conclusion

This study investigated how transition directions (soft-to-stiff ($\Delta VTD_{subR} < 0$) and stiff-to-soft ($\Delta VTD_{subR} > 0$)) affected dynamic load magnitudes (in terms of ϕ) at various train speeds and track structures, using data from the MRail and IWS systems. This investigation distinguishes itself from prior studies by focusing on the entire railway track, in contrast to research limited to specific track sections. This study employed extensive datasets acquired through instrumented railcar while moving along the track, showcasing the distinctive methodology adopted for this evaluation. These comprehensive datasets covered various track structures over 340 km of in-service track. The results demonstrated that soft-to-stiff transitions amplify dynamic load magnitudes while stiff-to-soft transitions attenuate the dynamic loads. Soft-to-stiff transitions had ϕ values approximately 10% higher than stiff-to-soft transitions. This study further examined how subgrade track stiffness

(VTD_{sub}) influences the effectiveness of transition directions on the magnitude of dynamic loads. This evaluation revealed that subgrade conditions (i.e., good-average and poor) affect the impact of transition directions on dynamic load magnitudes. Poor subgrade conditions consistently led to higher dynamic loads across both transition scenarios than good and average conditions.

This research also examined the performance of predictive models presented by Behnia et al. (2022) and AREMA (2021) for four specific speeds associated with North American track classes (1 through 3) and the maximum speed with a reasonable number of data points. The equations developed by Behnia et al. (2022) (Equations 6-8 and 6-9) tended to underestimate ϕ values by more than 10% in soft-to-stiff transitions, although this underestimation declined to 5% for stiff-to-soft transitions. Regarding the estimates provided by AREMA (2021) (Equation 6-10), the underestimation increased to 15-30% for soft-to-stiff transitions and 10-25% for stiff-to-soft transitions. The substantial underestimations were primarily associated with nontangent sections. This study identified a critical range for subgrade stiffness variation (ΔVTD_{sub}) in poor subgrade conditions ($VTD_{sub} > 4.4$), between 0.02 and 0.05, based on ϕ value estimates from Behnia et al. (2022) (smaller ΔVTD_{sub} values correspond to higher train speeds). This study also underscored the significance of considering train speed when evaluating the influence of ΔVTD_{sub} on ϕ variations. The impact of speed drew attention to the need to optimize maintenance techniques based on track classes and their maximum allowable speeds. Further research is warranted to evaluate the impact of subgrade track stiffness variations (ΔVTD_{sub}) on ϕ values while considering various track conditions and variations in car types and conditions. In future studies, it is also crucial to investigate the impact of transition directions on tangential forces along the track, which can complement this study.

6.10. Acknowledgement

The authors thank the Canadian National Railway for their support and facilitation of this project and specifically Tom Edwards for facilitating the collection of these datasets. This research was made possible through the Canadian Rail Research Laboratory (www.carrl.ca). Funding was provided by the Natural Sciences and Engineering Research Council of Canada (NSERCIRC 523369-18), Canadian National Railway, the National Research Council Canada, and Transport Canada.

6.11. References

- AREMA (American Railway Engineering and Maintenance of Way Association). (2021). *Manual for railway engineering*. Lanham, MD: AREMA.
- Arnold, R., Lu, S., Hogan, C., Farritor, S., Fateh, M., & El-Sibaie, M. (2006). Measurement of vertical track modulus from a moving railcar. In *Proceedings of the AREMA Annual Conference, Louisville, KY*.
- ASTM. (2021). *Standard practice for dealing with outlying observations*. ASTM E178-02. West Conshohocken, PA: ASTM.
- Bartlett, I.I.J.E., Kotrlík, J.W., & Higgins, C.C. (2001). Organizational research: Determining appropriate sample size in survey research. *Inf Technol Learn Perform J*, 19(1), 43.
- Behnia, D., & Hendry, M.T. (2024a). Impact of subgrade track stiffness on dynamic loads: a comprehensive evaluation using instrumented wheelset and MRail measurements. *Journal of Civil Structural Health Monitoring*, Springer (Submitted).
- Behnia, D., & Hendry, M.T. (2024b). Quantifying the impact of rail profile changes on the magnitude of dynamic loads through instrumented wheelset measurements. *Journal of Vehicle System Dynamics*, Taylor & Francis (Submitted).

- Behnia, D., Hendry, M.T., Haji Abdulrazagh, P., & Wahba, A. (2022). Railway dynamic load factors developed from instrumented wheelset measurements. *Journal of Transportation Engineering, Part A: Systems*, 148(7), 04022042.
- Berggren, E. (2009). *Railway track stiffness: dynamic measurements and evaluation for efficient maintenance*. Doctoral dissertation, KTH Royal Institute of Technology, Stockholm.
- Burrow, M., Teixeira, P., Dahlberg, T., & Berggren, E. (2009). Track stiffness considerations for high-speed railway lines. In *Railway transportation: policies, technology, and perspectives* (Ed. Scott NP). Nova Science Publishers, 303-354.
- Cai, Z., Raymond, G.P., & Bathurst, R.J. (1994). Estimate of static track modulus using elastic foundation models. *Transportation Research Record*, 1470, 65.
- Chen, R., Zhao, X., Wang, Z., Jiang, H., & Bian, X. (2013). Experimental study on dynamic load magnification factor for ballastless track-subgrade of high-speed railway. *Journal of Rock Mechanics and Geotechnical Engineering*, 5(4), 306-311.
- Davis, D.D., Otter, D., Li, D., & Singh, S. (2003). Bridge approach performance in revenue service. *Railway Track Structures*, 99(12).
- Ebersohn, W., Trevizo, M.C., & Selig, E.T. (1993). Effect of low track modulus on track performance. In *Proceedings of the Fifth International Heavy Haul Conference*, 379-388.
- Esveld, C. (2001). *Modern railway track, 2nd Ed.* Zaltbommel, Netherlands: MRT-Productions.
- Fallah Nafari, S., Gül, M., Hendry, M.T., & Cheng, J.R. (2018a). Estimation of vertical bending stress in rails using train-mounted vertical track deflection measurement systems. *Proceedings of the Institution of Mechanical Engineers, Part F: Journal of Rail Rapid Transit*, 232(5), 1528-1538.

- Fallah Nafari, S., Gül, M., Hendry, M.T., Otter, D., & Cheng, J.J.R. (2018b). Operational vertical bending stresses in rail: Real-life case study. *J Transp Eng Part A Syst*, 144(3), 05017012.
- Farritor, S. (2006). Real-time measurement of track modulus from a moving car. (No. DOT/FRA/ORD-05/05). Washington, DC: U.S. Dept. of Transportation.
- Farritor, S., & Fateh, M. (2013). Measurement of vertical track deflection from a moving rail car. (No. DOT/FRA/ORD-13/08). United States Federal Railroad Administration, Office of Research and Development.
- Greisen, C.J. (2010). Measurement, simulation, and analysis of the mechanical response of railroad track. *M.Sc. dissertation, Department of Mechanical Engineering, University of Nebraska, Lincoln, NE.*
- Hunt, G.A., & Wood, J. (2005). Review of the effect of track stiffness on track performance. *RSSB Research Project 372.*
- Leishman, E.M., Hendry, M.T., & Martin, C.D. (2017). Canadian main track derailment trends, 2001 to 2014. *Canadian Journal of Civil Engineering*, 44(11), 927-934.
- Li, D., & Selig, E.T. (1995). Evaluation of railway subgrade problems. *Transportation Research Record*, 1489, 17.
- Li, M.X.D., & Berggren, E.G. (2010). A study of the effect of global track stiffness and its variations on track performance: simulation and measurement. *Proceedings of the Institution of Mechanical Engineers, Part F: Journal of Rail Rapid Transit*, 224(5), 375-382.
- Li, D., Hyslip, J., Sussmann, T., & Chrismer, S. (2015). *Railway geotechnics*. CRC Press.
- Liu, X., Saat, M.R., & Barkan, C.P.L. (2012). Analysis of causes of major train derailment and their effect on accident rates. *Transportation Research Record*, 2289, 154–163.

- Lu, S. (2008). Real-time vertical track deflection measurement system. *Ph.D. dissertation, Department of Mechanical Engineering, University of Nebraska, Lincoln, NE.*
- McVey, B., Norman, C., Wood, N., Farritor, S., Arnold, R., Fateh, M., & El-Sibaie, M. (2005). Track modulus measurement from a moving railcar. In *Proceedings of the AREMA Annual Conference, Chicago, IL.*
- Norman, C., Farritor, S., Arnold, R., Elias, S.E.G., Fateh, M., & Sibaie, M.E. (2004). Design of a system to measure track modulus from a moving railcar. In *Proceeding of Railway Engineering*. Edinburgh, UK: Engineering TechnicsPress.
- Oberkampff, W.L., DeLand, S.M., Rutherford, B.M., Diegert, K.V., & Alvin, K.F. (2002). Error and uncertainty in modeling and simulation. *Journal of Reliability Engineering and System Safety*, 75(3), 333-357.
- Peters, N. (2010). *CN railway engineering course*. Montreal: McGill University.
- Read, D., Chrismer, S., Ebersöhn, W., & Selig, E. (1994). Track modulus measurements at the Pueblo soft subgrade site. *Transportation Research Record*, 1470, 55.
- Roghani, A., & Hendry, M.T. (2016). Continuous vertical track deflection measurements to map subgrade condition along a railway line: Methodology and case studies. *J Transp Eng Part A Syst*, 142(12), 04016059. [https://doi.org/10.1061/\(ASCE\)TE.1943-5436.0000892](https://doi.org/10.1061/(ASCE)TE.1943-5436.0000892).
- Roghani, A., & Hendry, M.T. (2017). Quantifying the impact of subgrade stiffness on track quality and the development of geometry defects. *Journal of Transportation Engineering, Part A: Systems*, 143(7), 04017029.
- Roghani, A., Macciotta, R., & Hendry, M. (2015). Combining track quality and performance measures to assess track maintenance requirements. In *Proceeding of ASME/IEEE Joint Rail Conference (Vol. 56451, p. V001T01A009)*. American Society of Mechanical Engineers.

- Roghani, A., Macciotta, R., & Hendry, M.T. (2017). Quantifying the effectiveness of methods used to improve railway track performance over soft subgrades: methodology and case study. *Journal of Transportation Engineering, Part A: Systems*, 143(9), 04017043.
- Sadeghi, J. (2012). New advances in analysis and design of railway track system. *Journal of Reliability and Safety Railway*, 30(3), 75-100.
- Sussman, T.R., Ebersöhn, W., & Selig, E.T. (2001). Fundamental nonlinear track load-deflection behavior for condition evaluation. *Transportation Research Record*, 1742(1), 61-67.
- TSB (Transportation Safety Board of Canada). (2013). *Statistical summary railway occurrences*. Cat. No. TU1-2/2013, Gatineau, Canada.
- UIC Code. (2008). *19R Earthworks and track bed for railway lines*. Paris: Union Internationale des Chemins de Fer, 117.
- Woelfle, A. (2016). Report for the national research council. In *Analysis of wheel-rail forces during (MRail) rolling deflection tests*. Gloucester, ON, Canada: National Research Council Canada, Automotive and Surface Transportation.
- Zarembski, A.M., & Palese, J. (2003). Transitions eliminate impact at crossings. *Railway Track Structures*, 99(8), 28–30.

7. Conclusions & Recommendations

Rail breaks and failures in track components are a primary factor contributing to derailments in Canada. In light of the ongoing problem of rail failures, it is worth revisiting the understanding of the magnitude of loads the rail is subjected to. This study enhances our comprehension of how railway track characteristics influence dynamic load magnitudes across Canadian freight railway lines. Such insights could lead to better railway design and heightened network safety and reliability.

The research objectives were twofold: to address gaps in previous studies and to investigate the primary factors contributing to the increase and variability of dynamic loads on tracks. Firstly, the study evaluated the impact of super-structural track features (e.g., grade crossings and switches) and rail surface changes on dynamic load magnitudes. Secondly, it provided a detailed quantitative analysis of how subgrade track stiffness affects these loads. Given the significant impact of the dynamic load factor (ϕ) on railway design, particularly concerning aspects such as rail steel and cross-sectional (weight), this research concentrated on scrutinizing various parameters by evaluating this crucial factor (ϕ).

The following sections explain the conclusions corresponding to each objective of this research.

7.1. Quantifying the impact of observable track characteristics on dynamic load magnitudes

Chapter 3 comprehensively evaluated the impact of observable track characteristics (structures) on dynamic load magnitudes, including tangent track, curve, grade crossing, bridge, and switch. This approach differs from previous studies that relied on instrumented track sections, which captured dynamic load magnitudes from various car types and conditions passing over the site but under constant track conditions. In contrast, the IWS system provided measurements of dynamic

loads under constant car types and conditions but across diverse track conditions. The results of this chapter demonstrated that the impact of track conditions is significant, resulting in ranges of dynamic loads and ϕ that the track may experience well over that provided by common means of estimating, especially for non-tangent track (inclusive of curves, switches, grade crossings, and bridges). Equations were also developed to represent the dynamic load factor (ϕ) in terms of speed, addressing both tangent and non-tangent tracks and offering a method to quantify the observed variation.

7.2. Quantifying the effect of surface track vertical deviation on dynamic load magnitudes

Chapter 4 quantified the impact of train speed and rail profile variations on the dynamic load factor (ϕ), reflecting dynamic load changes along the track. In contrast to previous studies that focused on specific track sections (instrumented sections), this chapter adopts a different approach by evaluating the impact of rail profile variations along the railway track, encompassing various track structures. The dynamic loads, measured by the IWS system, were assessed in terms of train speed, rail profile variations, and track characteristics. The findings demonstrated that dynamic load magnitudes (ϕ values) were significantly influenced by rail profile changes, train speed, and track structures, particularly in non-tangent sections.

This chapter also evaluated two equations for ϕ values, one being the commonly used equation from AREMA (2021) and the other a recently formulated equation by Behnia et al. (2022) in the context of North American freight railways. When rail profile variations reached the upper limit (18-20 mm), these equations underestimated the values by approximately 15% on tangent tracks. The underestimation was more pronounced on non-tangent tracks, with Behnia et al. (2022) and AREMA (2021) values underestimated by 15% and 36%, respectively. These results suggest that equations developed by Behnia et al. (2022) may offer more accurate estimates for dynamic loads

on in-service tracks, presenting an opportunity to optimize maintenance schedules and timely grinding procedures for rail break prevention. These findings enhance our understanding of how surface longitudinal level deviations affect dynamic load magnitudes and contribute to rail defects.

7.3. Quantitative evaluation of subgrade track stiffness effects on dynamic load magnitudes

Chapter 5 comprehensively evaluated dynamic load magnitudes (i.e., in terms of ϕ) by integrating data from the IWS system with subgrade track stiffness measurements (VTD_{sub}) from MRail. This analytical approach distinguishes itself from previous studies focusing on specific track sections. The results of this phase highlighted the substantial impact of track subgrade stiffness (i.e., VTD_{sub}) and variations in train speed on dynamic loads, with magnitudes surpassing those of prior estimates. The critical range for observed increases in ϕ values was identified under average track conditions ($VTD_{sub} = 3.1\text{--}4.4$ mm). In curves, the analysis reveals that increases in VTD_{sub} , especially on tracks with average to poor conditions, significantly elevate dynamic loads on the lower rail compared to a good track.

This study supported the better performance of the estimation models proposed by Behnia et al. (2022) over those presented by AREMA (2021). The $\phi_{Behnia et al.}$ values demonstrated an underestimation of less than 10% in good subgrade track conditions, surpassing the performance of ϕ_{AREMA} values, which consistently underestimated ϕ values by more than 20% for tangent tracks and approximately 30% for non-tangent tracks. This discrepancy was particularly pronounced in Class 1 tangent tracks ($S \leq 16$ km/h or 10 mph).

7.4. Quantitative evaluation of transition directions impacts on dynamic load magnitudes

Chapter 6 presented a quantitative evaluation of dynamic load fluctuations regarding ϕ values across various track structures, utilizing data from the IWS system. The ϕ values were assessed in light of transition directions, categorized as soft-to-stiff and stiff-to-soft. The evaluation also

considered changes in subgrade track stiffness (ΔVTD_{sub}) and subgrade track conditions (VTD_{sub}) derived from MRail measurements. The secant slope procedure was employed to quantify the transition directions (ΔVTD_{subR}). A positive ΔVTD_{subR} value ($\Delta VTD_{subR} > 0$) signifies a transition from stiff to soft, while a negative value ($\Delta VTD_{subR} < 0$) indicates a transition from soft to stiff. The findings indicated that soft-to-stiff transitions amplify dynamic load magnitudes, whereas stiff-to-soft transitions attenuate them. Notably, soft-to-stiff transitions resulted in ϕ values approximately 10% higher than those in stiff-to-soft transitions.

Recognizing the influence of subgrade track stiffness conditions on dynamic load magnitudes, the subsequent phase of the study examined the interplay between this parameter and the relationship between transition directions and dynamic load magnitudes. Data were thus categorized into two groups based on subgrade track conditions: good-average and poor. The analysis suggested that subgrade track conditions modulate the impact of transition direction, potentially diminishing the differences between the two transition scenarios. The significance lies in emphasizing that the influence of subgrade track conditions plays a more pivotal role in determining the magnitude of dynamic loads than the transitions' directions.

The research scrutinized the accuracy of predictive models proposed by Behnia et al. (2022) and AREMA (2021) across four specific speeds corresponding to North American track classes (1 through 3) and the maximum speed with a sufficient number of data points (i.e., 75 km/h). The models by Behnia et al. (2022) tended to underestimate ϕ values by more than 10% in soft-to-stiff transitions, though this underestimation decreased to 5% for stiff-to-soft transitions. Conversely, the ϕ values provided by AREMA (2021) exhibited a more significant underestimation, ranging from 15-30% for soft-to-stiff transitions to 10-25% for stiff-to-soft transitions, with significant

discrepancies predominantly observed in non-tangent sections. The study underscored the necessity of considering train speed when evaluating the impact of ΔVTD_{sub} on ϕ variations.

7.5. Contributions of track parameters to railway dynamic load factor

This study investigated the influence of various track characteristics on dynamic load magnitudes in railway systems, focusing on observable track structures, surface geometry, subgrade stiffness, and transition directions. This study, therefore, quantified the contributions of these factors, revealing that subgrade stiffness is the primary determinant of dynamic loads in both tangent and non-tangent tracks. Specifically, in good subgrade conditions, rail profile (also known as the longitudinal level of the rail or rail surface) variations predominantly affect dynamic loads. However, in average and poor subgrade conditions, subgrade stiffness becomes the dominant factor, with its influence being particularly pronounced in poor tracks. Additionally, the results of this investigation indicated that the impact of rail surface variations intensifies during transitions from stiff to soft subgrade conditions. However, subgrade stiffness remains the primary influence on dynamic loads. These findings underscore the critical role of subgrade stiffness in managing dynamic loads across varying track conditions.

7.6. Implications of this study

The main contribution of this research is to provide greater quantitative insight into the effect of various track features (i.e., observable track structures, track surface changes, subgrade stiffness variations) on the magnitude of dynamic loads along the freight railway lines. Understanding the magnitude of dynamic loads is paramount in railway engineering, as it informs decisions related to track design, material selection, and overall system safety. This understanding is crucial for informing decisions in railway engineering, such as track design, material selection, and overall system safety. Additionally, the text discusses the importance of dynamic load analysis in railway

maintenance scheduling, as it enables proactive maintenance to prevent structural deficiencies and reduce unplanned maintenance activities.

The other important aspects of this study can contribute to figuring out the point of interest regarding rail breaks and defects. The augmentation of dynamic load magnitudes can result in fatigue life in rail. Hence, the quantitative evaluation of dynamic loads is crucial for understanding how they affect the fatigue life of rails, assisting engineers in developing strategies to alleviate stress concentrations, improve material durability, and prolong the operational longevity of railway tracks. In this research, an extensive data analysis over 340 km of track with a wide variety of track structures (e.g., more than 30 bridges, 100 grade crossings, and 50 switches with more than 56×10^6 vertical dynamic load measurements), variations in track surface, and track subgrade conditions were conducted to quantify the extent of the impact of these parameters on dynamic load magnitudes (regarding ϕ values). The insights provided are valuable for the railway industry as they have the potential to diminish the risk of train derailments and considerably enhance track safety.

7.7. Recommendations

This thesis enhances the understanding of how various track features, including observable characteristics, surface changes, and subgrade conditions, influence dynamic loads on freight railways. This knowledge can be utilized to optimize railway design and enhance safety measures.

The following tasks are recommended for future work:

- Investigating temperature/environmental effects: Current datasets, confined to July and August 2015, represent summer conditions. Collecting data during winter and comparing it with the existing dataset can quantify how temperature, specifically cold weather, affects

the wheel-rail dynamic interactions. This analysis can improve understanding of dynamic load magnitudes along the railway track.

- Evaluating the conditions that increase rail break frequency: Recent studies have highlighted the impact of track surface roughness and subgrade conditions on dynamic load magnitudes, which are critical factors contributing to variability and increasing dynamic load magnitudes. Given rail fatigue life as an early indicator of potential rail breaks, examining these parameters alongside AREMA regulations can help quantify conditions that increase rail break occurrences. This approach can offer ample opportunities to revisit rail fatigue life and provide a comprehensive understanding of factors exacerbating rail break frequency.
- Evaluating other track surface geometry parameters: Investigating additional track geometry parameters such as alignment, twist, and warp can improve insights into their effects on dynamic load magnitudes. Examining these parameters in curved track sections and differentiating between their impacts on the low and high rails is suggested.
- Incorporating diverse railcar types and static loads: A limitation of the IWS measurements is their dependence on a single car type and load, in contrast to wayside measurements (instrumented section) that capture a broader spectrum of conditions. For a comprehensive understanding of wheel-rail dynamic interactions, it is recommended to combine these measurements to enhance the comprehension of the magnitude of dynamic loads along the railway track.
- Evaluating subgrade conditions and transition directions on tangential forces: Tangential forces play a pivotal role in defining the frictional properties and wear patterns on rail tracks. Understanding the impact of these forces on rail track behavior is essential for

improving system reliability and developing effective maintenance strategies. Investigating the effect of subgrade conditions (soft and stiff) and transition directions on tangential forces can present a pertinent opportunity to evaluate the effects of subgrade stiffness conditions on the degradation of surface tracks.

8. References

- Ágh, C. (2023). Connection between track geometry quality and dynamic vehicle response at various speeds. *The Baltic Journal of Road and Bridge Engineering*, 18(3), 169-187.
- Andersson, R., Torstensson, P. T., Kabo, E., & Larsson, F. (2015). The influence of rail surface irregularities on contact forces and local stresses. *Vehicle System Dynamics*, 53(1), 68-87.
- AREMA. (2012). *Manual for railway engineering*. American Railway Engineering and Maintenance of Way Association. Lanham, MD, USA.
- AREMA. (2021). *Manual for railway engineering*. American Railway Engineering and Maintenance of Way Association. Lanham, MD: AREMA.
- Arnold, R., Lu, S., Hogan, C., Farritor, S., Fateh, M., & El-Sibaie, M. (2006, September). Measurement of vertical track modulus from a moving railcar. In *Proceedings of the AREMA Annual Conference*, Louisville, KY.
- Asplund, M., & Söderström, P. (2022). Field validation of force response from defective wheel. In *12th International Conference on Contact Mechanics and Wear of Rail/Wheel Systems*, 4-7 September 2022, Melbourne, Victoria, Australia.
- ASTM. (2021). *Standard practice for dealing with outlying observations*. *ASTM E178-02*. West Conshohocken, PA: ASTM.
- Balasubramanian, V., Ho, S. S., & Vovk, V. (Eds.). (2014). *Conformal prediction for reliable machine learning: theory, adaptations and applications*. Newnes.
- Barbosa, R. S. (2016). Evaluation of railway track safety with a new method for track quality identification. *Journal of Transportation Engineering Part A: Systems*, 142(11), 04016053. [https://doi.org/10.1061/\(ASCE\)TE.1943-5436.0000855](https://doi.org/10.1061/(ASCE)TE.1943-5436.0000855).

- Bartlett II, J.E., Kotrlik, J.W., and Higgins, C.C. (2001). Organizational research: Determining appropriate sample size in survey research. *Information Technology, Learning, and Performance Journal*, 19(1), 43.
- Behnia, D., & Hendry, M. T. (2024, Submitted). Quantifying the impact of rail profile changes on the magnitude of dynamic loads through instrumented wheelset measurements. *Journal of Vehicle System Dynamics*, Taylor & Francis.
- Behnia, D., & Hendry, M.T. (2024, Submitted). Impact of subgrade track stiffness on dynamic loads: a comprehensive evaluation using instrumented wheelset and MRail measurements. *Journal of Civil Structural Health Monitoring*, Springer.
- Behnia, D., Hendry, M. T., Haji Abdulrazagh, P., & Wahba, A. (2022). Railway Dynamic Load Factors Developed from Instrumented Wheelset Measurements. *Journal of Transportation Engineering, Part A: Systems*, 148(7), 04022042.
- Berggren, E. (2009). Railway Track Stiffness – Dynamic Measurements and Evaluation for Efficient Maintenance. Doctoral Thesis, Rail Vehicles, KTH, TRITA AVE 2009:17, ISBN 978-91-7415-293-7, Stockholm, Sweden, 2009.
- Berggren, E. G., Li, M. X., & Spännar, J. (2008). A new approach to the analysis and presentation of vertical track geometry quality and rail roughness. *Journal of Wear*, 265(9-10), 1488-1496.
- Berggren, E., Jahlénus, Å., & Bengtsson, B. E. (2002). Continuous track stiffness measurement: An effective method to investigate the structural condition of a track. *Proc. Int. Conf. of Railway Engineering*, Engineering Technics Press, London.
- Berggren, E., Jahlenius, A., Bengtsson, B., & Berg, M. (2005). Simulation development, and field testing of track stiffness measurement vehicle. In *Proceedings of the 8th International Heavy Haul Conference*, Rio de Janeiro, Brazil, June 14-16 (pp. 763-771).

- Bianculli, A. J. (2001). *Trains and Technology: Track and Structures (Vol. 1)*. University of Delaware Press.
- Birmann, F. (1965, June). Paper 5: Track parameters, static and dynamic. In *Proceedings of the Institution of Mechanical Engineers, Conference Proceedings, 180(6)*, 73-85. Sage UK: London, England: SAGE Publications.
- Bracciali, A., Cavaliere, F., & Macherelli, M. (2014, April). Review of instrumented wheelset technology and applications. In *Proceedings of the 2nd International Conference on Railway Technology: Research, Development and Maintenance* (pp. 1-16).
- Burrow, M., Chan, A., & Shein, A. (2007). Falling weight deflectometer based inverse analysis of ballasted railway tracks. *Geotechnical Engineering, Proceedings of the Institution of Civil Engineers, Issue GE3*, pp 169–177, July.
- Burrow, M., Teixeira, P., Dahlberg, T., & Berggren, E. (2009). Track stiffness considerations for high-speed railway lines. In *Railway transportation: policies, technology, and perspectives* (Ed. Scott NP). Nova Science Publishers, 303-354.
- Bury, K. V. (1999). *Statistical Distributions in Engineering*. Cambridge University Press.
- Cai, X., Zhang, Q., Wang, Q., Cui, X., & Dong, B. (2022). Effects of the subgrade differential arch on damage characteristics of CRTS III slab track and vehicle dynamic response. *Construction and Building Materials*, 327, 126982.
- Cai, Z., Raymond, G. P., & Bathurst, R. J. (1994). Estimate of Static Track Modulus Using Elastic Foundation Models. *Transportation Research Record 1470*, pp. 65-72.
- Cakdi, S., Cummings, S., & Punwani, J. (2015, March). Heavy haul coal car wheel load environment: Rolling contact fatigue investigation. In *ASME/IEEE Joint Rail Conference (Vol. 56451, p. V001T02A005)*. American Society of Mechanical Engineers.

- Canadian National (CN) Railway. (2011). Wheel Impact Load Detectors: The Early History on CN. In: *Proceedings of the 31st Annual North American Rail Mechanical Operations Seminar*, St. Louis, Missouri, March.
- Cannon, D. F., Edel, K. O., Grassie, S. L., & Sawley, K. (2003). Rail defects: an overview. *Fatigue and Fracture of Engineering Materials and Structures*, 26(10), 865-886.
- Carr, G. A. (1999, September). Dynamic response of railroad track induced by high speed trains and vertical stiffness transitions with proposed method of measurement. *Tufts University*.
- Caughron, B. M., Saat, M. R., & Barkan, C. P. L. (2012). Identifying and Prioritizing Shared Rail Corridor Technical Challenge. In: *Proceedings of the 2012 Annual AREMA Conference*, Chicago, Illinois, September.
- Chen, R., Zhao, X., Wang, Z., Jiang, H., & Bian, X. (2013). Experimental study on dynamic load magnification factor for ballastless track-subgrade of high-speed railway. *Journal of Rock Mechanics and Geotechnical Engineering*, 5(4), 306-311.
- Cochran, W. G. (1977). *Sampling techniques*. John Wiley & Sons.
- Code, U. I. C. (2008). *719R Earthworks and track bed for railway lines*. Paris: Union Internationale des Chemins de Fer, 117.
- Collell, G., Prelec, D., & Patil, K. R. (2018). A simple plug-in bagging ensemble based on threshold-moving for classifying binary and multiclass imbalanced data. *Neurocomputing*, 275, 330-340.
- Crow, E. L. (1956). "Confidence intervals for a proportion." *Biometrika*, 43(3/4), 423-35. <https://doi.org/10.2307/2332920>.
- Dahlberg, T. (2010). Railway Track Stiffness Variations-Consequences and Countermeasures. *International Journal of Civil Engineering*, 8(1).

- Davis, D.D., Otter, D., Li, D., & Singh, S. (2003). Bridge approach performance in revenue service. *Railway Track Structures*, 99(12).
- Di Leo, G., & Sardanelli, F. (2020). Statistical significance: p value, 0.05 threshold, and applications to radiomics—reasons for a conservative approach. *European radiology experimental*, 4, 1-8.
- Dimasi, F., & Weinstock, H. (1978). A parametric study to relate railcar speed to permissible combinations of track geometry deviations.
- Dingqing, L., & Selig, E. T. (2018). “Wheel/track dynamic interaction: track substructure perspective.” In E. Schiehlen (Ed.), *Interaction of Railway Vehicles with the Track and Its Substructure* (pp. 183-196). Routledge.
- Do, N. T., Gül, M., & Nafari, S. F. (2020). Continuous evaluation of track modulus from a moving railcar using ANN-based techniques. *Vibration*, 3(2), 149-161.
- Doyle, N. F. (1980). *Railway track design: A review of current practice*. Canberra, WA: Australian Government Publishing Service.
- Dung, T. A., Van Tham, M., & Le Hai, H. A. (2022). A Study on Derailment at Railway Turnout Using Multi-body Dynamics Simulation. *Journal of Materials and Engineering Structures (JMES)*, 9(4), 499-505.
- Dybala, J., and S. Radkowski. (2013). Reduction of Doppler effect for the needs of wayside condition monitoring system of railway vehicles. *Mechanical Systems and Signal Processing*, 38(1), 125–136. <https://doi.org/10.1016/j.ymsp.2012.03.003>.
- Ebersohn, W. (1998). “Implementing a railway infrastructure maintenance system.” In *Conference on Railway Engineering Proceedings: Engineering Innovation for a Competitive Edge* (pp. 395-402). Rockhampton, Qld: Central Queensland University.

- Ebersöhn, W., & Selig, E. T. (1994). Track modulus measurements on a heavy haul line. *Transportation Research Record (1470)*, 73–82.
- Ebersohn, W., Trevizo, M.C., & Selig, E.T. (1993). Effect of low track modulus on track performance. In *Proceedings of the Fifth International Heavy Haul Conference*, 379-388.
- El-Sibaie, M. (2000). Computer model developed to predict rail passenger car response to track geometry (No. RR000-04). Washington, DC: United States. Federal Railroad Administration.
- Esveld, C. (2001). *Modern railway track, 2nd Ed.* Zaltbommel, Netherlands: MRT-Productions.
- Faizi, K., Beetham, P., & Kromanis, R. (2023). Performance evaluation of rail track bed stiffness: pre and post stabilisation. *Construction and Building Materials*, 407, 133452.
- Fallah Nafari, S. (2017). Quantifying the Distribution of Rail Bending Stresses along the Track using Train-Mounted Deflection Measurements.
- Fallah Nafari, S., Gül, M., Hendry, M. T., & Cheng, J. R. (2018). Estimation of vertical bending stress in rails using train-mounted vertical track deflection measurement systems. *Proceedings of the Institution of Mechanical Engineers, Part F: Journal of Rail and Rapid Transit*, 232(5), 1528-1538.
- Fallah Nafari, S., Gül, M., Hendry, M. T., Otter, D., & Roger Cheng, J. J. (2018). Operational vertical bending stresses in rail: Real-life case study. *Journal of Transportation Engineering, Part A: Systems*, 144(3), 05017012.
- Fallah Nafari, S., M. Gül, M. T. Hendry, D. Otter, and J. J. Roger Cheng. (2018). Operational vertical bending stresses in rail: Real-life case study. *Journal of Transportation Engineering Part A: Systems*, 144(3), 05017012. <https://doi.org/10.1061/JTEPBS.0000116>.
- Farritor, S. (2006). Real-time measurement of track modulus from a moving car. (No. DOT/FRA/ORD-05/05), U.S. Dept. of Transportation, Washington, DC.

- Farritor, S., & Fateh, M. (2013). Measurement of vertical track deflection from a moving rail car. (No. DOT/FRA/ORD-13/08). United States. Federal Railroad Administration. Office of Research and Development.
- Federal Railroad Administration (FRA). (2004). A preliminary design of a system to measure vertical track modulus from a moving railcar (Rep. No. RR04-03). *U.S. Department of Transportation, Federal Railroad Administration, Washington, D.C., August 20, 2009.*
- Federal Railroad Administration (FRA). (2007). *Track Safety Standard Compliance Manual.* Washington, DC: USDOT.
- Federal Railroad Administration (FRA). (2014). Track and rail and infrastructure integrity compliance manual. *Federal Railroad Administration, Washington DC, USA.*
- Greisen, C. J. (2010). Measurement, Simulation, and Analysis of the Mechanical Response of Railroad Track. *M.Sc. Thesis, Department of Mechanical Engineering, University of Nebraska at Lincoln.*
- Greisen, C., Lu, S., Duan, H., Farritor, S., Arnold, R., GeMeiner, B., ... & Carr, G. (2009, January). Estimation of rail bending stress from real-time vertical track deflection measurement. In *Joint Rail Conference (Vol. 43383, pp. 175-182).*
- Greisen, C.J. (2010). *Measurement, simulation, and analysis of the mechanical response of railroad track.* (M.Sc. Thesis). University of Nebraska–Lincoln, Department of Mechanical Engineering.
- Grossoni, I., Andrade, A. R., Bezin, Y., & Neves, S. (2019). The role of track stiffness and its spatial variability on long-term track quality deterioration. *Proceedings of the Institution of Mechanical Engineers, Part F: Journal of Rail and Rapid Transit, 233(1), 16-32.*

- Grubbs, F. E. (1969). Procedures for detecting outlying observations in samples. *Technometrics*, *11*(1), 1–21. <https://doi.org/10.1080/00401706.1969.10490657>.
- Guan, Q., Zeng, J., & Jin, X. (2014). An angle of attack-based derailment criterion for wheel flange climbing. *Proceedings of the Institution of Mechanical Engineers, Part F: Journal of Rail and Rapid Transit*, *228*(7), 719-729.
- Guo, Y., Shi, C., Zhao, C., Markine, V., & Jing, G. (2022). Numerical analysis of train-track-subgrade dynamic performance with crumb rubber in ballast layer. *Construction and Building Materials*, *336*, 127559.
- Hawari, H. M., & Murray, M. H. (2008, January). Deterioration of railway track on heavy haul lines. In *Conference on Railway Engineering* (pp. 7-10).
- Hay, W. W. (1982). *Railroad engineering*. New York: Wiley.
- Heelis, M. E., Collop, A. C., Dawson, A. R., Chapman, D. R., & Krylov, V. V. (1999). Predicting and measuring vertical track displacements on soft subgrades. *Loughborough University. [Conference contribution](#)*.
- Hendry, M. T. (2011). The geomechanical behaviour of peat foundations below rail-track structures. Ph.D. Thesis, *University of Saskatchewan, Saskatoon, Canada*.
- Hendry, M. T., Edwards, T., Martin, C. D., & Barbour, S. (2011). Assessing the Condition of Peat Subgrades Subjected to Heavy Axle Loads: Effectiveness of the use of Piles to Strengthen Embankment. *2011 International Heavy Haul Association Conference - Railroading in Extreme Conditions*, Calgary, AB, June 19-22.
- Hendry, M., & Roghani, A. (2015). Rolling Measurement of Vertical Deflection: Assessing a technology for the measurement of the deflection of track structure and its use to map poor

- subgrade locations. *Technical Report prepared for the Transportation Development Centre of Transport Canada*, 30 pp.
- Hendry, M., Martin, D., Barbour, S., & Edwards, T. (2008). Monitoring cyclic strain below a railway embankment overlying a peaty foundation using novel instrumentation. In *61st Canadian Geotechnical Conference*, Edmonton, Alberta, September 21-24, Paper No. 443.
- Heydari, H. (2023). Evaluating the dynamic behavior of railway-bridge transition zone: numerical and field measurements. *Canadian Journal of Civil Engineering*.
- Higgins, R. L., Otter, D. E., & Martin, R. W. (1992, January). High accuracy load measuring wheelset. In *Tenth International Wheelset Congress: Sharing the Latest Wheelset Technology in Order to Reduce Costs and Improve Railway Productivity; Preprints of Papers* (pp. 181-188). Barton, ACT: Institution of Engineers, Australia.
- Holder, D. E., Csenge, M. V., Qian, Y., Dersch, M. S., Edwards, J. R., & Van Dyk, B. J. (2017). Laboratory investigation of the Skl-style fastening system's lateral load performance under heavy haul freight railroad loads. *Engineering Structures*, 139, 71-80.
- Hsu, H. H., Chang, C. Y., & Hsu, C. H. (Eds.). (2017). Big data analytics for sensor-network collected intelligence. Morgan Kaufmann.
- Hunt, G.A., & Wood, J. (2005). Review of the effect of track stiffness on track performance. *RSSB Research Project 372*.
- Hyslip, J. P. (2002). *Fractal Analysis of Geometry Data for Railway Track Condition Assessment* (Doctoral dissertation). Department of Civil Engineering, University of Massachusetts, Amherst, MA.
- Hyslip, J. P. (2002). Fractal analysis of track geometry data. *Transportation research record*, 1785(1), 50-57.

- Ibrahim, A., Huat, B. B., Asadi, A., & Nahazanan, H. (2014). Foundation and embankment construction in peat: An overview. *Electronic Journal of Geotechnical Engineering*, 19(2014), 10079-10094.
- Indraratna, B., Nimbalkar, S., & Rujikiatkamjorn, C. (2012). "Future of Australian rail tracks capturing higher speeds with heavier freight." Australian Geomechanics Society Sydney Chapter Symposium, (October 2012).
- Indraratna, B., Sajjad, M. B., Ngo, T., Correia, A. G., & Kelly, R. (2019). Improved performance of ballasted tracks at transition zones: A review of experimental and modelling approaches. *Transportation Geotechnics*, 21, 100260.
- Johnson, K. L. (1989). The strength of surfaces in rolling contact. *Proceedings of the Institution of Mechanical Engineers, Part C: Mechanical Engineering Science*, 203(3), 151-163.
- Judge, A., Ho, C., Huang, H., Hyslip, J., & Gao, Y. (2018). Field investigation and modeling of track substructure performance under trains moving at critical speed (Report No. DOT/FRA/ORD-18/21).
- Karaduman, G., Karaköse, M., & Akin, E. (2012, December). Experimental fuzzy diagnosis algorithm based on image processing for rail profile measurement. In *Proceedings of 15th International Conference Mechatronika* (pp. 1-6). IEEE.
- Karttunen, K., Kabo, E., & Ekberg, A. (2012). A numerical study of the influence of lateral geometry irregularities on mechanical deterioration of freight tracks. *Proceedings of the Institution of Mechanical Engineers, Part F: Journal of Rail and Rapid Transit*, 226(6), 575-586.
- Kasy, M. (2019). Uniformity and the delta method. *Journal of Econometric Methods*, 8(1), 20180001.

- Kerr, A. D. (1983). A Method for Determining the Track Modulus Using A Locomotive Or Car On Multi-Axle Trucks. *Proceedings of the American Railway Engineering Association*, 84, 269-286.
- Kerr, A. D. (2003). *Fundamentals of Railway Track Engineering*. Omaha, NE: Simmons-Boardman Books, Inc.
- Kish, A., & Samavedam, G. (2013). *Track buckling prevention: theory, safety concepts, and applications* (No. DOT/FRA/ORD-13/16). John A. Volpe National Transportation Systems Center (US).
- Konrad, J.-M., Grenier, S., & Garnier, P. (2007). Influence of repeated heavy axle loading on peat bearing capacity. In: 60th Canadian Geotechnical Conference, Ottawa, ON, pp. 1551-1558.
- Kotrlik, J. W., & Higgins, C. C. (2001). "Organizational research: Determining appropriate sample size in survey research." *Journal of Information Technology, Learning, and Performance*, 19(1), 43.
- Krejcie, R. V., & Morgan, D. W. (1970). Determining sample size for research activities. *Educational and psychological measurement*, 30(3), 607-610.
- Kumar, S. (2006). A study of the rail degradation process to predict rail breaks. Ph.D. thesis, Luleå tekniska universitet.
- Kurowicka, D., & Cooke, R. M. (2006). *Uncertainty analysis with high dimensional dependence modelling*. John Wiley & Sons.
- Lasisi, A. (2019). *Dimension reduction techniques in track geometry quality analysis and safety*. University of Delaware.
- Lehmann, E. L., & Casella, G. (2006). *Theory of point estimation*. Springer Science & Business Media.

- Leishman, E. M., M. T. Hendry, and C. D. Martin. (2017). Canadian main track derailment trends, 2001 to 2014. *Can. J. Civ. Eng.*, 44(11), 927–934. <https://doi.org/10.1139/cjce-2017-0076>.
- Lenth, R. V. (2001). Some practical guidelines for effective sample size determination. *The American Statistician*, 55(3), 187-193.
- Leong, J., & Murray, M. H. (2008, February). Probabilistic analysis of train–track vertical impact forces. In *Proceedings of the Institution of Civil Engineers-Transport*, 161(1), 15-21.
- Leong, J., Murray, M., & Steffens, D. (2007). Examination of railway track dynamic models capabilities against measured field data. In *Proceedings International Heavy Haul Conference Specialist Technical Session* (pp. 257-267). International Heavy Haul Association.
- Lestoille, N., Soize, C., & Funfschilling, C. (2016). “Sensitivity of train stochastic dynamics to long-term evolution of track irregularities.” *Vehicle System Dynamics*, 54(5), 545-567.
- Li, D., & Selig, E.T. (1995). Evaluation of railway subgrade problems. *Transportation Research Record*, 1489, 17.
- Li, D., Hass, K., & Meddah, A. (2002, June). Moving closer to performance-based track geometry inspection. *Railway Track and Structures*, 15-17.
- Li, D., Hyslip, J.P., Sussmann, T.R., & Chrismer, S.M. (2015). *Railway geotechnics*. Taylor and Francis Group LLC, Boca Raton, FL, USA.
- Li, D., Thompson, R., Marquez, P., & Kalay, S. (2004). Development and Implementation of a Continuous Vertical Track-Support Testing Technique. *Transportation Research Record: Journal of the Transportation Research Board*, No. 1863, TRB, National Research Council, Washington, D.C., 2004, pp. 68–73.

- Li, M. X. D., & Berggren, E. G. (2010). A study of the effect of global track stiffness and its variations on track performance: simulation and measurement. *Proceedings of the Institution of Mechanical Engineers, Part F: Journal of Rail and Rapid Transit*, 224(5), 375-382.
- Liu, W., & Wang, W. (2002). Study on dynamic stiffness and damp measurement of railway crushed stone ballast. *Journal of the China Railway Society*, 24(6), 99-104.
- Liu, X., Saat, M. R., & Barkan, C. P. L. (2012). Analysis of causes of major train derailment and their effect on accident rates. *Transportation Research Record*, 2289, 154–163.
- Lu, S. (2008). *Real-time vertical track deflection measurement system*. (Ph.D. Thesis). University of Nebraska at Lincoln, Department of Mechanical Engineering.
- Lu, S., Hogan, C., Minert, B., Arnold, R., Farritor, S., GeMeiner, W., & Clark, D. (2007, January). Exception criteria in vertical track deflection and modulus. In *ASME/IEEE Joint Rail Conference (Vol. 4787, pp. 191-198)*.
- Lundqvist, A., & Dahlberg, T. (2005). “Railway Track Stiffness Variation-Consequences and Countermeasures.” In *19th IAVSD Symposium of Dynamics of Vehicles on Roads and Tracks*, Milano, August 29-September 2, 2005. Department of Mechanical Engineering, Politecnico di Milano.
- Maglio, M., Vernersson, T., Nielsen, J. C., Ekberg, A., & Kabo, E. (2024). Influence of railway wheel tread damage on wheel–rail impact loads and the durability of wheelsets. *Railway Engineering Science*, 32(1), 20-35.
- McVey, B. (2006). A nonlinear approach to measurement of vertical track deflection from a moving railcar. *M.Sc. dissertation, Department of Mechanical Engineering, University of Nebraska-Lincoln, Lincoln, NE*.

- McVey, B., Farritor, S., Norman, C., Wood, N., Arnold, R., Fetei, M., & El-Sibaie, M. (2005). Track modulus measurement from a moving railcar. In *Proceedings of the Annual Conference, American Railway Engineering and Maintenance of Way Association*, Chicago, IL, Sept. 25-28.
- Mei, H., Leng, W., Nie, R., Tu, R., Li, Y., & Dong, J. (2019). Experimental research on the dynamic response characteristics of the transition subgrade induced by heavy-haul train passage. *Proceedings of the Institution of Mechanical Engineers, Part F: Journal of Rail and Rapid Transit*, 233(9), 974-987.
- Memon, M. A., Ting, H., Cheah, J. H., Thurasamy, R., Chuah, F., & Cham, T. H. (2020). Sample size for survey research: Review and recommendations. *Journal of Applied Structural Equation Modeling*, 4(2):1-20.
- Milne, D., Harkness, J., Le Pen, L., & Powrie, W. (2021). "The influence of variation in track level and support system stiffness over longer lengths of track for track performance and vehicle track interaction." *Vehicle System Dynamics*, 59(2), 245-268.
- Mohammadzadeh, S., & Ghahremani, S. (2012). Estimation of train derailment probability using rail profile alterations. *Structure and Infrastructure Engineering*, 8(11), 1034-1053.
- Naeimi, M., Zakeri, J. A., Esmacili, M., & Shadfar, M. (2015). Influence of uneven rail irregularities on the dynamic response of the railway track using a three-dimensional model of the vehicle-track system. *Vehicle System Dynamics*, 53(1), 88-111.
- Nanjundeswaraswamy, T. S., & Divakar, S. (2021). Determination of sample size and sampling methods in applied research. *Proceedings on engineering sciences*, 3(1), 25-32.

- Nemeth, I., & Schleinzer, G. (2008). Investigation into the indirect determination of wheel-rail surface roughness. In *Proceedings of the 11th Mini Conference on Vehicle System Dynamics, Budapest* (pp. 135-146).
- Ngamkhanong, C., Ming, Q. Y., Li, T., & Kaewunruen, S. (2020). Dynamic train-track interactions over railway track stiffness transition zones using baseplate fastening systems. *Engineering Failure Analysis*, 118, 104866.
- Nielsen, J. C., Lundén, R., Johansson, A., & Vernersson, T. (2003). Train-track interaction and mechanisms of irregular wear on wheel and rail surfaces. *Vehicle System Dynamics*, 40(1-3), 3-54.
- Norman, C. (2004). Measurement of track modulus from a moving railcar. *MSc. Thesis, Department of Mechanical Engineering, University of Nebraska at Lincoln*.
- Norman, C., Farritor, S., Arnold, R., Elias, S. E. G., Fateh, M., and Sibaie, M. E. (2004). Design of a system to measure track modulus from a moving railcar. In: *Proceeding of Railway Engineering, Engineering Technics Press, Edinburgh, U.K.*
- Oberkampf, W. L., DeLand, S. M., Rutherford, B. M., Diegert, K. V., & Alvin, K. F. (2002). "Error and uncertainty in modeling and simulation." *Journal of Reliability Engineering and System Safety*, 75(3), 333-357.
- Odashima, M., Azami, S., Naganuma, Y., Mori, H., & Tsunashima, H. (2017). Track geometry estimation of a conventional railway from car-body acceleration measurement. *Mechanical Engineering Journal*, 4(1), 16-00498. DOI: <https://dx.doi.org/10.1299/mej.16-00498>
- Olofsson, U., & Telliskivi, T. (2003). Wear, plastic deformation and friction of two rail steels—a full-scale test and a laboratory study. *Wear*, 254(1-2), 80-93.

- Panunzio, A. M., Puel, G., Cottureau, R., Simon, S., & Quost, X. (2017). "Construction of a stochastic model of track geometry irregularities and validation through experimental measurements of dynamic loading." *Vehicle System Dynamics*, 55(3), 399-426.
- Pearson, R. K. (2005). *Mining imperfect data: Dealing with contamination and incomplete records*. Philadelphia, PA: Society for Industrial and Applied Mathematics.
- Peters N. (2010). *CN Railway Engineering Course*. Retrieved from McGill University Civil Engineering Graduate Studies class.
- Powrie, W., & Le Pen, L. (Ed.). (2016). *A Guide to Track Stiffness: August 2016*. University of Southampton Department of Civil & Environmental Engineering.
- Prause, R. H., H. C. Meacham, H. D. Harrison, T. G. John, and W. A. Glaeser. (1974). *Assessment of design tools and criteria for urban rail track structures: Volume I. At-grade tie-ballast track*. Washington, DC: DOT, Urban Mass Transportation Administration Office of Research and Development.
- Punetha, P., & Nimbalkar, S. (2023). An innovative rheological approach for predicting the behaviour of critical zones in a railway track. *Acta Geotechnica*, 18(10), 5457-5483.
- Puzavac, L., Popović, Z., & Lazarević, L. (2012). Influence of track stiffness on track behaviour under vertical load. *Promet-Traffic&Transportation*, 24(5), 405-412.
- Rail Safety and Standard Board Limited. (2011). Track system requirements. *United Kingdom, London*.
- Raymond, G. P. (1985). Analysis of track support and determination of track modulus. *Transportation Research Record*, 1022, 80-90.
- Raymond, G.P. (1978). Design for railroad ballast and subgrade support. *Journal of the Geotechnical Engineering Division, ASCE*, 104, 45-59.

- Read, D., Chrismer, S., Ebersöhn, W., & Selig, E. (1994). Track modulus measurements at the Pueblo soft subgrade site. *Transportation Research Record*, 1470, 55.
- Remennikov, A. M., & Kaewunruen, S. (2008). A review of loading conditions for railway track structures due to train and track vertical interaction. *Structural Control and Health Monitoring: The Official Journal of the International Association for Structural Control and Monitoring and of the European Association for the Control of Structures*, 15(2), 207-234.
- Ren, Y., and J. Chen. (2019). A new method for wheel–rail contact force continuous measurement using instrumented wheelset. *Vehicle system Dynamics*, 57(2), 269–285. <https://doi.org/10.1080/00423114.2018.1460853>.
- Roghani, A., and M. T. Hendry. (2016). Continuous vertical track deflection measurements to map subgrade condition along a railway line: Methodology and case studies. *Journal of Transportation Engineering Part A: Systems*, 142(12), 04016059. [https://doi.org/10.1061/\(ASCE\)TE.1943-5436.0000892](https://doi.org/10.1061/(ASCE)TE.1943-5436.0000892).
- Roghani, A., and M. T. Hendry. (2017). Quantifying the impact of subgrade stiffness on track quality and the development of geometry defects. *Journal of Transportation Engineering Part A: Systems*, 143(7), 04017029. <https://doi.org/10.1061/JTEPBS.0000043>.
- Roghani, A., Macciotta, R., & Hendry, M. (2015). Combining track quality and performance measures to assess track maintenance requirements. In *Proceeding of ASME/IEEE Joint Rail Conference (Vol. 56451, p. V001T01A009)*. American Society of Mechanical Engineers.
- Roghani, A., Macciotta, R., & Hendry, M. T. (2017). Quantifying the effectiveness of methods used to improve railway track performance over soft subgrades: methodology and case study. *Journal of Transportation Engineering, Part A: Systems*, 143(9), 04017043.

- Roghani, A., R. Macciotta, and M. Hendry. (2015). Combining track quality and performance measures to assess track maintenance requirements. In *Proceeding, ASME/IEEE Joint Rail Conf.* Washington, DC: ASME.
- Roghani, A., R. Macciotta, and M. T. Hendry. (2017). Quantifying the effectiveness of methods used to improve railway track performance over soft subgrades: Methodology and case study. *Journal of Transportation Engineering Part A: Systems*, 143(9), 04017043. <https://doi.org/10.1061/JTEPBS.0000071>.
- Sadeghi, J. (2010). Development of railway track geometry indexes based on statistical distribution of geometry data. *Journal of Transportation Engineering*, 136(8), 693-700.
- Sadeghi, J. (2012). New advances in analysis and design of railway track system. *Journal of Reliability and Safety Railway*, 30(3), 75-100.
- Sadeghi, J., & Barati, P. (2010). Evaluation of conventional methods in analysis and design of railway track system. *International Journal of Civil Engineering*, 8(1), 44–56.
- Sadeghi, J., & Barati, P. (2010). Improvements of conventional methods in railway track analysis and design. *Canadian Journal of Civil Engineering*, 37(5), 675-683.
- Sajjad, M. B., Indraratna, B., Ngo, T., Kelly, R., & Rujikiatkamjorn, C. (2023). A computational approach to smoothen the abrupt stiffness variation along railway transitions. *Journal of Geotechnical and Geoenvironmental Engineering*, 149(8), 04023063.
- Scanlan, K. M., Hendry, M. T., & Martin, C. D. (2016). “Evaluating the Equivalency Between Track Quality Indices and the Minimum Track Geometry Threshold Exceedances Along a Canadian Freight Railway.” In: *ASME/IEEE Joint Rail Conference* (Vol. 49675, p. V001T01A012). American Society of Mechanical Engineers.

- Schramm, G. (1961). Permanent way technique and permanent way economy. *Darmstadt, Germany: Otto Elsner Verlagsgesellschaft, Elsner.*
- Selig, E. T., & Li, D. (1994). Track modulus: its meaning and factors influencing it. *Transportation Research Record 1470*, 47-54.
- Selig, E. T., & Waters, J. M. (1994). Track Geotechnology and Substructure Management. *Thomas Telford ISBN: 0-07277-2013-9.*
- Sendra-Perez, C., Sanchez-Jimenez, J. L., Marzano-Felisatti, J. M., Encarnacion-Martinez, A., Salvador-Palmer, R., & Priego-Quesada, J. I. (2023). Reliability of threshold determination using portable muscle oxygenation monitors during exercise testing: a systematic review and meta-analysis. *Scientific Reports*, *13*(1), 12649.
- Serfling, R. J. (2009). *Approximation theorems of mathematical statistics*. John Wiley & Sons; September 25.
- Shi, C., Zhou, Y., Xu, L., Zhang, X., & Guo, Y. (2023). A critical review on the vertical stiffness irregularity of railway ballasted track. *Construction and Building Materials*, *400*, 132715.
- Smith, L., Doe, B., Li, D., Otter, D., & Uppal, S. (2003). Study of bridge approach and track transition degradation: Factors and mitigation.
- Smith, S. W. (1997). *The scientist and engineer's guide to digital signal processing*. California Technical Publication, San Diego.
- Soleimani, H., & Moavenian, M. (2017). Tribological aspects of wheel–rail contact: a review of wear mechanisms and effective factors on rolling contact fatigue. *Urban Rail Transit*, *3*(4), 227-237.
- Srinivasan M. (1969). Modern permanent way. *Mumbai, India: Somaiya Publications.*

- Srivastava, J. P., Sarkar, P. K., & Ranjan, V. (2014). Contact stress analysis in wheel–rail by Hertzian method and finite element method. *Journal of The Institution of Engineers (India): Series C*, 95, 319-325.
- Sun, Y., Dhanasekar, M., & Roach, D. (2004). Effect of track geometry irregularities on wheel-rail impact forces.
- Sussman, T. R., Ebersöhn, W., & Selig, E. T. (2001). Fundamental nonlinear track load-deflection behavior for condition evaluation. *Transportation Research Record*, 1742(1), 61-67.
- Sussmann, T. R., O’Hara, K. R., Kutrubes, D., Heyns, F. J., & Selig, E. T. (March 2001). Development of ground penetrating radar for railway infrastructure condition detection. *Proceedings of the Symposium on the Application of Geophysics to Engineering and Environmental Problems, Denver, CO*.
- Taber, K. S. (2018). The use of Cronbach’s alpha when developing and reporting research instruments in science education. *Research in science education*, 48, 1273-1296.
- TC (Transport Canada). (2011). *Rules respecting track safety*. Ottawa, ON, Canada: TC.
- Thompson, R., & Li, D. (2002, February). Automated Vertical Track Strength Testing Using TTCI’s Track Loading Vehicle. *Technology Digest.1489*, 17–25.
- Tong, P., Brantman, R., Greif, R., & Mirabella, J. (1979). *Tests of the Amtrak SDP-40F Train Consist Conducted on Chessie System Track* (No. DOT-TSC-FRA-79-14). United States. Federal Railroad Administration. Office of Research and Development.
- Tong, Y., Liu, G., Yousefian, K., & Jing, G. (2022). Track vertical stiffness–value, measurement methods, effective parameters and challenges: A review. *Transportation Geotechnics*, 37, 100833.
- Transport Canada (TC). (2011). *Rules Respecting Track Safety*. Ottawa, ON, Canada: TC.

- Transportation Safety Board of Canada. (2013). *Statistical Summary Railway Occurrences*. Cat. No. TU1-2/2013, Gatineau, Canada.
- Transportation Safety Board of Canada. (2016). *Statistical Summary - Railway Occurrences 2015 - Data Tables*. Retrieved from <http://www.bst-tsb.gc.ca/eng/stats/rail/2015/sser-ssro-2015-tbts.asp> [cited 11/12 2023].
- TSB (Transportation Safety Board of Canada). (1999). *Railway Investigation Report R99Q0019*. The Transportation Safety Board of Canada (TSB).
- TSB (Transportation Safety Board of Canada). (2008). *Railway Investigation Report R04Q0040*. Cat. No. TU3-6/04-2E, ISBN 978-0-662-47573-6.
- TSB (Transportation Safety Board of Canada). (2013). *Statistical summary railway occurrences*. Cat. No. TU1-2/2013, Gatineau, Canada.
- UIC (International Union of Railways). (2008). *Best Practice Guide for Optimum*. Proceedings of the Edition Techniques Ferroviaires; UIC: Paris, France.
- Van Dyk, B. (2015). Characterization of the loading environment for shared-use railway superstructure in North America. *M.Sc. thesis, University of Illinois at Urbana-Champaign*.
- Van Dyk, B. J., Dersch, M. S., Edwards, J. R., Ruppert Jr, C., & Barkan, C. P. (2013, April). Quantifying shared corridor wheel loading variation using wheel impact load detectors. In *ASME/IEEE Joint Rail Conference (Vol. 55300, p. V001T01A002)*. American Society of Mechanical Engineers.
- Van Dyk, B. J., Edwards, J. R., Dersch, M. S., Ruppert Jr, C. J., & Barkan, C. P. (2017). "Evaluation of dynamic and impact wheel load factors and their application in design processes." In: *Proceedings of the Institution of Mechanical Engineers, Part F: Journal of Rail and Rapid Transit*, 231(1), 33-43.

- Wang, P., Wang, L., Chen, R., Xu, J., Xu, J., & Gao, M. (2016). Overview and outlook on railway track stiffness measurement. *Journal of Modern Transportation*, 24, 89-102.
- Wang, W., & Li, G. X. (2012). Development of high-speed railway vehicle derailment simulation—Part I: A new wheel/rail contact method using the vehicle/rail coupled model. *Engineering Failure Analysis*, 24, 77-92.
- Wangqing, W., Geming, Z., Kaiming, Z., & Lin, L. (1997). Development of inspection car for measuring railway track elasticity. *Proc., 6th Heavy Haul Conf., International Heavy Haul Association, Cape Town, South Africa*.
- Wei, Z. (2018). Modelling and monitoring of dynamic wheel-rail interaction at railway crossing. *Ph.D. thesis, Ph.D. thesis, Delft Technical University, Delft*.
- Wiley, R., & Elsaleiby, A. (2011). A Review of Wheel Impact Measurement Variation. *TD-11-007. Transportation Technology Center, Incorporated, Pueblo, Colorado*.
- Woelfle, A. (2016). Report for the national research council. In *Analysis of wheel-rail forces during (MRail) rolling deflection tests*. Gloucester, ON, Canada: National Research Council Canada, Automotive and Surface Transportation.
- Yu, F., & Hendry, M. T. (2019). A new strain gauge configuration on the rail web to decouple the wheel–rail lateral contact force from wayside measurement. *Proceedings of the Institution of Mechanical Engineers, Part F: Journal of Rail and Rapid Transit*, 233(9), 951-960.
- Zarembski, A. M. & Choros, J. (1979). On the measurement and calculation of vertical track modulus. *Proceedings of the American Railway Engineering Association*, 81, 156-173.
- Zarembski, A.M., & Palese, J. (2003). Transitions eliminate impact at crossings. *Railway Track Structures*, 99(8), 28–30.

- Zerbst, U., Lundén, R., Edel, K. O., & Smith, R. A. (2009). Introduction to the damage tolerance behaviour of railway rails—a review. *Engineering fracture mechanics*, 76(17), 2563-2601.
- Zhang, D., Zhai, W., & Wang, K. (2017). Dynamic interaction between heavy haul train and track structure due to increasing axle load. *Australian Journal of Structural Engineering*, 18(3), 190–203. <https://doi.org/10.1080/13287982.2017.1363126>.
- Zhang, P., He, C., Shen, C., Dollevoet, R., & Li, Z. (2024). Comprehensive validation of three-dimensional finite element modeling of wheel-rail high-frequency interaction via the V-Track test rig. *Vehicle System Dynamics*, 1-25.
- Zhao, X., Li, Z., & Liu, J. (2012). Wheel–rail impact and the dynamic forces at discrete supports of rails in the presence of singular rail surface defects. *Proceedings of the Institution of Mechanical Engineers, Part F: Journal of Rail and Rapid Transit*, 226(2), 124-139.

A. Appendix A: Summary of the Dynamic Load Factors (ϕ) Equations Presented in the Literature for Passenger Railways

Examples of equations for the upper envelope of ϕ and dynamic loads for passenger railways are presented as follows:

$1 + \frac{4.5S^2}{10^5} - \frac{1.5S^3}{10^7}$	Equation (A-1)	German Railways $\{V \leq 200\}$ (Schramm 1961)
$(1 + 3.86 \times 10^{-5}S^2)^{\frac{2}{3}}$	Equation (A-2)	WMATA (Prause et al. 1974)
$1.098 + 8 \times 10^{-4}S + 10^{-6}S^2$	Equation (A-3)	Iran Railways (Sadeghi 2010)
$1 + 0.021 \frac{S}{D}$	Equation (A-4)	Talbot (Hay 1982)
$1 + 4.92 \frac{S}{D}$	Equation (A-5)	South African Railways (Doyle 1980)
$1 + \frac{S}{58.14\sqrt{U}}$	Equation (A-6)	Indian Railways (Srinivasan 1969)
$1 + \frac{19.65S}{D\sqrt{U}}$	Equation (A-7)	Clark formula (Doyle 1980)
$1 + \delta\eta t$	Equation (A-8)	Eisenmann formula (Esveld 2001)
$\frac{8.784(\alpha_1 + \alpha_2)S}{P_S} \sqrt{\frac{D_j P_u}{g}}$	Equation (A-9)	British Railways (Doyle 1980)

where S = train speed (km/h); D = wheel diameter (mm); U = track modulus; δ = track maintenance condition; η = speed factor; t = upper confidence limits regarding the probability of exceedance; P_S = static load (kN); $\alpha_1 + \alpha_2$ = total rail joint dip angle (radians); D_j = track stiffness at joints (kN/mm); P_u = un-sprung load on one wheel (kN); and g = acceleration due to gravity (m/s²).

B. Appendix B: Developed Dynamic Load Factor (ϕ) Equations in Miles per Hour (m/h)

The following are Eqs. (3-5) and (3-6) modified to be used with speed (S) in units of miles per hour.

From Equation (3-5)

$$\phi_{Tan} = 1.16 \times 10^{-5}S^2 + 8.7 \times 10^{-4}S + 1.19 \quad \text{Equation (B-1)}$$

From Equation (3-6)

$$\phi_{NTan} = 1.16 \times 10^{-5}S^2 + 1.55 \times 10^{-3}S + 1.27 \quad \text{Equation (B-2)}$$

C. Appendix C: Supplemental Materials for Chapter 4

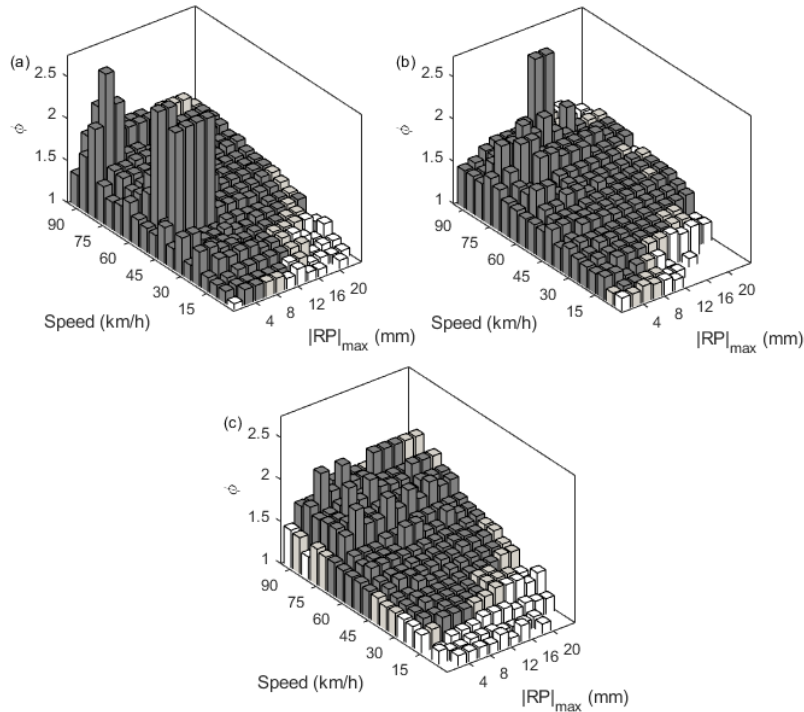


Figure C-1. IWS and rail profile measurements based on maximum values of dynamic load factor (ϕ) for 5 km/h increments of train speed and 2 mm increments of rail profile: (a) tangent sections; (b) curves; and (c) track assets.

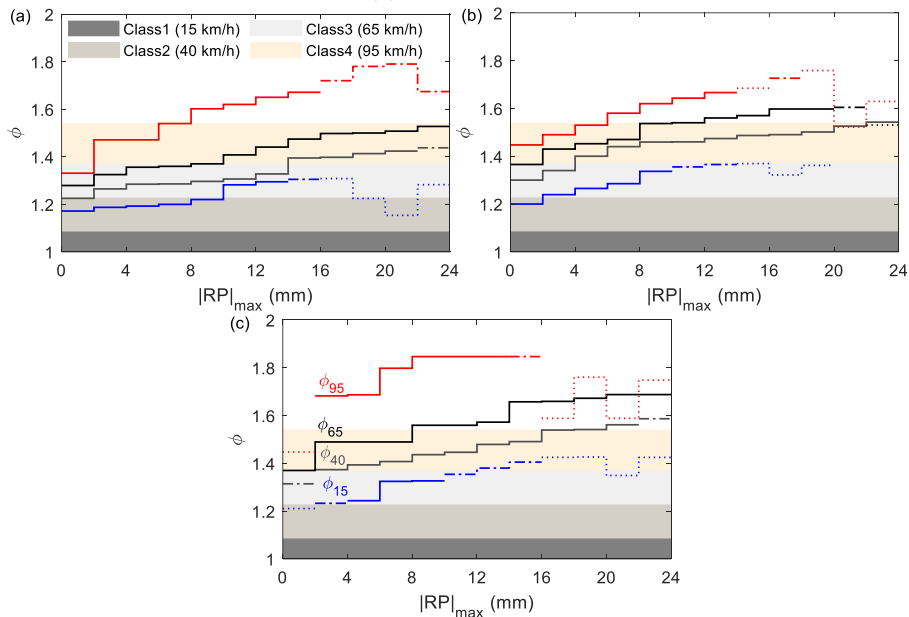


Figure C-2. IWS and rail profile measurements based on the maximum Grubbs' test values of ϕ values for 2 mm increments of rail profile regarding the statistical significance conditions for four track classes, including Class 1 ($S_{max}=15$ km/h [~ 10 mph], ϕ_{15}), Class 2 ($S_{max}=40$ km/h [25 mph], ϕ_{40}), Class 3 ($S_{max}=65$ km/h [~ 40 mph], ϕ_{65}), and Class 4 ($S_{max}=95$ km/h [~ 60 mph], ϕ_{95}), compared to AREMA (2021) (ϕ_{AREMA} (Equation (4-2))) estimations, in: (a) tangent tracks; (b) curves; and (c) track assets.

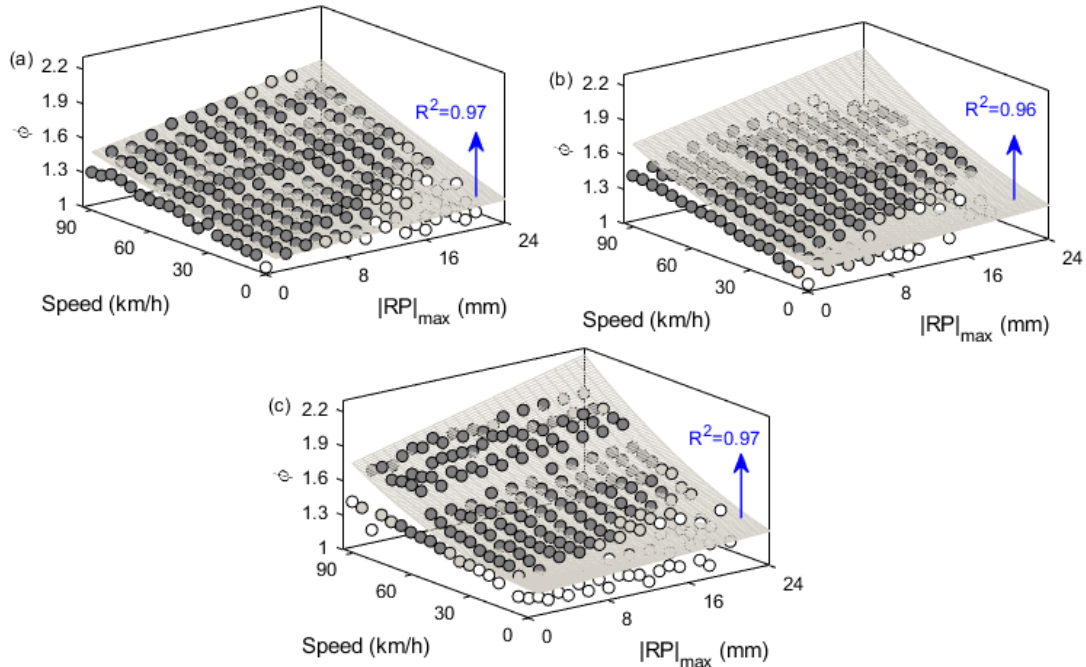


Figure C-3. Fitted surfaces over dynamic loads (in terms of ϕ) from IWS, with train speed increments of 5 km/h and rail profile increments of 2 mm: (a) tangent tracks; (b) curves; and (c) track assets (i.e., grade crossings, bridges, and switches). Note: Dark grey, light grey, and white markers represent high-, moderate-, and low-reliability zones, respectively. Fitted surfaces are based on data from the high- and moderate-reliability zones.

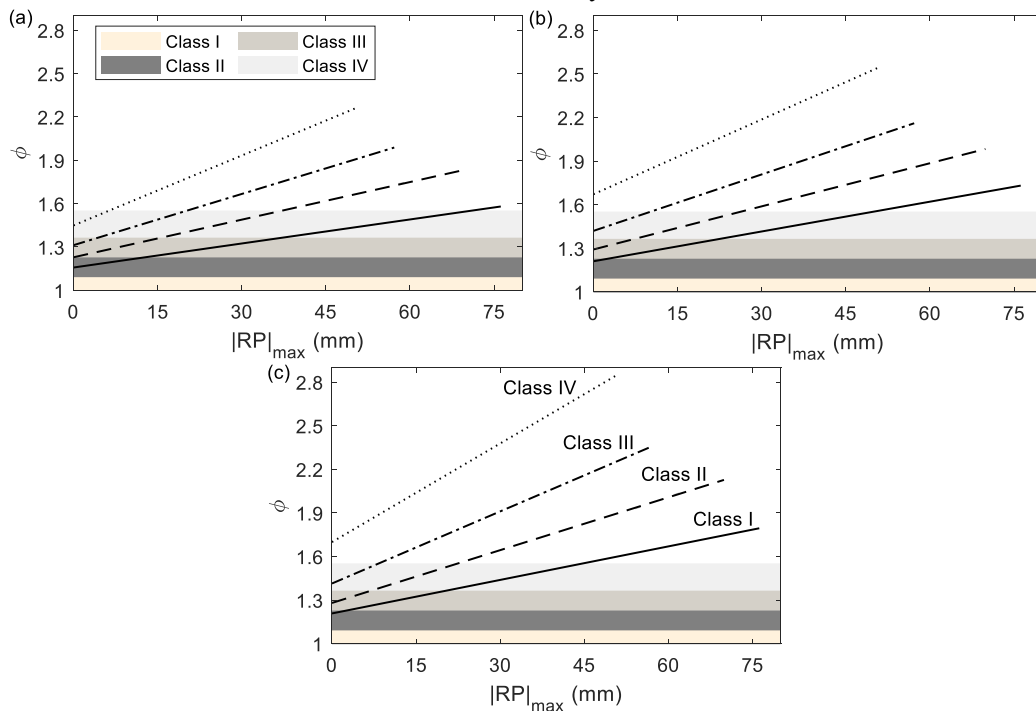


Figure C-4. ϕ trends across North American track classes: Comparative analysis showcasing ϕ changes based on fitted surfaces for defined rail profile threshold values within each track class, in (a) tangent tracks, (b) curves, and (c) track assets. Note: The shaded areas represent estimated values for each track class, according to AREMA (2021) (Equation 4-2).

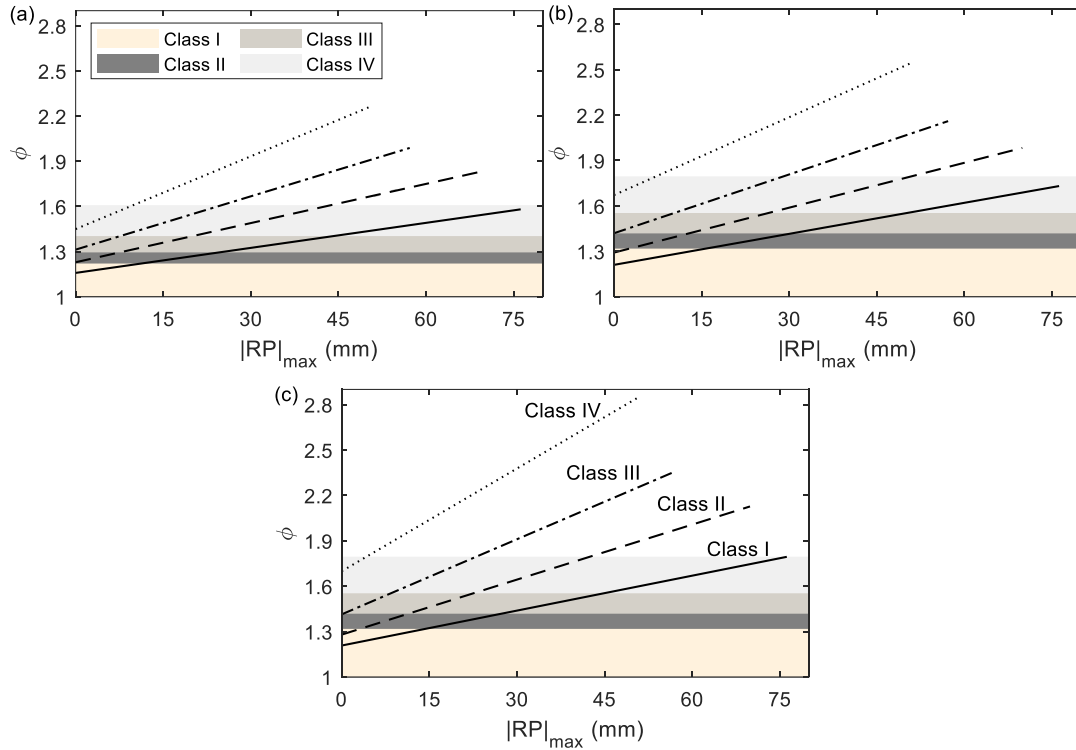


Figure C-5. ϕ trends across North American track classes: Comparative analysis showcasing ϕ changes based on fitted surfaces for defined rail profile threshold values within each track class, in (a) tangent tracks, (b) curves, and (c) track assets. Note: The shaded areas represent estimated values for each track class, according to Behnia et al. (2022) (Equations 4-3 and 4-4).

D. Appendix D: Supplemental Materials for Chapter 5

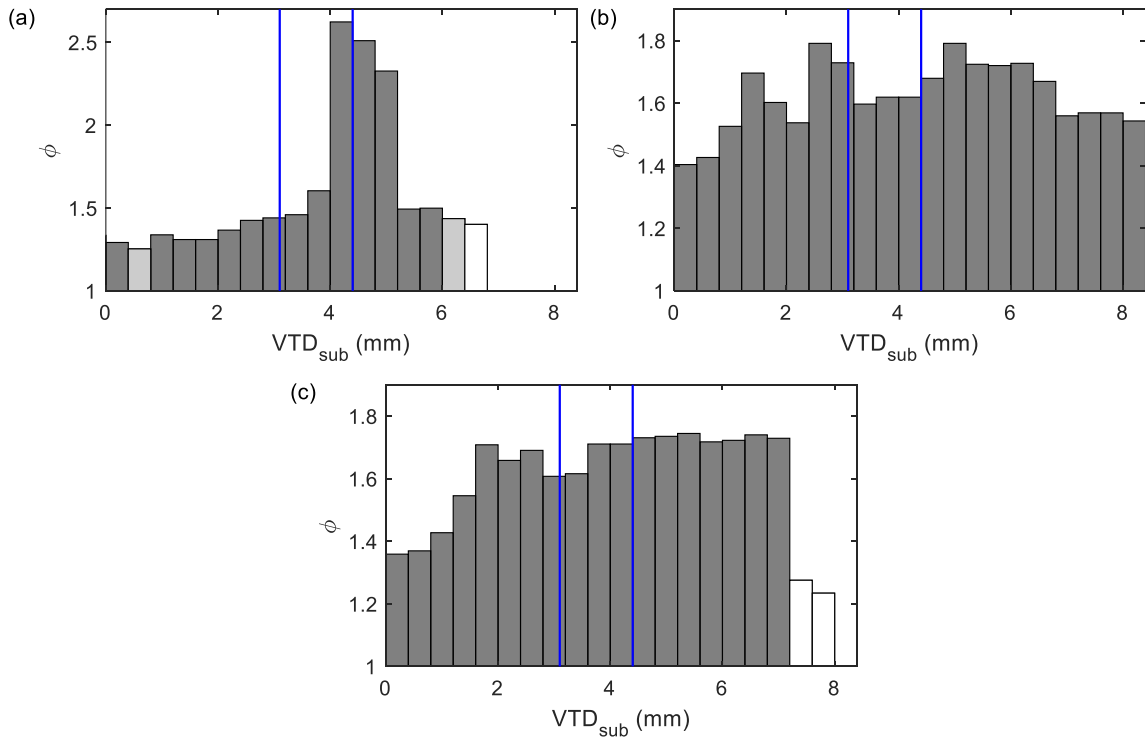


Figure D-1. IWS and VTD_{sub} measurements based on maximum values of the dynamic load factor ($\phi \geq 1.1$) for 0.4 mm increments of subgrade track stiffness (VTD_{sub}) on: (a) tangent sections; (b) curve sections; and (c) track assets. The graph is segregated into three sections by blue lines, indicating good ($VTD_{sub} \leq 3.1$), average ($3.1 < VTD_{sub} \leq 4.4$), and poor ($VTD_{sub} > 4.4$) tracks.

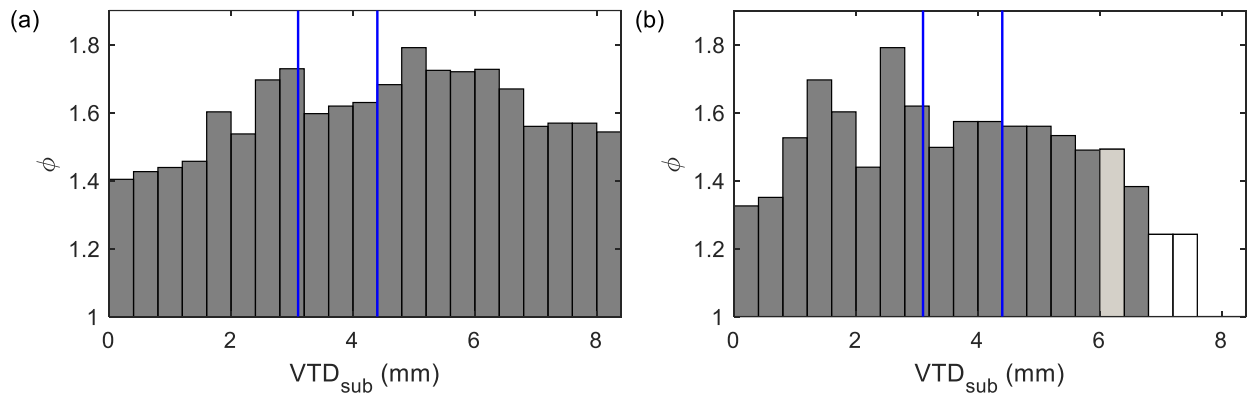


Figure D-2. IWS and VTD_{sub} measurements based on maximum values of the dynamic load factor ($\phi \geq 1.1$) for 0.4 mm increments of subgrade track stiffness (VTD_{sub}) on curves: (a) low (inner) rail; and (b) high (outer) rail. The graph is segregated into three sections by blue lines, indicating good ($VTD_{sub} \leq 3.1$), average ($3.1 < VTD_{sub} \leq 4.4$), and poor ($VTD_{sub} > 4.4$) tracks.

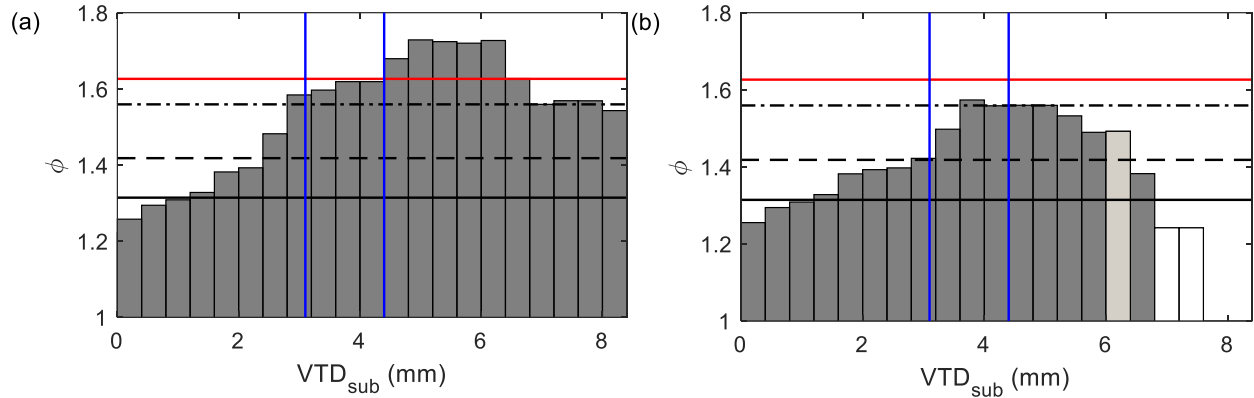


Figure D-3. IWS and VTD_{sub} measurements based on the Grubbs values of the dynamic load factor ($\phi \geq 1.1$) for 0.4 mm increments of subgrade track stiffness (VTD_{sub}) on: (a) curve sections; and (b) high (outer) rail in curve sections. Note the horizontal lines are based on equations provided by Behnia et al. (2022), where the ϕ_{C1} line is for 15 km/h (~10 mph), ϕ_{C1} line is for 40 km/h (~25 mph), ϕ_{C1} line is for 65 km/h (~40 mph), and ϕ_{C1} line (75 km/h~ 47 mph) is for the maximum speed with a reliable number of data points. The graph is segregated into three sections by blue lines, indicating good ($VTD_{sub} \leq 3.1$), average ($3.1 < VTD_{sub} \leq 4.4$), and poor ($VTD_{sub} > 4.4$) tracks.

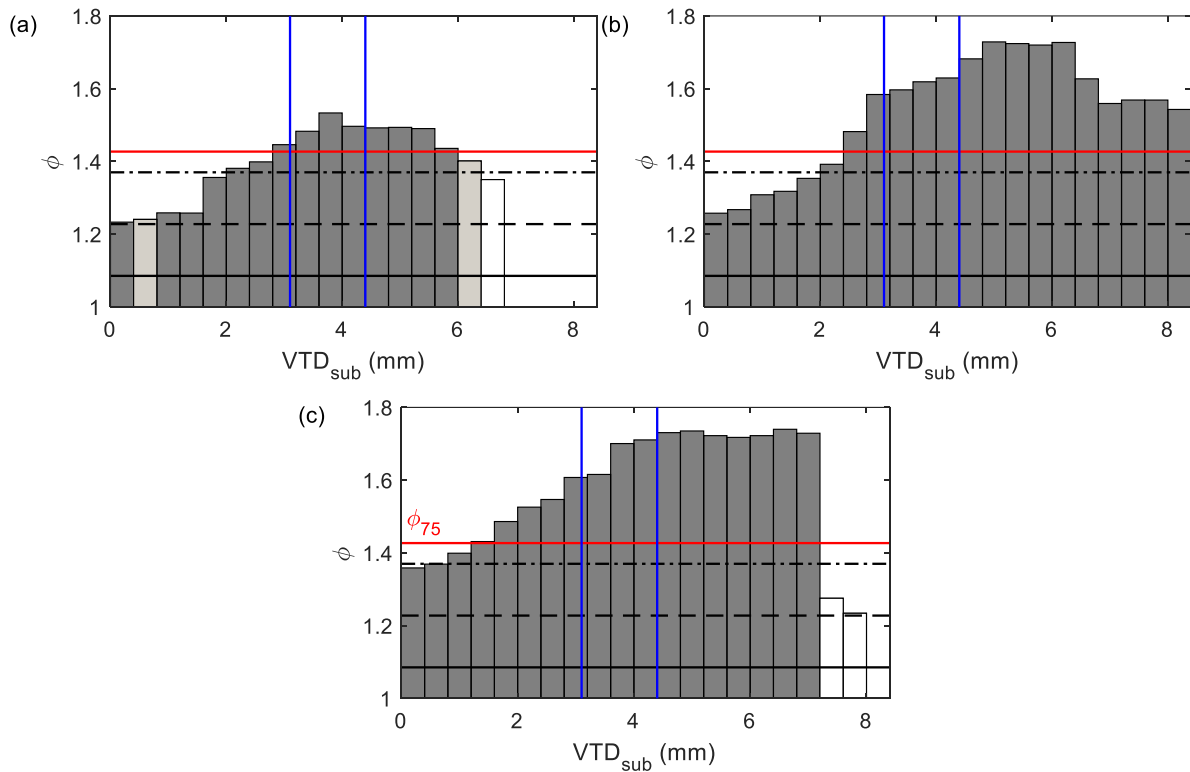


Figure D-4. IWS and VTD_{sub} measurements based on the Grubbs values of the dynamic load factor ($\phi \geq 1.1$) for 0.4 mm increments of subgrade track stiffness (VTD_{sub}) on: (a) tangent sections; (b) low (inner) rail in curve sections; and (c) track assets. Note the horizontal lines are based on the equation provided by AREMA (2021), where the ϕ_{C1} line is for 15 km/h (~10 mph), ϕ_{C2} line is for 40 km/h (~25 mph), ϕ_{C3} line is for 65 km/h (~40 mph), and ϕ_{75} line (75 km/h~ 47 mph) is for the maximum speed with a reliable number of data points. The graph is segregated into three sections by blue lines, indicating good ($VTD_{sub} \leq 3.1$), average ($3.1 < VTD_{sub} \leq 4.4$), and poor ($VTD_{sub} > 4.4$) tracks.

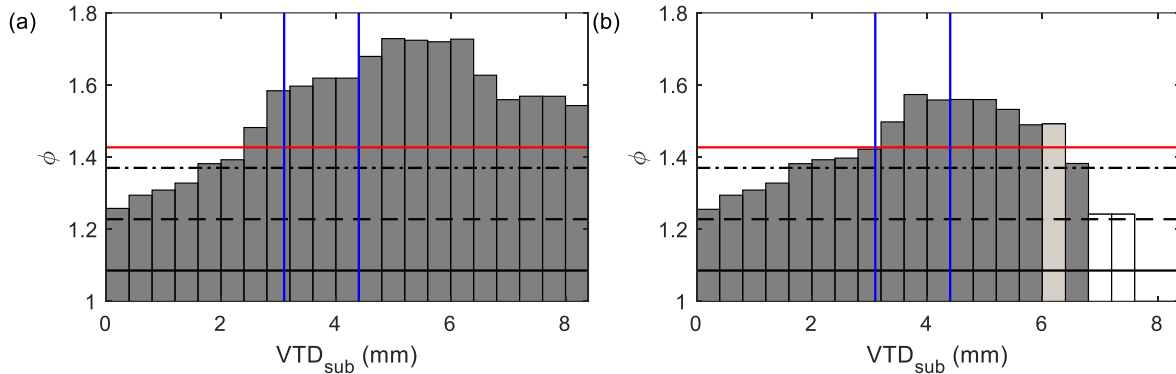


Figure D-5. IWS and VTD_{sub} measurements based on the Grubbs values of the dynamic load factor ($\phi \geq 1.1$) for 0.4 mm increments of subgrade track stiffness (VTD_{sub}) on: (a) curve sections; and (b) high (outer) rail in curve sections. Note the horizontal lines are based on the equation provided by AREMA (2021), where the ϕ_{C1} line is for 15 km/h (~10 mph), ϕ_{C2} line is for 40 km/h (~25 mph), ϕ_{C3} line is for 65 km/h (~40 mph), and ϕ_{75} line (75 km/h~ 47 mph) is for the maximum speed with a reliable number of data points. The graph is segregated into three sections by blue lines, indicating good ($VTD_{sub} \leq 3.1$), average ($3.1 < VTD_{sub} \leq 4.4$), and poor ($VTD_{sub} > 4.4$) tracks.

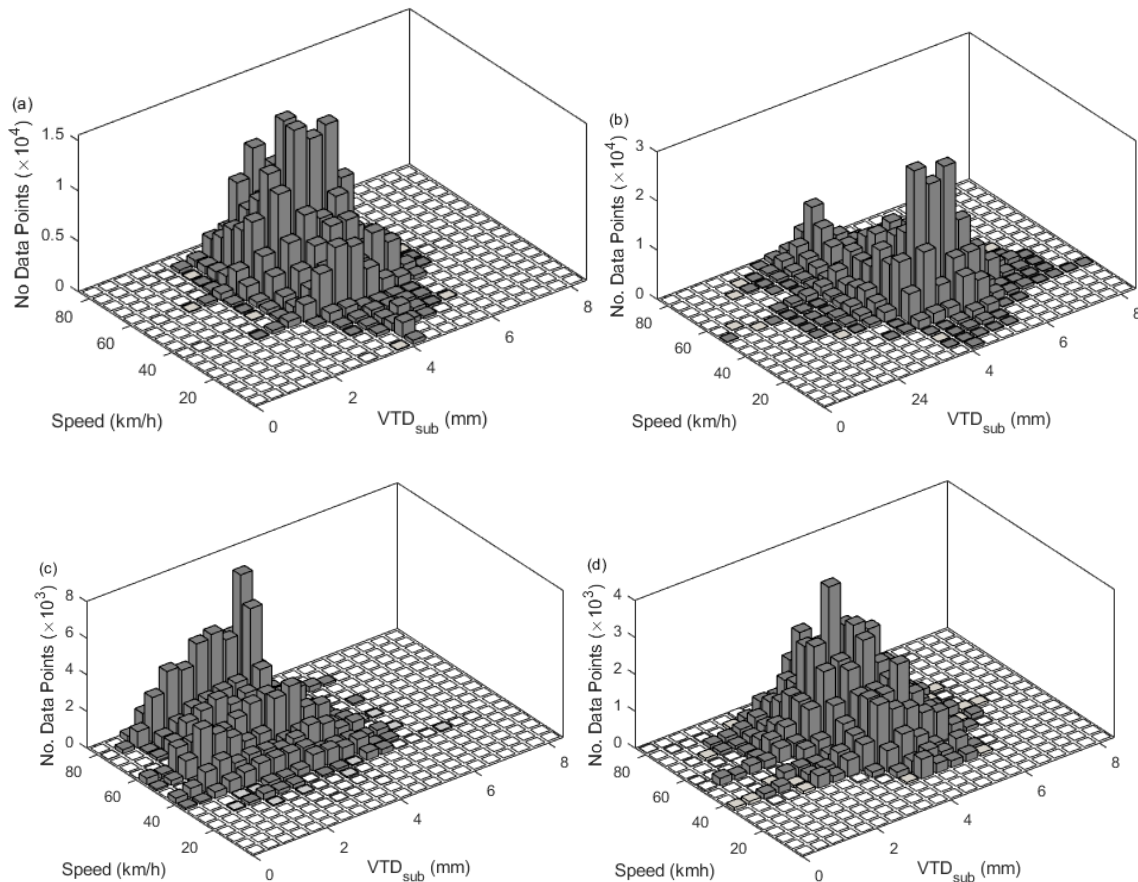


Figure D-6. Number of data points for 5 km/h increments of train speed and 0.4 mm increments of VTD_{sub} on: (a) tangent track; (b) low (inner) rail in curve sections; (c) high (outer) rail in curve sections; and (d) track assets.

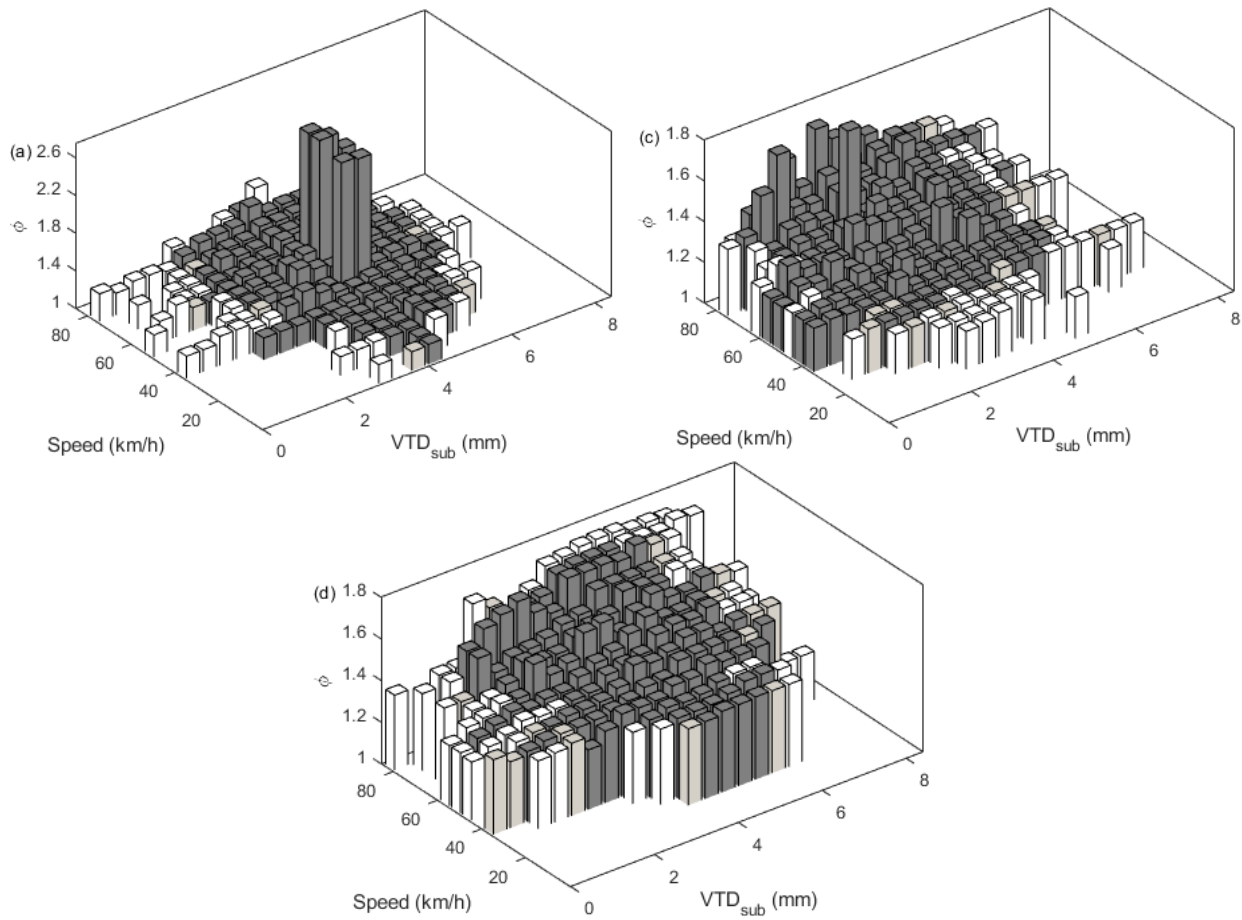


Figure D-7. Maximum values of the dynamic load factor ($\phi \geq 1.1$) values for 5 km/h increments of train speed and 0.4 mm increments of VTD_{sub} on: (a) tangent track; (b) low rail in curve sections; (c) high rail in curve sections; and (d) track assets.

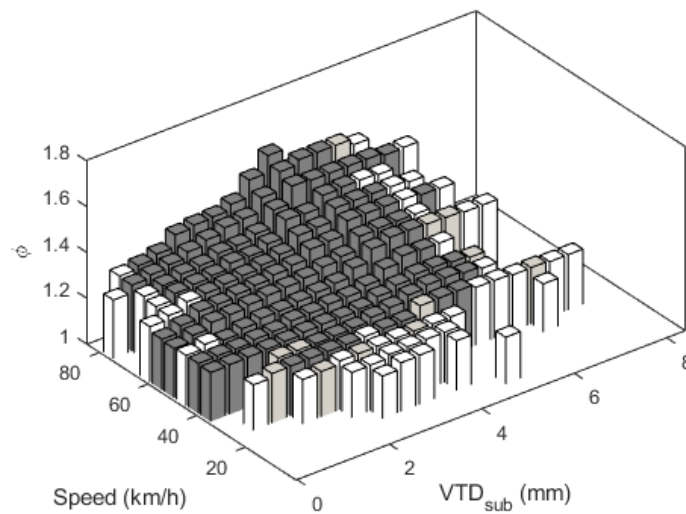


Figure D-8. Grubbs values of the dynamic load factor ($\phi \geq 1.1$) for 5 km/h increments of train speed and 0.4 mm increments of VTD_{sub} for the high rail in curves.

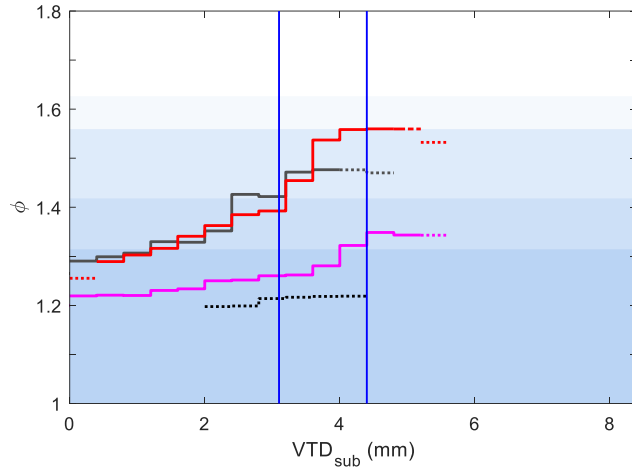


Figure D-9. IWS and VTD_{sub} (measured by MRail) measurements based on the Grubbs values of the dynamic load factor ($\phi \geq 1.1$) for 0.4 mm increments of VTD_{sub} with respect to statistical significance conditions for four specific train speeds on the high rail in curve sections. Note the specific speeds include $S = 15$ km/h (~ 10 mph, in black), 40 km/h (~ 25 mph, in magenta), 65 km/h (~ 40 mph, in grey), and 75 km/h (~ 47 mph, in red); and the shaded regions represent the ϕ values based on the specific speeds (ϕ_{C1} , ϕ_{C2} , ϕ_{C3} , and ϕ_{75}) and equations developed by Behnia et al. (2022). The graph is segregated into three sections by blue lines, indicating good ($VTD_{sub} \leq 3.1$), average ($3.1 < VTD_{sub} \leq 4.4$), and poor ($VTD_{sub} > 4.4$) tracks.

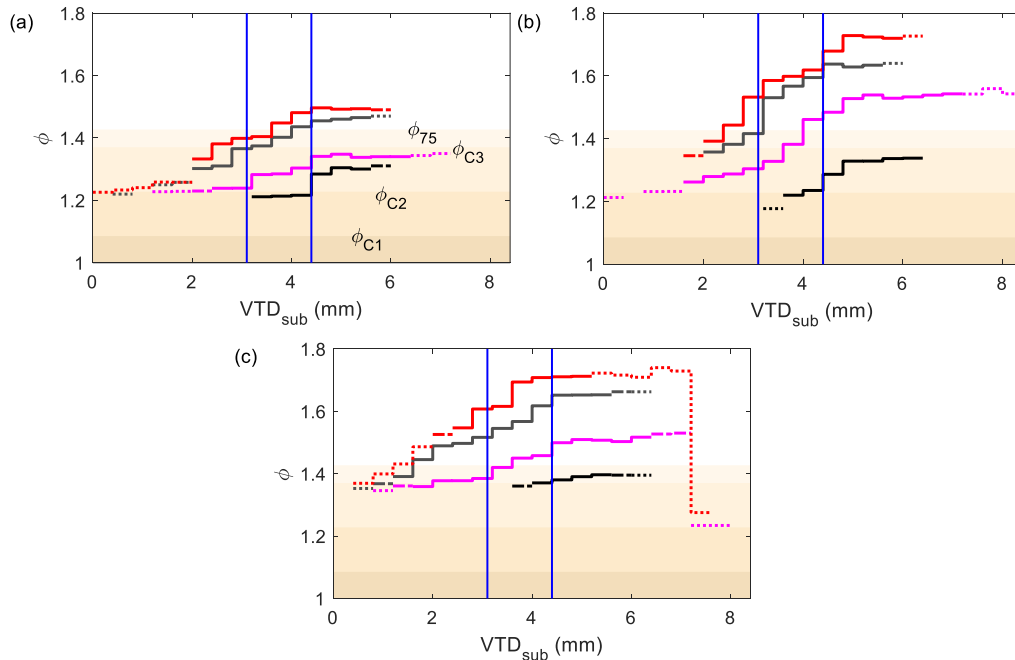


Figure D-10. IWS and VTD_{sub} (measured by MRail) measurements based on the Grubbs values of the dynamic load factor ($\phi \geq 1.1$) for 0.4 mm increments of VTD_{sub} with respect to significance conditions for four specific train speeds on: (a) tangent track; (b) the low rail in curves; and (c) track assets. Note the specific speeds include $S = 15$ km/h (~ 10 mph, in black), 40 km/h (~ 25 mph, in magenta), 65 km/h (~ 40 mph, in grey), and 75 km/h (~ 47 mph, in red); and the shaded regions represent the ϕ values based on the specific speeds (ϕ_{C1} , ϕ_{C2} , ϕ_{C3} , and ϕ_{75}) and equations developed by AREMA (2021). The graph is segregated into three sections by blue lines, indicating good ($VTD_{sub} \leq 3.1$), average ($3.1 < VTD_{sub} \leq 4.4$), and poor ($VTD_{sub} > 4.4$) tracks.

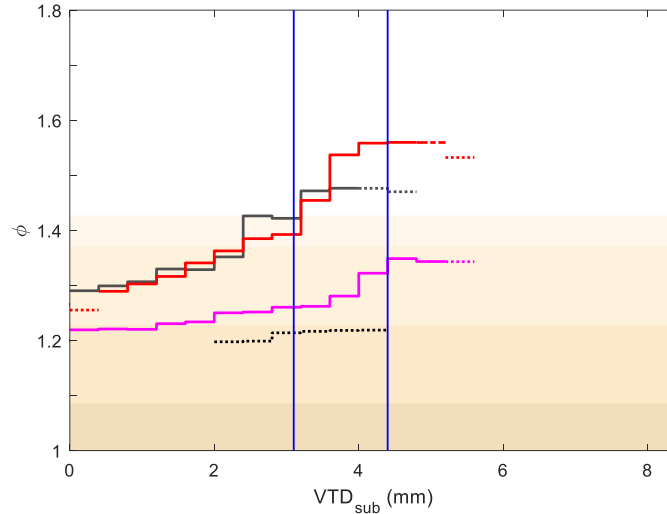


Figure D-11. IWS and VTD_{sub} (measured by MRail) measurements based on the Grubbs values of the dynamic load factor ($\phi \geq 1.1$) for 0.4 mm increments of VTD_{sub} with respect to significance conditions for four specific train speeds on the high rail in curve sections. Note the specific speeds include $S = 15$ km/h (~10 mph, in black), 40 km/h (~25 mph, in magenta), 65 km/h (~40 mph, in grey), and 75 km/h (~47 mph, in red); and the shaded regions represent the ϕ values based on the specific speeds (ϕ_{C1} , ϕ_{C2} , ϕ_{C3} , and ϕ_{75}) and equations developed by AREMA (2021). The graph is segregated into three sections by blue lines, indicating good ($VTD_{sub} \leq 3.1$), average ($3.1 < VTD_{sub} \leq 4.4$), and poor ($VTD_{sub} > 4.4$) tracks.

Table D-1. Statistical measures from probability distributions of dynamic vertical load measurements from the IWS system.

Track type	μ (kN)	Median (kN)	σ (kN)	Maximum (kN)	99.9th (kN)
All	144.8	144.3	10.0	377.8	190.9
Tangent track	144.6	144.2	8.2	377.8	184.3
Curve	145.0	144.5	11.5	258.0	192.8
Grade crossing	145.7	144.9	13.2	246.7	208.8
Bridge	145.3	145.0	11.5	243.5	209.3
Switch	145.4	144.8	14.3	219.5	200.7

Note: Data include all four instrumented wheels and two passes; μ = mean; σ = standard deviation; and 99.9th= 99.9th percentile value.

Table D-2. Statistical measures from probability distributions of VTD_{sub} measurements from the MRail system.

Track type	μ (mm)	Median (mm)	σ (mm)
All	4.1	4.2	0.9
Tangent track	4.2	4.2	0.6
Curve	3.9	4	1.2
Grade crossing	4.4	4.4	0.9
Bridge	4.6	4.5	0.7
Switch	4.5	4.4	0.8

Note: Data include all four instrumented wheels and two passes; μ = mean; and σ = standard deviation.

E. Appendix E: Supplemental Materials for Chapter 6

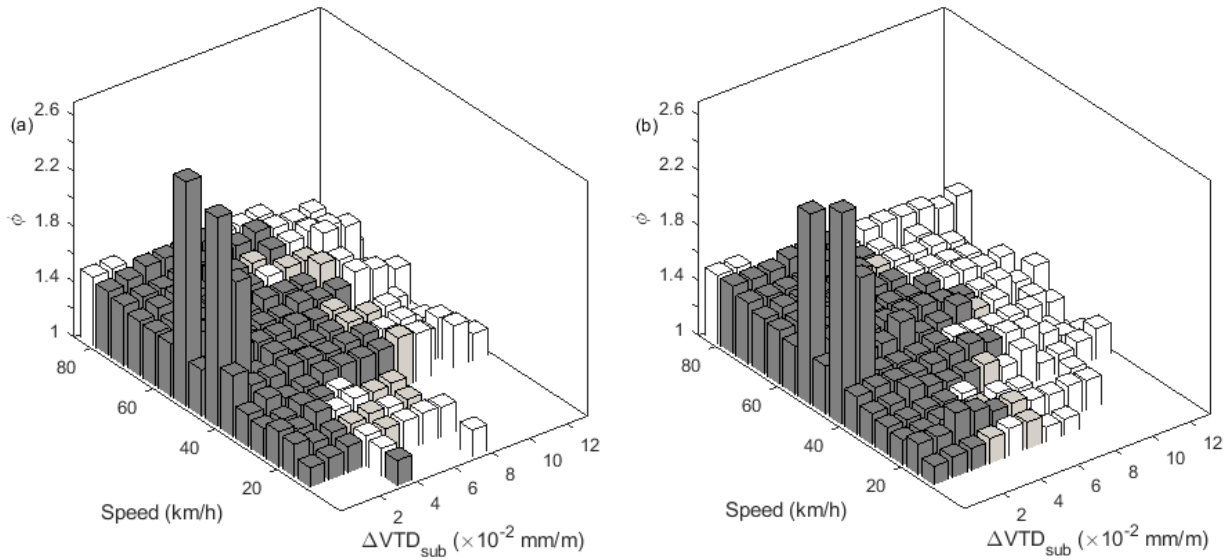


Figure E-1. Maximum ϕ values for 5 km/h increments of train speed and 0.01 mm/m increments of ΔVTD_{sub} on tangent track for: (a) soft-to-stiff transitions; and (b) stiff-to-soft transitions.

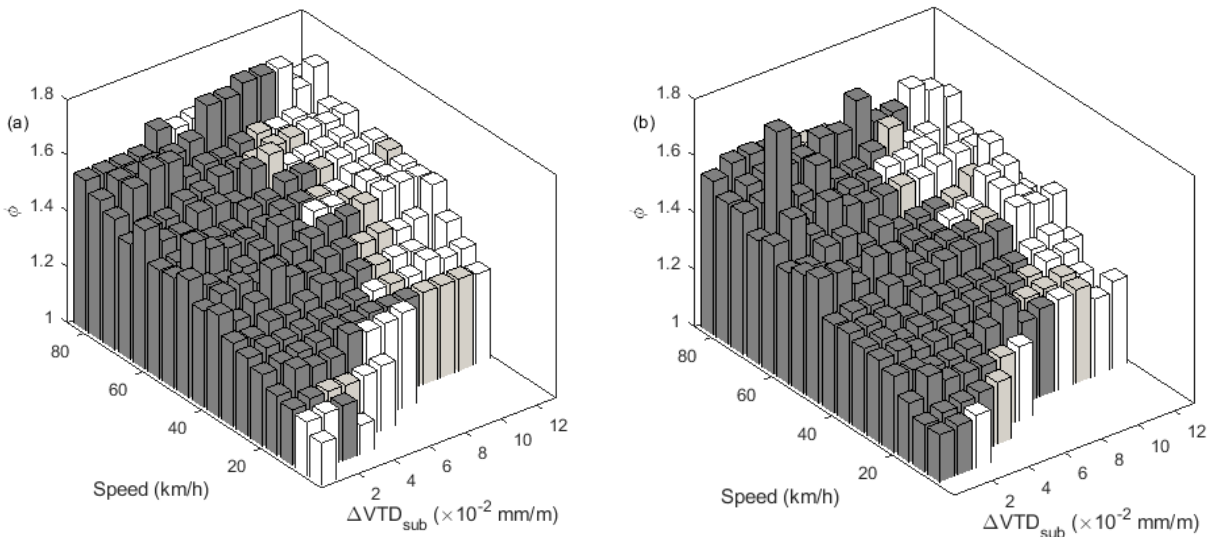


Figure E-2. Maximum ϕ values for 5 km/h increments of train speed and 0.01 mm/m increments of ΔVTD_{sub} on curve sections for: (a) soft-to-stiff transitions; and (b) stiff-to-soft transitions.

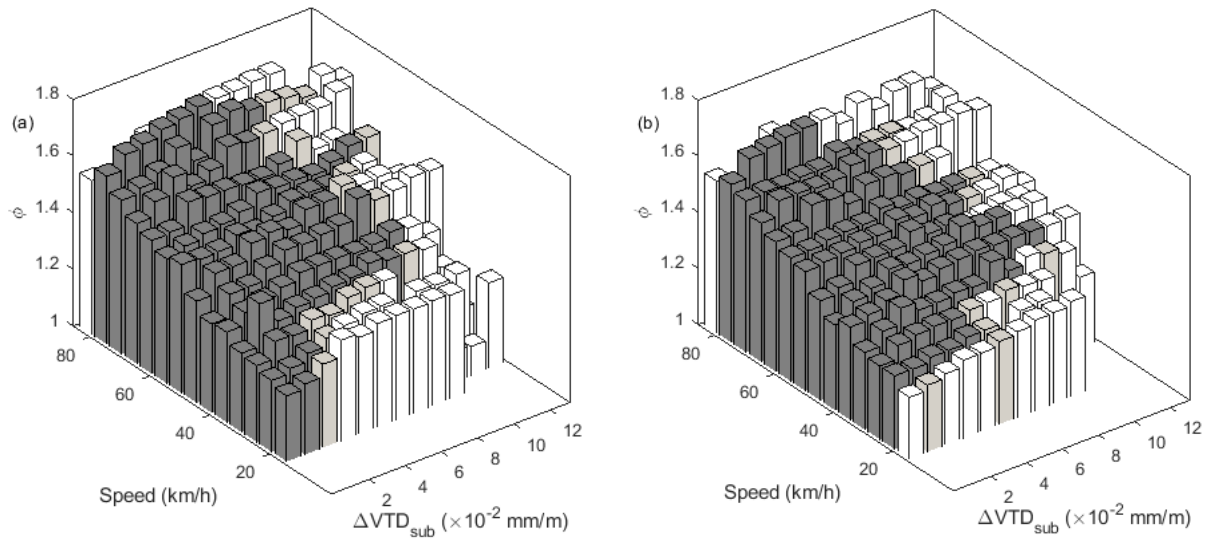


Figure E-3. Maximum ϕ values for 5 km/h increments of train speed and 0.01 mm/m increments of ΔVTD_{sub} on track assets for: (a) soft-to-stiff transitions; and (b) stiff-to-soft transitions.

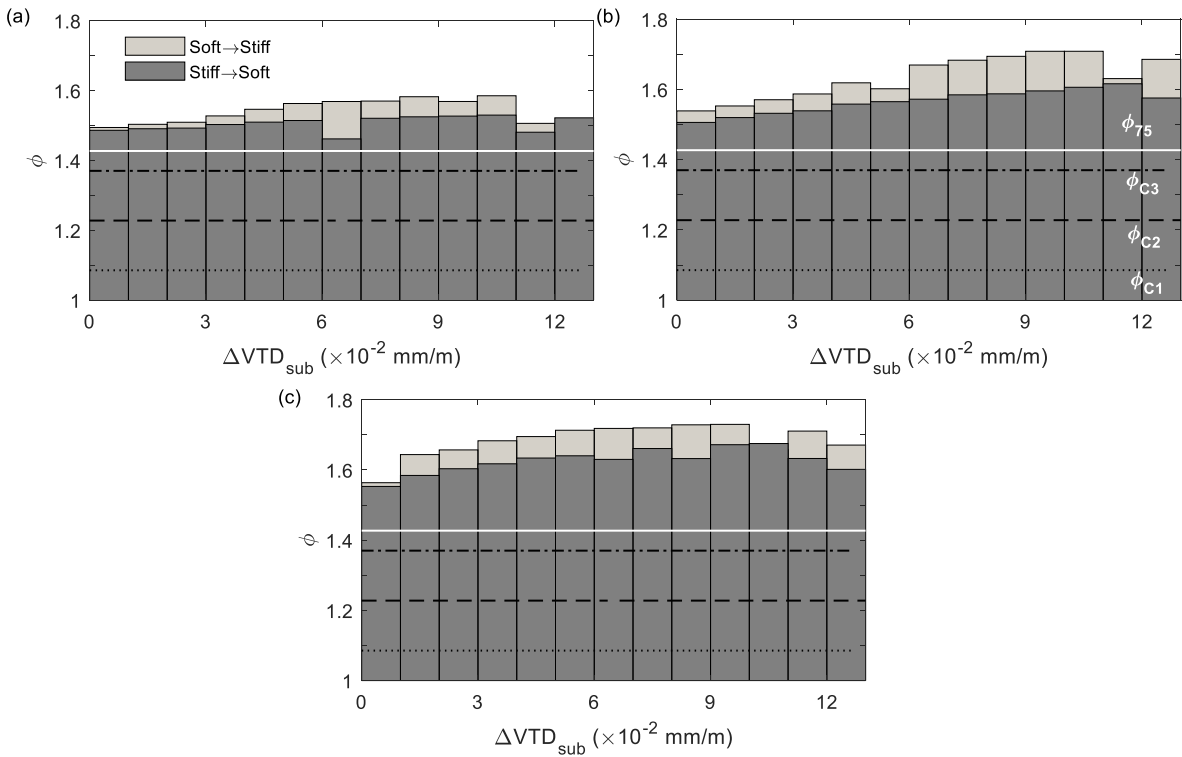


Figure E-4. Comparing the AREMA (2021) line regarding the track classes with ϕ value changes regarding the ΔVTD_{sub} with 0.01 mm/m increments for $\phi \geq 1.1$ for: (a) tangent track; (b) curve sections; and (c) track assets.

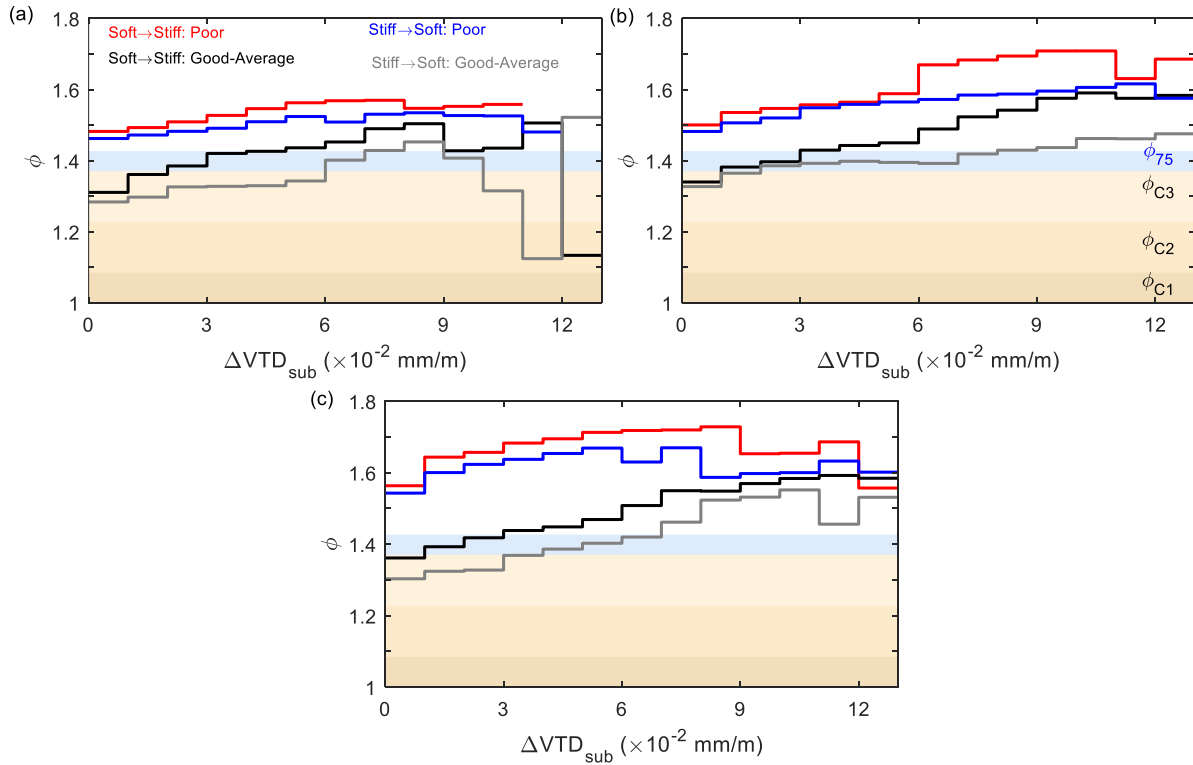


Figure E-5. Comparing the AREMA (2021) line regarding the track classes and conditions (i.e., good-average and poor tracks) with ϕ value changes regarding the ΔVTD_{sub} with 0.01 mm/m increments for $\phi \geq 1.1$ for: (a) tangent track; (b) curve sections; and (c) track assets.

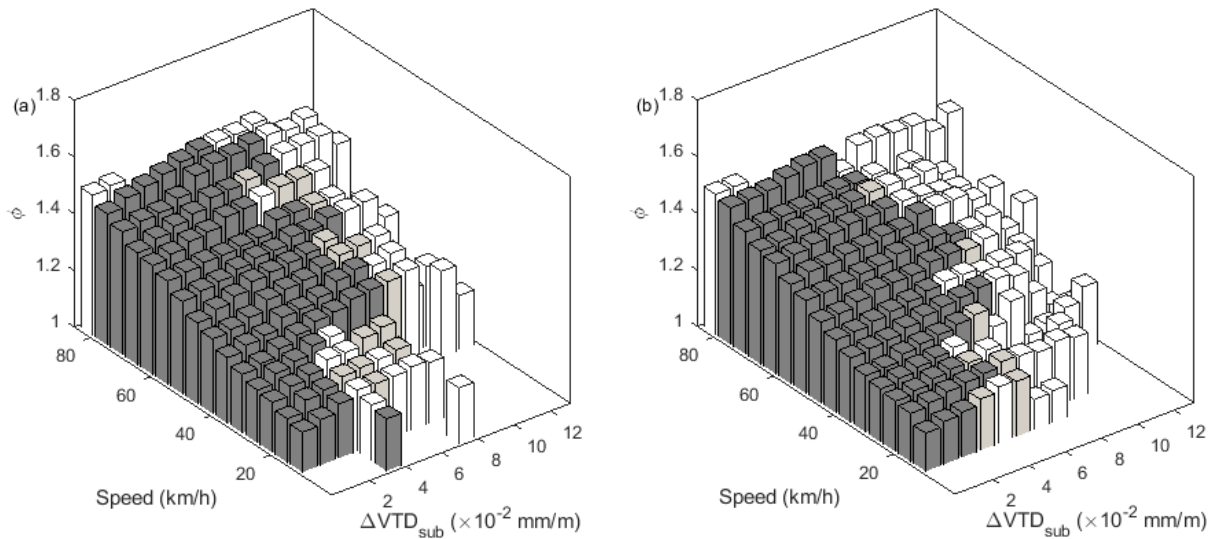


Figure E-6. The Grubbs test values of ϕ for 5 km/h increments of train speed and 0.01 mm/m increments of ΔVTD_{sub} on tangent track for: (a) soft-to-stiff transitions; and (b) stiff-to-soft transitions.

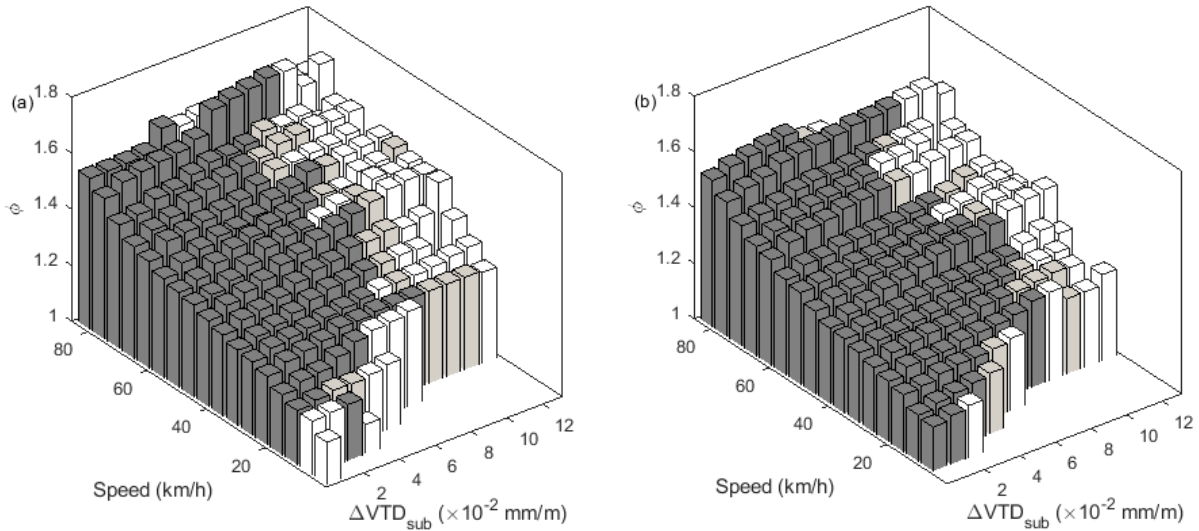


Figure E-7. The Grubbs test values of ϕ for 5 km/h increments of train speed and 0.01 mm/m increments of ΔVTD_{sub} on curve sections for: (a) soft-to-stiff transitions; and (b) stiff-to-soft transitions.

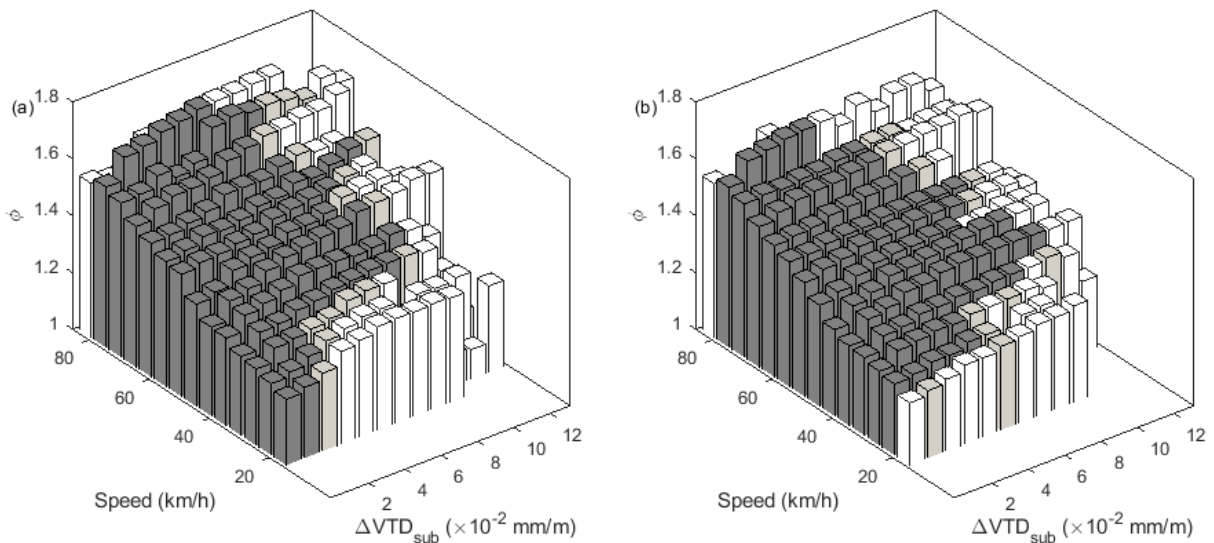


Figure E-8. The Grubbs test values of ϕ for 5 km/h increments of train speed and 0.01 mm/m increments of ΔVTD_{sub} on track assets for: (a) soft-to-stiff transitions; and (b) stiff-to-soft transitions.

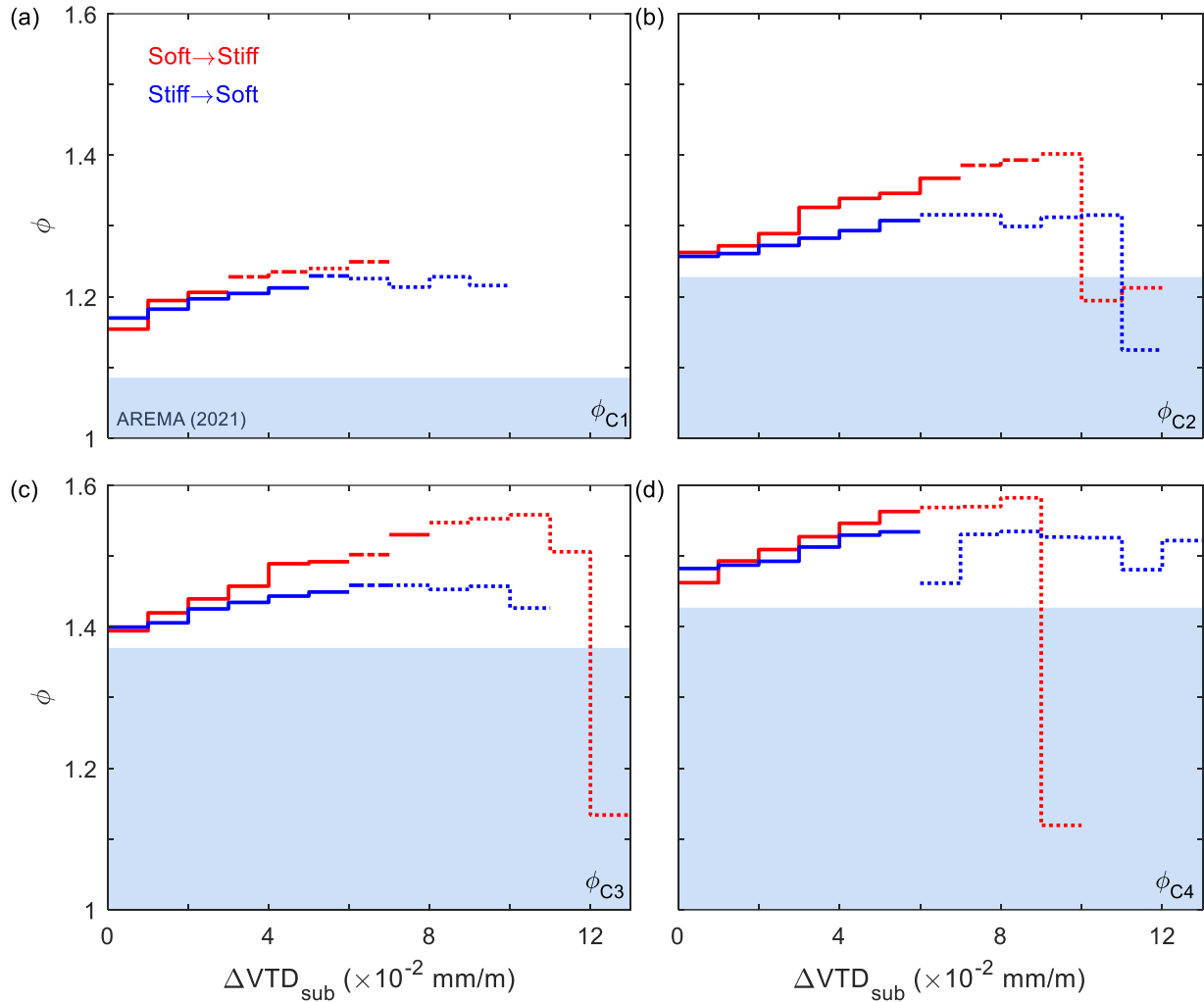


Figure E-9. IWS and MRail measurements for tangent track based on the Grubbs test values of dynamic load factor (ϕ) for 0.01 mm/m increments of ΔVTD_{sub} regarding the estimated ϕ values by AREMA (2021) (Equation 6-9) and reliability (confidence level) conditions for four specific train speeds: (a) 15 km/h (~10 mph, as Class 1, ϕ_{C1}); (b) 40 km/h (25 mph, as Class 2, ϕ_{C2}); (c) 65 km/h (~40 mph, as Class 3, ϕ_{C3}); and (d) 75 km/h (~47 mph, as the maximum speed with appropriate number of data points, ϕ_{75}). Note: the solid, dash-dot, and dotted lines respectively correspond to zones of high, moderate, and low reliability.

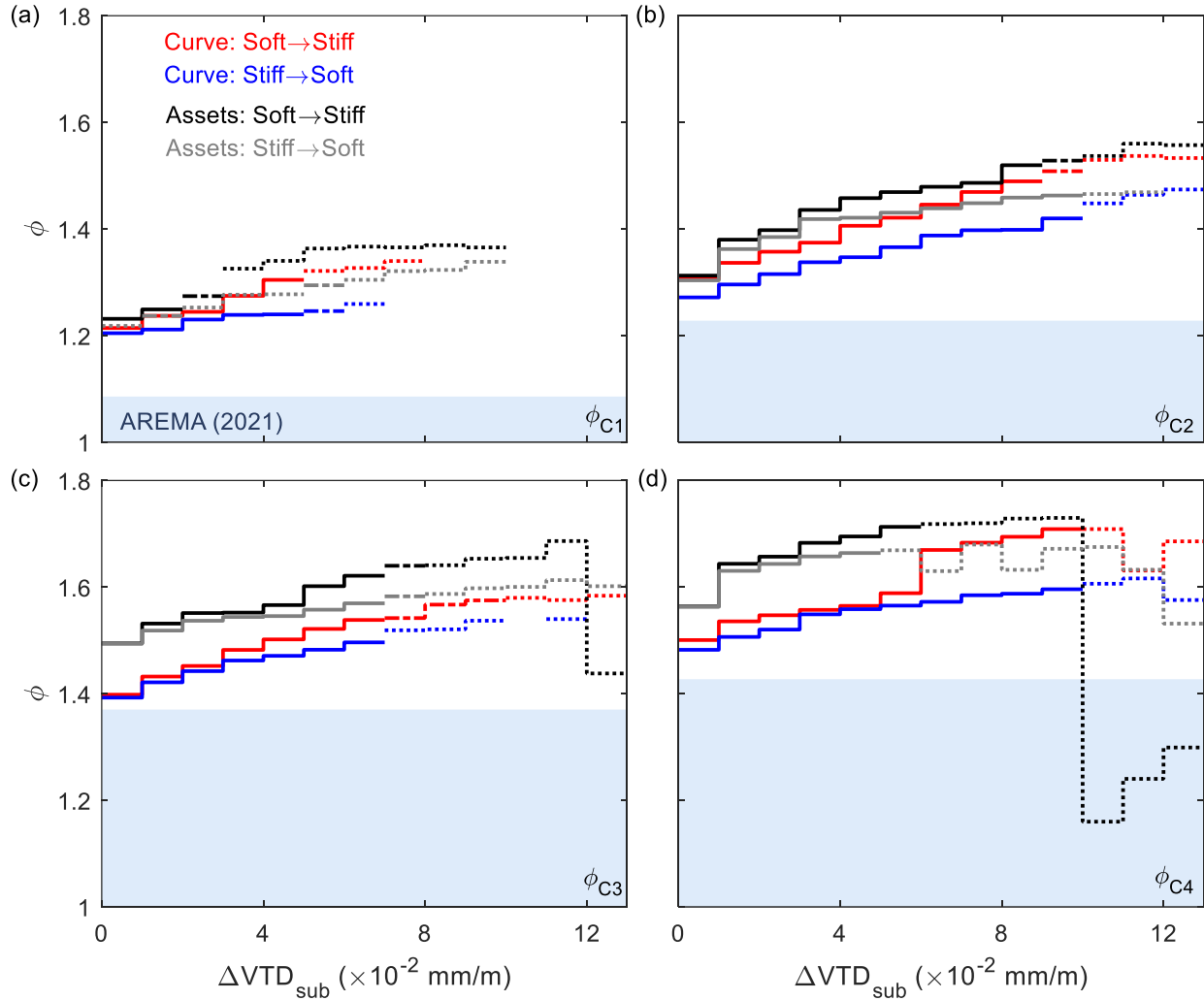


Figure E-10. IWS and MRail measurements for non-tangent track (inclusive of curve sections and track assets) based on the Grubbs test values of dynamic load factor (ϕ) for 0.01 mm/m increments of ΔVTD_{sub} regarding the estimated ϕ values by AREMA (2021) (Equation 6-9) and reliability (confidence level) conditions for four specific train speeds: (a) 15 km/h (~10 mph, as Class 1, ϕ_{C1}); (b) 40 km/h (25 mph, as Class 2, ϕ_{C2}); (c) 65 km/h (~40 mph, as Class 3, ϕ_{C3}); and (d) 75 km/h (~47 mph, as the maximum speed with appropriate number of data points, ϕ_{75}). Note: the solid, dash-dot, and dotted lines correspond to zones of high, moderate, and low reliability, respectively.

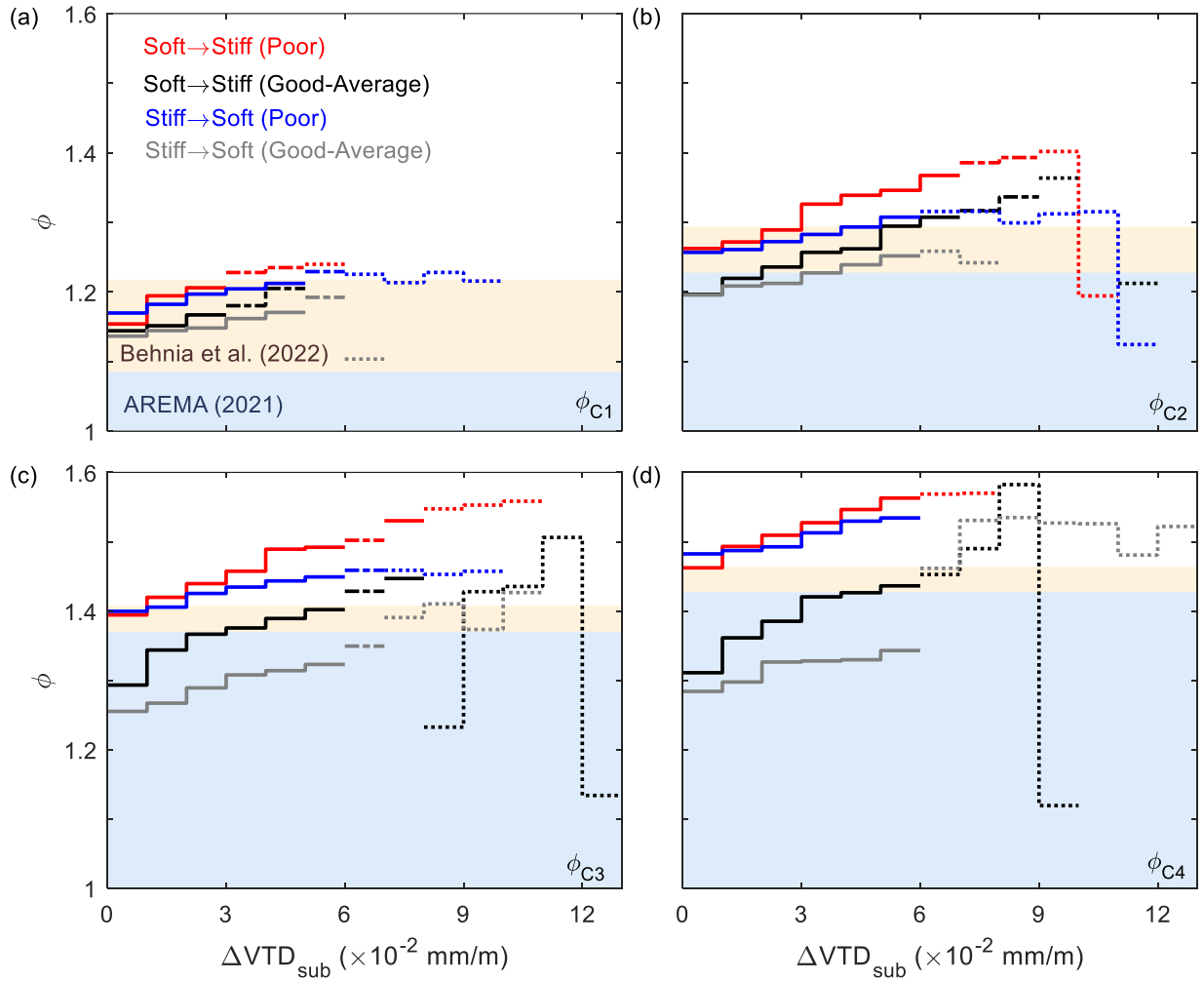


Figure E-11. IWS and MRail measurements in tangent track based on the Grubbs test values of dynamic load factor (ϕ) for 0.01 mm/m increments of ΔVTD_{sub} regarding the estimated ϕ values by Behnia et al. (2022) (Equation 6-7) and AREMA (2021) (Equation 6-9) and reliability (confidence level) conditions and track conditions (i.e., good-average and poor subgrade conditions of track) for four specific train speeds: (a) 15 km/h (~10 mph, as Class 1, ϕ_{C1}); (b) 40 km/h (25 mph, as Class 2, ϕ_{C2}); (c) 65 km/h (~40 mph, as Class 3, ϕ_{C3}); and (d) 75 km/h (~47 mph, as the maximum speed with appropriate number of data points, ϕ_{75}). Note: the solid, dash-dot, and dotted lines respectively correspond to zones of high, moderate, and low reliability.

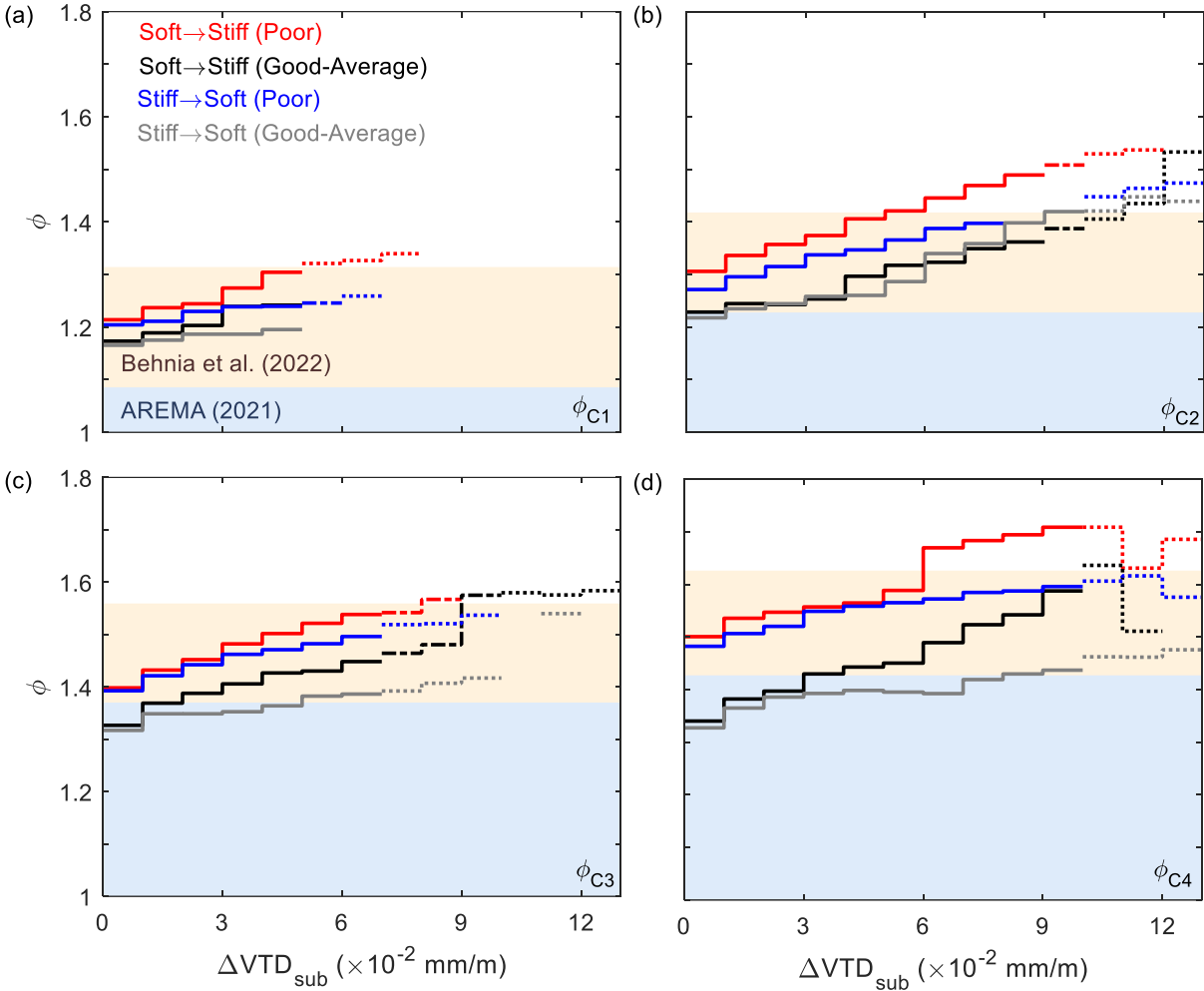


Figure E-12. IWS and MRail measurements in curve sections based on the Grubbs test values of dynamic load factor (ϕ) for 0.01 mm/m increments of ΔVTD_{sub} regarding the estimated ϕ values by Behnia et al. (2022) (Equation 6-8) and AREMA (2021) (Equation 6-9) and reliability (confidence level) conditions and track conditions (i.e., good-average and poor subgrade conditions of track) for four specific train speeds: (a) 15 km/h (~10 mph, as Class 1, ϕ_{C1}); (b) 40 km/h (25 mph, as Class 2, ϕ_{C2}); (c) 65 km/h (~40 mph, as Class 3, ϕ_{C3}); and (d) 75 km/h (~47 mph, as the maximum speed with appropriate number of data points, ϕ_{75}). Note: the solid, dash-dot, and dotted lines respectively correspond to zones of high, moderate, and low reliability.

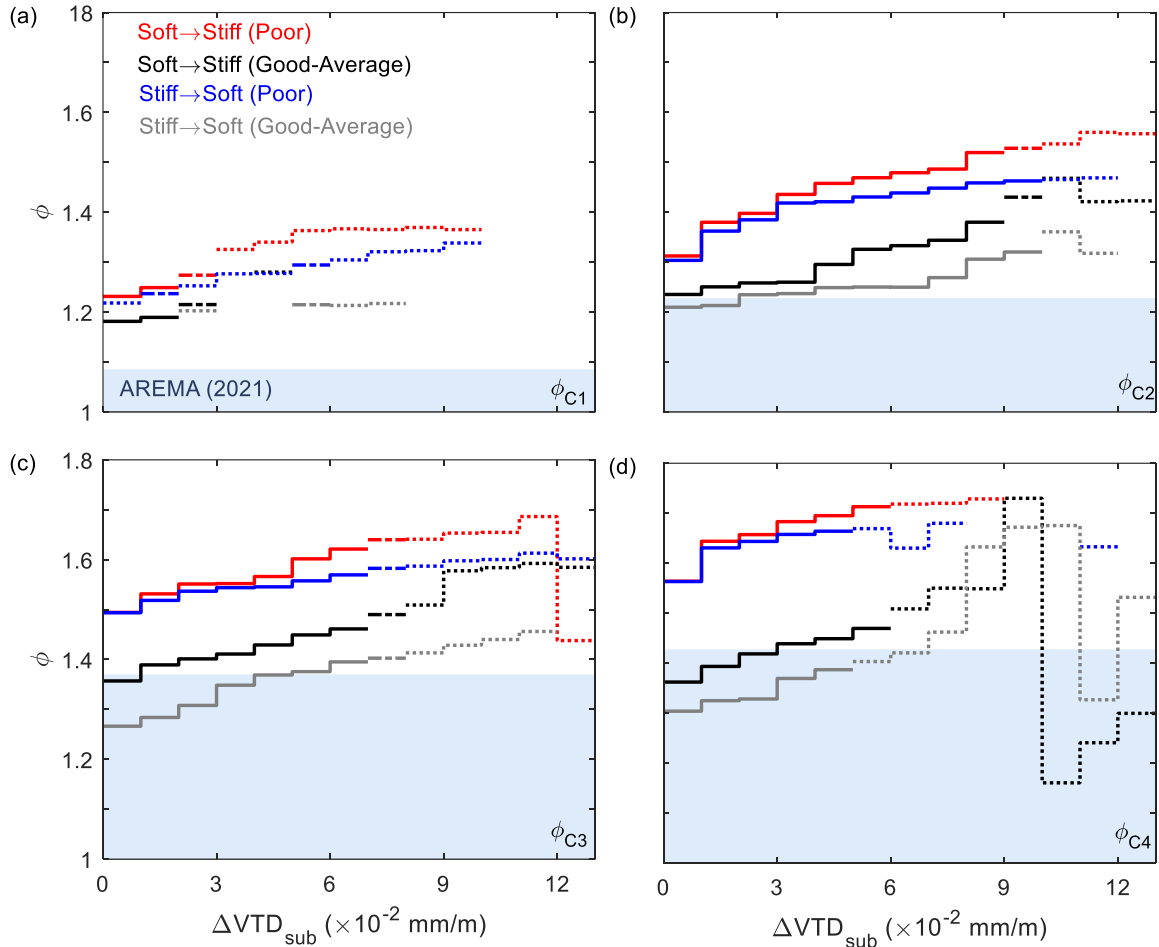


Figure E-13. IWS and MRail measurements in track assets based on the Grubbs test values of dynamic load factor (ϕ) for 0.01 mm/m increments of ΔVTD_{sub} regarding the estimated ϕ values by AREMA (2021) (Equation 6-9) and reliability (confidence level) conditions and track conditions (i.e., good-average and poor subgrade conditions of track) for four specific train speeds: (a) 15 km/h (~10 mph, as Class 1, ϕ_{C1}); (b) 40 km/h (25 mph, as Class 2, ϕ_{C2}); (c) 65 km/h (~40 mph, as Class 3, ϕ_{C3}); and (d) 75 km/h (~47 mph, as the maximum speed with appropriate number of data points, ϕ_{75}). Note: the solid, dash-dot, and dotted lines respectively correspond to zones of high, moderate, and low reliability.

Table E-1. Comparison of ϕ_{75} line developed by AREMA (Equation 6-9) and the maximum Grubbs test values from the IWS system based on transition direction and track conditions (derived from Figure E10).

Track type	Soft \rightarrow Stiff		Stiff \rightarrow Soft	
	Good-average track [Δ (%)]	Poor track [Δ (%)]	Good-average track [Δ (%)]	Poor track [Δ (%)]
Tangent	6	11	7	8
Curve	12	20	4	14
Track assets	12	22	8	17

Note: all ϕ values pass the ϕ_{75} line provided by AREMA (2021).